UTS UNIVERSITY OF TECHNOLOGY SYDNEY

Towards learning from demonstration for industrial assembly

by Victor Hernandez Moreno

Thesis submitted in fulfilment of the requirements for the degree of

Doctor of Philosophy

under the supervision of Univ.-Prof. Dr.-Ing. Jochen Deuse

University of Technology, Sydney

Faculty of Engineering and Information Technology

July 2024

Certificate of Original Authorship

I, Victor Hernandez Moreno, declare that this thesis is submitted in fulfilment of the requirements for the award of Doctor of Philosophy, in the School of Mechanical and Mechatronic Engineering at the University of Technology Sydney.

This thesis is wholly my own work unless otherwise referenced or acknowledged. In addition, I certify that all information sources and literature used are indicated in the thesis.

This document has not been submitted for qualifications at any other academic institution.

This research is supported by the Australian Government Research Training Program.

Production Note:
Signed: Signature removed prior to publication.

Date: 15 July 2024

Towards learning from demonstration for industrial assembly

by

Victor Hernandez Moreno

A thesis submitted in fulfilment of the requirements for the degree of Doctor of Philosophy

Abstract

The industrial assembly sector is confronted with a confluence of challenges arising from demands for mass customisation, labour shortages, and competitive pressure. To address this unique combination, automation systems appear beneficial that can rapidly adapt to new tasks and be operated by non-technical personnel. The Learning from Demonstration (LfD) concept emerges as a promising solution, enabling non-expert operators to teach robots new tasks without the complexities of traditional programming. This concept also empowers robots to apply learnt tasks in changed situations, fostering flexibility for competitive solutions. Despite being a well-explored field in research, the effective deployment of LfD in industrial settings remains an unmet challenge.

This thesis delves into the application of prominent LfD methods towards industrial assembly tasks and investigates how the concept can be leveraged to benefit this sector. Through a comprehensive analysis of LfD solutions in research and a comparison with industrial practices, key obstacles hindering the seamless integration of promoted solutions in an industrial environment are identified. These challenges include issues of practicability, task complexity and diversity, generalisability, performance evaluation, and integration concepts. With the goal of developing a framework that enhances applicability in the industrial assembly industry, this thesis promotes improvements in the three phases of characteristic LfD: human demonstration, robot learning, and robot reproduction.

In contrast to the prevailing kinaesthetic teaching application, a guiding graphical interface is developed based on the Hausdorff approximation planner (HAP) framework, providing human operators with insights into the robot's kinematic constraints during demonstration. The robot learning phase is enhanced by combining the primarily employed trajectory-based Dynamic Movement Primitives (DMPs) method with the well-established Methods-Time Measurement (MTM-1) industrial taxonomy for extended generalisability across custom skills. Addressing challenges during reproduction in changing environments, a reactive control approach is presented that employs a novel multibody approximation scheme. This scheme informs potential fields generating wrenches of repulsion and attraction for robust reproduction given new environmental situations. A unified framework incorporating these novel methods is established and demonstrated through a physical demonstrator, allowing for real-world evaluation of the proposed methods.

This thesis contributes a comprehensive framework to promote increased applicability of LfD for the industrial assembly sector, addressing key challenges in prevailing LfD research approaches, and providing a pathway towards effective deployment of robotic solutions in a competitive and evolving industrial landscape.

Acknowledgements

I wish to convey my sincere appreciation to those whose guidance and support have been instrumental in the realisation of this work.

First and foremost, I extend my sincere appreciation to my esteemed supervisors, Prof Jochen Deuse and Dr Marc G. Carmichael. Their unwavering commitment to excellence, scholarly guidance, and patience have been the cornerstones of my academic development. Their insightful feedback and continuous support have been instrumental in shaping this thesis. I am truly grateful for their mentorship, which has not only refined my research skills but has also enriched my overall academic experience.

I feel gratitude for the opportunity to collaborate with numerous fantastic co-authors, colleagues, and fellow students who have been steadfast companions through both successes and challenges. I want to extend a special acknowledgement to Fouad Sukkar and Louis Fernandez for an inspiring and fruitful collaboration, as well as their unwavering dedication to creating impactful contributions. I also want to express a particularly warm thank you to Richardo Khonasty, Sheila Sutjipto, and Hongkyoon Byun for engaging in diverse conversations, sharing in challenges, and offering motivating words — your support has been truly invaluable.

Beyond the academic realm, I am deeply grateful to my family for their endless love, encouragement, and sacrifices. Their unwavering support sustained me through the challenges of this doctoral journey. I am particularly grateful to my wife, Adhara Ferra Gutierrez, for being my pillar of strength, understanding the demands of this undertaking, and providing unconditional support, patience, and encouragement.

This accomplishment would not have been possible without the support of these individuals and the broader academic community from the School of Mechanical and Mechatronic Engineering and the Robotics Institute. Thank you for being an integral part of this transformative chapter in my life.

Contents

List of Figures

List of Tables

Acronyms & Abbreviations

AI	Artificial Intelligence
CAD	Computer-aided Design
CAM	Computer-aided Manufacturing
CDMPs	Cartesian space Dynamic Movement Primitives
DMPs	Dynamic Movement Primitives
DoF	Degrees of Freedom
FIRAS	Force Inducing an Artificial Repulsion from the Surface
GUI	Graphical User Interface
HAP	Hausdorff approximation planner
IK	inverse kinematics
IRL	Inverse Reinforcement Learning
LfD	Learning from Demonstration
LfD-IA	Learning from Demonstration for Industrial Assembly
ML	Machine Learning
MOST	Maynard Operation Sequence Technique
MTM	Methods-Time Measurement
OEE	Overall Equipment Effectiveness

PbD Programming by Demonstration

PCB Printed Circuit Board

PMTS Predetermined Motion Time System

PRISMA Preferred Reporting Items for Systematic Reviews and Meta-Analyses

ProMPs Probablisitic Movement Primitives

RBFs Radial Basis Functions

RL Reinforcement Learning

ROS Robot Operating System

RTM Robot Time and Motion

TWI Training within Industry

WF Work Factor

WoS Web of Science

Nomenclature

General Formatting Style

i	generally used index indicating distinct list values
x	scalar variable
$\mathbf{x}$	vector variable
$f(\cdot)$ or $\mathbf{f}(\cdot)$	scalar / vector valued function
$\lvert \cdot \rvert$	absolute value
$\lVert \cdot \rVert$	vector length and normalised vector
$[\cdot]^T$	transpose
$\overline{\{\cdot\}}$	inverse
$log(\cdot)$	logarithm
$\frac{\partial}{\partial x}$	partial derivative to x
$\nabla_{\mathbf{x}}$	vector derivative to $\mathbf{x}$

Subscriptions

$\{\cdot\}_{\mathbf{x}}$ or $\{\cdot\}^{\mathbf{x}}$	position related variable
$\{\cdot\}_{\mathbf{q}}$ or $\{\cdot\}^{\mathbf{q}}$	quaternion related variable
$\{\cdot\}_{dem}$	subscript for demonstration related value
$\{\cdot\}_{rep}$	subscript for reproduction related value
$\{\cdot\}_{rel}$	subscript for relative position
$\{\cdot\}_{stat}$	subscript for static variable
$\{\cdot\}_{dyn}$	subscript for dynamic variable

Region of non-reproducible motions

$\mathcal{S}$	system that performs a motion
$\mathcal{C}$	space in which a system performs a motion
λ	motion trajectory as a set of discrete states over time
Λ	discrete states
Γ	control policy
π	executable control
$\mathcal{R}$	region of reproducible motion
$\mathcal{R}^*$	region of reproducible motion that maximises coverage

Dynamic Movement Primitives

x, $\dot{x}$, $\mathbf{x}$, $\dot{\mathbf{x}}$	translational trajectory data and its 1st derivative
$\tilde{v}$, $\dot{\tilde{v}}$, $\tilde{\mathbf{v}}$, $\dot{\tilde{\mathbf{v}}}$	translational velocity and acceleration scaled with temporal scaling parameter
$\tilde{\mathbf{w}}$, $\dot{\tilde{\mathbf{w}}}$	rotational velocity and acceleration scaled with temporal scaling parameter
$\mathbf{e_q}$	quaternion error
$\mathbf{x}_0$, $\mathbf{x}_T$, $\mathbf{q}_0$, $\mathbf{q}_T$	initial and goal position / quaternion
τ	temporal scaling parameter
s	phase variable
α_s	scaling parameter of canonical system
$f, \mathbf{f}^x, \mathbf{f}^q$	forcing term for different spaces
$\varphi_{\tilde{v}}$, $\varphi_{\tilde{a}}$	coupling term on velocity and acceleration level
K, $\mathbf{K}^x$, $\mathbf{K}^q$	stiffness gain in different spaces
D, $\mathbf{D}^x$, $\mathbf{D}^q$	damping gain in different spaces
ψ_n	Radial Basis Function
n, N	Number of Radial Basis Functions (n=1,2,...N)
h_n, c_n	centres and widths of Radial Basis Functions

ω_n	weights of Radial Basis Functions

Superquadrics, Potential Fields, and Wrenches

$\mathbf{x}_B$	point in the superquadric's canonical coordinate system
x_B, y_B, z_B	individual dimensions of $\mathbf{x}_B$
$F(\mathbf{x}_B)$	inside-outside function
$H_{1,2,3}$	term of the inside-outside function with absolute coordinates
a, b, c	volumetric expansion of superquadric (radii)
ε_1, ε_2	roundness parameters of superquadric
$\mathbf{r}_s$	intersecting vector of superquadric
$\mathbf{c}_{i,j}$	vector between the centres of superquadric i and j
U	potential field
$p(\mathbf{x})$	shortest distance between two points
p_0	distance of desired influence
ζ, A	scaling parameter of static potential field
λ, ι, η	scaling parameters of dynamic potential field
θ	angle between velocity vector and potential field related vector
β	scaling parameter for intersecting vector
$\mathbf{A}(\mathbf{q})$	transformation matrix from absolute to canonical coordinate system

Chapter 1

Introduction

1.1 Background and Motivation

The first industrial robot was installed in 1961 by Unimation on a production line at the GM Ternstedt plant in Trenton, NJ, to automate the handling of distinct hardware components [3]. Since then, robots have become a popular tool in the industrial sector and are increasingly present in public and private life. In science-fiction movies, robots have ever since been portrayed as intelligent and capable of communicating through intuitive approaches, such as direct conversation or simple gestures. However, reality continues to challenge many people when it comes to programming modern robots.

With the rationale of transmitting an intended behaviour to a robotic system through user-friendly and intuitive methods, a variety of techniques have been developed since the invention of robots. Most of the approaches that emerged in the first decades of the robotics era are still common among today's industrial practice, including teach pendants from the 1970s, offline programming using Computer-aided Design (CAD) / Computer-aided Manufacturing (CAM) from the 1980s, and lead-through technology (1987) where a robot is physically guided through the task. [4]

At about the same time, a highly visionary idea emerged that gained attention in the manufacturing industry. The so-called Learning from Demonstration (LfD) concept, known then as Programming by Demonstration (PbD), envisioned the ability of robots to be taught new tasks by end users without the need for explicit and tedious manual programming. Thus, the desire for more efficient ways to program robots grew, in contrast to

the prevailing trial-and-error *tabula rasa* approaches, and simultaneously extending the robot's operability to a wider range of potential users. [5]

The first implementations of PbD date back to the early 1980s, when industrial robots were still extremely limited in their capabilities. Sensorimotor information recorded of the end-effector was initially segmented by discrete key subgoals such as a relative pose between objects or absolute goal poses. To mimic the motion presented, the key points were traversed using *primary actions* in the form of simple point-to-point movements of the industrial robot. Due to the sheer variability in human motions, these linear state-action-state sequences were soon transformed into symbolic *if-then* rules within graph-based representations, allowing symbolic reasoning to unify different task approaches. With the influence of the emerging field of machine learning, the PbD community shifted expectations from recording and playing back scenarios to generalisable capabilities, introducing challenges such as *how to generalise a task* or *how to reproduce a skill in a completely novel situation*. The initial two-step approach that incorporated *human demonstration* and *robot reproduction* experienced a rethinking in which an intermediate phase of a necessary *robot learning* of the task's nature was considered. As a consequence, the necessity for adaptive robot controllers and an active role of the user was established to ensure appropriate learning of the intended task. [6]

Driven by the progressive development towards generalisability in combination with innovations in robotics technology, the expectations around LfD expanded increasingly into interdisciplinary challenges. With increasing interest in mobile and humanoid robots, trends toward robot behaviour similar to that of living beings were awakened. Influential studies of primate neural mechanisms and children's imitation capacities led to the biologically inspired branding of *imitation learning*. Recent developments such as the new category of collaborative robots that have been in use since late 2008 [7] and revolutionary technologies in the field of artificial intelligence [8] have added additional stimuli to the current progression surrounding LfD. [6]

Today, the traditional idea of PbD is considered an interdisciplinary field with a variety of unique challenges to tackle and desires to meet depending on the application explored. LfD is known under several conceptually comparable approaches, including *learning from observation*, *programming from demonstration*, *imitation learning*, or *apprenticeship learning*. However, all continue to follow the initial general paradigm of endowing robots with the ability to learn new tasks from human demonstrations. Categorised as a programming approach based on direct human demonstration rather than learning on its own,

LfD promises, in particular, to reduce the complexity of search spaces for learning [5], resulting in more efficient and human intention-driven learning.

Due to the wide range of possible applications and approaches investigated so far, there exists no overarching blueprint for the realisation of an LfD solution. As a general framework, the generic questions formulated in the early 2000s, namely, *who to imitate*, *when to imitate*, *what to imitate*, and *how to imitate*, provide indicative guidance [6]. However, many implementations continue to follow a procedural structure that divides an LfD approach into three consecutive phases: *demonstration*, *learning*, and *reproduction* (see Figure 1.1).

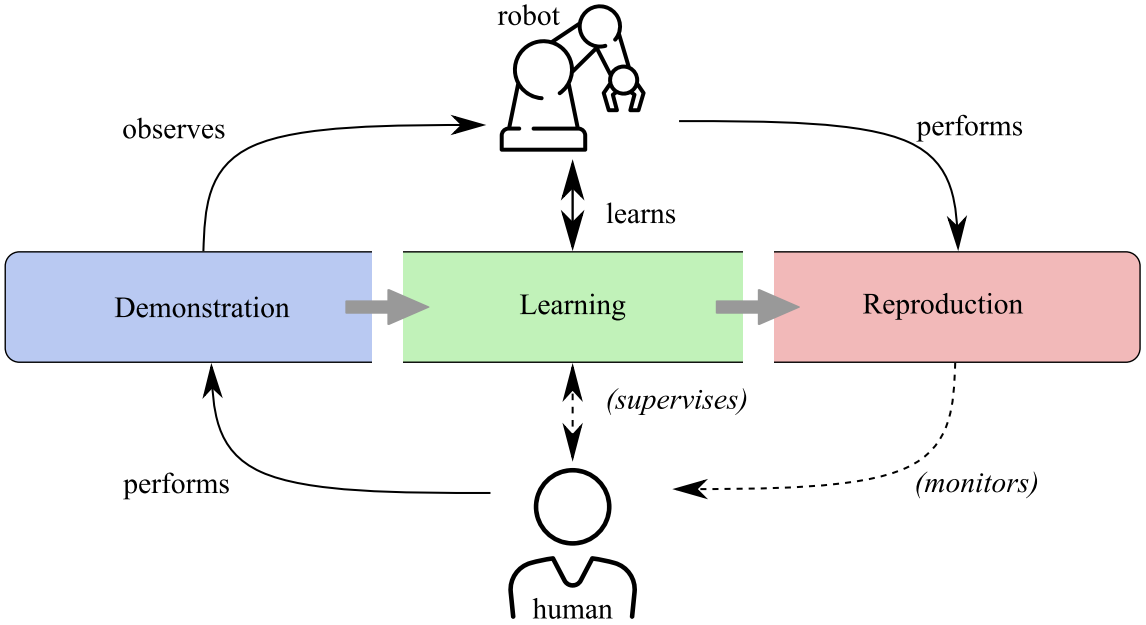

FIGURE 1.1: Conceptual procedure of Learning from Demonstration

In the first phase, the human takes an active role in performing the task that the robot shall reproduce afterward, while the robotic system observes the happenings passively. The wording 'observation' highlights the passivity of the robot and does not imply the perceptual solution with which this is implemented. In fact, observation can be carried out in mainly three different ways, including *kinaesthetic teaching*, *teleoperation*, and *passive observation* [9]. In kinaesthetic teaching, the human guides the robot physically through the desired motion by manually adjusting its end-effector position. The robot follows passively while compensating for any gravitational effects. On the contrary, teleoperation refers to the robot's ability to be controlled from a certain distance, resulting in no physical contact between the human and the robot, but requires still the simultaneous performance of the task. A robot-independent task demonstration is considered as a passive observation

technique, where the human performs the task using their own capabilities while being tracked from various sensors.

Related to the choice of the demonstration method is the appearance of two critical correspondence problems, namely physical and perceptual inequality [5]. The former thematises the differences in human's and robot's embodiment that may result in distinct actions / movements to accomplish the same physical effect. The perceptual issue describes the difference between the human's and robot's sensory capabilities, which may produce dissimilar observations of the actions/scene. Regarding tactile impression, for example, the human skin allows the simultaneous sense of contact forces, temperature, and surface procurement, while most tactile robot sensors perceive only information of contact through force interaction.

During the *learning* phase, the robot is assigned to actively learn the essence of the task taught through the implemented LfD learning framework. While aiming for a generalised understanding capable of reproducing the task under differing circumstances, this phase is considered highly impactful on the final outcome of any LfD solution. The selected technique defines the required information of the demonstration, the technique's ability to generalise to differing circumstances, and the robot's capability of translating the technique's outcome to physical motion. Generally speaking, common techniques can be classified on the basis of their outcomes. An outcome can be a *policy* in the form of trajectories or low-level actions, a *plan* consisting of primitive sequences or primitive hierarchies, or a *cost/reward* for trajectory optimisation or Inverse Reinforcement Learning (IRL) [9]. Depending on the demonstration's quality and the task's nature, the human teacher usually supervises the learning and provides, if necessary, guiding/correcting feedback or new demonstrations to the robot. By monitoring and intervening during the learning process, the human ensures that the robot is adequately understanding the expected behaviour.

Once the human is satisfied with the task learnt within the controlled environment, the final phase of autonomous *reproduction* commences. Success is mainly driven by the generalisability to new unknown situations. Due to growing expectations, the situation may today consider changes in motion, such as spatial or temporal scaling, in the environment, such as appearing obstacles or uncertainties within the real world, as well as in the task by performing a manipulation on similar but not identical objects. Depending on the application, the task may incorporate the collaboration between the human and the robot during reproduction, requiring a more responsive acting of the robot. However, in most cases, the human is passive during reproduction and optionally monitors the continuous

appropriate performance of the robot. Table 1.1 summarises the technical categories that are commonly encountered when implementing an LfD solution.

Demonstration Method	**Learning Methods Outcomes**	**Reproduction Generalisability**
Kinaesthetic Teaching	Policy: • trajectory • low-level actions	changes in motion (spatial / temporal scaling)
Teleoperation	Plan: • primitive sequence • primitive hierarchy	changes in environment (e.g. obstacles)
Passive Observation	Cost/Reward: • trajectory optimisation • inverse reinforcement learning	changes in task (e.g. differing objects)

TABLE 1.1: Technical categories of Learning from Demonstration approaches

As the spectrum of potential robot usage has expanded beyond industrial settings in recent years, LfD has received increasing attention in a variety of application areas [8]. Ranging from manufacturing and assembly [10, 11], surgery and rehabilitation [12, 13], personal assistance, to construction tasks [14], LfD approaches promise to make the communication between humans and robots more accessible to non-robot experts and to strengthen the robot's task performance against varying circumstances.

Originated in the manufacturing industry, LfD continues to be a highly promising technology with the potential to revolutionise the prevailing practices. The assembly industry, which accounts for a significant share of up to 70% of the time allocated within the production process [15], faces emerging factors that threaten to limit its growth. Although the availability of the workforce is expected to be reduced in the near future due to demographic changes [16, 17], the assembly process continues to be carried out predominantly manually [18]. Simultaneously, a shift from mass production to mass customisation is observable [19, 20], limiting the applicability of customised assembly systems, while products tend to generally shrink in dimensions, making manual assembly more challenging or even impossible in certain industries [21]. These challenges requiring modern solutions in the assembly industry favour the deployment of user-friendly, intuitively programmable, and flexible robotic systems. Based on the anticipated capabilities of the LfD concept, such approaches are considered highly promising to tackle the present challenges. Despite its

great potential proven within the research environment and few commercial products, such as MIRAI [22], LfD has not yet been widely deployed in the assembly industry.

This thesis presents an investigation into techniques that improve the applicability of LfD for industrial assembly tasks. Extending existing approaches based on application-specific requirements and expectations can promote a relevant boost of the concept for practical consideration in the near future and assist in coping with modern challenges in the targeted field.

1.2 Research Questions

Existing research on LfD for assembly-related tasks have mainly focused on methodological functionality rather than exploiting sufficiently the distinctive characteristic entailed in assembly-specific requirements. Satisfactory results were often achieved based on simplified scenarios, either by targeting a specific subskill that has limited conclusive value in isolation, or oversimplified representation of objects and environments which hinders the transferability to practical settings. Another distinction is drawn from the driving goals of research trends and the practical use of LfD in industrial assembly. Industrial assembly emphasises efficiency, productivity, and cost effectiveness [23], contrary to assembly-related experiments in research where effectiveness is less critical and success rates above 50% are considered satisfactory.

Based on decades of research efforts, the numerous contributions in LfD provide a solid foundation for assembly-related applications, and the assembly industry is considered a field of application that will benefit significantly from application-targeted LfD solutions. In light of the situation described above, this thesis investigates the research question of how state-of-the-art LfD approaches can be leveraged toward practical industrial assembly capabilities. In line with the characteristic LfD procedure, this is linked to the following aspects: (1) Is the prevailing demonstration method designed for effective and efficient teaching? (2) How can specific tasks of a typical industrial assembly be effectively embodied in an LfD framework? (3) How can LfD ensure robust reproduction in realistic situations?

1.3 Scope

Following the formulated research question, this research seeks to develop a framework that incorporates techniques to improve the applicability of LfD in an industrial assembly context. In detail, this thesis aims to: (1) *examine* currently prevailing methods with respect to the requirements and expectations in the targeted field of application (2) *enhance* preexisting methods to overcome identified obstacles limiting the applicability of LfD in the outlined context (3) *develop* a framework embodied in an application-oriented experimental physical demonstrator.

To make the technical scope of this thesis attainable, specific assumptions have been established, in particular, surrounding the envisioned application. In the scope of this thesis, a scenario of repetitive assembly operations is depicted in which the task-experienced non-robot experts, referred to as human operators, are assumed to perform the teaching of the required task to the robotic system. Due to the industrial context, demonstration, learning, and reproduction are envisaged under certain time constraints, and the availability of resources is taken into account. Once human-driven demonstration and robot-driven learning are finalised, the robot is expected to perform the task autonomously under varying scenery conditions, including changes in motion and environment. All physical operations are limited to a workspace of a small workbench setup assuming that all necessary components are in reach for a human operator and no larger body motion is required. Tasks that require the collaboration between the human operator and the robot during reproduction are not considered. The scope of this thesis is restricted to investigating the improved applicability of LfD methods in the industry-inspired scenario described.

Further constraints are drawn with respect to the interdisciplinary field of LfD. In light of the achievements of previous academic contributions, the development of completely novel demonstration technologies, learning methods, or reproduction characteristics is considered neither within the scope of this thesis nor necessary due to the wide preexisting range of LfD techniques. As a result, the selection of foundational LfD techniques is driven by the requirements extracted from the specified scenario. This includes predominantly the assumption that the human operator is an expert of the intended task favouring a demonstration-driven learning procedure. As a consequence, self-driven approaches emphasising Artificial Intelligence (AI) and Machine Learning (ML)-inspired techniques are considered out of scope.

Finally, the thesis presents fundamental research aimed at enhancing state-of-the-art LfD features tailored to assembly-related skills. Criteria identified from a comprehensive literature review inform key requirements investigated for LfD systems to improve their applicability in industrial contexts. Laboratory experiments, both in simulation and real-world settings, demonstrate how the proposed framework achieves these improvements. An evaluation or deployment in industrial practice is out of scope, as the desired outcomes can be adequately reflected in the given scenarios.

1.4 Principal Contributions

The research contributions that emerged from the work associated with this thesis can be framed around the three-phase LfD procedure discussed above and summarised as in Figure 1.2. Individual contributions are described as follows:

- C1: A systematic literature review that provides insights into the state-of-the-art LfD research for assembly-related applications and a discussion of the similarities and obstacles identified compared to industrial practices and expected requirements.
- C2: A method for robust transferability of a human demonstration in the absence of the robotic system, allowing more efficient and reliable resource occupation when applying LfD approaches in industrial practice.
- C3: A learning technique designed for assembly tasks in industrial environments that combines the prevailing LfD approach with the industry-established Methods-Time Measurement that is used to model assembly operations.
- C4: A method for robust reproduction under environmental changes and motion alteration based on potential fields between multi-volumetric objects represented as superquadrics.

1.5 Publications

The contributions presented within this thesis have been partially featured in the directly related publications P1-4 listed below. To elaborate, the systematic literature review was published in P1. The content of contribution C2 corresponds to what was presented in P2, while the material in P3 served as a template for the content of contribution C3. As of the submission of this thesis, the content of the contribution C4 is prepared for submission to the IEEE Robotics and Automation Letters (RA-L) Journal under the title ‘Multibody

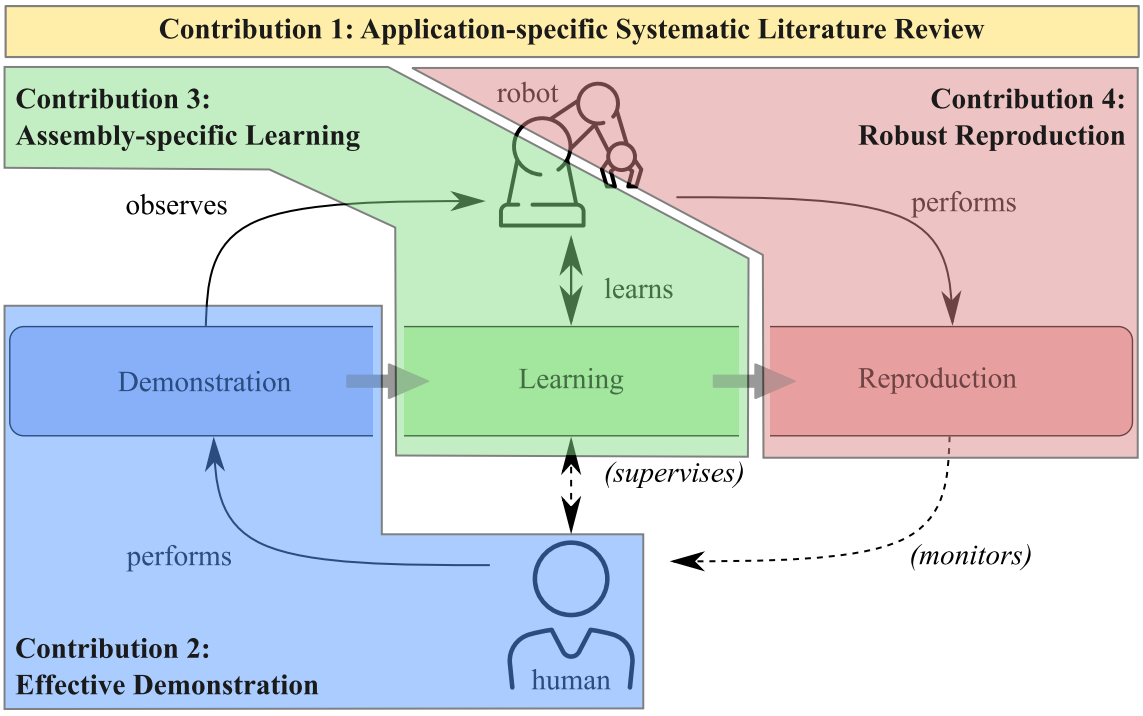

FIGURE 1.2: Contribution overview

collision avoidance using superquadrical potential fields'. All publications influenced the thesis conclusion and the prospects for future work. Victor Hernandez Moreno was the main contributor to all of these publications.

- P1 [24]: **Victor Hernandez Moreno**, Steffen Jansing, Mikhail Polikarpov, Marc G. Carmichael, and Jochen Deuse. Obstacles and Opportunities for Learning from Demonstration in Practical Industrial Assembly: A Systematic Literature Review. *Robotics and Computer-Integrated Manufacturing*, accepted, 2024
- P2 [25]: Fouad Sukkar*, **Victor Hernandez Moreno***, Teresa Vidal-Calleja, and Jochen Deuse. Guided Learning from Demonstration for Robust Transferability. *IEEE International Conference on Robotics and Automation (ICRA)*, accepted, 2023
- P3 [26]: **Victor Hernandez Moreno**, Marc G. Carmichael, and Jochen Deuse. Towards Learning by Demonstration for Industrial Assembly Tasks. *Manufacturing Handling Industrial Robotics (MHI) Conference*, published, 2022.
- P4 [27]: **Victor Hernandez Moreno**, Louis F. Fernandez, Marc G. Carmichael, and Jochen Deuse. Multi-volume Potential Fields for Effective Learning from Demonstration. *IEEE International Conference on Automation Science and Engineering*, accepted, 2024.

1.6 Thesis Outline

The thesis is organised as follows:

Chapter 2 explores relevant literature and shows the obstacles identified in the current research of LfD for assembly-related tasks with the intention of industry deployment. The summary incorporates a scoped outline of the framework that aims to improve the applicability of LfD for industrial assembly.

Chapter 3 details a novel technique to improve the efficiency of the demonstration process in the absence of the physical robot using an interactive interface that provides information about the robot's kinematic constraints.

Chapter 4 presents a learning framework that addresses the individual characteristics of assembly-related tasks. A prominent LfD learning technique is enhanced with an industry-established task discretisation system. The creation of generalised skills allows their individual characterisation for improved performance.

Chapter 5 contributes a technique for robust reproduction that allows the robotic reproduction of the learnt task in new contexts. Considered changes include the relocation of task-related objects and the appearance of unrelated obstacles while respecting boundaries of an artificially introduced workspace and being attracted to the desired final state.

Chapter 6 consolidates the three techniques from Chapters 3, 4, and 5 into a unifying framework. A physical demonstrator is proposed that embodies the established framework.

Chapter 7 concludes the presented work by providing a summary of the contributions elaborated, together with a discussion of their limitations and potential future research avenues.

Chapter 2

Literature Review

The work in this thesis investigates the potential to leverage LfD to the specified industry-focused scenario of assembly tasks. This Chapter surveys the state-of-the-art of LfD approaches explored in research for assembly-related tasks and depicts their obstacles based on the comparison to industrial practice. In detail, it reviews the literature with the purpose of answering the following questions:

- (Q1) What are the prevalent LfD methods and problem domains explored in research?
- (Q2) How do state-of-the-art LfD approaches align with the training techniques and learning behaviour of human operators in the industry?
- (Q3) What are the primary obstacles that hinder the practical implementation of LfD solutions in the traditional repetitive assembly industry?

An evidence-based approach was performed in the form of a systematic literature review, known to produce reliable, reproducible, and transparent research results with minimal bias and errors [1, 28, 29]. It was carried out according to the updated Preferred Reporting Items for Systematic Reviews and Meta-Analyses (PRISMA) guideline [1].

The Chapter is structured as follows: Based on the systematic approach described in Section 2.1, the findings with respect to Q1 are summarised in Section 2.2. In light of Q2, Section 2.3 reviews a common training technique to teach human operators new manual assembly tasks and discusses its similarities and differences to LfD dominant research trends. Identified obstacles are described in Section 2.4 reflecting Q3. Finally, a summary and justified specification of the research narrative investigated in this thesis are given in Section 2.5. This Chapter was derived from [24].

2.1 Systematic Approach

The following reports on the information sources interrogated, the search strategy chosen, the eligibility criteria selected, and details regarding the data collection process. Potential limitations of the chosen approach are discussed in the end.

2.1.1 Information Sources and Search Strategy

The systematic review of the literature was based on the interrogation of the well-recognised databases Scopus and Web of Science (WoS) [30]. Web of Science has been searched using the *Core Collection* and the *Exact Search* option.

To query representative records of state-of-the-art robot LfD for assembly applications, both aspects were embedded in the search string. It incorporated the LfD variations from Section 1.1 and a list of assembly-related terms established through a preliminary screening of abstracts that included the term 'assembly' combined with the assembly taxonomy of [23] (see Table 2.1). A consistent selection of relevant reports was achieved using the automatic filter mechanisms described in Table 2.1 and manual screening based on the eligibility criteria defined in Section 2.1.2. The final database interrogation was conducted on 31 March 2023.

2.1.2 Eligibility Criteria

In addition to the application scenario described in Section 1.3, physical relatable experiments are considered essential to evaluate the state-of-the-art LfD approaches applied to assembly tasks. Therefore, records were included that show demonstrations done by humans and reproduced motions made by physical robots. Although physical experiments were required, practical implementation in an industrial environment was not necessary.

In order to establish coverage of high-quality records, additional reputation criteria were applied in the form of a grouping approach inspired by [31]. The first group of eligible records includes all records published in 2022 despite the citation count to acknowledge and emphasise the most recent efforts in the field of interest. Records published between 2013 and 2021 are recognised as eligible should the threshold of at least three citations on average per year be reached.

Database	Search String and Filter Parameters
Scopus	TITLE-ABS-KEY(((learning OR programming OR teaching) PRE/2 (demonstration OR observation)) OR ((imitation OR apprenticeship) PRE/2 learning) AND robot*) **AND** TITLE-ABS-KEY (assembl* OR (peg W/2 (hole OR insertion)) OR interlocking OR (pick W/1 place) OR rivet* OR wiring OR fastener OR jamming OR glue OR gluing OR (reach* W/2 grasp*) OR weld* OR stacking OR screw* OR retainer OR ((press OR snap) W/1 fit) OR adhesiv* OR crimp*)
	Publication Year: 2013 – 2023 Subject Area: Computer Science, Engineering, Mathematics Language: English Document Type Exclusion: Conference Review, Editorial
Web of Science	TS=((((learning OR programming OR teaching) NEAR/2 (demonstration OR observation)) OR ((imitation OR apprenticeship) NEAR/2 learning) AND robot*) **AND** (assembl* OR (peg NEAR/2 (hole OR insertion)) OR interlocking OR (pick NEAR/1 place) OR rivet* OR wiring OR fastener OR jamming OR glue OR gluing OR (reach* NEAR/2 grasp*) OR weld* OR stacking OR screw* OR retainer OR ((press OR snap) NEAR/2 fit) OR adhesiv* OR crimp*))
	Publication Year: 2013 – 2023 Subject Area: Robotics, Computer Science, Automation Control Systems, Engineering, Mathematics Language: English

Table 2.1: Information Sources and Search Strategy

In summary, the following exclusion criteria (EX1-6) were defined, which supplement the parameters for automatic filtering of Table 2.1:

- EX1: The study was published between 2013 and 2021, but the annual average citation count is below the threshold at the time of final database access (citation requirement).
- EX2: The terms LfD and assembly are used in an unrelated context.
- EX3: The full text of the study is not available.
- EX4: The study is a review or survey.
- EX5: The study deals with collaborative applications between humans and robots in which the task is reproduced jointly.
- EX6: The study has not evaluated the proposed method with the execution of a physical robot.
- EX7: The study has not evaluated the proposed method with demonstrations performed by humans.

2.1.3 Selection and Data Collection Process

The systematic literature review was performed following the three consecutive phases of the PRISMA 2020 [1] guideline, namely *identification*, *screening*, and *data collection* (see Figure 2.1). Within the initial identification phase, the interrogation of the selected databases Scopus and WoS, resulted in n = 330 and n = 265 identified records, respectively. The automated filtering system of both databases, following the parameters specified in Table 2.1, removed a total of n = 136 records. Using software and manual comparison of authors, title, and abstract, n = 190 records were identified as duplicates and merged. Furthermore, the average annual citation value was calculated for each record, which marked a total of n = 156 publications as ineligible with respect to the citation requirement (EX1). Within the consecutive screening phase, the preliminary review of the title and abstract revealed that n = 12 records were not related to the field of interest (EX2), while the full text of all records was accessible (EX3). The full reports were assessed for eligibility following the exclusion criteria EX4 to EX7. In this context, n = 4 reports were identified as reviews or surveys (EX4), n = 17 reports only discussed human-robot collaboration (EX5), and n = 15 + 4 reports did not evaluate the proposed method in an end-to-end solution with human and robot performing the task physically (EX6 + EX7). Consequently, a total of n = 61 studies were verified as appropriate for the present study and accordingly used for the data collection process. Appendix A.1 and A.2 provide a corresponding table of all included studies of the literature review conducted. The included studies were reviewed for the following data: LfD methods, applications, and experimentally evaluated capabilities. Particular attention was paid to the experimental evaluation and the results presented.

2.1.4 Limitations of the Systematic Approach

With the intention of comparing the state-of-the-art achievements of learning from demonstration research to industrial requirements, the systematic literature deliberately focusses on end-to-end solutions performed physically by humans and robots. Consequently, potential impactful theoretical findings may be excluded either intentionally by the authors or unintentionally due to uncontrollable circumstances. An acute reason for unintentional limitation was the COVID-19 pandemic, which affected physical work in laboratories and workplaces between 2020 and 2022. Such exclusions are covered by criteria EX6 and EX7 (assessment performed in order: EX6 before EX7). Figure 2.2 illustrates the chronological distribution of excluded studies as a percentage of included+EX6/7. Outliers in 2015 and

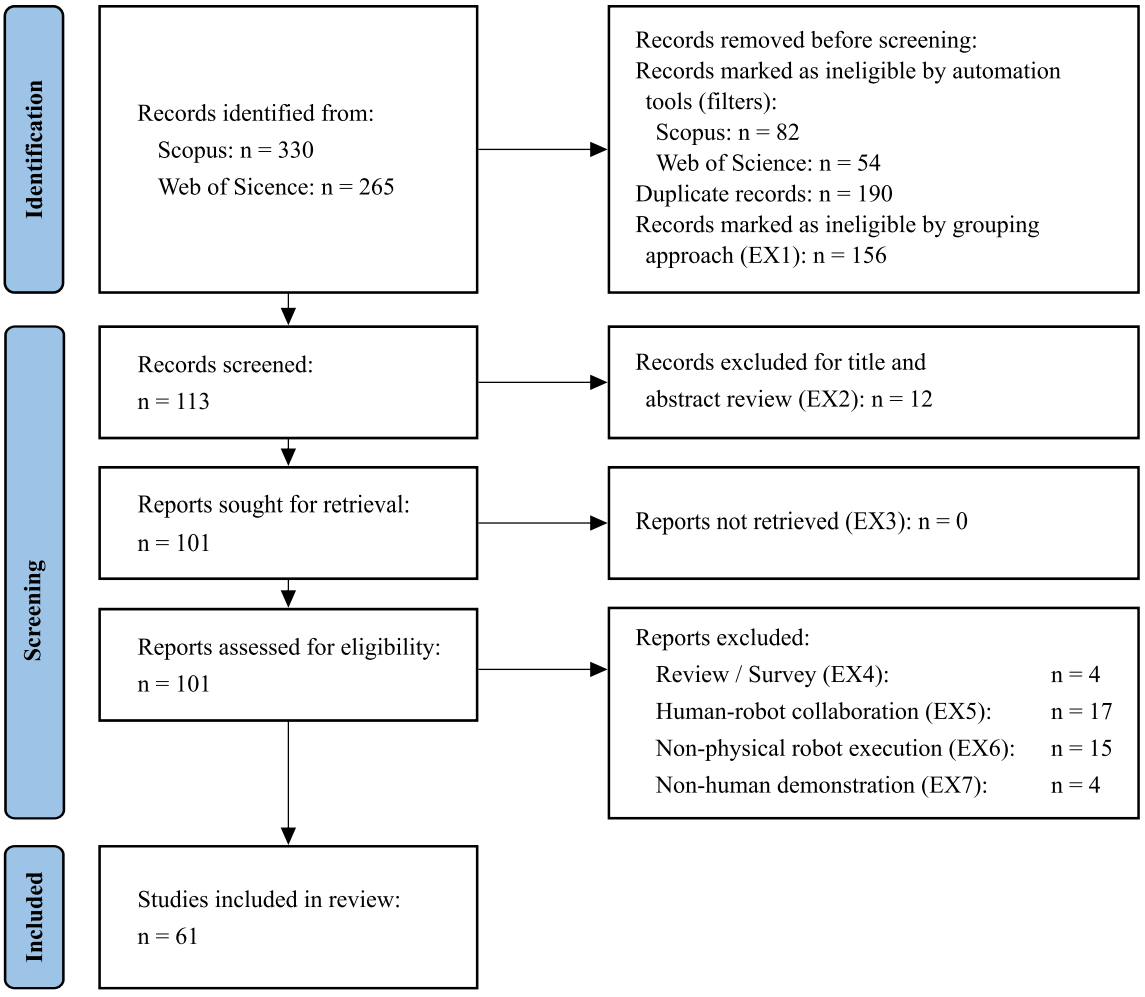

FIGURE 2.1: PRISMA 2020 flow diagram [1]

2019 are attributable to only two included versus two excluded records. The remaining outliers for 2018 and 2020 are based on two out of seven excluded records. Hence, the COVID-19 pandemic did not have an exclusive impact on the results of the conducted systematic review of the literature. Regarding the deliberate omission of physical experiments, it is assumed that the impactful fundamental theoretical achievements without physical evaluation are covered by reviews and surveys that emphasise LfD methodologies [24]. Finally, the chosen citation requirement might have excluded valuable studies. However, to the best knowledge of the author, the systematic literature review reflects comprehensively current trends and procedures in academic research on LfD for assembly-related tasks.

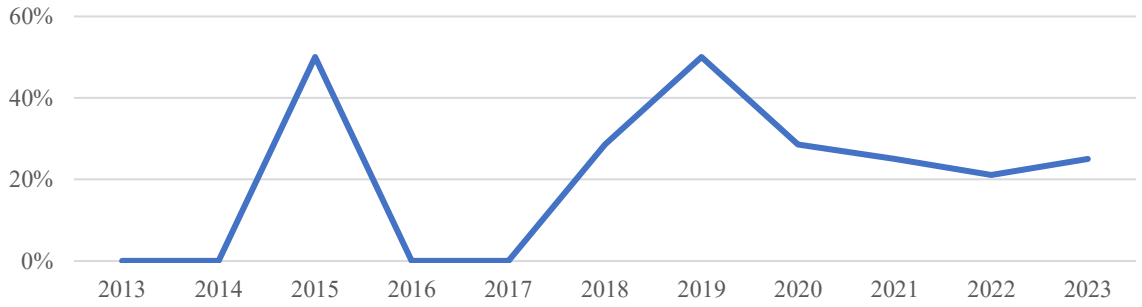

FIGURE 2.2: Chronological percentage of excluded studies based on non-human demonstration (EX6) or non-physical robotic reproduction (EX7)

2.2 Findings

This section summarises the analytical findings acquired by reviewing the studies identified using the systematic approach of Section 2.1. The following provides a statistical analysis of the methods utilised during the demonstration and learning phases, investigated use cases, performed assembly skills, including a qualitative analysis of the main research trends, achieved generalisability capabilities, and reported performances.

2.2.1 Demonstration and Learning Methods

Figure 2.3a illustrates the resulting statistical comparison of the methods applied for human demonstration. As can be seen, kinaesthetic teaching and passive observation prevail with 41% and 30% as preferred methods for teaching assembly-related tasks. Teleoperation was exclusively selected only in 13 out of 56 cases. Five studies provided two demonstration methods, either for initial skill acquisition and testing [32, 33], consecutive skill correction [34], or teaching distinctive task aspects [35]. Abu-Dakka et al. [36] used teleoperation and kinaesthetic teaching to meet the requirements of different robotic platforms. In general, passive observation was achieved in various ways. The most common approach is to use camera streams or images of the recorded human demonstration (see, e.g., [37]). However, other studies used customised demonstration tools [38], sensor-augmented objects [39], mock-up objects with distinctive properties (e.g., a lighter object than what the robot handles [40]), or tangible instruction 'blocks' [41]. Similarly, teleoperation was achieved through the robot's teach pendant [42], commercial tools [43], or by mimicking the human manipulation path with identical objects in real time [33].

In addition to the demonstration method, the number of demonstrations required is considered an important indicator of applicability. Within the 61 analysed studies, a tendency is

noticeable towards requiring two to ten demonstrations, which was considered in 26 cases. On the contrary, 15 studies built on a single demonstration and eight experimental evaluations required more than ten instructions. The remaining 12 studies have not quantified (using phrases such as 'multiple', 'set', 'few', or 'several') or have not specified the required number of demonstrations at all.

As can be seen in Figure 2.3, learning methods based on trajectory policies as learning outcomes prevail in assembly-related LfD research, endorsed by 35 of the 61 studies that used it as their selected approach. The second most prominent method is the representation of tasks in the form of plans based on primitive sequences reported in 23.0% of the studies. The least reported category of applied learning methods is based on cost/reward-driven outcomes with a joint share of 13.1%. Among the most prominent techniques are the so-called Dynamic Movement Primitives (DMPs) and Reinforcement Learning (RL). These techniques were explored in a total of 19 and 14 studies, respectively, and applied independently and in combination with other techniques. Furthermore, the analysis of learning methods in terms of preferred demonstration methods shows that 54.3% of the studies used kinaesthetic teaching when targeting trajectory policy outcomes, while 64.3% preferred passive observation for outcomes in the form of primitive sequences (see Appendix A.1 and A.2).

2.2.2 Use Cases

In the context of application scenarios, the experimental reports are analysed regarding their practicability for real-world scenarios and to which extent research approaches respond to actual assembly scenarios in the industrial sector. Therefore, three categories of practicability are defined. Studies that evaluate their LfD approach in a practical industrial use case that assembles realistic objects are classified as *practical*. The second level of practicability considers the handling of *related* objects. This includes objects that are only handled in a subsidiary manner in the industry, objects interesting for specific industry sectors but not practically applied, or benchmark models mimicking industrial challenges. All experiments using objects that do not meet the above categories are considered *unrelated*.

The collection of identified studies features six practical assembly scenarios with realistic objects that mainly target the electronics industry (see Figure 2.4). Hu et al. [44, 45] investigated the Printed Circuit Board (PCB) assembly on the bottom case of a cursor mouse, which required fitting two locating pins and three resilient fasteners (see Figure 2.4a).

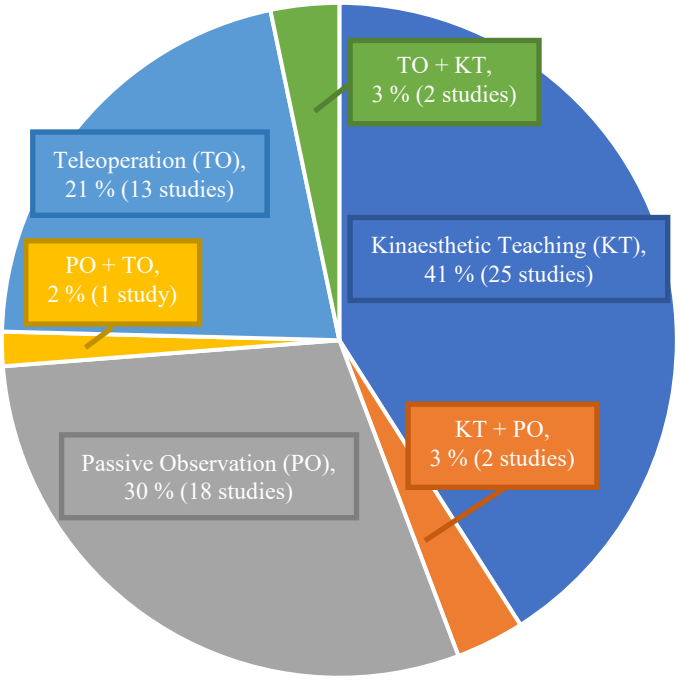

(A) Demonstration methods (five studies used a combination of two demonstration methods)

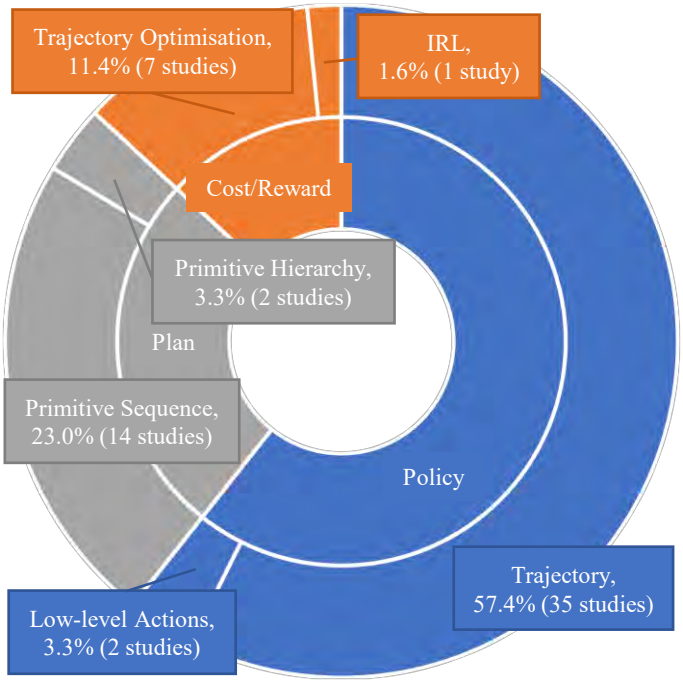

(B) Learning methods based on the learning outcome

FIGURE 2.3: Classification of applied demonstration and learning methods

Similarly, Haage et al. [46] investigated the PCB assembly based on passive visual observation. Yan Wang et al. [47, 48] carried out experiments on a circuit breaker condenser

assembly task (see Figure 2.4c) that required an L-shaped insertion motion. More complex task sequences in an industrial scenario were emphasised by Ji et al. [32], who evaluated the proposed LfD solution in the assembly of power breakers and set-top boxes (see Figure 2.4d). Precision insertion and gluing capabilities for joining micro sleeve-cavities and coil-cylinders with $10\mu m$ clearance fit were explored by Qin et al. [49]. Finally, Yue Wang et al. [50] investigated the assembly of a switch through passive observation, including placing, screwing and pushing motions.

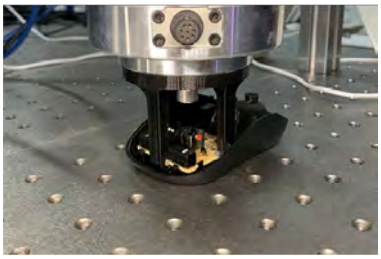

(A) PCB assembly of cursor mouse [44, 45]

(B) PCB assembly [46]

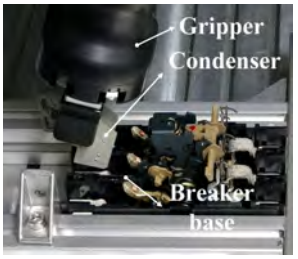

(C) condenser assembly [47, 48]

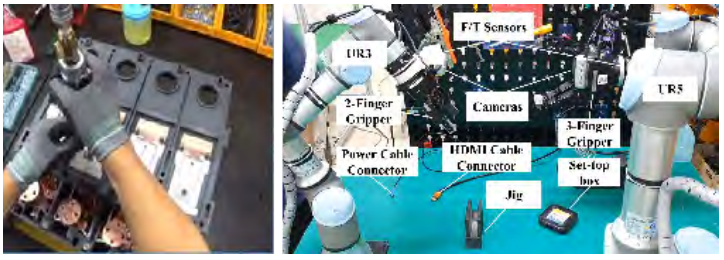

(D) power breaker (left) and set-top box (right) assembly [32]

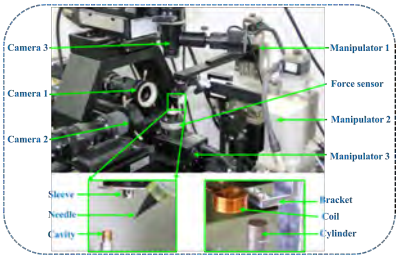

(E) sleeve-cavity and coil-cylinder assembly [49]

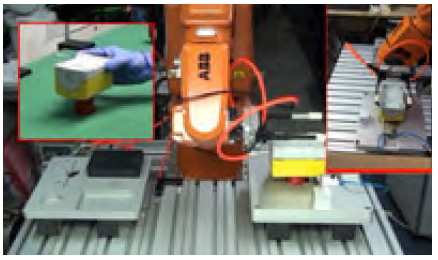

(F) switch assembly [50]

FIGURE 2.4: Practical use cases

Related use cases do not represent a direct practical application, but offer experimental evaluation with objects that are realistically transferable to industrial environments (see Figure 2.5). A prominent example is the standardised connector plug-in, including RJ-45 connectors, USB sticks, power plugs, and HDMI connectors (see Figures 2.5a to 2.5c). Specific industries, including the medical, construction and microscale assembly sectors, were targeted by [51–53]. The experiments demonstrated the ability to sew personalised stent

grafts whose dimensions were provided by current stent graft manufacturers, construct timber structures and perform precision peg insertion tasks (see Figures 2.5d to 2.5f). Some researchers chose benchmark models for assembly-associated tasks to evaluate their proposed method (see Figures 2.5g and 2.5h). These include the U.S. National Institute of Standards and Technology assembly board #3 [54] and the Cranfield benchmark model [55]. The latter has been used primarily for peg insertion capabilities [33, 36, 56]. The remaining 45 studies have used industry-unrelated objects. These include arbitrary toy parts or generic machined and 3D-printed components.

(A) RJ-45 connector [43]

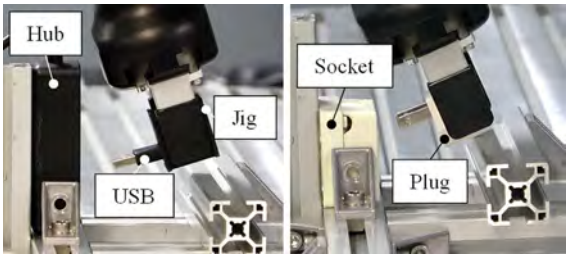

(B) USB stick and power plug [57]

(C) HDMI connector [47, 48]

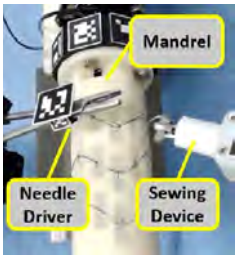

(D) personalised stent grafts [51]

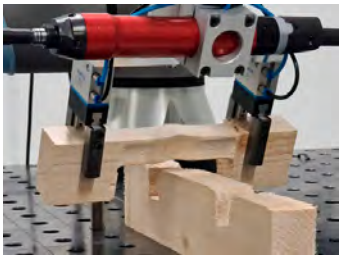

(E) timber structure assembly [52]

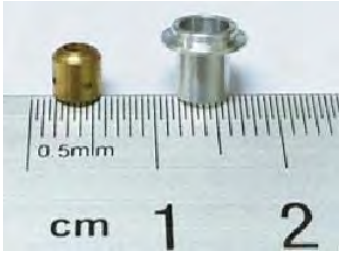

(F) micro-scale peg insertion [53]

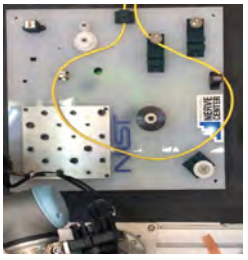

(G) NIST assembly board #3 [58]

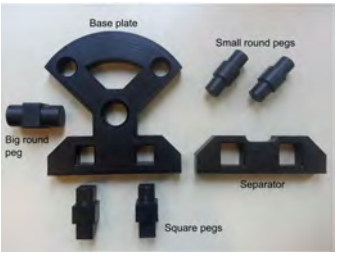

(H) Cranfield benchmark [36]

FIGURE 2.5: Related use cases

In terms of industrial relevance, some efforts are worth mentioning owing to their outstanding experimental setups. As illustrated in Figure 2.6a, Kramberger et al. [52] proposed a LfD platform in which the so-called teaching and execution cells were separated, leading to increased execution space and improved productivity. Huang et al. [51] extended the reachability of two surrounding robotic serial arms through an actuated assembly base,

allowing sewing motions on all sides of the object (see Figure 2.6b). Challenged by microscale assembly, Ma et al. [53] emphasised LfD precision capabilities and built a set-up incorporating a three translational Degrees of Freedom (DoF) manipulator achieving a resolution of $1\mu m$. Furthermore, the three rotational DoF platform was equipped with a force torque sensor that reaches a force resolution of approximately $\frac{1}{128}N$ and two microscopic cameras with zoom lenses surround the workspace to precisely measure the poses of the components. A similar system was proposed by Qin et al. [49].

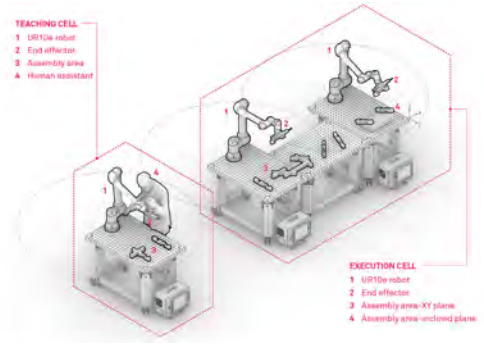

(A) teaching and execution cell separation [52]

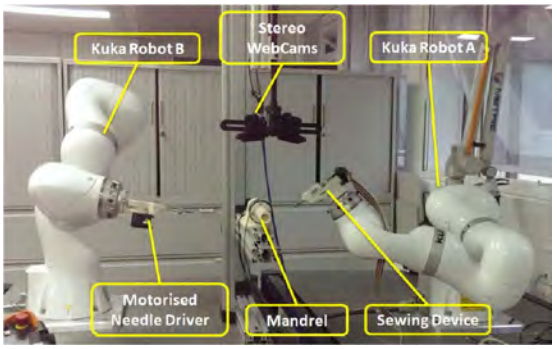

(B) extended reachability through rotating objects [51]

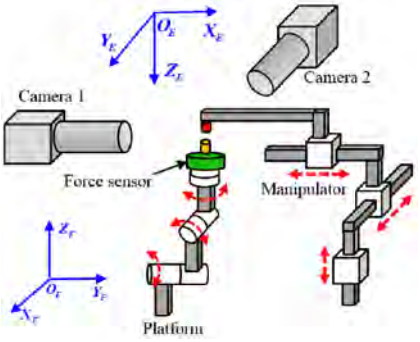

(C) micro-scale precision assembly [53]

FIGURE 2.6: Outstanding experimental setups

2.2.3 Assembly Skills

In a general sense, the assembly process can be described by superimposed steps of mating and joining parts. Nof et al. [23] refer to mating skills as all those motions that bring two (or more) parts into contact or align with each other. In turn, joining skills are responsible for the final fastening of parts to hold them together. Both are usually necessary to perform the assembly successfully and ensure the designated function of the final product for its expected lifetime.

As pursued in the applied search strategy (see Section 2.1.1), various forms of mating and joining skills are considered associated with assembly-related skills. The 61 analysed studies provide experimental evaluations on 11 distinct assembly skills with a total of 77 references. These include *peg insertion*, *pick-and-place*, *stacking*, and *bin picking/sorting* as instances of mating skills, as well as the joining skills of *screwing*, *bolting*, *gluing*, *wiring*, *hammering*, *interlocking*, and *sewing*. Compared to the applied search strategy, no evidence has been reported in the studies on the remaining considered joining skills, including *jamming*, *riveting*, *fastening*, *welding*, *retaining*, *press fitting*, *snap fitting* and *crimping*.

Figure 2.7 illustrates the statistical distribution of the experimental evidence on the assembly skills investigated and shows the allocation to the level of practicalability discussed in Section 2.2.2. As can be seen, the skill of *peg insertion* attains exceptional dominance in academic research. In general, 46.8% of all experimental references conducted this specific mating skill, followed by general *pick-and-place* skills, covering 23.4% of all reported evaluations. *Stacking* and *bin picking/sorting* were considered in 7 and 3 experiments, respectively. Joining capabilities are significantly less explored, with only 16.9% of the 77 assembled skills discovered. There is a slight preference for *screwing* skills. In terms of practicability, all assembly skills were primarily explored using unrelated use cases.

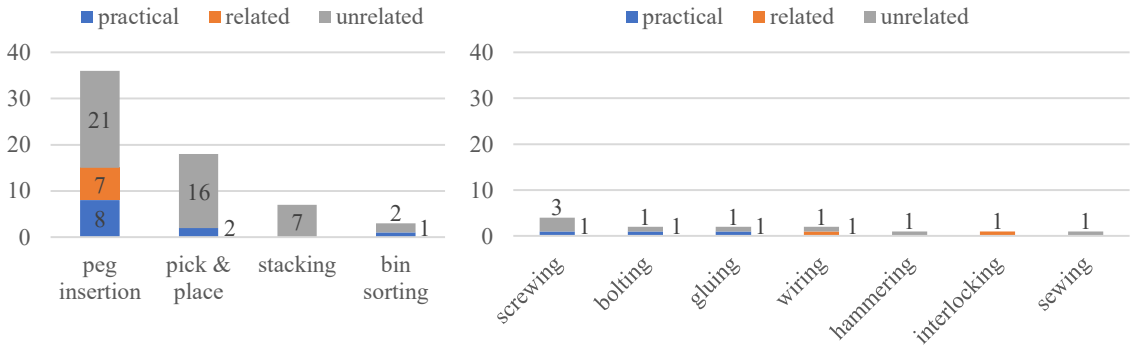

(A) mating skills (B) joining skills

FIGURE 2.7: Classification of assembly scenario according to investigated assembly skills and their practicability level

The following provide further qualitative insights, with an emphasis on targeted challenges, methodological approaches, and achievements.

2.2.3.1 Mating

The most examined mating skill in the reviewed studies is the insertion of an object or part of an object, in this context, colloquially called a 'peg', into its dedicated hole. Although seemingly simple in nature, the challenge of peg insertion lies particularly in the high-precision requirements often demanded due to tight clearances between the objects. It is considered one of the most essential skills required to be solved for automated assembly [56, 59, 60]. Equally necessary and, in fact, inevitable for the completion of the mating operation, the skill of picking up an object from one location and placing it elsewhere is arguably the most widely used skill in general robot manipulation tasks. Although often requiring less strict tolerances to be maintained, pick-and-place operations are challenged by the complexity of grasping different objects safely and performing large motions without colliding with surrounding obstacles. *Stacking*, *bin picking*, and *sorting* are considered special cases of pick-and-place skills with additional requirements for the positioning of the object with respect to others.

In the context of bringing two parts into contact and achieving their alignment while in contact, peg insertion is mainly challenged by task uncertainties. These occur due to variable grasps of the peg, inprecise locations of the hole, and unmodeled manufacturing defects of the involved components [61]. To encounter such slight deviations from the assumed poses, several studies investigated the use of compliant controllers, including variations of admittance [33, 49, 56, 62] and impedance [36, 42, 63–65] control methods that allow an adjustment of the robot motion based on measured contact forces. Although some experiments relied on learning from a single demonstration, for example [56], trajectory-based methods show a decrease in the success rate when the spatial parameters of the execution deviate significantly from the demonstration poses [60]. Therefore, others proposed the consideration of multiple demonstrations to create generalised [64] or prescribed [42] force profiles that cover a wider spectrum of potential conditions. Furthermore, Wang et al. [47, 48] developed a compliant control policy based on RL in combination with a nominal motion trajectory through a hierarchical imitation learning framework, while [63] investigated the applicability of the recently developed generative adversarial imitation learning approach to high-precision peg insertion. The idea of compliant controllers was furthermore evaluated in robot systems with reduced capabilities, including industrial robots with non-backdrivable mechanisms and strict tolerance requirements [66], position-controlled industrial robots [67], or even without a force sensor using ergodic exploration [61]. Beyond the dominant case of single-peg insertion, several achieved multi-peg insertion by reacting on force measurements [53, 62, 68].

In contrast to tackling task uncertainties with compliant controllers, some studies investigated strategic approaches to carry out the peg insertion successfully. Wan et al. [40] suggested the calculation of an optimal path by mathematically reducing the demonstrated motion to the alignment of the axis. Ti et al. [39] defined an intermediate three-point contact state with a representation of the assembly angle for round peg insertion tasks. Abu-Dakka et al. [56] proposed an exception strategy for systematic hole search by initially starting with deterministic translational variation followed by a stochastic search with random increments. In case of misalignment or external disturbance, Stepputtis et al. [62] combined a phase estimator with an admittance controller to enable the robot to correct or even reverse the progress of the task. Taking into account the differentiation of errors parallel and perpendicular to the assembly surface, Ahn et al. [69] developed two separate trajectory generators to respond to the alignment and insertion processes.

A common approach to tackling motions beyond contact-rich skills is the development of appropriate subskills or subgoals that are separately learnt and joined afterwards to achieve the expected assembly outcome. The distinction between different assembly operations motivated the definition of distinguished image-featured guided and force-constrained motions [49] or approaching and assembling motions [45]. The latter was created based on the idea that within the industrial field, the generalisation ability to environmental constraints is of more importance during the approaching phase, while object constraints matter during the assembly phase. Sefidgar et al. [41] developed a tangible programming technique with predefined objects to indicate subskills that translate into a sequence of robot functions, including instances of pick-up-from-top, pick-up-from-side, place-at, and drop. In contrast to this deterministic approach, Wang et al. [50] proposed an automatic programming method for robotic assembly that estimates the present assembly skill and the parts involved in a recorded video segment. This framework distinguished between the predefined skills of placing, screwing, taking, pushing, and labelling. In the context of stacking capabilities, Kang et al. [70] defined reaching, picking, carrying, and placing as base skills and argued that the skills connecting those are challenging to obtain via demonstrations due to their arbitrary nature. Therefore, the proposed base skills were acquired using expert demonstrations, while the bridge skills were trained through RL. Pinosky et al. [71] proposed a similar idea, where actions were artificially synthesised when the policy was uncertain, i.e. regions where expert demonstration was lacking. A more abstract approach was pursued by Liu et al. [72], who modelled manipulation tasks as a series of what-where-how elements, reducing the attention to the selected object and action for improved adaptability. Finally, Savarimuthu et al. [33] created a sophisticated three-level architecture that extends the adaptation of sensorimotor skills [36] with keyframe-based

semantic and pre- and postconditioned planning levels. Additional techniques for self-learning and human interaction were incorporated to facilitate efficient decision-making.

An alternative stream of research efforts investigated the automatic extraction of the required action sequence based on determined keyframes [46, 73], goal images [74, 75], positions of interest [38], and key hand points [76]. Duque et al. [37] investigated the applicability of Petri nets to automatically generate work plans according to the available objects within the workspace and to generalise to new scenarios. To capture the complexity and possible transitions when performing multistep assembly tasks, Chen et al. [77] developed a universal functional object-orientated network that optimised the assembly sequence from multiple demonstrations. Similarly, Guo et al. [78] proposed a framework evaluated on an inspection and bin-sorting task that established coordination schemes to select the correct sequence of skill primitives, ensuring an appropriate grasp orientation. Wu et al. [75] achieved zero-shot generalisation to unseen tasks through a novel method of rearrangement of image data, while Eiband et al. [79] specialised in an automated segmentation method of trajectory data into logical and classified skills. These were implemented using symbolic pre-/post-conditional recognition and data-driven sliding windows, respectively.

Motivated by the idea of minimal demonstration input, Berscheid et al. [74] proposed a method that learns from goal state images allowing them to succeed in generic pick-and-place and peg insertion tasks with $1mm$ tolerance. Evaluating comprehensively practical assembly tasks that incorporate peg insertion, (bin-) picking, and placing skills, Ji et al. [32] used similarly passive observation to reduce human effort to automate robotic assembly. Based on the extracted assembly sequence, state transitions, grasping modes and involved objects, the proposed framework automatically generates a robot assembly script considering the different embodiments by utilising pre-trained robot skills, self-exploration, self-reproduction, and self-improvement capabilities. Such self-driven learning after the initial human demonstration is common practice for LfD methods based on RL techniques. While defining distinctive primitive skill libraries for the hole search and peg insertion, Cho et al. [59] used RL to optimise the generated motion based on previously experienced or newly defined skill instances. Davchev et al. [43] applied model-free RL to learn a residual correction policy. The RL-based controller by Wang et al. [57] is capable of learning the control policies of a specific class of complex contact-rich insertion tasks based on the trajectory profile of a single instance that enables generalisation to similar objects. Considering the cost and burden on the human operator of each demonstration, Ma et al. [53] artificially increased the number of demonstrations, reducing the required number

to one third for the consecutive RL-based self-learning assembly phase. Although studies highlighting the above capabilities assume the existence of perfect demonstrations, Pervez et al. [80] explored the situation in which the operator may not provide multiple complete demonstrations. The developed stochastic model allows the execution of the given task based on one full demonstration and multiple incomplete/inconsistent attempts.

In addition to the fundamental concepts above for generic pick-and-place-related skills, several studies target specific capabilities that promise valuable contributions to the robustness of LfD approaches in practical environments. Of particular interest is the secured performance in dynamic situations. Ghalamzan et al. [81] emphasised the dynamic work environment in which the robot was capable of avoiding collisions with moving obstacles. Motivated by reducing the execution time, Meszaros et al. [34] investigated an interactive correction method to iteratively speed up the non-zero-velocity picking skills of objects. Wang et al. [82] optimised an LfD technique to eliminate errors from human demonstrations by smoothing reproduced motions into appropriate segments. To improve the robustness of the robot's performance, Iovino et al. [83] introduced additional verbal interaction to clarify potential disambiguation in the scene, e.g., when identical objects are present in the workspace, and Wu et al. [84] developed a method that enabled the robot to quantify its learning progress and guide the user to efficient demonstrations. Incorporating external forces, Zhang et al. [85] proposed a method that reduced the impact of external disturbances, which was demonstrated by the example of task completion despite physical interaction with the robot arm. Alternatively, Ugur et al. [86] suggested the use of external forces in uncertain situations to manually adjust the ongoing movement by physical interaction with the robot.

2.2.3.2 Joining

As indicated in Figure 2.7, *screwing* was the most investigated joining skill in the reviewed studies with four experimental evaluations. Ji et al. [32] and Wang et al. [50] developed comprehensive assembly systems, both using passive observation with consecutive assembly skill estimation, part recognition, and robot embodiment strategies, capable of performing distinctive assembly skills, including *bolting* and *screwing*, respectively. Experimental evaluations provide limited information on their performance, in addition to mentioning failed attempts [50] and identified issues attributed to insertion tolerances [32]. Using toy components, Gu et al. [35] evaluated an assembly sequence including *bolting*, *hammering*, and *screwing* skills through passive observation of human performance. To reach the state of the finished *screw* assembly, eight turns were required. The repetitive

turning characteristic was tackled by two identical markers on the screw that allowed 180-degree rotations to be performed in either configuration. In this setup, *screwing* was identified as the most challenging skill due to complex motion in addition to small screw slots, while *hammering* was considered the simplest task due to the simplicity of the movement and the accuracy of the loose strike. Putting emphasis on unstructured demonstrations, Niekum et al. [87] proposed a method for automatic skill segmentation and interactive human intervention. In terms of the assembly of table legs with protruding screws, the system performed the *screwing* task after interactive correction using recovery behaviour for difficult grasping angles or distant leg locations. Based on a skill library that includes *screwing* (clockwise + anticlockwise) and stacking, Yu et al. [88] proposed an RL-centred method that maps new scenarios to a sequence of a few library instances. The evaluation was carried out using a simplified task design with loose clearances and no contact with the environment, limiting the practicability evaluation of the method for realistic *screwing* tasks.

Motivated by precision assembly challenges, Qin et al. [49] demonstrated *gluing* capabilities on a sleeve-cylinder assembly task after insertion using a predefined force-constrained motion action class. As described in Section 3.2.2, (Eiband et al., 2023) focused on the automatic segmentation of the demonstration data where the gluing motion was abstracted to a sliding skill with slight pressure against the surface. The experimental gluing motion was performed under loose spatial or task-related requirements.

In the case of *wiring*, it requires handling and routing of deformable wires. Keipour et al. [58] developed a spatial representation graph that enables wire rerouting, considered a pick-and-place task, towards a goal configuration. Emphasising the enhancement of kinaesthetic teaching through online impedance shaping, Meattini et al. [89] evaluated its method on a wiring task consisting of the pick-up of a cable's extremity and inserting it into a connector. The execution behaviour was furthermore altered at run-time through physical interaction to perform a rerouting of the cable.

Although *sewing* represents a highly repetitive task and is considered the most challenging skill in the manufacture of personalised stent grafts, Huang et al. [51] developed a robotic system capable of extending a single demonstrated stitch cycle to the whole stitching task through design specifications, rigid transformations, and an actuated mandrel. Kramberger et al. [52] investigated a robotic interlocking method that enables timber-timber joinery without the need for additional steel fasteners through the optimal structural truss design and a particular rotational insertion strategy.

2.2.4 Generalisability

The capability of generalising and expanding to unseen scenarios is one of the key aspects distinguishing LfD concepts from intuitive programming techniques and promises to enable robotic systems to deal with dynamic environments and product variations in industrial settings. In the context of assembly-related application scenarios, six major generalisation capabilities were identified, which have been explored in the reviewed studies. These include the ability to reproduce the task under distinct spatial or temporal requirements (execution scaled to demonstration), cope with task uncertainties, adjust the path or skill sequence, and execute the task with objects similar but not equal to the one used for demonstration (transferability). Note that the following quantification only reflects capabilities that have been evaluated in physical experiments and does not necessarily show all capabilities of the underlying learning method.

With 46 reported evaluations, spatial scaling is the most common generalisation capability explored in LfD methods, incorporating distinguished start and goal poses for trajectories and object positions. While assuming that the robot knows the theoretical location of the objects, the existence of task uncertainties has mainly driven the field of LfD methods applied to peg insertion tasks. 18 experimental reports have contributed to counteracting measures. Commonly addressed with RL-techniques, path optimisation was mentioned in eight applications to improve robot execution, while graph-based sequence optimisation was only explored twice in experimental reports [77, 78]. Although an equally intrinsic feature as spatial scaling of LfD learning methods, temporal scaling capabilities are often neglected, reaching two mentions in the reviewed studies [43, 90].

Generalising over similar objects has mainly emerged as an investigated capability in most recent studies. Experimental contributions examined similar objects with distinguished properties [40, 53], objects of the same task class but distinguished shapes [43, 57, 59, 69] or entirely unknown objects [34, 74]. Depending on the learning method, the LfD approach may not necessarily require any generalisation process [59, 69], only a few update steps [43] or interactive adaptation [34]. In general, adapting existing knowledge to slightly distinguished situations/objects is promoted with less required effort than demonstrating the task from scratch.

2.2.5 Performance Evaluation

To provide a valid experimental evaluation of a proposed method, different performance metrics were used in the reviewed studies. These include, in particular, the reporting of the success of a task or its success rate over several attempts, accuracy analyses, effectiveness compared to competing approaches, and achievable efficiency. Although all studies present at least one successful physical execution, a total of 41 studies report achieved success rates over at least three attempts (seven have not specified the number of attempts used to determine the success rate). The success rate reported on the number of attempts is visualised in Figure 2.8 using the classification of mating and joining skills. As can be seen, mating skills tend to be evaluated using more attempts and generally achieve higher success rates.

In the special case of peg insertion, success was often challenged by tight tolerances that are required to overcome. In total, 26 peg insertion skills with specified tolerances were assessed (ten did not provide specifications). In general, tolerances between $0.006mm$ [63] and $6mm$ [67] with an average of $0.708mm$ were considered. Furthermore, some studies chose specifications according to the ISO 286 standard [65, 66], interference or clearance fit [49, 53] or a hole chamfer of $1mm$ [66]. Further accuracy analyses with respect to other skill classes reflect the analysis of trajectory deviations from the demonstrated motion [76, 91] as well as the final pose errors in tasks such as pose alignment [49, 91] or placement [74].

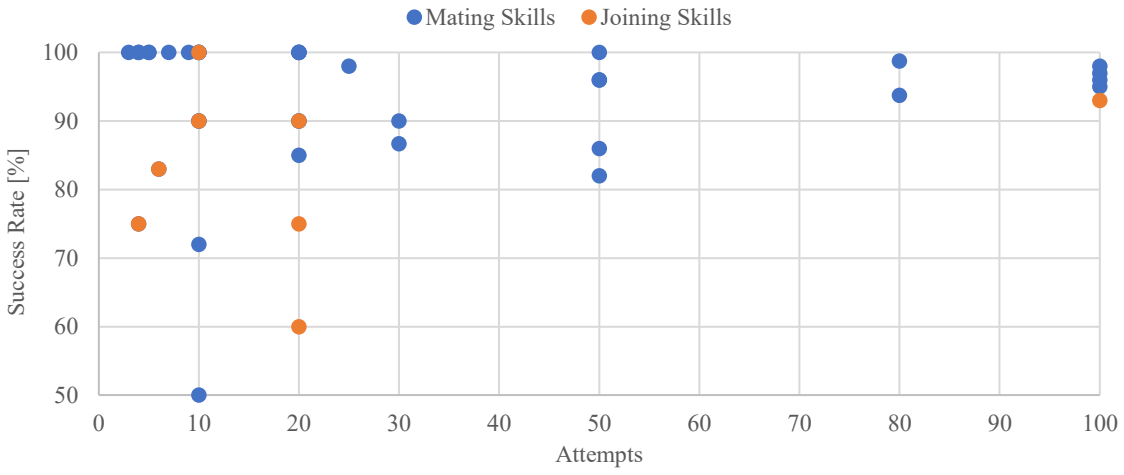

FIGURE 2.8: Reported success rates over attempts distinguished between mating and joining skills

Based on a deep background in LfD research, evidence of the effectiveness of the proposed method compared to competitive approaches is a common evaluation practice. This can be the ground truth for automated recognition [35, 79], comparable techniques [64, 72, 84], the baseline method when extended [43, 68], or the comparison to other representative LfD approaches [67, 69].

In addition, some studies reported performance assessments towards procedure efficiency. In addition to reports on a reduced number of required execution steps [57] or sequenced actions [77], several researchers provide evidence of an improved execution speed [34, 36, 43, 59, 64]. Through interactive correction techniques, Meszaros et al. [34] extend efficiency evaluation to training time, reporting a four-fold faster approach compared to the initial demonstration method. Similar demonstration-time reduction efforts were promoted by [57, 72]. Wang et al. [47] used simulation before training to reduce the time required on the real robot. As reducing computing time is equally important for improved efficiency, Wang et al. [82] optimised the underlying learning technique and Keipour et al. [58] developed a routing method efficient enough to run online. On the other hand, Xu et al. [92] raised performance concerns regarding the proposed RL-centred method when confronted with more complicated tasks. Specifically targeting 3C product assembly operations with optical motion capture, Hu et al. [44] proposed a performance evaluation protocol including performance indicators for static and trajectory evaluations.

2.3 Comparison to Industrial Practice

In addition to the technical competence proposed by LfD solutions, the integration of the new technology into existing processes is considered an equally important factor in analysing its applicability to industrial practice. In this context, mimicking the capabilities of human operators to learn and execute new tasks is assumed beneficial to promote the acceptance of LfD technology in the traditional assembly industry [24].

Traditional industrial assembly is based on well-established and historically preserved methodologies for instructing human operators that have proven great effectiveness. In traditional manual industrial assembly, instruction refers to the systematic learning of knowledge and skills to perform a task that operators are expected to perform in a production environment, but have not previously fully known or mastered [93]. Instruction concepts are a measure of operator qualification and human resource development, and the theoretical concepts are correspondingly diverse. A primary distinction can be made

between training on the job, along the job, near the job, and off the job [94]. According to Schelten et al. [95], instruction procedures can be further differentiated depending on the learning domain (sensorimotor, sensorimotor and cognitive, cognitive) and the degree of participation (instructor emphasised, instructor and learner involved, learner emphasised).

As described in Section 2.2, research efforts towards LfD solutions for assembly-related applications emphasise on-the-job instructions for sensorimotor capabilities. This promotes the comparison of state-of-the-art LfD trends with the so-called four-step method, an industrially relevant and well-established method. It is based on the principles of the Training within Industry (TWI) approach, which was developed in the USA during the Second World War [96] and has been considered in Germany since the 1950s as the 'REFA-Vierstufenmethode' for work instruction [97, 98]. It focusses on repetitive, relatively short-cycled and simplistic tasks that must be performed repetitively according to a standardised sequence, allowing a certain degree of transferability to automated practice [98]. The subsequent discussion highlights identified synergies and discrepancies between the four-step method and LfD trends.

Preparation

In the first phase of the four-step method, the learning location is prepared for the instruction, and a suitable learning objective is defined based on the learner's existing knowledge. Attention must be paid to the interpersonal factors that enable the instructor to arouse the interest and motivation of the learner.

The reviewed LfD approaches show, in principle, transferable competencies to deal with workplace requirements, including varying settings and dynamic environments. Therefore, the preparation of the learning location is considered comparable. However, effective interaction with the robotic system relies on the instructor's active involvement with the programming method, understanding the system's capabilities, limitations, and expected performance. This changes the necessary recognition of interpersonal factors to the instructor's interest and motivation, which must be aroused by a suitable design of the robotic system. The emerging interest in advanced generalisability, that is, the transfer of knowledge and skills to similar objects and situations, is an essential prerequisite to imitating the prior knowledge repertoire of humans.

Demonstration and Explanation

This step requires a high level of performance from the instructor and involves the physical demonstration of the task. The instructor performs the task while explaining the reasoning and important details verbally. These help the learner to improve their understanding of the assembly task and achieve high quality during self-performance.

The active demonstration of the task corresponds to the first phase of the characteristic LfD procedure (see Figure 1.1). The applied demonstration method determines the required level of participation of the robotic system. Using passive observation techniques provides a method comparable to conventional human instruction with no involvement of the physical robot. Furthermore, the four-step method promotes simultaneous physical demonstration and verbal explanation. In contrary, most research efforts rely on a single predefined channel (see Figure 2.3a) that limits the instructor's communication abilities. An additional distinction emerges from the ability to fully understand the task, as most LfD approaches target the acquisition of sensorimotor skills. Only few investigations provide ideas on communicating the robot's understanding to the instructor, immediately or subsequently, to increase the instructor's confidence in the perceived demonstration.

Execution and Explanation

After passively observing the instructor's demonstration of the task, this step involves mimicking the task by the learner and justifying the key aspects in the learner's own words. The instructor observes and intervenes when necessary. An important aspect is to ensure that learning objectives are met and understood.

Incorporating the transition of the robotic system from a passive observer to an active executor corresponds to the second phase of the characteristic LfD procedure (see Figure 1.1. Synergies are identified, in particular, regarding the performance of the task on the basis of the robot's own understanding and skills. Several studies have also presented ways of communication between the robot and the instructing human operator during execution to reason the actions performed, communicate the learning progress, or visualise the task understanding. This often involves the creation of collaborative situations with intentional interaction that allows the human operator to intervene and improve the understanding of the task until the learning objective is met.

Practice

The last step of the four-step method has the purpose of providing the opportunity for the learner to practice the new skill and apply the acquired knowledge. This step is important for solidifying learning, building confidence, and becoming more efficient. The goal is to achieve a defined performance under the premise of error-free assembly.

The learning behaviour of humans can generally be illustrated by learning curves [93, 99]. These show the learning progress, i.e. the time required per execution, as a function of the number of repetitions. During the process of understanding the required contexts and actions, the curve drops at first. The learning effect then decreases steadily with an increasing number of repetitions until a routine of working is finally developed, and the assembly process is increasingly internalised. The description of the functional relationship of the learning curve is based on the task to be performed, as well as a variety of factors that depend on the learner [100].

Promoting the teacher-independent task performance, this step aligns with final phase of the characteristic LfD procedure in which the robot reproduces the task with minimal human intervention (see Section 1.1). In light of the usually targeted challenges in LfD approaches, this phase consolidates on the robot's capability to provide generalisability and meet certain performance criteria. As outlined in Section 2.2.5, the performance is often quantified by the success rate performing the same task repeatedly. The generalisability capabilities enable the robot to cope with changes in task, motion and environment.

Compared to the practise required in conventional settings, most LfD approaches provide the ability to start at a higher performance level from the beginning. However, due to the strongly narrow cognitive abilities and hardware limitations, most of the proposed LfD solutions have rather flat learning curves. The ability to improve their own performance in a self-controlled manner can be observed in ML-based solutions, which has been applied for this purpose in various studies, and can be named a key enabler. In the reviewed literature, no prediction of expected efficiency has been discussed.

2.4 Identified Obstacles

Although several synergies with the four-step method have been identified that promote reasonable potential, some fundamental aspects are lagging behind in creating a smooth integration of LfD solutions into industrial practices. Based on the findings above, the

following provides an educated summary of identified obstacles in LfD research to drive its progression toward meaningful deployment. These include aspects regarding practicability, task complexity and diversity, generalisability, performance evaluation, and integration concepts.

Practicability

The practical evaluation of promising solutions that have emerged from research marks a pivotal moment in gauging their potential interest for industrial sectors. Demonstrating significant advantages, along with robustness to withstand industrial conditions, instils a willingness to invest in the proposed technologies.

Academic advances in the field of LfD over the course of the last decades exhibit a robust level of maturity within the research landscape. State-of-the-art studies successfully demonstrate the features of popular techniques and expand their interest in niche challenges. However, the analysis of practicability reveals that only very few studies have presented the application of the proposed LfD methods in practical or related task designs, resulting in a severe limitation in evaluations using mainly unrelated tasks and objects. This is particularly evident in methodologies based on ML techniques. The consecutive transition to realistic scenarios is presumed to work smoothly.

Moreover, the identified practical and related application scenarios can be characterised as tasks which are predisposed for automation. Exploring the potential expansion of a robot's functionalities into tasks that currently fall outside the scope of automation, particularly those involving assembly situations primarily carried out by human operators, remains an area that requires more comprehensive exploration. While practical LfD solutions for the currently emphasised capabilities continue to proliferate and promise valuable influence in the assembly industry, extension to tasks carried out predominantly manually can have an exceptional impact on industrial practice.

Task Complexity and Diversity

The advantage of LfD-equipped robotic systems, as opposed to specialised machinery designed for defined assembly operations, lies in their improved user experience and increased applicability. The latter requires a high degree of adaptability to different complexities and varieties of tasks, which must be anchored in the applied LfD solution.

Contrary to this industrial requirement, the literature review discloses that the developed solutions predominantly focus on individual assembly skills with a strong bias toward peg insertion. While the latter covers a certain portion of industrially performed tasks, there exists a significant shortcoming in the development of LfD methods that address other skills, particularly joining skills, which are necessary for the completion of many assembly tasks.

Studies investigating pick-and-place-related tasks offer conceptual ideas for handling compound tasks, including automatic extraction of abstract task interpretation and appropriate sequencing of skills. However, the proposed frameworks possess mostly limited skill repertoires that were designed for specialised assembly situations. To address the needs of the industrial sector, it is crucial to expand the scope of the capabilities of LfD methods to have a higher degree of achievable task complexity and a wider range of assembly skills.

Generalisability

In addition to the necessary adaptability to different complexities and varieties of tasks, the incorporation of LfD solutions in the industrial sector holds, in particular, the promise of a significant degree of adaptability to various tasks and environmental conditions. Expected generalisability is seen as one of the key advantages of the LfD frameworks to manage the predicted shift from mass production to mass customisation.

The analysis of the generalisability of state-of-the-art LfD solutions shows that recent studies focus on experimental evaluations of encounters with changes in motion (see Table 1.1). This includes, in particular, the spatial scaling which considers relocating objects between the demonstration and reproduction phases. The results are perceived as appropriate in the context of current industrial requirements.

Furthermore, the qualitative analysis shows an emerging cluster dealing with realistic changes in the environment, especially in pick-and-place-related contexts. The learning of corresponding skill sequences contributes decisively to generalisation capabilities favouring the seamless transfer to realistic industrial tasks.

However, these features represent only a fraction of the cognitive abilities that human operators possess. Transferability to similar tasks, in terms of similar component groups or sequence structures, is an essential property that increases the applicability of LfD solutions in the field of industrial assembly. This is particularly true with regard to the ability to handle product variants, which is one of the decisive challenges in the automation

of industrial assembly. To address this feature, further research is to be carried out in the area of cross-product generalisation skills.

Performance Evaluation

The primary objectives of industrial assembly lie in its pursuit of efficiency, productivity, and cost-effectiveness [23]. An established method to analyse the economic benefits of automation solutions is given by the Overall Equipment Effectiveness (OEE) that incorporates productivity losses caused by setup and waiting times, reduced execution speeds, scrap and rework [101]. Alternative performance metrics are provided by standardisation organisations such as the National Institute of Standards and Technology [102].

The literature review conducted revealed the use of different performance metrics to evaluate the proposed LfD solutions. These include, in particular, quantifying success rates and mastered tolerances in the case of peg insertion tasks. Furthermore, common practice is to compare against competitive LfD approaches assessing the methods' effectiveness. Only a small part deals with the efficiency of the system, which was evaluated based on the processing or execution time. To promote the viability of LfD solutions for industrial deployment, a more comprehensive evaluation of the performance of the system as a whole is necessary.

Integration Concepts

Since their invention, collaborative robots have been an emerging technology that is steadily migrating into the industrial world to assist humans with their work tasks. For a seamless integration of such systems, human safety is essential. Apart from physical hazards, ethical, social, and psychological aspects are equally important [103]. Framing factors outside of technical solutions will determine the ability to transfer research results to industrial environments.

The literature review conducted reveals a dominant focus on understanding sensorimotor skills to succeed in physical tasks. However, for systematic integration into the working environment, it is equally important to develop a comprehensive framework that considers aspects beyond technical succession. Consequently, further research potentials are emerging in the context of integration concepts.

2.5 Summary and Framework Outline

The literature review conducted aimed to explore the factors that discourage the limited adoption of LfD solutions within the repetitive assembly industry. Physical experiments were quantitatively and qualitatively analysed to determine current trends, interests, and achievements within the relevant contributions of the past decade. A comparison was made with the industry-established four-step instruction technique for human operators to identify synergies and discrepancies of LfD solutions with industrial assembly practice. Promising synergetic concepts were found in demonstration methods, approaches for the interactive elaboration of the task's understanding, and the subsequent improvement during independent execution. However, the remaining obstacles were identified primarily in real-world applicability with respect to the practicability and complexity of the tasks. In summary, the research field of LfD has developed to a point where its potential and capabilities have been shown to be valuable in laboratorial environments and highly promising for a variety of applications. However, further research is required to promote the applicability of the concept to industry-relevant assembly scenarios.

In light of the situation identified, this work focuses on contributing to the field of LfD research by addressing several aspects of the remaining obstacles that hinder the transition of LfD to industrial deployment for repetitive assembly tasks. Although not guided by an industry-driven use case, the primary interest lies in the development of industry-inspired methods with enhanced robustness to increase future transferability to industrial practice. With the goal of enhanced robustness, this thesis presents a framework that explores improvements in the three phases of the characteristic LfD procedure (see Figure 1.1). In detail, it contributes by developing techniques for efficient demonstration, assembly-specific learning, and robust reproduction. These align with the identified obstacles as follows:

- The efficient demonstration technique focuses on the human operator and primarily explores how to make the demonstration more *practicable* compared to the prevailing approach. It takes into account that the intended application scenario favours efficient solutions to minimise the workload for the human operator. This implicitly addresses the psychological aspect of the *integration* challenges for the human operator, who may feel increased frustration if the demonstration takes too long or does not lead to the expected behaviour.
- The assembly-specific learning technique explores how the learning phase of an LfD can be improved to meet the requirements of the repetitive assembly industry. This

mainly addresses the *complexity and diversity* of potential tasks that may occur in industrial settings.

- Robust reproduction takes into account dynamic situations during the reproduction phase. It aims at practicality in realistic industrial environments by improving the prevailing methods in terms of their *generalisability* with respect to motion and environmental changes.

Finally, the developed hardware demonstrator is designed to provide intuitive and user-friendly communication that touches on the identified hurdle with respect to concepts of *integration*. In future work, further proposed improvements for effective *integration* and *evaluation* are discussed to eventually create an industry-relevant LfD framework.

Chapter 3

Guided Demonstration for Robust Transferability

In the first phase of the characteristic LfD procedure, the human operator actively demonstrates the desired task. Although this can be accomplished in several ways, recent statistics (see Figure 2.3a) show a tendency towards methods that involve guiding the reproducing robot through the task. Most LfD solutions restrict the demonstration to occur on the robot using kinaesthetic teaching (illustrated in Figure 3.1a), where the human operator physically moves the robot in a gravity-compensating mode. Performing the intended task directly on the robot has the benefit that its kinematic capabilities and constraints are considered at any time, resulting in guaranteed faithful motion reproduction. However, such an approach presents some disadvantages in relation to expected efficiency and productivity when considered for deployment in realistic industrial scenarios, e.g., the application scenario described in Section 1.3. Relying on kinaesthetic teaching requires the presence of the robot and the human operator to rethink the task from the robot's point of view. Depending on the task, this may necessitate the inconvenient movement of multiple joints simultaneously for multihanded or complex motions [5] or being particularly difficult with bulky robots performing precise assembly tasks [39]. As a result, the demonstration of the task may be perceived as impractical, lengthy, or too intricate. Furthermore, some resistance may be encountered in industrial practice due to the difference from conventional instruction techniques (see Section 2.3).

Based on these limitations of kinaesthetic teaching and teleoperation, the use of passive observation (illustrated in Figure 3.1b) is encouraged in the application scenario under

consideration. The passive observation method has several advantages in terms of practicability and productivity. Performing the demonstration through the human operator's own motion directly is considered more user-friendly and intuitive. Furthermore, a demonstration phase that occurs in the absence of the robot enables the utilisation of the robot in other tasks in parallel.

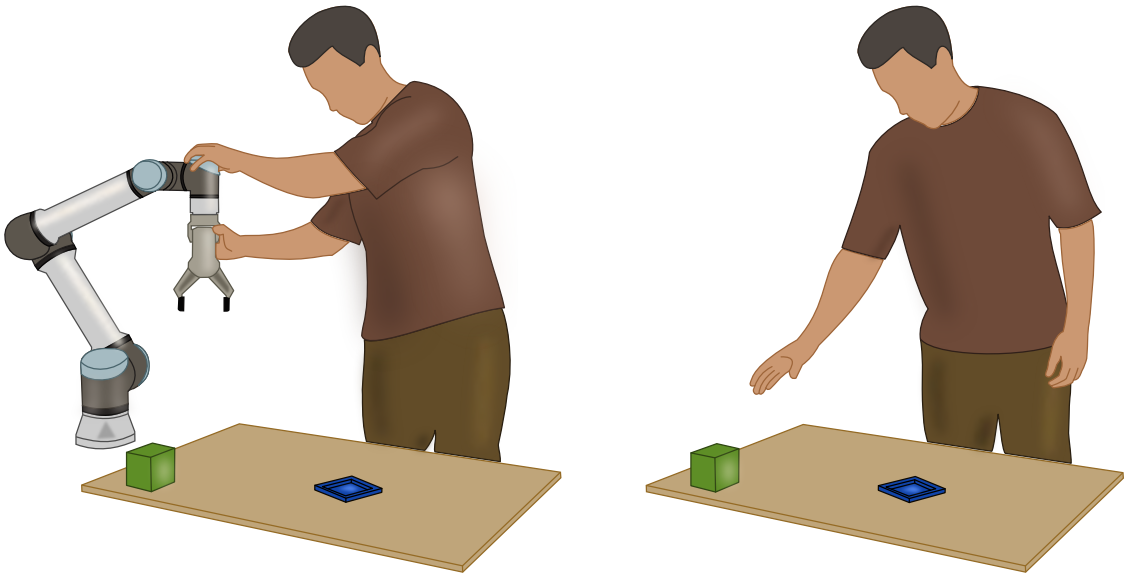

(A) Demonstration using kinaesthetic teaching

(B) Demonstration relying on passive observation

FIGURE 3.1: Illustrations of preferred demonstration methods in LfD research

Allowing the demonstration to be performed on a system different from the reproducing system generates further motivating context: an unconstrained mock-up of a heavy/-dangerous tool detached from the robot can be used to demonstrate comfortably, or a dangerous/labour-intensive task can be demonstrated on a smaller/safer robot contrary to a reproducing powerful robot. However, preserving this independence can result in demonstrated motions that are not reproducible by the reproduction system due to its different kinematic structure. In the present context, *reproducible* motion refers to a faithful reproduction by the reproducing system without deviating from the demonstrated path or colliding with the environment or itself. As a consequence, non-reproducible motions are typically considered failure and only discovered during the reproduction phase, which may cause a safety hazard or require repeated demonstration. Such unnecessary iteration through the LfD procedure reduces the efficiency of the method and potentially increases the level of frustration of the human operator.

Assuming a kinematically constrained reproduction system, this Chapter explores how the motion of the human operator can be artificially restricted to demonstrate motions that are reproducible on the robot in mind. In the absence of the physical reproduction system, the objective is defined by achieving robust transferability between the systems to reduce the number of failed reproduction attempts and therefore increase the productivity of the proposed LfD method.

In light of the goal described above, Section 3.2 formulates the problem in a generalised setting. It results in the necessity of determining the region of reproducible motions accessible to the reproducing system. Leveraging on an existing motion planning framework, Section 3.3 describes how such regions can be found. The presentation of the acquired information to the human operators preventing them from demonstrating non-reproducible motions is discussed in Section 3.4. A visualisation in the form of an interactive Graphical User Interface (GUI) was chosen. The explanation of the utilised LfD learning framework, consisting of so called Dynamic Movement Primitives is outlined in Section 3.5. Finally, Section 3.6 provides experimental results of the proposed method, including a validation and a comprehensive user study, and Section 3.7 summarises the presented contribution. This Chapter was derived from [25].

3.1 Related Work on Transferability

The transferability of a specific motion presented by a demonstration system, e.g. a hand-held tool, a distinctive robot or the human's tracked motion, to a reproducing robot that differs in its physical embodiment is known in LfD research as one of the correspondence problems [5] (see Section 1.1).

A common strategy is to design the demonstration method to track movements in relation to the intended end-effector trajectory of the robot. This is achieved by using simplified mock-ups of the robot's end-effector tool [38, 51] or sensor-enhanced replicas of the part to be assembled [39, 40]. Alternatively, the human operator's hand and / or the movement of the manipulated object is recorded directly and translated to the desired end-effector motion [32, 44, 74, 76, 77, 92]. All methods result in a common representation of the motion that can be interpreted [8, 9], but are not necessarily reproducible by the target system due to its kinematic limitations.

An approach often found to implicitly reduce the likelihood of erroneous movements reproduced is the use of a redundant robot for motion reproduction [32, 38, 44, 46, 51, 70,

74, 75, 77]. These robots have more DoF than dimensions that exist in the task space [104] and can use null-space control methods. As a consequence, kinematic constraints, such as avoiding obstacles, singularities, and joint limits, may be better satisfied whilst maintaining faithful reproduction of the demonstrated end-effector motion [5].

In many applications, especially in the context of industrial use, a non-redundant arm may be preferable for reproduction over a redundant arm, for example a six-DoF over a seven-DoF, due to being relatively lower cost, exhibiting higher payload-to-weight ratio and having simpler kinematics for control and planning. However, in certain cases, these arms cannot exploit null-space control [104] due to their kinematic structure and, as a consequence, may require large joint changes between intermediate points of a demonstrated trajectory to satisfy kinematic constraints. Despite their similar prominence in physical LfD research [33, 37, 39–41, 50, 58, 66, 76, 92], potential constraints to avoid unfaithful reproduction are typically neglected. Instead, tasks are intentionally designed to succeed by specifying clear limitations of the method and informing the human operator of any avoidable behaviour prior to the demonstration phase, e.g., placing objects outside a predefined workspace [33, 41, 46].

A more robust and practicable alternative is seen in artificially restricting the motions of the demonstrator during the physical demonstration. Some work explored this approach by providing additional visual information using a GUI [105] or augmented reality [106–108]. However, these methods usually only consider verifying, adjusting, or adding loosely defined workspace / task constraints, and do not directly consider the kinematic constraints of the target system.

This work builds on the trend to guide the human operator during the demonstration phase, preventing non-reproducible motions from being demonstrated. This promises to increase the efficiency of the underlying LfD framework and improve the practicability of the method for industrial use.

3.2 Problem Formulation

Based on the envisioned goal of guiding the human operator during demonstration through motions that are reproducible by the reproduction system in mind, the following presents a generalised formulation of the investigated problem. It extends to the broader non-trivial LfD scenario in which a motion demonstrated on one system shall be successfully

reproduced on another system with different kinematic structure. While the demonstration system can be anything, including the demonstrator's hand, a mock-up tool, or a passively moved robot, the reproduction system is typically considered a robot with kinematic constraints, for example, providing only six DoFs.

The problem is framed around assumptions about the environment, the demonstration system, and the reproduction system. Figure 3.2 provides an illustrative example of the problem setup. The environment consists of static elements, such as fixtures and equipment, that are known a priori and physically present during demonstration and reproduction. Dynamic objects can be added and removed in real-time during demonstration and kept static during reproduction. The demonstration system is defined as $\mathcal{S}_{dem}$ and can move freely within the demonstration space $\mathcal{C}_{dem}$. The desired motion is captured during the demonstration as a set of discrete states over time $\lambda_{dem} = \{t_i, \Gamma_i\}\big|_{i=0}^{T}$ with $\Gamma_i \in \mathcal{C}_{dem}$. λ_{dem} is fed to a policy-driven LfD learning framework capable of interpreting and processing the information to generate a trajectory λ_{rep} for reproduction. The calculated trajectory is reproduced on the reproduction system $\mathcal{S}_{rep}$ within $\mathcal{C}_{rep}$ which consists of the subset of its reachable space and a predefined operational space. With $\mathcal{S}_{rep}$ selected prior to the demonstration, its kinematic model is assumed to be accessible at any time. Furthermore, it is assumed that $\mathcal{C}_{dem}$ and $\mathcal{C}_{rep}$ are in a common representation space that is chosen as $SE(3)$ since motions within this space can be interpreted by all anticipated systems. The apparent assumption of $\mathcal{C}_{dem} \cap \mathcal{C}_{rep} \neq \emptyset$ is necessary to allow for any reproducible motion. To realise the motion reproduced on the reproduction system $\mathcal{S}_{rep}$ it is necessary to interpret λ_{rep} and generate executable controls, $\Pi : \lambda_{rep} \mapsto \pi_{rep}$, where π_{rep} is a sequence of control actions.

Following the setup above, the problem arises once $\mathcal{S}_{dem}$ and $\mathcal{S}_{rep}$ provide different kinematic structures and $\mathcal{C}_{rep}$ may not entirely cover $\mathcal{C}_{dem}$, that is, $(\mathcal{C}_{dem} \cap \mathcal{C}_{rep}) \subset \mathcal{C}_{dem}$. Furthermore, not all λ_{dem} are reproducible on $\mathcal{S}_{rep}$. Thus, to improve the robustness of the reproduction process, $\mathcal{C}_{dem}$ is expected to be artificially constrained such that it is bounded within $\mathcal{C}_{rep}$ and any λ_{dem} within this constraint space is reproducible by $\mathcal{S}_{rep}$. More concretely, the reproducible motion is defined as λ_{dem} such that the resulting λ_{rep} when mapped through Π results in a short, smooth and collision-free path in C_{rep}. Accordingly, the problem can be formulated as follows:

Problem 1 (Region of reproducible motions)**.** *Find a region $\mathcal{R} \subset \mathcal{C}_{dem}$ such that it is contained within C_{rep} and any λ_{dem} through this region is a reproducible motion. In the case that multiple distinct regions exist, find $\mathcal{R}^*$ that maximises coverage of the anticipated operational space.*

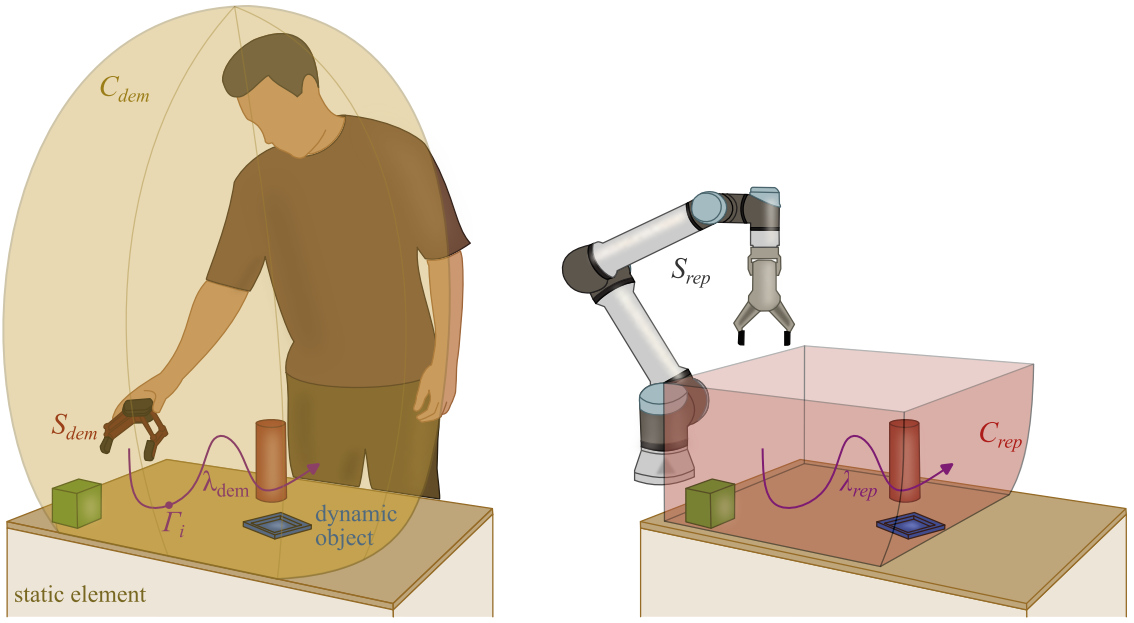

(A) Demonstration with mock-up tool (for better readability, $\mathcal{C}_{dem}$ is limited to the reachable space of the demonstrator's right arm)

(B) Reproduction on six-DoF robot (for better readability, $\mathcal{C}_{rep}$ is limited to an approximated workspace)

FIGURE 3.2: Illustration of the problem's setup

3.3 Finding Regions of Reproducible Motions

In Section 3.2, the challenge faced by potential unfaithful reproduction after performing a robot-independent demonstration was translated into the problem of finding the region of reproducible motions with the highest coverage, $\mathcal{R}^*$. Demonstrating motions within this space promotes robust transferability to the reproducing system in mind.

To solve the stated Problem 1 of finding $\mathcal{R}^*$ based on the assumptions defined in Section 3.2, an existing robotic manipulator planning framework called Hausdorff approximation planner (HAP) [109] was used. Originally developed to effectively sequence trajectory queries, HAP enables motion planning in a user-defined task space (end-effector poses) with an emphasis on planning and execution time efficiency. This is achieved by an underlying algorithm that determines one or more distinctive subspaces of the given task space such that the path between two points close to each other maps to a short, smooth, and collision-free configuration space trajectory. As a result, continuous task space trajectories can be constructed through these subspaces, which translate into configuration space trajectories with a bounding relation in terms of trajectory distance. This mapping between metric spaces is called the ϵ-Gromov-Hausdorff approximation (ϵ-GHA) [109].

In the context of this work, these subspaces with the properties described correspond to the desired regions of reproducible motions. As formulated in Problem 1, the subspace that occupies most of the user-defined operational space is considered the desired region of reproducible motions $\mathcal{R}^*$. Any demonstrated λ_{dem} contained within this region of $\mathcal{C}_{rep} \subset SE(3)$ satisfies the reproducibility condition, assuming that the generated λ_{rep} is spatially identical to λ_{dem}.

The HAP method for finding subspaces is described in the following, with an illustrative example shown in Figure 3.3. First, the models of the reproducing robot and the environment encountered including all static elements are defined (see Figure 3.3a) and introduced into the framework. Based on a set of granularity parameters, the anticipated operational space is discretised, representing the task space of interest (see Figure 3.3b). An undirected graph is then constructed over the discrete task space, where poses within a ball radius of each other are connected by an edge. An optimisation routine then iteratively maps unique configurations to each pose while ensuring that neighbouring poses, i.e. those connected by an edge, are within some specified bounded distance. Kinematic constraints, such as avoiding collisions and remaining within joint limits, are also considered. The ϵ-GHA that minimises the sum of all path costs through the graph is kept. This process can be repeated multiple times with a penalty added to the paths that pass through previously mapped poses to find multiple distinct subspaces (see Figure 3.3(c) and (d)). The subspace with the highest percentage of task space covered is selected as the desired region of reproducible motions $\mathcal{R}^*$, i.e. the subspace depicted in Figure 3.3c.

Following the procedure to determine $\mathcal{R}^*$, a constraint space within the task space is found which is bounded within $\mathcal{C}_{rep}$ and any λ_{dem} through this region is reproducible by $\mathcal{S}_{rep}$. The resulting outcome of HAP is a set of discrete six-dimensional poses in $SE(3)$ - translation and orientation, which quantify $\mathcal{R}^*$. The remaining task space consists of poses that do not meet the transferability condition and are referred to as $\overline{\mathcal{R}^*}$. Poses belonging to $\overline{\mathcal{R}^*}$ can be assigned to one of three reasons for producing non-reproducible motions, i.e. failure during reproduction, when considered within the HAP subspace currently under consideration. Figure 3.4 illustrates, through colour-coded voxels, all three cases for different orientations of the end-effector in the given example of 3.3. The green voxels behind the wall are blocked due to requiring a large change about the wrist to avoid collision with the wall or workbench, which would violate the condition for a region of reproducible motions. The red voxels indicate regions where no inverse kinematics (IK) solution is possible without environmental collision. The blue voxels indicate regions outside the reachability of $\mathcal{S}_{rep}$.

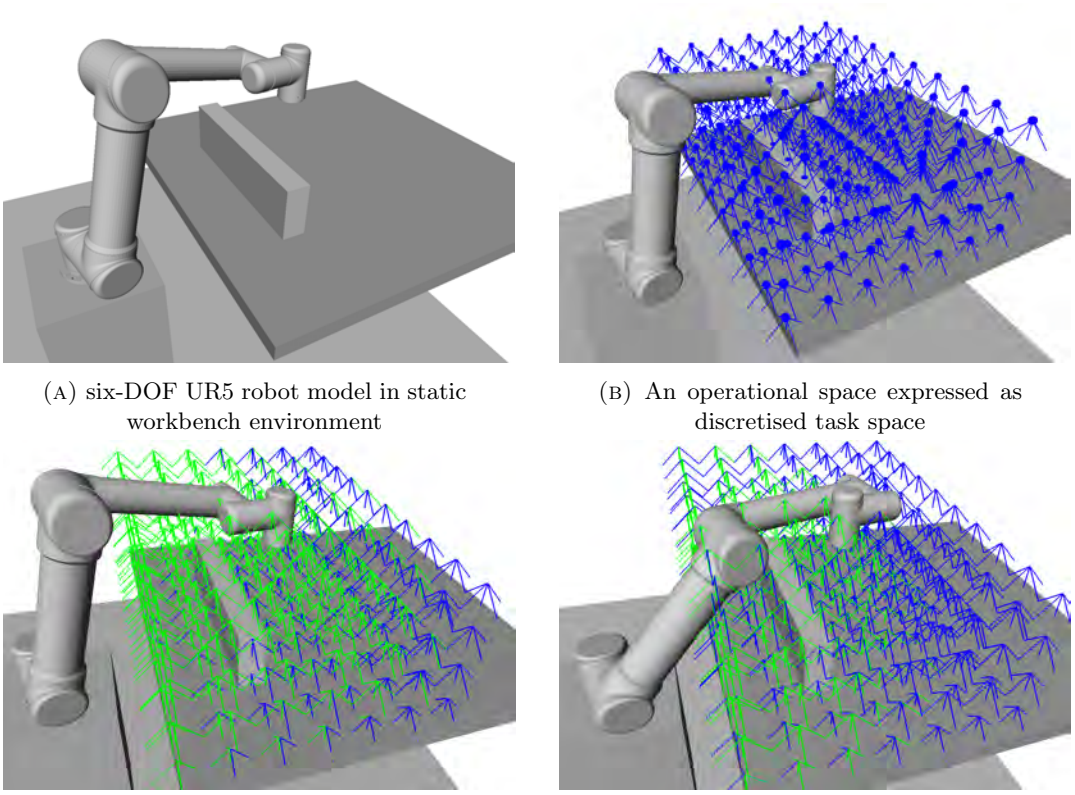

(A) six-DOF UR5 robot model in static workbench environment

(B) An operational space expressed as discretised task space

(C) A region found with 66% coverage and mapped 'wrist-out' configuration

(D) A region found with 35% coverage and mapped 'wrist-in' configuration

FIGURE 3.3: Illustrative procedure of finding regions of reproducible motions (green) using HAP

Extending on HAP, dynamic objects in the scene were accounted for by performing an update to $\mathcal{R}^*$ rather than completely recomputing $\mathcal{R}^*$, which is computationally expensive. This update is performed by iterating over all mapped configurations and checking that they are still collision-free, and if not, they were removed from $\mathcal{R}^*$.

3.4 Visual Guidance during Demonstration

In order to obtain an efficient demonstration method, the information accessible through $\mathcal{R}^*$ and $\overline{\mathcal{R}^*}$ is used to demonstrate motions that can be faithfully reproduced by the reproducing system in mind. This is achieved by guiding the human operator during the demonstration to perform motions such that $\lambda_{dem} \subset \mathcal{R}^*$. In other words, preventing the human operator from moving $\mathcal{S}_{dem}$ into the regions of $\overline{\mathcal{R}^*}$ promises a successful reproduction afterward.

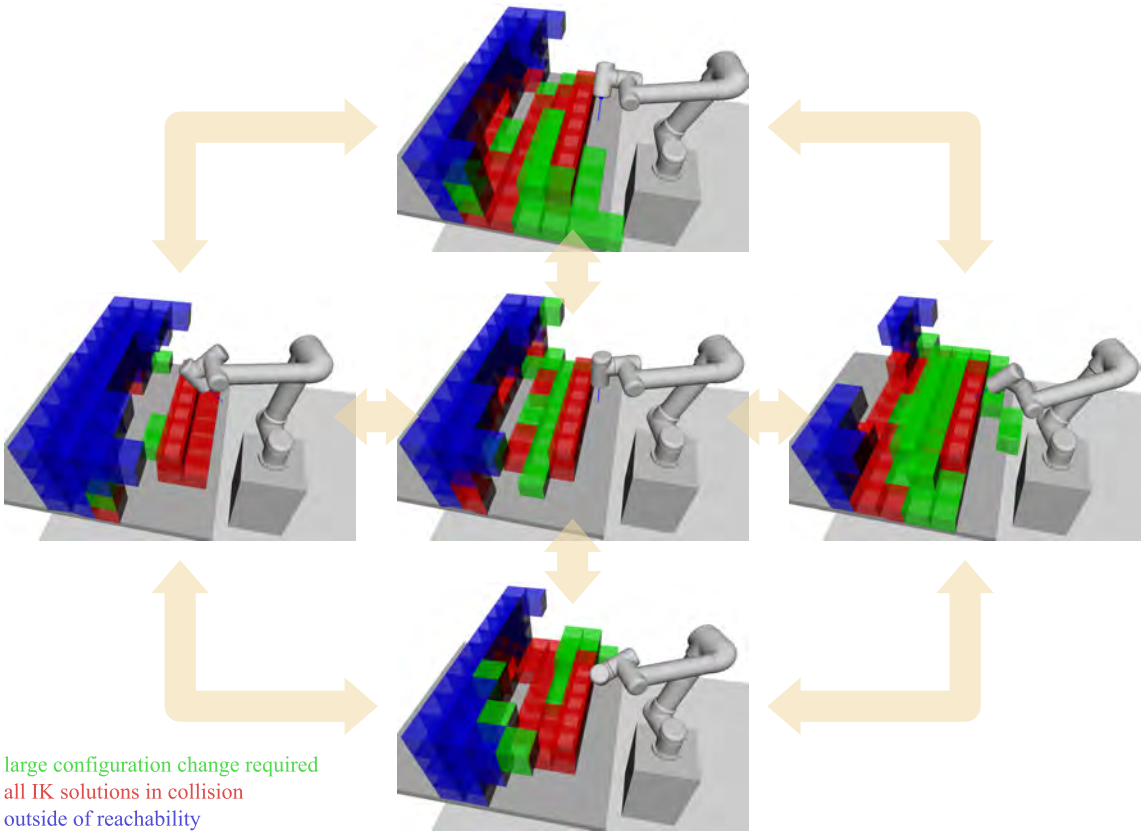

FIGURE 3.4: Illustration of orientation-dependent regions of non-reproducible motions

In the context of this work, a user-friendly GUI was designed to guide human operators through the demonstration by informing them about regions that may affect transferability. The design of the interface is crucial to promote its acceptance for use. In light of the application scenario described, it was designed to be intuitive enough for a non-expert human to interpret and make effective use of it without any knowledge of the underlying kinematics of $\mathcal{S}_{dem}$. Therefore, the following design choices were made with respect to the appearance of the physical components in action, the transferability information condensed in $\mathcal{R}^*$ and $\overline{\mathcal{R}^*}$, and additional adjustments for improved readability.

The physical components of interest include the static environment, dynamic objects, the demonstration system, and the reproduction system. The static environment is considered an exact replica of the physical components encountered by the human operator during the demonstration. While still displayed for reference, its visibility is reduced by a monotonous grey colouring. The rendering of dynamic objects, on the other hand, is considered to be more important, and accordingly acknowledged through a colourful appearance. In terms of visualising the human-controlled $\mathcal{S}_{dem}$, its location in the scene is reduced to a simple blue arrow instead of displaying an entire model of $\mathcal{S}_{dem}$. This was chosen to effectively

reduce the chance of occluding regions of interest. Following the same reasoning, the robot model $\mathcal{S}_{rep}$, although fully accessible, was intentionally removed from the GUI. Besides potential occlusion, it may also distract the human operator from the actual task.

In addition to the physical components of interest, the core information to effectively guide the human operator is found in $\mathcal{R}^*$ and $\overline{\mathcal{R}^*}$, which combined are considered overwhelming and mostly redundant. In light of their opposing characteristic, the visualisation of only $\overline{\mathcal{R}^*}$ was chosen to improve the visibility of the free space in which $\mathcal{S}_{dem}$ can be moved. However, to perform motions such that $\lambda_{dem} \subset \mathcal{R}^*$, it is not necessarily relevant to provide information about the different types of failure (see Figure 3.4), especially since the human operator may not be familiar with their meaning. Therefore, the colour coding was translated to a uniform red representation with reduced opacity.

As $\mathcal{R}^*$ and $\overline{\mathcal{R}^*}$ are quantified as sets of poses in the six-dimensional space, its proper visualisation on a two-dimensional interface is crucial for acceptable readability. As can be seen in Figure 3.3, displaying a static dense grid of arrows is considered to be too cluttered and confusing for the user to follow. Instead, the six-dimensional space was compacted into three dimensions by dynamically activating the regions in $\overline{\mathcal{R}^*}$ when necessary. This is the case for all red voxels in poses that are within a similar orientation to the current pose of $\mathcal{S}_{dem}$. The similarity is computed by taking the dot product between the forward pose axes of $\mathcal{S}_{dem}$ and $\overline{\mathcal{R}^*}$ and only showing voxels corresponding to poses within a given similarity threshold. The result is that red voxels appear to the human operator in positions in the environment to indicate a potential violation of the transferability condition once penetrated from $\mathcal{S}_{dem}$ in its current orientation. Similarly, these red voxels may disappear when the human operator changes the orientation of $\mathcal{S}_{dem}$ so that the region becomes accessible again. An example of this activation and deactivation that occurs for different end-effector orientations was shown in Figure 3.4. This activation occurs in real time and in response to the human operator moving $\mathcal{S}_{dem}$.

Based on the explained approach, the interactive GUI displays static and dynamic environmental elements, the pose of $\mathcal{S}_{dem}$ in real-time, as well as $\mathcal{S}_{dem}$-dependent regions of red voxels, which indicate where the transferability condition may be violated. Confronted with the apparent challenge of visualising a three-dimensional space on a two-dimensional screen, further design decisions were made to improve readability. If $\mathcal{S}_{dem}$ is in proximity to any currently activated red voxel, the appearance of the $\mathcal{S}_{dem}$-representing arrow changes from blue to luminous red. In addition, any voxel separated by a certain distance from the current pose of $\mathcal{S}_{dem}$ was further reduced in opacity and all layers above $\mathcal{S}_{dem}$'s current height were completely removed. A representative example of the interactive GUI

developed to guide human operators confidently through demonstrations of reproducible motions is shown in Figure 3.5.

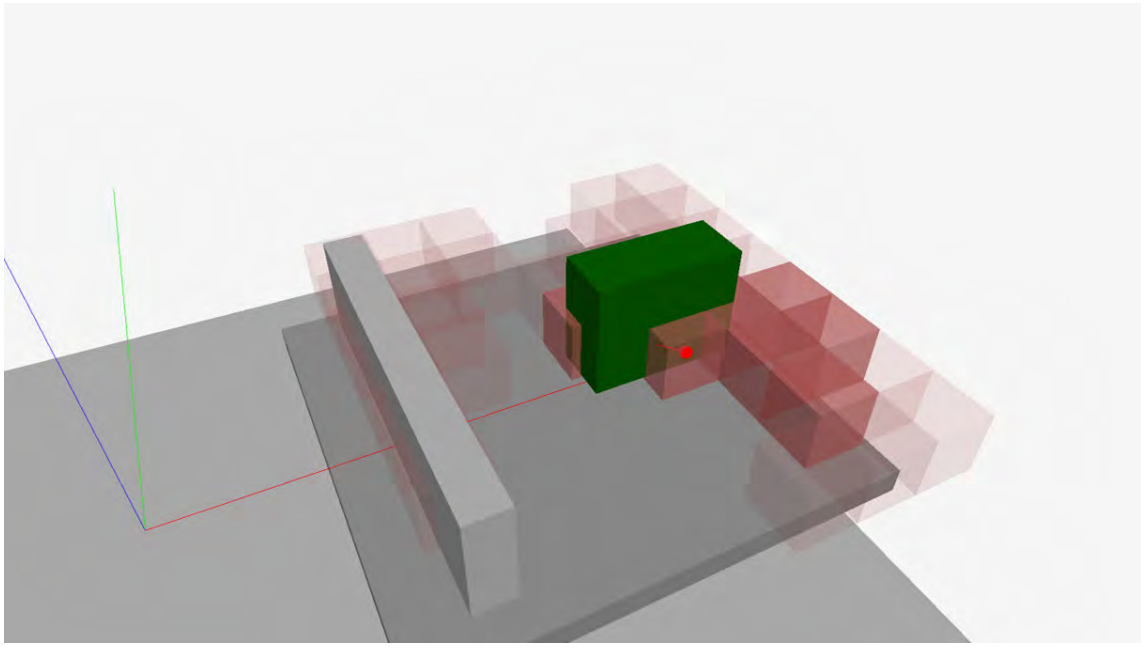

FIGURE 3.5: Representative example of the GUI presented to the human operator for guidance during demonstration

3.5 LfD Learning Framework

Guided by the interactive GUI during demonstration, the human operator is able to perform motions that reflect the intended task while avoiding regions of non-reproducible motions such that $\lambda_{dem} \subset \mathcal{R}^*$. As a result, the recorded demonstration is represented as $\lambda_{dem} = \{t_i, \Gamma_i\}\big|_{i=0}^{T}$ with Γ_i being Cartesian poses, i.e., positions $\mathbf{x}_i$ and quaternions $\mathbf{q}_i$. With the given common representation space of $SE(3)$ it suggests itself to source a policy-driven LfD method for learning with trajectorial outcome. This also aligns with the prevailing trend in recent LfD research (see Figure 2.3). Moreover, the most prevalent technique, the so-called Dynamic Movement Primitives (DMPs), was selected as the applied LfD learning framework. DMPs are a compact, single shot, deterministic motion learning algorithm that incorporates spatial and temporal scaling capabilities and generates smooth and continuous trajectories.

Originating from research around movement imitation with nonlinear dynamical systems [110–113], DMPs were first formally introduced by S. Schaal, J. Peters, J. Nakanishi,

and A. Ijspeert in 2003 [114–116]. Promoted as an efficient framework for robot control, planning, learning, and imitation, DMPs were established for discrete and rhythmic motion control policies. Due to the exclusive usage of discrete DMPs in the remainder of this thesis, the term DMPs refers to this variation if not stated otherwise. Based on observations of converging force fields in frogs [117], Hoffmann et al. proposed in 2008 a revised, biologically-inspired DMPs formulation which tackled the original's failure in the case of coinciding start and goal positions [118]. Since then, several modifications have been proposed for various application-specific adjustments [90, 119–126] and DMPs continue to be a popular subject in ongoing research [127–130]. However, the original and biologically-inspired formulations remain the most applied forms of DMPs in the context of LfD.

The classic learning and smooth reproduction of a single dimension using the DMPs framework is based on a set of non-linear differential equations, called the transformation system (3.1) and the canonical system (3.2):

$$\begin{aligned} \tau\,\dot{\tilde{v}} &= K\,(\,x_T\,-\,x\,)\,-\,D\,\tilde{v}\,-\,K\,(\,x_T\,-\,x_0\,)\,s\,+\,K\,f(s) \\ \tau\,\dot{x} &= \tilde{v} \end{aligned} \tag{3.1}$$

$$\tau\,\dot{s}\;=\;-\,\alpha_s\,s \tag{3.2}$$

where x and $\tilde{v}$ are the motion variables for the position and the velocity scaled by τ, x_0 and x_T are the initial and final trajectory values, and K and D represent stiffness and damping gains. The parameter τ facilitates the temporal scaling capability where as the phase variable s creates the system's time independence through the canonical system, which is parameterised with α_s. The force variable $f(s)$ that preserves any nonlinear characteristic of the given demonstration is modelled as a linear combination of N weighted nonlinear Radial Basis Functions (RBFs), such that:

$$f(s)\;=\;\frac{\sum_{n=1}^{N}\psi_n(s)\,\omega_n}{\sum_{n=1}^{N}\psi_n(s)}\,s\;\;with:\;\;\psi_n(s)\;=\;e^{-\,h_n\,(\,s\,-\,c_n\,)^2} \tag{3.3}$$

with ω_n, c_n, h_n being the i's RBFs weight, centre, and width, respectively. Common practice is to parameterise DMPs according to the following guidelines for guaranteed convergence, critical damping and RBFs equally distibuted in time:

$$\tau > 0\;;\;D = 2\sqrt{K}\;;\;c_n = e^{-\alpha_s\frac{n-1}{N-1}}\;;\;h_n = \frac{1}{(c_{n+1}-c_n)^2}\;;\;h_N = h_{N-1} \tag{3.4}$$

To learn a specific motion, the transformation system computes the unknown RBFs weights ω_n based on the demonstrated trajectory $\{t_i, x_i, v_i, \dot{v}_i\}\big|_{i=0}^{T}$ (if not available, $v_i, \dot{v}_i$ are typically approximated numerically) using Locally Weighted Regression. Task-specific information is compactly stored in the weights ω_n and the parameters K, D, N, α_s. During reproduction, the transformation system is reversed using the learnt weights ω_n to calculate the accelerations, resulting in a smooth and continuous trajectory of the given dimension [127].

Processing multiple independent dimensions, such as joint configurations or Cartesian positions, is achieved by vectorising the transformation system (3.1) while sharing the same one-dimensional canonical system (3.2) for temporal synchronisation. However, rotational dimensions such as unit quaternions or rotation matrices are of a constrained nature. The first attempt of quaternion-DMPs explored the independent calculation of each quaternion element with a post-normalisation step [131]. Subsequent studies proposed to express them in a single vectorised formulation to appropriately incorporate the constrained characteristic of quaternions [132–136]. In 2014, Aleš Ude et al. proposed in [133] formulations for quaternions and rotation matrices and formally introduced the nomenclature of CDMPs.

In the context of this thesis, the term CDMPs is used for DMPs covering poses in the robot's operational space, expressed as positions $\mathbf{x}$ and quaternions $\mathbf{q}$. In detail, the LfD learning framework is based on the revised biologically-inspired CDMPs formulation by Koutras et al. [136, 137] which is considered state-of-the-art. It consists of transformation systems for translational and rotational dimensions that read as follows:

$$\begin{aligned} \tau\, \dot{\tilde{\mathbf{v}}}_{\mathbf{x}} &= \mathbf{K}^{\mathbf{x}} \left(\mathbf{x}_T - \mathbf{x} \right) - \mathbf{D}^{\mathbf{x}}\, \tilde{\mathbf{v}}_{\mathbf{x}} - \mathbf{K}^{\mathbf{x}} \left(\mathbf{x}_T - \mathbf{x}_0 \right) s + \mathbf{K}^{\mathbf{x}}\, \mathbf{f}^{\mathbf{x}}(s) \qquad (3.5) \\ \tau\, \dot{\mathbf{x}} &= \tilde{\mathbf{v}}_{\mathbf{x}} \end{aligned}$$

$$\begin{aligned} \tau\, \dot{\tilde{\mathbf{w}}}_{\mathbf{q}} &= -\mathbf{K}^{\mathbf{q}}\, \mathbf{e}_{\mathbf{q}} - \mathbf{D}^{\mathbf{q}}\, \tilde{\mathbf{w}}_{\mathbf{q}} - \mathbf{K}^{\mathbf{q}}\, 2\, log(\mathbf{q}_T * \bar{\mathbf{q}}_0)\, s + \mathbf{K}^{\mathbf{q}}\, \mathbf{f}^{\mathbf{q}}(s) \qquad (3.6) \\ \tau\, \dot{\mathbf{e}}_{\mathbf{q}} &= \tilde{\mathbf{w}}_{\mathbf{q}} \end{aligned}$$

where $\mathbf{x}$, $\tilde{\mathbf{v}}_{\mathbf{x}}$ are the vectorised variables of translational motion and $\mathbf{q} \in SO(3)$ represents a unit quaternion. $\mathbf{e}_{\mathbf{q}}$ is defined as the quaternion error between the current and goal orientation values and is calculated as follows:

$$\mathbf{e}_{\mathbf{q}} = 2\, log(\mathbf{q}_T * \bar{\mathbf{q}}). \qquad (3.7)$$

Its derivative scaled by τ is given by $\tilde{\mathbf{w}}_{\mathbf{q}}$. The parameters $\mathbf{x}_0$, $\mathbf{x}_T$, $\mathbf{q}_0$, $\mathbf{q}_T$, $\mathbf{K}^i$, $\mathbf{D}^i$ and the force variable $\mathbf{f}^i$ are vectorised variations of the expressions x_0, x_T, K, D, f introduced

above for each transformation system. All dimensions remain synchronised using the one-dimensional canonical system in (3.2) and build on the linearisation in (3.3).

Following the procedure described above with a given λ_{dem}, CDMPs are applied to generate a continuous smooth motion λ_{rep} represented as Cartesian poses in $SE(3)$ over time. On a redundant robot, this information can be fed to a local null space control to achieve physical motion. However, considering the kinematic constraints of the reproduction system $\mathcal{S}_{rep}$ in mind, an additional motion generator was developed to translate λ_{rep} into a sequence of reproducible arm configurations, $\pi_{rep} = \{\phi_1, \phi_2, ..., \phi_T\}$. However, the poses in λ_{rep} are in a continuous space where as the ϵ-GHA mapping is defined over a discrete task space. Therefore, to remain within $\mathcal{R}^*$ a configuration is assigned to each $\phi \in \pi_{rep}$ that is close to the ϵ-GHA mapping. This is achieved by computing all IK solutions for each $\Gamma \in \lambda_{rep}$ and choosing the IK solution that minimises the Euclidean distance to any of the k closest mapped configurations in $\mathcal{R}^*$. The approach described integrates tightly the CDMPs and HAP frameworks and results in robust transferability of the generated motions λ_{rep} that are spatially identical to λ_{dem}.

3.6 Experimental Evaluation

By preventing the human operator during demonstration from infiltrating regions of non-reproducible motions $\overline{\mathcal{R}^*}$ with $\mathcal{S}_{dem}$, the developed method based on HAP and CDMPs promises to generate reproducible motions on a structurally different $\mathcal{S}_{rep}$. The following experimental evaluation, including a validation experiment and a comprehensive user study, presents the proposed guided demonstration approach for an efficient and robust LfD framework on two distinct setups. In the context of this evaluation, special attention is paid to the demonstration phase in which the method is applied. This includes how the method can be used to circumvent poor decisions in situations that can be considered trivial, as well as how the intuitive GUI helps to make the demonstration process more efficient and robust. The detailed functionality of CDMPs used in LfD for learning and reproducing the motion are comprehensively examined in the following Chapters.

3.6.1 Validation Experiment

Envisioning an application in which two kinematically distinct robot arms are used, the validation experiment is designed to demonstrate the non-trivial challenge of transferring motions acquired on a redundant robot to a reproducing kinematically constrained robot.

In this context, a seven-DoF Sawyer arm was used as the demonstration system and moved kinesthetically during demonstration (see Figure 3.6). The reproducing system is a simulated six-DoF UR5 (see Figure 3.3a). Both exist within an identical static environment consisting of a workbench and an obstructive wall obstacle. The modelling of the environment, kinematics, and collisions as well as motion control for the UR5 is performed in a high-fidelity simulator called OpenRAVE. In case of a naive approach, that is, without using the proposed method for robust transferability, the motion reproduction is generated by a local Cartesian space controller.

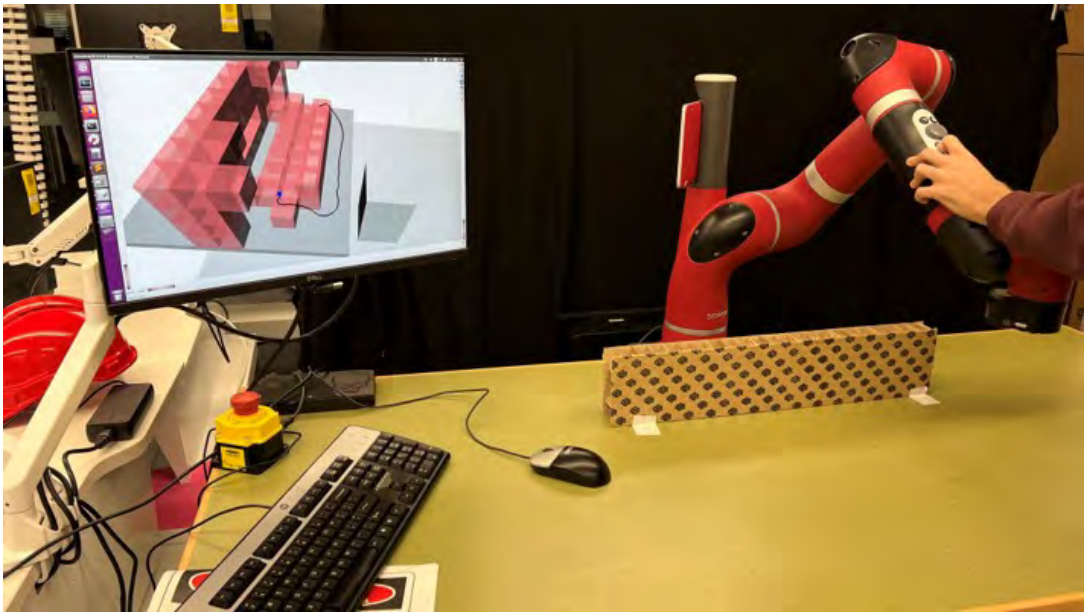

FIGURE 3.6: Demonstration setup for validation experiment

In this experiment, the operator's task is to perform a circular motion around the wall obstacle with the Sawyer's end-effector while remaining as close as possible to the wall and workbench. The motion demonstrated is then processed through CDMPs and transferred to the UR5 with the goal of obeying its kinematic constraints. The task is considered successful when the end-effector of the UR5 performs a movement identical to the demonstration. For this task, the operational space was designed with all poses pointing roughly down with variations of 45°, as exemplified in Figure 3.3b, resulting in $\mathcal{R}^*$ in Figure 3.3c. For a better explanation of accessible $\mathcal{R}^*$, the GUI was used without the additional measures for depth visualisation discussed in Section 3.4.

The first attempt represents the naive approach, in which no help is provided during demonstration regarding the motion's feasibility. The naive operator intuitively hugs the wall with the Sawyer end-effector in a downward facing orientation. The interactive GUI

that was not accessible to the operator in this attempt clearly indicates in the sequence in Figure 3.7(a)-(d) how multiple red voxels, representing regions of non-reproducible motions, were crossed. As a result, the simulated UR5 performs a poorly reproduced end-effector trajectory, as can be seen on the black line in the exemplary sequence of reproduced states in Figure 3.7(e)-(h). The explanation for this is that the UR5 must perform several large configuration changes along the trajectory, reorienting its wrist and shoulder to avoid collision with the wall. The UR5 is unable to faithfully reproduce the demonstrated motion, which was conveniently demonstrated on the Sawyer, afforded by its extra DoF.

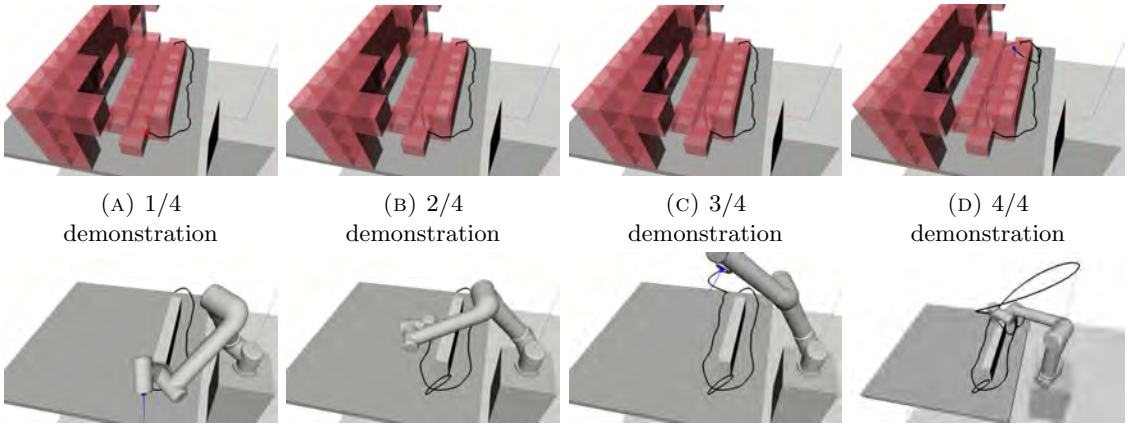

(A) 1/4 demonstration (B) 2/4 demonstration (C) 3/4 demonstration (D) 4/4 demonstration

(E) 1/4 reproduction (F) 2/4 reproduction (G) 3/4 reproduction (H) 4/4 reproduction

FIGURE 3.7: Example sequence of the naive, unguided approach: (a)-(d) hidden GUI and (e)-(h) simulative reproduction on UR5

In contrast, the operator informed by the proposed method is able to actively avoid these problematic regions, as shown in the exemplary sequence in Figure 3.8(a)-(d). On reaching the right side of the wall, the interactive GUI assists in finding a strategy to carry out the task faithfully. By pivoting the wrist forward, several red voxels disappear and non-restricted space behind the wall becomes accessible (compare Figures 3.8(a)/(b)). However, even after doing so, two red voxels remain and block the path (see Figure 3.8b). As a result, the GUI allows the operator to assess the new situation and intentionally trace a path around this region before approximating the workbench again and continuing the task. As can be seen in the reproduction sequence in Figure 3.8(e)-(h), the UR5 is able to reproduce the demonstrated motion faithfully.

This observed behaviour validates the proposed method for this particular scenario and confirms the claim that reproduction can fail if the kinematics of the reproduction system is not considered during demonstrations, even in a relatively simple environment.

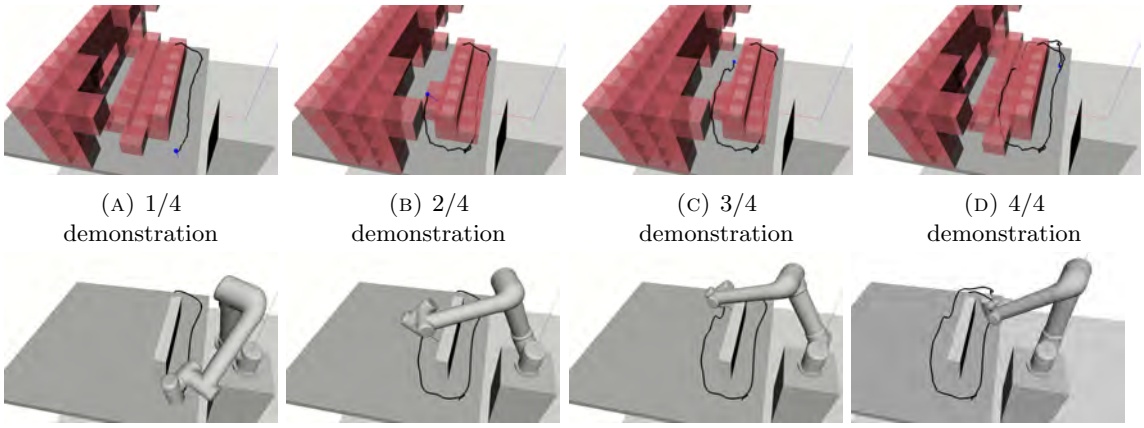

(A) 1/4 demonstration (B) 2/4 demonstration (C) 3/4 demonstration (D) 4/4 demonstration

(E) 1/4 reproduction (F) 2/4 reproduction (G) 3/4 reproduction (H) 4/4 reproduction

FIGURE 3.8: Example sequence of the approach using the proposed method: (a)-(d) guiding GUI and (e)-(h) simulative reproduction on UR5

3.6.2 User Study

After showcasing the importance of considering the kinematics of the reproducing system in Section 3.6.1, a subsequent user study was conducted to evaluate the usability of the proposed method. To remove any physical limitation arising from demonstrating kinaesthetically on a robot, $\mathcal{S}_{dem}$ was embodied by a freely movable 3D printed mock-up tool tracked by a VICON motion capture system. The reproduction system $\mathcal{S}_{rep}$ and the static environment were kept identical to the setup of the validation experiment. A physical hardware setup of the reproducing system was also prepared to showcase successful reproduction. An additional dynamic object is introduced into the scene for the purpose of the given task. In total, nine users participated in the study consisting of three women and six men, five of whom had little or no experience with robot arms.

In this experiment, the users were asked to perform a mock weld operation along a predefined marked edge on the dynamic object. For this purpose, the object is to be placed within the available space on the workbench so that a reproducible motion that mimics welding can be demonstrated. Although the object can be repositioned as often as desired, once a location is selected, the weld motion is to be performed in full on the stationary object. After the demonstration, the validity of the demonstrated motion is evaluated in simulation and, if successful, reproduced on the physical robot. The goal is to perform a weld motion that is transferable to the given reproduction system. Figure 3.9 shows an example of a demonstration (left), which was guided by the proposed interactive GUI (top) and afterwards reproduced on the physical UR5 (right).

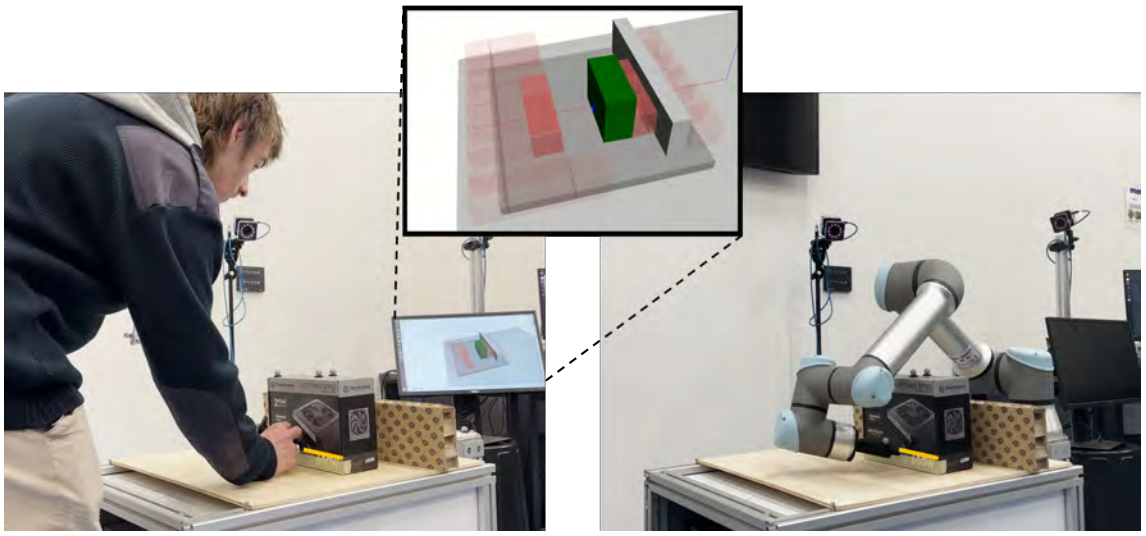

FIGURE 3.9: Experimental setup for the user study

The user study was conducted as follows: First, each user was asked to perform the task without the guidance of the interactive GUI. They were given a maximum of three attempts, which involved carrying out the demonstration and then verifying that it was reproducible on a simulated UR5 in the same environment. If successful, the reproduction was carried out on the real UR5 robot. Subsequently, the user was asked to perform the same task with the guidance of the proposed GUI, again with a maximum of three attempts. If the user was successful in the unguided attempt, the task goal was amended to find an alternative valid placement of the weld object.

Due to the experimental setup, two demonstration scenarios are valid. These include the placement of the box close to the maximum reach of the UR5 with the edge facing the wall (see Fig. 3.10a) and a placement near the wall with the edge facing away (see Fig. 3.10b). Alternatively, the UR5 fails to reproduce the motion by performing large configuration changes (see Figure 3.10c) or reaching its physical limits and deviating from the demonstrated path (see Figure 3.10d).

The main advantage provided by the accessible information through the interactive GUI was that it helped users make an informed decision about where to place the weld object. Furthermore, users were able to place the object and then update the region of feasible motion before carrying out the demonstration. As a result, a potential failure was identified very early without the need to go through the whole process. Figure 3.11a shows the distribution of the number of trials required to successfully demonstrate the weld task. As can be seen, five participants were unable to successfully perform the task within the given three trail and error attempts. In comparison, six succeeded in the first guided

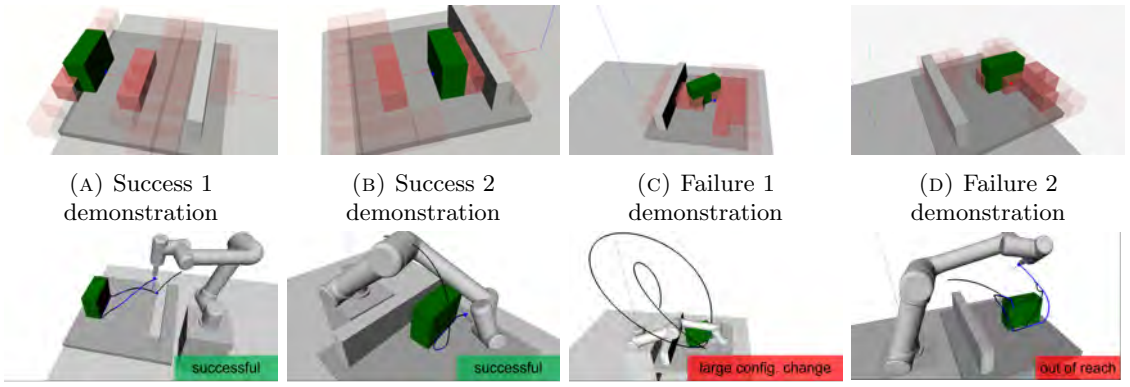

(A) Success 1 demonstration (B) Success 2 demonstration (C) Failure 1 demonstration (D) Failure 2 demonstration

(E) Success 1 reproduction (F) Success 2 reproduction (G) Failure 1 reproduction (H) Failure 2 reproduction

FIGURE 3.10: Types of successful and failed attempts observed in the user study

reproduction attempt after several repositioning of the box and explorations of feasible regions. In total, 36 reproduction attempts were conducted of which 13 were successful (seven by placing the object near the wall as in Figure 3.10b), 22 failed due to required large configuration changes (see Figure 3.10c), and two failed for demonstrating outside the UR5's reach (see Figure 3.10d). All reproduction attempts are shown in the Appendix B.1.

In addition to the quantitative analysis of the required attempts, the usability of the proposed method was evaluated using the subjective metric applied in a previous usability study on socially assistive robots [138]. Their study categorised their evaluation metrics into effectiveness, efficiency, and satisfaction with which users were able to perform given tasks [139]. In a similar fashion, the users were asked to rate on a 5-point scale how confident they were, how easy it was to carry out the task with and without the GUI and how surprised they were with the reproduced trajectory. The full questionnaire of this user study is provided in Appendix B.2.

Figure 3.11b shows the percentage of increase and decrease in each of the metrics questioned. As can be seen, almost all participants were more confident in carrying out the task when using the guidance of the GUI. The ease of use was comparable, which is a positive result considering the additional component of the GUI during demonstration. And users were less surprised by the reproduced motions when using the GUI, which can be explained by the absence of large spontaneous joint changes.

Users were additionally asked the following questions on a 5-point scale specifically about the effectiveness and design of the GUI:

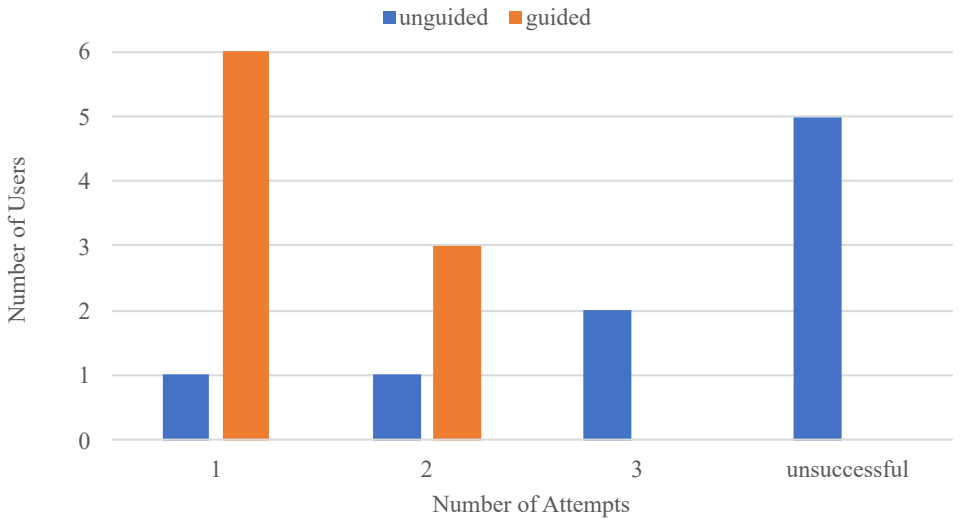

(A) Distribution of number of trials required for success

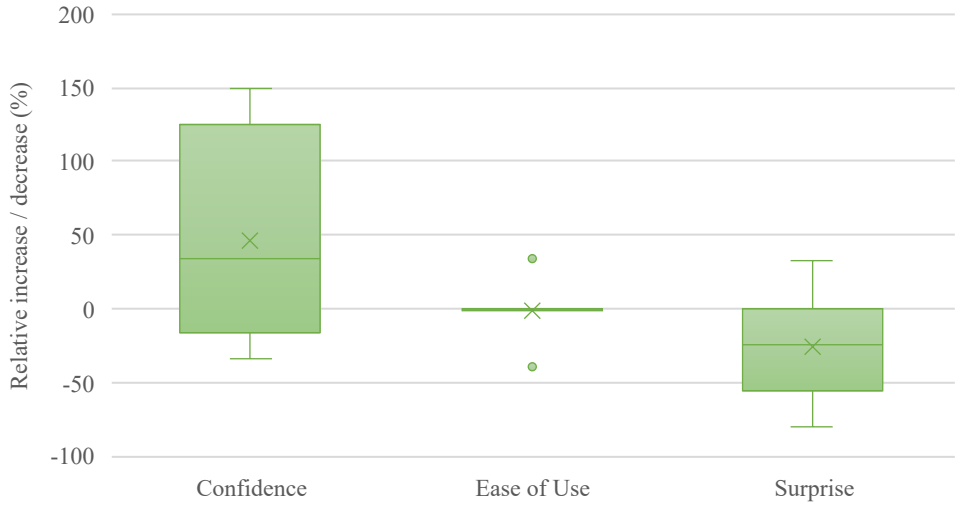

(B) Percentage increase/decrease in subjective metrics

FIGURE 3.11: Quantitative results of the user study

- How effective was the GUI at improving your decision of where to place the weld object?
- How intuitive was the GUI in assisting with the task?
- How effective was the GUI in providing spatial awareness, i.e., avoid red voxels?
- Is the extra effort to use the GUI worth it over trial and error (without any guidance)?

On average, users gave a rating of 4 and above, which indicates that our GUI design was overall effective and intuitive enough for assisting with the given task. Furthermore, all participants rated the last question with a 5, which reinforces the value of our method over a trial-and-error approach.

In terms of qualitative feedback, some participants desired more suggestive guidance. For example, providing recommended object placements to the user. Other suggested improvements included receiving more information on the source of failure when entering a red voxel and the option to display the simulated robot in the GUI.

3.7 Summary

In contrast to the prevailing tendency to demonstrate a desired task on the system that is expected to reproduce, significant advantages regarding applicability and practicability are envisioned for demonstrations conducted in the absence of the reproduction system. However, naively transferring a demonstrated motion to a system with differing kinematic structure withholds the potential of generating motions which differ drastically from the initial intention.

This Chapter presented a novel demonstration method that ensures the reproducibility of a demonstrated motion on the reproduction system in mind. To achieve this, an existing robotic manipulator planner was used to compute regions of reproducible motions. An intuitive GUI was designed to intuitively and effectively inform the human operator during demonstration about these regions preventing the performance of non-reproducible motions. The results of the conducted validation experiment and user study showcased the importance of being able to demonstrate reproducible motions reliably without the presence of the physical target system.

Chapter 4

Assembly-tailored Learning Framework

The second phase of the characteristic LfD procedure is determined by the robot's learning capabilities. During the previous demonstration phase, the human operator demonstrates a task that is to be learnt by the robot. The demonstrations performed are collected and function as input to the LfD learning framework. While passive monitoring by or active assistance from the human operator can be incorporated in this phase (see Figure 1.1), it typically focusses on the robot's self-driven ability to acquire a comprehensive understanding about the desired behaviour from the given demonstration data. As described in Section 1.1, learning frameworks can be categorised according to their outcomes in the form of policies, plans, or cost/reward functions. Recent statistics on assembly-related LfD research suggest a prevailing tendency towards policy-driven approaches that generate reproduction trajectories (see Figure 2.3). In this context, Dynamic Movement Primitives (DMPs) have been successfully applied to a variety of assembly-related use cases.

As introduced in Section 3.5, DMPs have several beneficial properties that favour their application within an LfD framework for assembly-related tasks. Given a single demonstrated trajectory, DMPs utilise a deterministic algorithm to generate a smooth and continuous trajectory representing an efficient one-shot learning method [127]. Furthermore, DMPs provide the ability to scale spatially and temporally between the demonstrated and reproduced trajectory. Such generalisability is achieved by alternating some of the parameters used in the transformation system (see (3.5) and (3.6)) between learning and reproduction. The learning set consists of the start/end points of the demonstrated trajectory as $\mathbf{x}_0$,$\mathbf{x}_T$ and the selected time constant τ_{dem} which is typically chosen as the duration of the

demonstration T_{dem} in seconds. Changing $\mathbf{x}_0$ and/or $\mathbf{x}_T$ results in spatial scaling while remaining topologically similar to the demonstrated trajectory [140]. Temporal scaling is achieved by selecting a time constant $\tau_{rep} \neq \tau_{dem}$. In other words, increasing τ_{rep} results in a proportionally extended reproduction duration. Figure 4.1 shows a simplified illustration of this generalisability using translational dimensions. Spatial scaling is visualised by amending the given positions $\mathbf{x}_0 = \mathbf{x}_T = (0, 0, 0)^T$ to $\mathbf{x}_{0/T} = (0, 0, \pm 0.5)^T$ (see Figure 4.1a). Similarly, τ_{rep} was set to $0.5\tau_{dem}$, creating a motion with a similar path, but twice the speed as seen in Figure 4.1b. This behaviour is similarly applicable to rotational dimensions by alternating $\mathbf{q}_{0,T}$ and the shared time constant τ_{rep}.

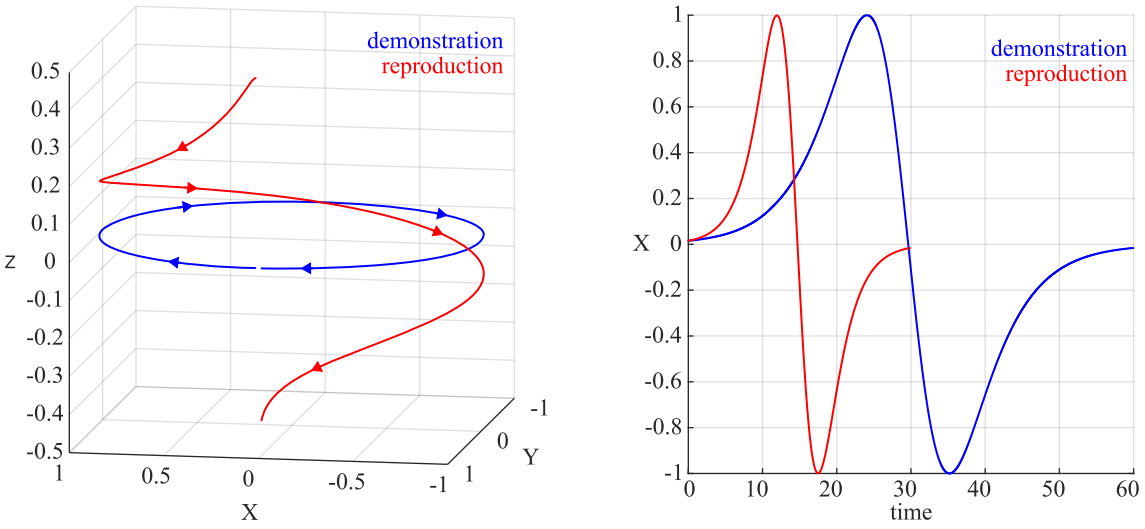

(A) spatial scaling exemplified in the z-dimension

(B) temporal scaling exemplified in the x-dimension

FIGURE 4.1: Example of spatial and temporal scaling capabilities of DMPs

As a representative trajectorial-based learning framework, DMPs provide the ability to reproduce movements accurately with generalisation applicable to a new set of desired bounding poses and duration. However, handling complex tasks remains a major bottleneck of DMPs and other trajectory-driven approaches [141] as distinctive parameterisation may be desired throughout the course of reproduction. An example of such a scenario is depicted by a pick-and-place task as illustrated in Figure 4.2a. Alternating the object's initial location while keeping its goal location and speeding up only a portion of the resulting trajectory is considered not achievable with the original DMPs formulation.

In contrast, the second most applied category of learning frameworks with outcomes in the form of plans typically extracts a sequence of key states that include their required pre / post conditions from given demonstrations (see illustration in Figure 4.2b). As a

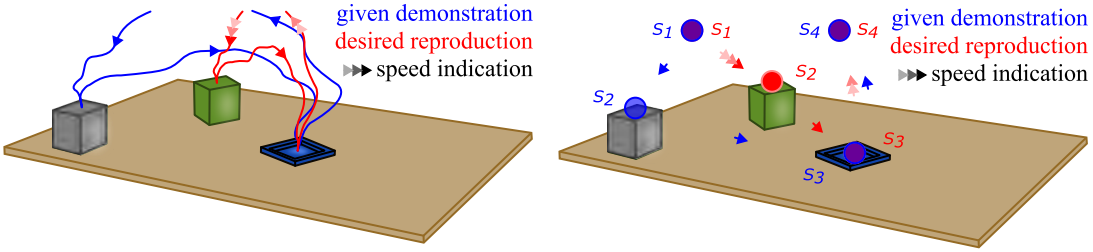

(A) trajectory-based learning: accurate motion reproduction achievable, but no separate relocation or partial velocity adjustment

(B) plan-based learning: sequential adjustments achievable, but no accurate motion reproduction

FIGURE 4.2: Illustration of conceptual limitations for trajectorial and plan-based learning frameworks

result, hierarchies, rules, and loops of complex tasks can be sequentially expressed, but accurate motion reproduction is limited, as reproduction relies on a set of predefined basic controllers [6]. This characteristic distinction between LfD learning frameworks based on trajectories and abstract plans has a long history [6]. The merging of both approaches is considered necessary to adequately learn and reproduce complex tasks [5, 110].

In light of the targeted application scenario (see Section 1.3), the prevailing DMPs learning framework provides suitable characteristics with respect to motion-related requirements. However, its standalone abilities do not adequately meet the requirements for desired task complexity and diversity encountered in assembly-related tasks (see Section 2.4). This Chapter investigates how DMPs can be extended by an abstract discretisation system to achieve increased generalisability tackling expected task complexity and diversity. In the context of this work, a *discretisation system* refers to a symbolic finite library of skills that can be sequenced to adequately describe assembly tasks. Compared to previous attempts with rudimentary discretisation systems, this work explores the use of preexisting systems that have been successful for abstracting assembly movements in an industrial context. Such a system provides several benefits, including its proven sophisticated level for appropriate coverage and abstraction, as well as its familiarity in industry, which promotes smoother integration into practical processes. Providing application-specific requirements, a suitable discretisation system is used to inform and structure the underlying sequence of individual DMPs that accurately fit motion-related characteristics. As a result, an assembly-tailored learning framework is established that promotes improvement with respect to the requirements considered essential for the practicability and applicability of LfD in the industrial environment.

This Chapter is structured as follows: Section 4.1 reviews the possibilities of expanding

DMPs with a discretisation layer and discusses approaches that have been explored in the past. Section 4.2 reviews existing industry-related discretisation systems for assembly tasks and selects the most suitable with respect to the context described. Its integration with the trajectory-based DMPs is proposed in Section 4.3 to establish the assembly-tailored LfD learning framework. Finally, Section 4.4 provides experimental results and a summary is given in Section 4.5. This Chapter was derived from [26].

4.1 Related Work on DMPs Complexity Enhancement

To achieve more complex motions than those produced by a single DMPs' expression, the literature suggests two major approaches [127]. One approach is built on the introduction of via-points as intermediate checkpoints with defined state constraints. This allows, in addition to the generalisability given by DMPs, the consideration of further constraints at specified states over the course of the reproducing motion. This approach was initiated by Kober et al. [119] who proposed a modification of DMPs to incorporate non-zero velocity conditions for the start and goal state. Ning et al. extended this idea by learning DMPs based on artificially generated sample trajectories that meet certain via-point criteria [142]. Weitschat et al. translated the desired via-points into via goals that were expressed as Gaussian kernels in a time-varying goal function that activated them in sequence [143]. The most recent contribution proposed so-called via-point movement primitives in which DMPs were extended by the probablistic framework of Probablisitic Movement Primitives (ProMPs) [144] to generate better inter- and extrapolation results.

Alternatively, complex motions can be achieved by combining separately processed DMPs to create a unifying reproducing motion. Saveriano et al. summarised in [145] three ways to merge DMPs. The first represents the trivial case in which any segment expressed via DMPs starts and ends in a steady state, allowing for unmodified sequential processing of the given DMPs. An intended 'handover' between DMPs with non-zero velocity at the point of transition is built upon [119] and is modelled as *reaching* a moving target that coincides with the desired 'handover' state. The third option is based on [146] and merges multiple DMPs into a single more complex mathematical expression, eliminating any transition between separate reproducing algorithms.

In the context of this work, considering merging consecutive DMPs is desirable as it allows access to the modelling and generalisation abilities of DMPs in each segment independently. This has been investigated in several recent studies, as reviewed in full in Section 2.2.3.

Explored task representations that extend policy-driven learning frameworks are typically designed to meet an application-specific narrative. As a result, various abstract naming of reproduction segments with varying points of interest were proposed. Examples include trajectorial properties such as contact-rich/-poor [49] or approaching/assembling [45], robot-inspired skills such as place-at/move-to [41, 110, 147], and high-level assembly-related skills such as screwing/placing/reaching [50, 70]. While reasonable task representations have been discussed for potential exploitation of generalised applicability, none are based on a sophisticated industry-proven structure, limiting their probability to endure realistic industrial assembly operations. Furthermore, proposed sequences of DMPs show only limited exploitation of their full potential for individualisation.

The presented work explores the usability of industry-related discretisation systems that have been applied to model practical industrial assembly movements. Such a sophisticated baseline in combination with the DMPs trajectorial generalisability and adaptability promises to establish an assembly-tailored learning framework that embodies the capabilities expected in practical environments.

4.2 Selection of Discretisation System

As stated above, several benefits arise from using an existing discretisation system instead of developing a new one. The approach of selecting a system that is or has been used in an industrial context for a similar purpose ensures the system's sophisticated robustness and capability to discretise most of the encountered assembly tasks. It is also assumed that it is familiar to human operators who may be confronted with the proposed LfD learning framework, making the eventual interaction more intuitive. Furthermore, as an elaborate system used in industrial practice, it may incorporate additional features that could be used in the learning framework.

Selecting a discretisation system from an industrial context is also feasible, as the assembly sector provides a sophisticated knowledge base that spans many decades. Influences from many disciplines and the persistent desire to shift towards automated solutions in the industry have produced a variety of potential starting points. In the following, several discretisation systems encountered in industrial practice are examined and evaluated with regard to their applicability in the context under consideration. This includes the criteria of providing a finite library of basic movements capable of modelling complex assembly tasks, being sufficiently granular for the framework in mind, providing intuitively understandable skill representations, and ideally being recognisable from human operators.

With the intention of translating a human-performed task to a robot, discretisation systems were exploited from human-centred and automation-centred methods. The first category includes, in particular, the so-called Predetermined Motion Time System (PMTS), which emerged mainly in the twentieth century and provide tools for modelling and analysing manual workflows found in industry. This is achieved by predefined sets of basic human movements with unique characteristics and distinct influential factors. Building on such a finite library of skills, most workflows encountered in industrial practice can be expressed as a discretised sequence or structure of elementary motions. Workflow analysis is carried out on the basis of scientifically benchmarked standard times for each elementary motion. This enables the evaluation and planning of existing or future workflows. The most popular PMTS in industrial practice are MTM, Work Factor (WF), and Maynard Operation Sequence Technique (MOST).

Methods-Time Measurement (MTM) was first introduced by H. B. Maynard et al. in 1948 [2] and distinguishes ten basic elements to model human movements in industrial environments (see Table 4.1). The average time to execute the actions after sufficient practice depends on different factors. For example, the length of movement and the precision at the goal state influence the standard time of move and reach, while the object's shape, position, and dimensions are decisive for grasp operations. As MTM is designed for detailed operation analysis, it is commonly considered for repetitive short-cycle assembly tasks during mass production. The profound set of rules established in this system allows the discretisation of complex tasks and even tool-assisted operations using the predefined basic elements in Table 4.1. In addition to its industrial importance for manual workflow analysis, recent research efforts explore its automated classification and transfer to automated systems [148–153]. Today, several variations exist, including MTM-1 (MTM), MTM-2, MTM-UAS, MTM-MEK, and MTM-SAM, which extend to different levels of granularity for diversified assembly scenarios.

With similar intentions, Quick et al. proposed in 1962 the Work Factor (WF) system [154]. Its original form consists of eight fundamental elements, which are listed in Table 4.1. In this system, the time required to perform the skills is affected by four main variables. These include the body part used, the distance travelled, the weight or resistance, and the type of manual control. Compared to MTM, it takes particular account of the mental component that occurs during the performance of assembly tasks. Today, several variations were proposed and are used in industry to cope with different levels of detail, including DWF, RFW, AWF, VWF, and BWF.

MTM-1	**WF**	**Basic MOST**
Reach		
Grasp	Grasp	Gain Control
Move	Transport	Controlled Move
Position	Assemble	Alignment
Release	Release	Placement
	Use	
		Action Distance
Turn		
Apply Pressure		
Disengage (separate)	Disassemble	
Body, legs, and foot Motions	Preposition	Body Motion
Eye Times	Mental Process	Process Time

TABLE 4.1: Elementary operations of considered Predetermined Motion Time Systems

Like the systems described above, the Maynard Operation Sequence Technique (MOST) is based on the idea that human movements in industrial assembly tasks can be described by repetitive movement sequences [155] and proposes a set of seven elementary operations (see Table 4.1). It was first released in Sweden in 1972 and has been known in the United States as Basic MOST since 1974. It was soon extended by two variations called Mini MOST and Maxi MOST. Contrary to MTM and WF, this method focuses on the sequence characteristic of assembly tasks and determined three essential building blocks that include a predefined sequence of elementary operations. The building blocks are the general move sequence, the controlled move sequence, and the tool use sequence.

Alternative discretisation systems are sourced from automation-centred taxonomies. Under the umbrella of effects on material flows, the VDI 2860 [156] provides a consistent description of automated handling processes using solution-neutral (device- and manufacturer-independent) motion modules. It was developed by the Association of German Engineers (VDI - 'Verein Deutscher Ingenieure') and first published in May 1990. The latest version from 2003 divides industrial handling activities into five functional areas of storage, variation of quantities, movement, security, and inspection. Subordinate to this classification are seven elementary functions which are represented through standardised symbols (see Figure 4.3a). These include divide, unite, turn, displace, stop, release, and test. Further functions were defined to represent industrially relevant compound handling processes that sequence multiple elementary functions.

Within the set of standards for manufacturing processes, the DIN 8593 presents a taxonomy for the joining capabilities encountered in industrial practice [157]. It consists of a discretisation system that covers the skill categories of putting together, filling, pressing

on/in, shapeless forming, forming, welding, soldering, bonding, and textile joining. Each subgroup is further divided into elementary functions, which are listed in Figure 4.3b using *putting together* and *pressing* as examples.

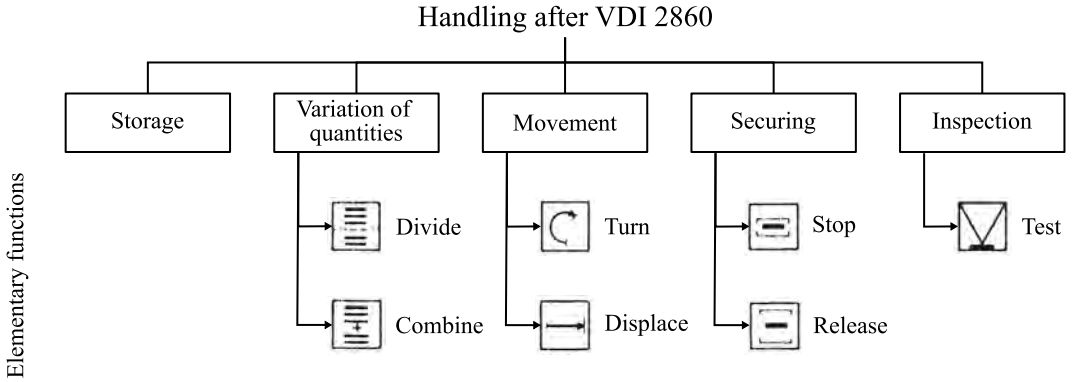

(A) Elementary handling functions after [158]

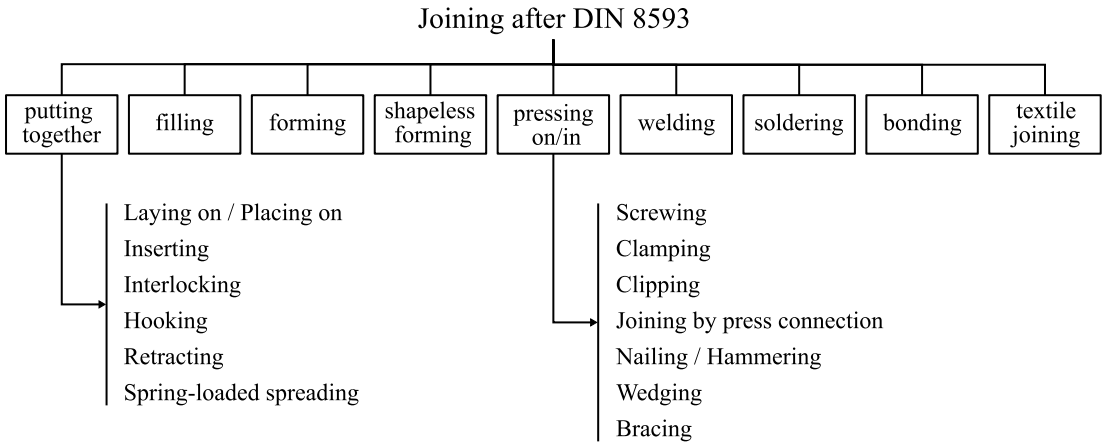

(B) Joining elements after [157]

FIGURE 4.3: Taxonomies provided by selected standards

Some research efforts have also investigated the merging of human-centred and automation-centred approaches. Based on the MTM system, Richard P. Paul and Shimon Y. Nof invented the Robot Time and Motion (RTM) system in 1979 to transfer the human-centred motion system to robot capabilities [159–161]. Its taxonomy consists of eight elements, including MTM-related *reaching*, *moving*, *grasping*, and *releasing*, as well as required robot-related vision, stopping on error/force, and process time-delay functions. Consecutive research investigated the usability of RTM in industrial scenarios [162–164]. In 1991, RTM was extended through elementary operations for mobile platforms [165] and recently for human-robot collaboration [166, 167].

The evaluation and selection of the most suitable discretisation system is driven by its applicability to the intended LfD learning framework for assembly tasks. Given the application scenario in mind and the trajectory-based CDMPs for skill learning and reproduction, the considered discretisation systems are reviewed according to their skill library, ability to abstract industry-relevant physical movements, and intuitiveness for human operators.

Promising systems were sourced mainly from human-centred PMTS and automation-centred standards. The latter provide profound and proven sets of elementary functions, but appear less intuitive for ordinary assembly tasks and are not directly related to expected physical movements, e.g. test. These disadvantages are not observed in PMTS approaches, which were designed to map and analyse human movements in an industrial context. Additionally, PMTS provide an established time analysis system that allows the exploration of predictive human-robot comparison. Based on the elementary operations listed in Table 4.1, MOST is not sufficiently detailed and its translation into robot movements is considered limited. Similarly, the decisive feature of WF is its consideration of mental factors that are not relevant for physical robot movements. MTM, on the other hand, provides a consistent set of elementary operations that are linked to reproducible physical movements on a robot. Even if human operators are not familiar with MTM-1 itself, the nomenclature used is considered intuitively understandable. Its modification for the automation-inspired discretisation given by RTM is seen as not advantageous as functionalities such as vision and process time delay were embedded that do not reflect human-based movements.

As a result, MTM-1 was selected as the most suitable discretisation system for the intended LfD learning framework. In the context of this work, assembly tasks are expected to be performed within a small workbench space (see Section 1.3). This reduces the explored set of predefined skills to the first five elementary operations of MTM-1, including *reach*, *grasp*, *move*, *position*, and *release*.

4.3 MTM-inspired CDMPs Learning Framework

With the goal of developing an LfD learning framework that is tailored to industry-orientated assembly tasks, this Section explores the combination of trajectory- and plan-based methods to source advantageous features of both approaches into one unified learning method. For this purpose, an enhancement of the prevailing CDMPs method with a discretisation system is envisioned. Based on the selection process in Section 4.2 that

identified MTM-1 as the most suitable system, the following explains the proposed MTM-inspired CDMPs learning framework. First, the basic elements given by MTM for manual workflow modelling are translated into robot-centred skills that exploit different customisation features of CDMPs. Then, two approaches for the sequential distinction between those skills from human demonstrations are discussed, followed by the derivation of a mechanism to cope with relocated objects.

4.3.1 MTM-inspired CDMPs skills

As explained in Section 4.2, this work is based on an assumed limited workspace that narrows the focus to the first five basic elements of MTM-1. A typical MTM-1 assembly cycle is depicted by the task of transporting an object of interest from an initial indeterminate location to a defined location relative to other objects. As such, assembly tasks are discretised following the illustrative sequence of *reaching* to a workpiece, *grasping* the workpiece, *moving* the workpiece in proximity of its desired location relative to an assembly point, *positioning* the workpiece accurately at its assembly point, and *releasing* it securely. This sequence is repeated if several workpieces are involved in the assembly process or alternated by given MTM-1 rules to discretise distinct motions, such as tool handling. The predominant purpose of the MTM-1 elements and the factors that influence manual workflows are summarised in Table 4.2. Details on the predetermined time data for MTM-1 are provided in Appendix C.1.

Basic element	**Predominant purpose**	**Influencing factors (manual workflow)**
Reach	move the hand to a destination or general location	distance of motion, condition of the target object, and pre/post velocity of the hand
Grasp	secure sufficient control of one or more objects with the fingers or the hand	properties of the object such as the size of the available contact area and its surroundings
Move	transport an object to a destination	transported object, and pre/post velocity of the hand
Position	align, orient, and engage one object with another object	insertion tolerance, joining pressure, and the object's symmetry
Release	relinquish control of an object by the fingers or hand	opening the fingers or letting go

Table 4.2: Properties of MTM-1 basic elements after [2]

The conventional trajectory-based CDMPs learning framework provides several opportunities to customise the reproduced motion according to the desired behaviour. As described above, CDMPs allow spatial and temporal scaling by alternating the parameters $\mathbf{x}_0, \mathbf{x}_T, \mathbf{q}_0, \mathbf{q}_T, \tau_{rep}$. The smoothness and precision of the reproduced CDMPs trajectory are indirectly determined by the parameter N that defines the number of RBFs to model the forcing terms $\mathbf{f}^i(s), i \in \{\mathbf{x}, \mathbf{q}\}$. Increasing N results in a more accurate imitation of the demonstrated motion, but also proportionally increased computational costs, which result from the calculation of the weights ω_n, since the matrices used by the locally weighted regression are of higher rank. Furthermore, several enhancements of the original CDMPs have been explored in previous studies that allow real-time path adjustments during reproduction, including external forces measured or artificially introduced and machine learning-based optimisation. These features are valuable for unique customisation of the CDMPs and their suitable applicability will be discussed without further details on their implementation. However, the particular ability to incorporate real-time collision avoidance is investigated in depth in Chapter 5 for robust reproduction.

The following derive unique CDMPs for each MTM-1 element to establish a finite skill library to learn and reproduce compound assembly tasks. The proposed framework is explained in detail below and summarised in Figure 4.4. *Remark*: the proposed framework provides only suggestions toward relative amendments (increase/decrease) for CDMPs parameterisation as optimal values are subject to the robot's capabilities and the application's requirements.

Reaching

As introduced above, the typical MTM-1 assembly cycle begins with approaching a workpiece that needs to be transported, aligned, and positioned relative to its assembly point. The spatial shape of motion is dictated by the starting position of the given demonstration system and the initial location of the workpiece. The expected duration to perform this element is mainly influenced by the distance between these two locations.

Translated into custom CDMPs, the focus is on the efficiency and adaptability of movement. The latter is achieved by using the spatial scaling capability of CDMPs. A new location of the workpiece serves as the goal pose of the reach model to adapt to the new scene (see Section 4.3.3). Since the distance travelled influences efficiency during *reaching*, the temporal scaling property of CDMPs becomes valuable, especially when the task was

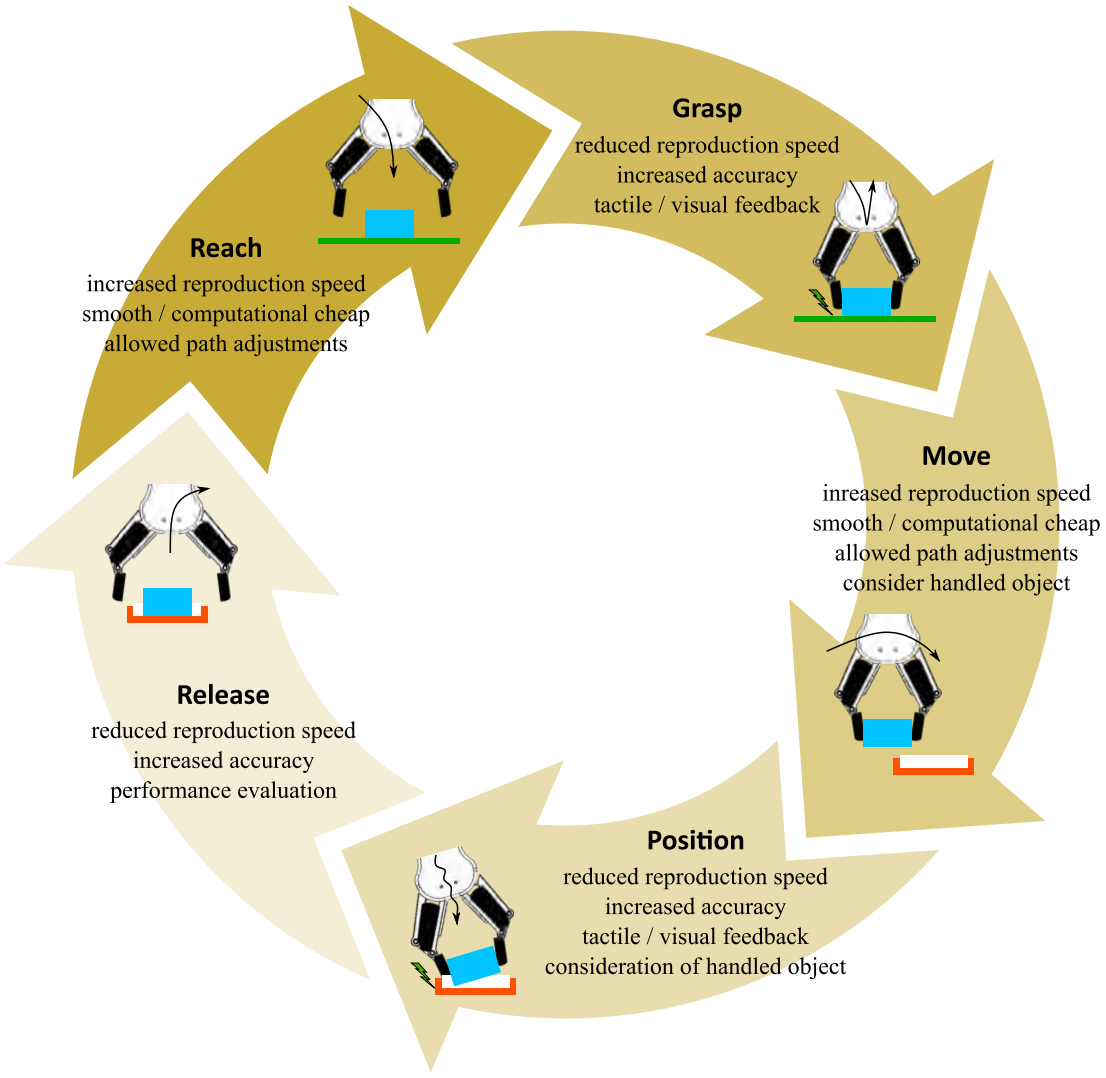

FIGURE 4.4: MTM-inspired CDMPs learning framework

demonstrated at reduced speed due to an inconvenient demonstration method. Reducing the time constant τ_{rep} provides an effortless adjustment of the robot's end-effector speed during reproduction. Since imitating the motion demonstrated with high precision is considered less important when approaching the object, it is recommended to choose a reduced number of RBFs. In doing so, a smoother trajectory is created and computational costs are reduced. The result of partially deviating from the demonstrated path is desirable, as unintentional noise that is not required for the success of the skill gets reduced. Considering that human demonstrations may not be optimal for robot kinematics due to the different kinematic structure, weights ω_n can be further optimised using Reinforcement Learning [127]. Additionally, CDMPs provide the functionality to further generalise by adjusting the resulting trajectory in case obstacles appear on its path (see Chapter 5).

Grasping

After *reaching* proximity to the object of interest, the basic element *grasping* commences. In contrast to *reaching*, this element typically takes place in a smaller space. However, it requires higher precision as a distinguishing characteristic, which dictates its success.

Based on this requirement, custom CDMPs replicating the demonstrated *grasping* are modelled with a higher number of RBFs (N). To reduce the risk of damage due to inertia forces or control limitations, a reproduction speed similar to or slower than the motion demonstrated is desirable and achievable by increasing the time constant τ_{rep}. As any relocation of the object is considered during *reaching*, the alternation does not affect *grasping*. As long as the hardware configuration allows, additional visual or force feedback may be considered to further improve accuracy, especially in the event of expected task uncertainties (see Section 2.2). Furthermore, gripper actuation may be reproduced through a set of DMPs, depending on the gripper's DoF, using the same canonical system to guarantee correct actuation timing.

Moving

Once grasped and lifted sufficiently to allow free movement, the *move* element starts to transport the object into proximity to the assembly point. As this basic element also reflects a large motion in which precision is considered less relevant, the same efficiency and generalisation ideas apply as introduced in the basic element *reach*. However, the properties of the transported object must be considered. This may include its weight, dimensions, and fragility.

In light of the requirements, the time constant τ_{rep} is adjusted appropriately. Reducing this parameter results in improved efficiency. A reduced number of RBFs (N) to reproduce the demonstration trajectory allows smoothing of shaky demonstration motions and reduces computational costs. When optimising the weights ω_n of the forcing terms $\mathbf{f}^i(s)$ through RL, as discussed for the *reaching* skill, the dimensions, fragility and weight of the object influence the reproduction. Regarding generalisation capabilities, the starting pose is provided by the ending pose of the preceding *positioning* CDMPs outcome. Adjustments to the end pose may be incorporated in real time, as discussed for the *reaching* skill. Similarly to RL augmentation, the dimensions of the workpiece affect collision avoidance methods (see Chapter 5).

Positioning

The *position* basic element describes the most challenging aspect of an assembly task. It covers the alignment, orientation, and engagement of the grasped object with its designated location relative to the assembly point. Similarly to the *grasp* element, precision is a vital factor for the success of this skill. However, a fundamental characteristic during *positioning* is the appearance of contact wrenches, which can significantly influence the appropriate execution.

To improve accuracy, a high RBFs density is recommended to replicate the demonstrated motion. Since accurate execution is of greater importance than its speed, a suitably low time constant τ_{rep} may be selected. Beyond the achievable spatial precision, the consideration of contact wrenches promises to enhance the robustness of the *positioning* skill. CDMPs provide different ways of incorporation [127].

Releasing

The *position* basic element terminates when the workpiece is aligned and orientated successfully and no interference wrenches are recorded. Once this state is reached, the *release* skill commences by actuating the gripper and ends after collision-free disengagement from the workpiece. Like the preceding *positioning* skill, a continued high precision and reduced reproduction speed characterise the *releasing* skill. An assessment of noticeable forces may be used to ensure that no intervention is made with the workpiece during disengagement.

4.3.2 Sequencing of MTM-inspired CDMPs skills

After establishing MTM-inspired CDMPs skills that are customised in their properties, their merging in transition states is discussed to be applied sequentially in complex assembly tasks. Given the method for determining standard times in MTM-1 by analysing recorded human workflows, transition states were elaborated based on changes in human states between consecutive frames. As such, the basic elements *reaching* and *moving* are distinct from others surrounding elements by incorporating any 'noticable motion' [2]. Taking into account the challenge associated with the basic element *positioning*, it includes also minor motion to perform the intended assembly step. This motion is quantified by a length of less than 1 inch. Any assembly motion that exceeds this threshold is treated as a separate *moving* element.

In the context of this work, transition states are redefined to suit the aimed LfD framework. Two options are envisioned to specify the transition states. The first option is based on the active manual specification of the human operator. This can be achieved in different ways, including additional input during the demonstration, such as vocal expressions, or generating characteristic behaviour that is identifiable in the recorded demonstration. This approach assumes that the human operator is familiar with the five predefined skills and their incorporated functionality.

Alternatively, the transition states can be automatically extracted from the given demonstration using the distances between relevant objects. As such, the human operator is not required to provide additional information or to know about the underlying skills. With respect to the five skills discussed in Section 4.3.1, this approach requires the tracking of the demonstration device, the workpiece and the assembly point. With this information, the L2-Norm is selected to calculate the distances between the relevant points. The case presented involves the distance between the demonstration device and the workpiece, the initial and current position of the workpiece, and the workpiece and the assembly point. Plateaus of identical distances over a longer time period are determined in each time series. Based on the nature of predefined skills and a common skill sequence, several plateaus are expected to occur, which are summarised in Table 4.3. Using a distance threshold for the workpiece and the assembly point, the plateaus inform the determination of the transition states.

<table>
<tr><th></th><th>distance:
demonstration device
and workpiece</th><th>distance:
workpiece's initial
and current position</th><th>distance:
workpiece and
assembly point</th></tr>
<tr><td>reaching</td><td rowspan="2">distance decreases</td><td>distance plateau</td><td>distance plateau</td></tr>
<tr><td>grasping</td><td rowspan="3">distance plateau</td><td rowspan="3">distance increases</td><td rowspan="3">distance decreases</td></tr>
<tr><td>moving</td></tr>
<tr><td>positioning</td></tr>
<tr><td>releasing</td><td>distance increases</td><td>distance plateau</td><td>distance plateau</td></tr>
</table>

TABLE 4.3: Characteristic patterns in the distances between entities of interest

The transition states between individual skills are determined from the information acquired above. In detail, the transition state between *reaching* and *grasping* is calculated from the starting state of the distance plateau between demonstrated motion and the

workpiece, and the latest penetration of the workpiece's proximity threshold. This ensures that multiple approaches without *grasping* the workpiece do not lead to false transitions. Similarly, the *grasping* skill transitions to the *moving* skill once the workpiece's barrier is penetrated again with the grasped workpiece (distance plateau between demonstrated motion and assembly point). The transition state from *moving* to *positioning* is determined from the final distance plateau between the workpiece and the assembly point and the latter's proximity threshold. As indicated in Table 4.3, the release skill begins once the final distance plateau starts between the workpiece and the assembly point. The remaining demonstrated motion is classified as either a *releasing* skill or a *reaching* skill based on the penetration of the assembly point's proximity threshold. A representative illustration of the transitions given is shown in Figure 4.5.

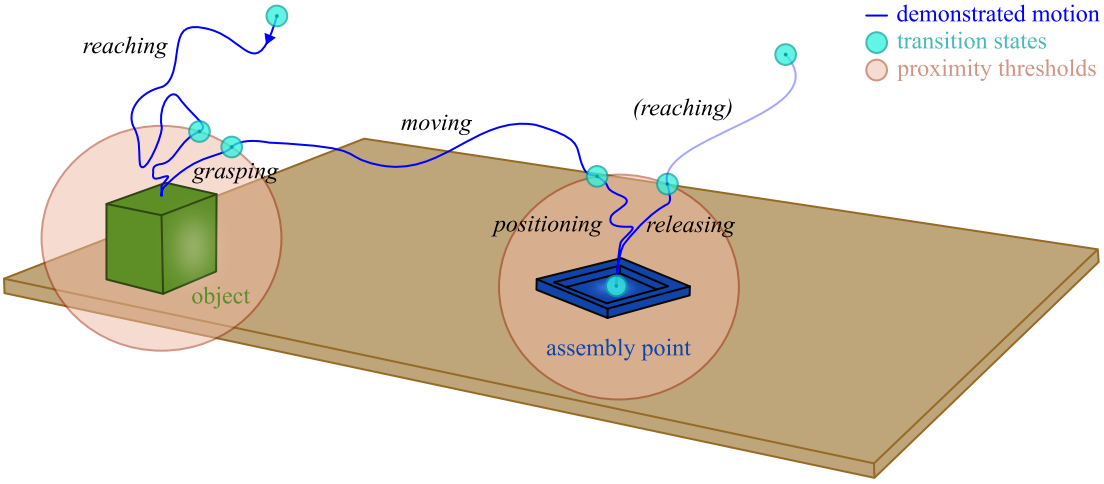

FIGURE 4.5: Illustration of distance based transition states for MTM-sequencing

After determining the transition states from a demonstrated motion, individual CDMPs skills are merged in the appropriate sequence. Section 4.1 discussed three options to combine CDMPs according to their initial and goal states. In the course of this work, the first option has been applied in all implementations, which requires a steady state at the transition states. Although this is partially not guaranteed in the sequencing approaches listed above, experimental tests show that low velocities at the transition states do not lead to negligible effects.

It should be noted that by defining the transition states distinct from the original MTM-1 system, an appropriate time comparison between assembly motions using MTM-1 methods-time data (see Appendix C.1) is not feasible. Although it promises additional advantages for industrial practice, the appropriate automatic classification of the basic MTM-1

elements of human motions recorded is non-trivial and subject of current research efforts [150, 152, 153]. The proposed learning framework and its applicability for comparison with manual labour will greatly benefit from the use of such an automatic and accurate classification algorithm, which will be investigated in future work.

4.3.3 Relocating Objects during Reproduction

The introduction of intermediate transition states, enables extended generalisation capabilities during reproduction compared to the conventional approach of learning and reproducing a demonstrated motion with a single CDMPs. Using amended values for the CDMPs parameters for initial and goal poses, the proposed learning framework is capable of coping with changes in motion resulting from distinct locations of the workpiece and the assembly point or alternated starting and end poses of the demonstration during reproduction.

The spatial scaling to a new setup is achieved by calculating the relative translational and rotational changes between demonstration and reproduction. Given the workpiece's absolute pose during demonstration $\mathbf{x}_{dem}, \mathbf{q}_{dem}$ and its absolute pose at the time of reproduction $\mathbf{x}_{rep}, \mathbf{q}_{rep}$, the relative relocation is given by

$$\mathbf{x}_{rel} = \mathbf{x}_{rep} - \mathbf{x}_{dem} \tag{4.1}$$

$$\mathbf{q}_{rel} = \mathbf{q}_{rep} \cdot \mathbf{q}_{dem}^{-1} \tag{4.2}$$

which applies similarly to the assembly point. The acquired relative poses are applied to the relevant goal parameters of the CDMPs skills, as illustrated in Figure 4.6. In detail, a relative change in the location of the workpiece affects the *reaching*, *grasping*, and *moving* goal states. The relocation of the assembly point results in a relative change of the *moving*, and *positioning* goal states. The alternate start and goal states of the desired motion are applied to the *reaching* initial state and the *releasing* goal state, respectively. As reduced accuracy may result in slightly deviated goal poses, the start pose of each skill is set to the previous CDMPs goal state.

4.4 Experimental Evaluation

By enhancing the trajectory-based CDMPs for learning and reproduction with a discretisation system allows the creation of distinctive motion segments that represent necessary

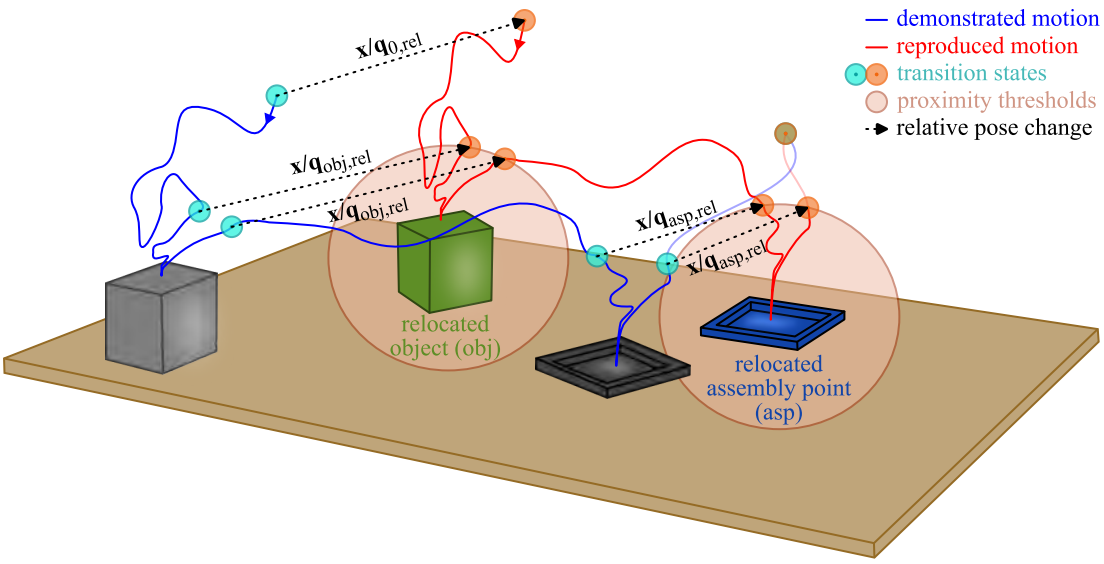

FIGURE 4.6: Illustration of how object relocation is translated into the goal states of the MTM-inspired CDMPs

skills for the success of the overall assembly task. The MTM-inspired learning framework proposed in Section 4.3 leveraged the preexisting industry-established discretisation system called MTM-1, which is commonly used to analyse and plan manual workflows in industry. As such, the developed framework used the finite library of defined basic elements, consisting of the *reaching*, *grasping*, *moving*, *positioning*, and *releasing* to propose inspired CDMPs skills to mimic human workflows by a robotic system. Unique skills were established using unique parameterisation and extensions, and different options of merging the skills to a compound assembly task were discussed.

This Section presents an experimental evaluation of the proposed learning framework on a simplified pick-and-place task. The workpiece is given by a toy dice with an equal edge length of $8cm$. The assembly point is embodied by a 3D printed part with a recess measuring $9cm \times 9cm \times 1cm$. The experimental setup consists further of a Universal Robots UR5e robot equipped with an OnRobot RG6 gripper and an ATI Axia80 F/T sensor that is installed beneath the assembly point. The setup is shown in Figure 4.7. Data points including the robot's end-effector poses and the Axia80's wrenches were recorded at 100 Hz. Offline processing of the demonstration data and CDMPs was carried out in MATLAB.

As discussed in Section 4.3.3, the proposed framework allows for the relocation of dice and/or the assembly jig, compared to the conventional one-model-fits-all approach, which is showcased in Chapter 6. Furthermore, the extension of CDMPs for collision avoidance is discussed in more detail in Chapter 5. Additional features that were expressed in

Section 4.3 but are not evaluated in any experiment are considered beyond the scope of this study and will be explored in future work.

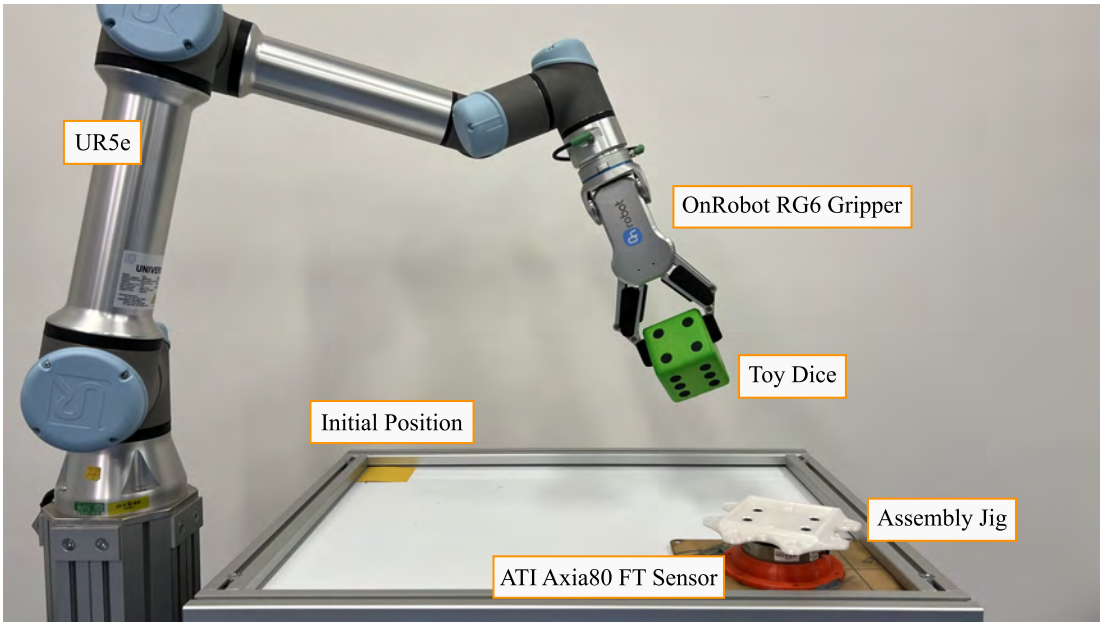

FIGURE 4.7: Experimental Setup

The human operator is tasked to pick up the dice from its initial location and place it on the stationary assembly jig. To do so, the UR5e is kinaesthetically moved during the demonstration phase using its free-drive mode. The desired transitions between the five skills were communicated by the human operator by briefly interrupting the movement. Once positioned to grasp or release the object of interest, the gripper is actuated manually using the teach-pendant. Given the single demonstration provided by the human operator performing the pick-and-place task, the proposed MTM-inspired CDMPs learning framework is compared to the conventional one-model-fits-all approach, in which a single CDMPs representation is used to imitate the entire motion demonstrated.

In view of the promising properties established from skill-dependent parameterisation, the proposed framework uses distinct values for the given MTM-inspired skills. The CDMPs were empirically parameterised to suit the given experimental setup and the task requirement. The applied values are summarised in Table 4.4. In detail, temporal scaling and reduced precision levelling were applied to the *reaching* and *moving* skills by alternating the temporal constant τ and the number of RBFs N. The spatial scaling property is incorporated by introducing an offset of +3cm in each translational dimension to the starting position of the demonstration data. All other parameters were kept the same for all skills, including stiffness gains and the canonical system parameter.

As the transition states between skills are introduced manually by interrupting movement, the naive sequencing approach of Section 4.3.2 was applied to merge the CDMPs into a compound task motion. In addition to alteration of the initial reproduction position, the goal pose of each skill served as the initial pose of its consecutive CDMPs ($x_{0,rep} = x_{T,pre}$).

	reaching	grasping	moving	positioning	releasing
temporal scaling: τ_{rep}	$\frac{1}{2}\tau_{dem}$	τ_{dem}	$\frac{1}{2}\tau_{dem}$	τ_{dem}	τ_{dem}
reproducing precision: N	10	200	10	200	200
spatial scaling: $x_{0,rep}$	$x_{0,dem} + (0.03, 0.03, 0.03)^T$	$x_{T,pre}$			
stiffness gains: K^i	100 for all i				
canonical system: α_s	T ln				
all other parameters	see guidelines in (3.4)				

TABLE 4.4: Parameterisation of the MTM-inspired CDMPs learning framework

The proposed framework was benchmarked against two conventional one-model-fits-all CDMPs. As such, the selected parameters determine the characteristic of the entire reproduced motion. The conventional models were implemented with two different precision levels quantified by the number of RBFs $N = 10$ and $N = 200$ per skill, respectively. No spatial or temporal scaling was applied to these models.

Given the demonstrated motion, both methods were processed to generate reproducing motions. The resulting comparison of the translational dimensions reproduced from the proposed framework and the one-model-fits-all approach with a low number of RBFs is shown in Figure 4.8, including the transition states and duration of each skill (see Appendix B.3 for all dimensions and models). As can be seen in Figure 4.8, the partial alteration of the temporal constant τ in the proposed learning framework during *reaching* and *moving* results in a reduced reproduction time of $10 seconds$. The $3cm$ offset introduced in each translational dimension were eliminated during *reaching* skill, demonstrating the ability of CDMPs to cope with alternate initial positions (green circles).

A jerky motion was recorded after approximately 30 seconds of demonstration (blue circles). Considered an unnecessary disturbance, approaches with a low number of RBFs demonstrate a smoothing characteristic that reduces the magnitude of the disturbance.

As appeared during the *moving* skill, this beneficial behaviour is reported in the proposed framework and the respective one-model-fits-all approach. However, the latter generates critical dips in the z-dimension in situations that require high precision, as highlighted by the red circles in Figure 4.8. On the contrary, the conventional one-model-fits-all approach with 200 RBFs per skill matches the demonstrated motion accurately, including the recorded disturbance (see Appendix B.3). Its computational costs to calculate the CDMPs weights ω_n were 36% higher than for the alternative low-precision one-model-fits-all approach. Compared to the low-precision approach, the MTM-inspired CDMPs learning framework increased computational costs by only 6%.

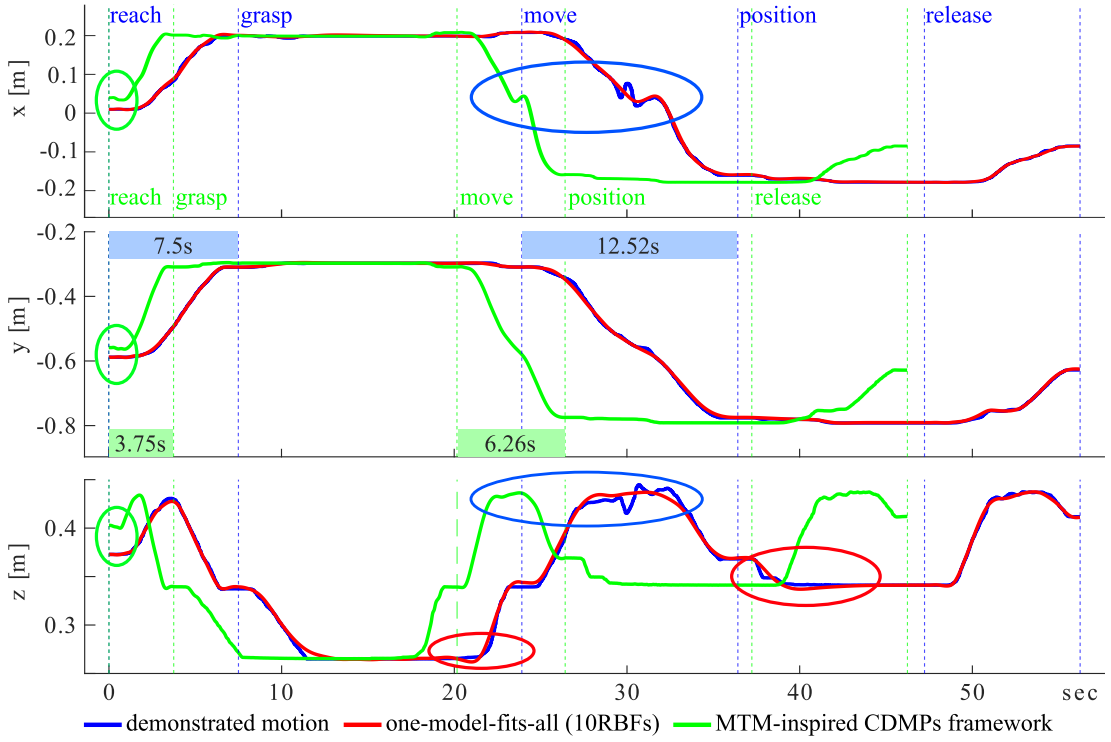

FIGURE 4.8: Trajectory comparison in translational dimensions

Given the additional F/T sensing capability at the assembly point, a qualitative assumption was derived from the assembly process. Figure 4.9 shows the measured forces in the z-direction during the *position* skill of the proposed learning framework. Based on a post-assessment of the force profile, the data verifies that the dice was successfully placed onto the assembly point through an identical end value. Furthermore, the forces that occurred during reproduction did not exceed those during the demonstration, suggesting a damage-free task reproduction. It is to be noted that the reduced force was not actively achieved but resulted from slight positional deviation during reproduction that turned out

favourably. In case a larger force is recorded, its active incorporation into CDMPs may be necessary as proposed in Section 4.3.

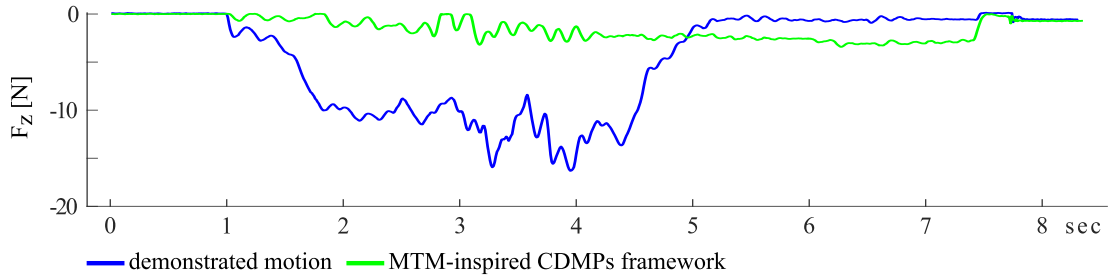

FIGURE 4.9: Recorded forces in z-dimension during *positioning* skill

In summary, the distinction between the five basic elements of MTM-1 and the design of characteristic CDMPs brings the decisive benefit of focussing on their unique requirements, paving the way for tackling complex and compound assembly tasks.

4.5 Summary

Following the dominant trend in assembly-related LfD approaches in applying learning methods with trajectorial outcome, these techniques lack the ability to reproduce complex tasks. Previous proposed extensions with predefined skill sets are often use case-specific and not appropriately defined for the variety of tasks potentially encountered during industrial assembly. Furthermore, the full potential of trajectory-based learning frameworks is rarely exploited in the design of discrete skills.

This Chapter presented a novel LfD learning framework that addresses these limitations by leveraging an industry-established discretisation system. Given the targeted application scenario and the accessible features of the systems, the Methods-Time Measurement (MTM-1) framework was determined to be the most suitable due to its intuitive skill set, its profound industry-proven compactness, and its potential extension to time analysis. By distinguishing discrete skills *reaching*, *grasping*, *moving*, *positioning* and *releasing*, the proposed MTM-inspired CDMPs learning framework defines unique CDMPs for each skill using their parameterisation and proven extensions. As a result, greater generalisability, comparison with human workflows, and time efficiency are promoted. The proposed method was evaluated on a pick-and-place assembly task, showing decisive benefits compared to the conventional one-model-fits-all CDMP approach. These include appropriate

time management, appropriate accuracy in the relevant periods of the assembly task, and force monitoring at the relevant times.

Chapter 5

Dynamic Potential Fields for Robust Reproduction

The last phase of the characteristic LfD procedure involves translating the learnt task understanding into physical motion on the robotic system, a step called *reproduction*. This is accompanied by the expectation that state-of-the-art LfD frameworks are capable of autonomously dealing with new circumstances without tedious reprogramming. A prominent aspect in this context is to incorporate an adequate response to changes in motion, which refers to spatial and temporal adjustment of the reproducing trajectory. The learning framework presented in Chapter 4 addressed this type of change through the inherent generalisability of CDMPs in combination with the discretisation system. As a result, demonstrated motions are translated to topologically similar reproduction motions considering new situations that are spatially and/or temporally scaled.

An additional beneficial capability of LfD solutions is depicted in coping with changes in the environment. In envisioning its application to realistic industrial scenarios, obstacles may be introduced during reproduction due to the dynamic surrounding or by relocating the objects of interest such that naive reproduction following a topologically similar path results in collision. An illustrated example of the latter situation is shown in Figure 5.1, in which the relocation of the workpiece and assembly point causes a motion that penetrates an environmental obstacle. As a result, a dynamic response during reproduction in new environments is necessary to deal effectively with environmental changes. As discussed in Chapter 4, this challenge is particularly present in larger displacements that occur during the proposed reaching and moving skills. As such, the proposed learning framework promoted the application of collision avoidance techniques in these custom CDMPs.

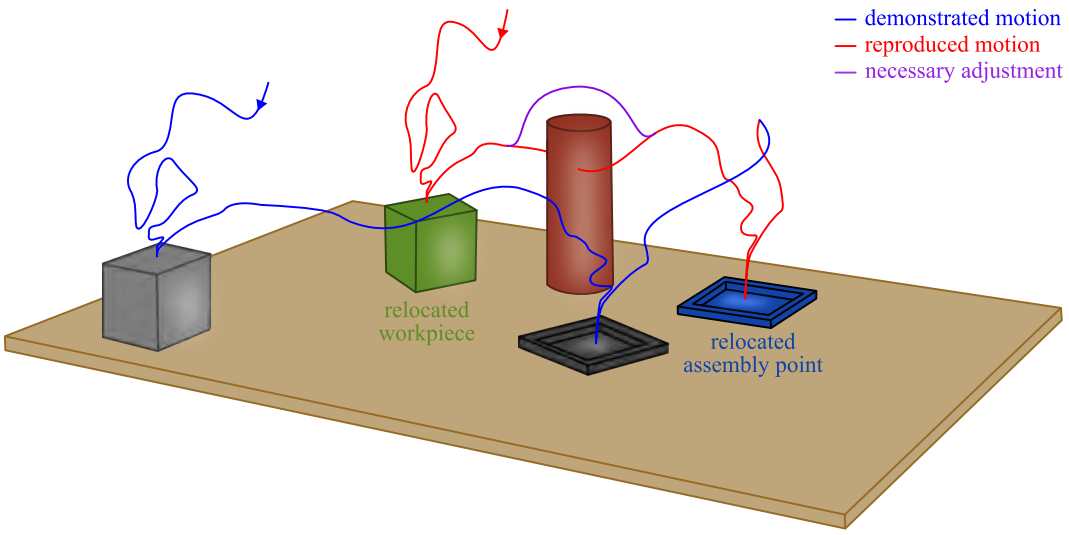

FIGURE 5.1: Illustrative example of topologically similar reproduction resulting in collision with the environment

In light of the depicted scenario, existing extensions of CDMPs for collision avoidance show promising approaches to encounter changes in the environment during reproduction. However, these methods consider a point-based trajectory that results in a purely translational deviation of the given path. Furthermore, only physical obstacles are considered, which limits the ability to adequately model the situation encountered. This Chapter investigates how learnt CDMPs-based trajectories can be increased in robustness during reproduction when faced with changed environmental situations by following one of the prevailing approaches that is based on potential fields. These are generated from modelled obstacles using superquadrics as volumetric approximations, resulting in repulsive forces that act on the reproducing path. The presented reproduction method extends existing approaches by representing the moving object of interest, in this case the robot's end-effector, as a volumetric entity. This allows for the exploitation of rotational deviations (provided that the application allows for it), making the reproduced motion more effective. Furthermore, the environmental model is extended by an imaginary workspace boundary and an attractive goal state. These are applied to robustly restrict the deviating path within the robot's expected workspace and create an attractive well for assisting the CDMPs-driven convergence to the desired final state.

This Chapter is structured as follows: After reviewing existing approaches to avoid collisions using CDMPs in Section 5.1, some technical fundamentals of the applied methods are presented in Section 5.2. Extending existing work, Section 5.3 proposes an approximation scheme of the environment with superquadrics by defining four types of object and

their separation distances. The latter serve as driving variables in the consecutive establishment of potential fields, and repulsive / attractive wrenches acting on the end-effector (see Section 5.4). The method developed for robust reproduction based on potential fields is evaluated in Section 5.5 and summarised in Section 5.6. This Chapter was derived from [27].

5.1 Related Work on Obstacle Avoidance with DMPs

Due to its benefits for safe operation of robots, obstacle avoidance is a highly researched field in robotics. Motion planning techniques to encounter changes in the environment differ predominantly based on their computational complexity, local or global considerations, and determinism versus probabilistic characteristic [168]. Solutions can be classified into five main categories: graph-based path planner, data-driven control, optimal control, collision control, and deterministic reactive obstacle avoidance. In the context of industrial scenarios, local, fast and deterministic approaches are preferable which is predominantly achieved by techniques within the latter category. Such techniques have also been dominantly investigated to create deviating motions that are directly incorporated into DMPs. A significant share of proposed approaches for extending DMPs with collision avoidance is held by real-time consideration of artificial forces acting on the reproducing trajectory through an additional forcing term in the DMPs transformation system. Illustrated on the single dimension formulation after (3.1), the extended transformation system reads

$$\begin{aligned} \tau\,\dot{\tilde{v}} &= K\,(\,x_T\,-\,x\,)\,-\,D\,\tilde{v}\,-\,K\,(\,x_T\,-\,x_0\,)\,s\,+\,K\,f(s)+\varphi_{\tilde{a}} \\ \tau\,\dot{x} &= \tilde{v}+\varphi_{\tilde{v}} \end{aligned} \tag{5.1}$$

where the additional variables are commonly referred to as coupling terms on the acceleration level $\varphi_{\tilde{a}}$ and on the velocity level $\varphi_{\tilde{v}}$. Methods exploiting this approach differ in the way the coupling term is calculated. Two approaches in particular have proved popular in research, utilising so-called potential fields and steering angles.

The first approach was promoted by Park et al. in 2008 [169], in which existing work on potential fields [170, 171] was applied to DMPs to avoid punctiform obstacles. The artificial potential field was sourced from the relative distance between the pointwise-modelled end-effector's and obstacle's positions and used to compute repulsive accelerations to manoeuvre the end-effector. The expression of initially point-based objects to

generate potential fields was recently extended by Ginesi et al. to non-pointwise, volumetric obstacles [172, 173]. To achieve this, a mathematical approximation of the object's contour was considered by modelling them with the so-called superquadrics. These methods were applied to different use cases, such as avoiding link collision by considering several points along the structure of the robot arm [174], joint manoeuvring of two robots due to task-required coupled motion [175–177], or navigating an arm-base robotic system around obstacles [178]. It has further inspired the development of application-specific potential fields [124] and the artificial online adaptation of the goal that converts to its destination while avoiding collision with a disturbing obstacle [179].

A similarly popular alternative was first introduced to DMPs by Hoffmann et al. [118] in 2009, who applied a modelled human-inspired behaviour for collision avoidance after [180]. This approach computes the steering angle between the end-effector's current velocity vector and the relative position vector between the end-effector and the obstacle. This approach was applied to various use cases, including bimanual tasks using coupling terms on the velocity and acceleration level [121, 181], and the navigation of mobile [182] and continuum robots [183, 184]. The original steering angle method was also extended with an impedance mechanism for smooth manoeuvring [185], for consideration in a hybrid joint / Cartesian framework [186] and with an appropriate parameterisation method to result in more effective avoidance trajectories [187, 188]. Recent approaches proposed its combination with superquadrics for effective consideration of volumetric obstacles [189] and with potential fields to merge both prevailing collision avoidance methods [190].

Some alternative approaches were proposed in addition to the prevailing methods discussed above. The so-called stylistic DMPs proposed by Matsubara et al. extend the set of path-shaping weights ω_n with a style parameter expressed by a probability distribution [191]. Based on multiple demonstrated trajectories, Stulp et al. developed a selection algorithm for the most suitable path to avoid collision with a given obstacle [192, 193]. Finally, a set of methods investigates ML-driven collision avoidance [194–198]. However, the latter typically requires an additional learning phase in order to respond appropriately to distinct environmental scenarios, which is not in the interest of the aimed efficient LfD framework and therefore not considered in the scope of this thesis.

Solutions utilising potential fields and steering angles have reached a solid standing in DMPs research for collision avoidance. The steering angle approach provides the advantage of guaranteed convergence to the goal position for arbitrarily-many static obstacles [199]. However, it is only applicable in ambient space (not joint space), and the repulsive forces sourced from obstacles are not dependent on its distance, giving any obstacle the same

importance which may result in oscillatory behaviour [172]. On the contrary, collision avoidance using potential fields does not always guarantee convergence, as the moving point may become caught in local minima [173, 200]. However, this is only possible if multiple obstacles occlude the path [201] and may be solved by introducing an additional perturbation term that releases the trajectory from these local minima in a way similar to that in which repulsive forces are integrated into the DMPs [172].

In terms of the recent trend of using superquadrics for the volumetric representation of obstacles [172, 173, 189, 201–203], it provides a decisive advantage in contrast to the previous representation of obstacles by points. Incorporating the volumetric expansion of obstacles using point clouds can lead to significant computational costs, making an instant response more challenging [189], and selecting critical points may result in non-smooth behaviour due to the need of reselecting in real time [173]. Therefore, the compact mathematical approximation of volumetric objects with superquadrics is considered beneficial, which further allows the fitting of most generic shapes with a low number of required parameters [172].

Considering the prevalent advantages that can be attributed to potential fields sourced from volumetric obstacle representations with superquadrics, this work elaborates further promising features to improve its effectiveness and robustness in realistic scenery. This includes, particularly, the modelling of the end-effector as a volumetric entity. While previous approaches considered the end-effector's expansion in artificially inflated volumetric obstacles or more conservative parameterisation of the coupling term, this approach represents the environment more accurately and enables the exploitation of rotational deviation for improved efficiency. Additionally, the set of considered object types emitting potential fields is extended to an imaginary workspace boundary and an attractive goal. This Chapter investigates these beneficial features and proposes an extension of CDMPs that promotes robust reproduction in alternated environmental scenery using potential fields between multiple superquadrics.

5.2 Fundamentals on Potential Fields and Superquadrics

Potential fields applied within the context of DMPs are generally based on the idea of expressing an increase in the calculated potential value when the distance between two entities decreases. Considering the intention of avoiding a collision of the robot's end-effector at position $\mathbf{x}$ with an obstacle, Khatib et al. initially proposed the application of

a simplified Force Inducing an Artificial Repulsion from the Surface (FIRAS) function for a potential field [170], which reads:

$$U_{stat,p}(\mathbf{x}) = \begin{cases} \frac{\zeta}{2}\left(\frac{1}{p(\mathbf{x})} - \frac{1}{p_0}\right)^2 & p(\mathbf{x}) \leq p_0 \\ 0 & p(\mathbf{x}) > p_0 \end{cases} \tag{5.2}$$

where $p(\mathbf{x})$ is the shortest distance between the end-effector and the obstacle and p_0 represents the region of desired influence. Park et al. outlined in [169] an issue of such a static potential field as non-smooth behaviour may be produced and suggested the inclusion of the end-effector's velocity $\mathbf{v}$ and direction of movement relative to the object's location θ. As a result, the following dynamic potential function was proposed.

$$U_{dyn,p}(\mathbf{x}, \mathbf{v}) = \begin{cases} \lambda(\cos(\theta)^{\iota} \frac{\|\mathbf{v}\|}{p(\mathbf{x})} & \frac{\pi}{2} < \theta < \pi \\ 0 & 0 \leq \theta \leq \frac{\pi}{2} \end{cases} \quad with \quad \cos\theta = \frac{\mathbf{v}^T\mathbf{x}}{\|\mathbf{v}\|p(\mathbf{x})} \tag{5.3}$$

Due to the disadvantages encountered with point-based object approximations, Ginesi et al. introduced in [172, 173] superquadrics as a volumetric approximation of obstacles to compute potential fields, following the trend of related contributions [201, 204]. Superquadrics are a family of parametric shapes that were initially proposed for computer graphics design [205] and incorporate shapes such as superellipsoids, superhyperboloids, and supertoroids [206]. Following its prominence in the literature, this work refers to superquadrics as a synonym for applied superellipsoids. They are mathematically expressed by the so-called inside-outside function $F(\mathbf{x}_B)$ [206] that reads

$$F(\mathbf{x}_B) = \left[\left(\frac{x_B}{a}\right)^{\frac{2}{\varepsilon_2}} + \left(\frac{y_B}{b}\right)^{\frac{2}{\varepsilon_2}}\right]^{\frac{\varepsilon_2}{\varepsilon_1}} + \left(\frac{z_B}{c}\right)^{\frac{2}{\varepsilon_1}} \tag{5.4}$$

where the parameters a, b, c are the volumetric expansion in each dimension (radii) and $\varepsilon_{1,2}$ represent the shape parameters that determine the superquadrics' roundness. Figure 5.2 shows some examples of superquadrics with distinct roundness parameters. Given any point at the location $\mathbf{x}_B$ in the superquadric's canonical coordinate system, F quantifies the isometric distance from its surface to that point. In detail, $F = 1$ indicates that the point lies on the superquadric's contour, while $F < 1$ and $F > 1$ specify that it is inside or outside the shape, respectively.

Given any point at $\mathbf{x}_B$, the scaled vector to this point that intersects the surface of the superquadrics is called $\mathbf{r}_s$ and is defined by $\mathbf{r}_s = \beta\mathbf{x}_B$ with $F(\mathbf{r}_s) = 1$. The scalar β is

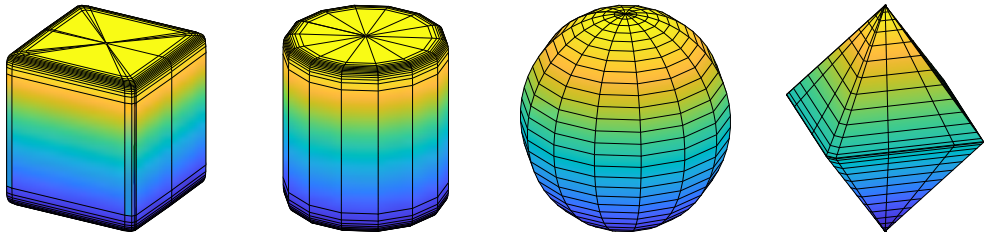

(A) $\varepsilon_1 = 0.1$, $\varepsilon_2 = 0.1$ (B) $\varepsilon_1 = 0.1$, $\varepsilon_2 = 1.0$ (C) $\varepsilon_1 = 1.0$, $\varepsilon_2 = 1.0$ (D) $\varepsilon_1 = 2.0$, $\varepsilon_2 = 2.0$

FIGURE 5.2: Examples of superquadrics with different ε_i

derived according to [206] as follows:

$$\begin{aligned} F(\beta \mathbf{x}_B) &= \left[\left(\frac{\beta x_B}{a} \right)^{\frac{2}{\varepsilon_2}} + \left(\frac{\beta y_B}{b} \right)^{\frac{2}{\varepsilon_2}} \right]^{\frac{\varepsilon_2}{\varepsilon_1}} + \left(\frac{\beta z_B}{c} \right)^{\frac{2}{\varepsilon_1}} = F(\mathbf{r}_s) \stackrel{!}{=} 1 \\ \Rightarrow \beta \; &= F(\mathbf{x}_B)^{\frac{\varepsilon_1}{2}} \end{aligned} \tag{5.5}$$

To express the inside-outside function of any superquadric with its absolute position $\mathbf{x} = [x, y, z]$, orientation $\mathbf{q} = [q_x, q_y, q_z, q_w]$ and the position of the point $\mathbf{p} = [p_x, p_y, p_z]$ in a given coordinate system, the following homogeneous transformation proposed by [201, 207] is applied to determine $\mathbf{x}_B$ in its canonical coordinate system:

$$\begin{bmatrix} x_B \\ y_B \\ z_B \end{bmatrix} = \underbrace{\begin{bmatrix} q_x^2 - q_y^2 - q_z^2 + q_w^2 & 2(q_x q_y + q_z q_w) & 2(q_x q_z - q_y q_w) \\ 2(q_x q_y - q_z q_w) & -q_x^2 + q_y^2 - q_z^2 + q_w^2 & 2(q_y q_z + q_x q_w) \\ 2(q_x q_z + q_y q_w) & 2(q_y q_z - q_x q_w) & -q_x^2 - q_y^2 + q_z^2 + q_w^2 \end{bmatrix}}_{\mathbf{A}(\mathbf{q})} \begin{bmatrix} x - p_x \\ y - p_y \\ z - p_z \end{bmatrix} \tag{5.6}$$

Leveraging on the property of superquadrics to generate spherical isopotential contours at large distances and shape-mimicking isopotentials in proximity [204], Ginesi et al. applied in [172] the Yukawa function [204] as the mathematical expression for a static potential field, which reads

$$U_{stat,vol}(\mathbf{x}) = \frac{A e^{-\zeta C(\mathbf{x})}}{C(\mathbf{x})} \tag{5.7}$$

where $C(\mathbf{x})$ denotes the distance between the robot's representing point and the surface of the obstacle, i.e. $C(\mathbf{x}) = F(\mathbf{x}_B) - 1$. Mimicking the dynamic potential function (5.3) for point-based potential fields, the converted formula for volumetric obstacles was proposed

as [173]:

$$U_{dyn,vol}(\mathbf{x},\mathbf{v}) = \begin{cases} \lambda(-\cos\theta)^{\beta}\frac{\|\mathbf{v}\|}{C^{\eta}(\mathbf{x})} & \frac{\pi}{2} < \theta < \pi \\ 0 & 0 \leq \theta \leq \frac{\pi}{2} \end{cases} \qquad with \;\; \cos\theta = \frac{\langle \nabla C(\mathbf{x}), \mathbf{v}\rangle}{\|\nabla C(\mathbf{x})\|\|\mathbf{v}\|} \tag{5.8}$$

Independent of the utilised potential field, the guiding repulsive force to avoid collision with the modelled obstacle is generated by the negative derivative of the given potential function:

$$\varphi_{\tilde{a}} = -\nabla_{\mathbf{x}}\left[U_i\right] \qquad with \;\; \nabla_{\mathbf{x}} = \left[\frac{\partial}{\partial x}\,,\, \frac{\partial}{\partial y}\,,\, \frac{\partial}{\partial z}\right] \tag{5.9}$$

5.3 Scene Approximation using Superquadrics

Based on the intended goal of improving robustness and effectiveness when encountering a new situation during robot reproduction, this Section presents an extended modelling approach to approximate the environmental scene. Contrary to the simplified interpretation of previous approaches, effectiveness is achieved through the consideration of a volumetric robot end-effector allowing the simultaneous exploitation of its translational and rotational freedom of movement. Following the prominent approach of approximating any physical obstacle in the scene of interest [173], the set of object types is extended by an imaginary workspace boundary and an imaginary shape specifying the end-effector's final state.

These four types of volumetric shapes are approximated by superquadrics to generate a simplified representation of the scene, which is illustrated as an example in Figure 5.3. To achieve robust reproduction, the end-effector is to manoeuvre in the given space such that its volume remains at any time outside of the volume occupied by the obstacle, within the volume representing the workspace, and finally converges toward the volume given by the goal shape. For simplification, the following references to any type of object refer to the volume approximated by its superquadric if not otherwise specified.

Following the general idea of potential fields, a collision-avoiding motion in a scene as illustrated in Figure 5.3 is driven by the distance between the given entities. Considering that the scene is created from multiple volumetric shapes, the separation distance between those is affected by their relative position and orientation, which is referred to as the attitude-distance effect in [201]. As such, the inside-outside function of each given superquadric is translated from its typical canonical coordinate system to a specified world coordinate system with absolute poses. Following the homogeneous transformation in

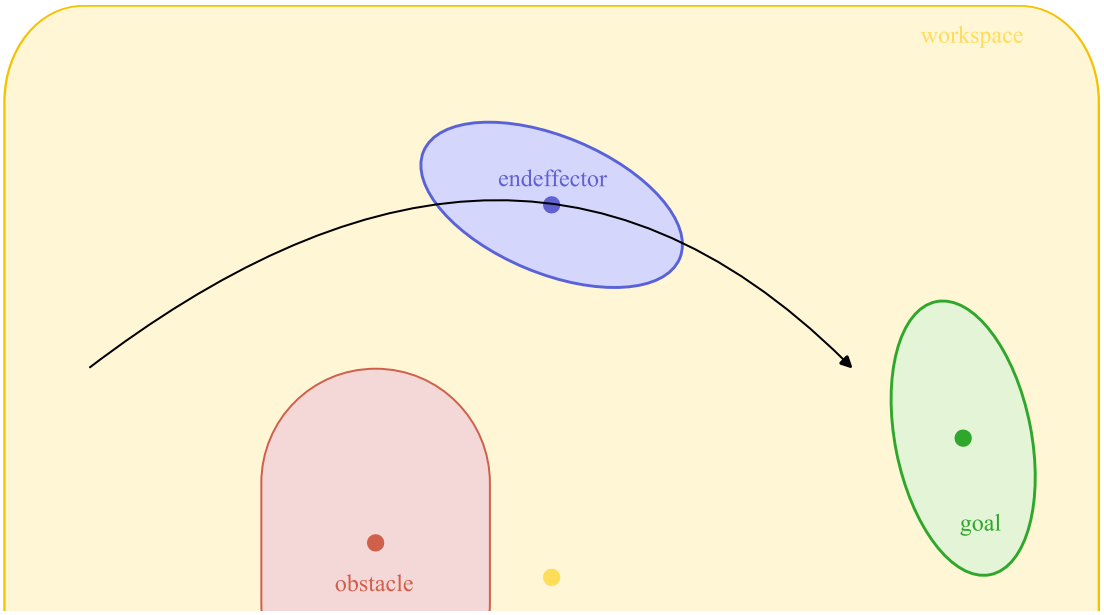

FIGURE 5.3: Illustration of the approximated scene encountered during reproduction based on superquadrics representing the end-effector, obstacles, workspace, and the goal state

(5.6), the inside-outside function for the four types of object reads:

$$F_i = \left[\left(\frac{x_{B,i}}{a_i} \right)^{\frac{2}{\varepsilon_{2,i}}} + \left(\frac{y_{B,i}}{b_i} \right)^{\frac{2}{\varepsilon_{2,i}}} \right]^{\frac{\varepsilon_{2,i}}{\varepsilon_{1,i}}} + \left(\frac{z_{B,i}}{c_i} \right)^{\frac{2}{\varepsilon_{1,i}}} \quad , \quad \mathbf{x}_{B,i} = \mathbf{A}(\mathbf{q}_i) * (\mathbf{x}_i - \mathbf{p})$$

$$F_i(\mathbf{x}_i, \mathbf{q}_i, \mathbf{p}) = \left[H_{1,i}(\mathbf{x}_i, \mathbf{q}_i, \mathbf{p})^{\frac{2}{\varepsilon_{2,i}}} + H_{2,i}(\mathbf{x}_i, \mathbf{q}_i, \mathbf{p})^{\frac{2}{\varepsilon_{2,i}}} \right]^{\frac{\varepsilon_{2,i}}{\varepsilon_{1,i}}} + H_{3,i}(\mathbf{x}_i, \mathbf{q}_i, \mathbf{p})^{\frac{2}{\varepsilon_{1,i}}} \tag{5.10}$$

where i refers to the end-effector ee, the obstacle obs, the workspace ws, or the goal state g and $\mathbf{p}$ is the absolute position of any point of interest.

In this work, it is assumed that the robot's end-effector is dynamically moving in the given space while the three other shapes remain stationary. Therefore, the separation distance of interest is defined between the end-effector and the other affecting shapes. Badawy et al. proposed in [201] four different approaches to approximate the distance with superquadric shapes. In the given context concerning the separation distance between two superquadrics, the so-called rigid body radial Euclidean distance applies. This method determines the separation distance between two superquadrics along the line that passes through the centre positions $\mathbf{x}_i$ of each superquadric. Following the illustrative derivation for the case of an affecting obstacle given in Figure 5.4a, the distance d_{obs} between the shape of the end-effector and the obstacle is calculated from the distance between the

centres $\mathbf{c}_{ee,obs}$ and the intersecting vectors $\mathbf{r}_{s,i}$ of both superquadrics and reads

$$d_{obs} \;=\; \|\mathbf{c}_{ee,obs}\| \;-\; \|\mathbf{r}_{s,ee}\| \;-\; \|\mathbf{r}_{s,obs}\| \tag{5.11}$$

By utilising the centre's position of the opposite's superquadric as the point of interest $\mathbf{p}$ in (5.10) and applying (5.5), (5.11) is simplified by expressing the intersecting vector through the inside-outside function and the scalar β_i. The separation distance between the end-effector and an obstacle is quantified as follows:

$$\begin{aligned} d_{obs} &= \|\mathbf{c}_{ee,obs}\| \;-\; \beta_{ee}\|\mathbf{c}_{ee,obs}\| \;-\; \beta_{obs}\|\mathbf{c}_{obs,ee}\| \\ &= \|\mathbf{c}_{ee,obs}\| \cdot \left[1 - F_{ee,obs}(\mathbf{x}_{ee}, \mathbf{q}_{ee}, \mathbf{x}_{obs})^{-\frac{\varepsilon_{1,ee}}{2}} - F_{obs,ee}(\mathbf{x}_{obs}, \mathbf{q}_{obs}, \mathbf{x}_{ee})^{-\frac{\varepsilon_{1,obs}}{2}}\right] \\ &\quad with\;\; \mathbf{c}_{ee,obs} = [x_{ee} - x_{obs}\;,\; y_{ee} - y_{obs}\;,\; z_{ee} - z_{obs}]^T \end{aligned} \tag{5.12}$$

With the intention of keeping the end-effector within the space occupied by the workspace, the separation distance between the end-effector and the workspace boundary is derived in a similar fashion. Here, the superquadric's symmetry property is applied, in which any intersecting vector $\mathbf{r}_s$ as in (5.5) is equal in length with the vector facing in the opposite direction. This is used to quantify the approximate distance between the superquadric's contours, as illustratively derived with the given approach in Figure 5.4b. It results in the following equation for d_{ws}, simplified with the inside-outside functions and the scaling parameter β_i:

$$\begin{aligned} d_{ws} &= \|\mathbf{r}_{s,ws}\| \;-\; \|\mathbf{r}_{s,ee}\| \;-\; \|\mathbf{c}_{ee,ws}\| \\ &= \beta_{ws}\|\mathbf{c}_{ws,ee}\| \;-\; \beta_{ee}\|\mathbf{c}_{ee,ws}\| \;-\; \|\mathbf{c}_{ee,ws}\| \\ &= \|\mathbf{c}_{ee,ws}\| \cdot \left[F_{ws,ee}(\mathbf{x}_{ws}, \mathbf{q}_{ws}, \mathbf{x}_{ee})^{-\frac{\varepsilon_{1,ws}}{2}} - F_{ee,ws}(\mathbf{x}_{ee}, \mathbf{q}_{ee}, \mathbf{x}_{ws})^{-\frac{\varepsilon_{1,ee}}{2}} - 1\right] \\ &\quad with\;\; \mathbf{c}_{ee,ws} = [x_{ee} - x_{ws}\;,\; y_{ee} - y_{ws}\;,\; z_{ee} - z_{ws}]^T \end{aligned} \tag{5.13}$$

The attractive goal is envisioned to function as a well that pulls the end-effector towards the volume occupied by its superquadric. Since in this case the overlapping of the two superquadrics is desired, the separation distance from the end-effector to the goal state volume is defined between the goal facing contour of the end-effector and the goal's contour on the opposite side. Using the approaches discussed above, this distance is quantified by

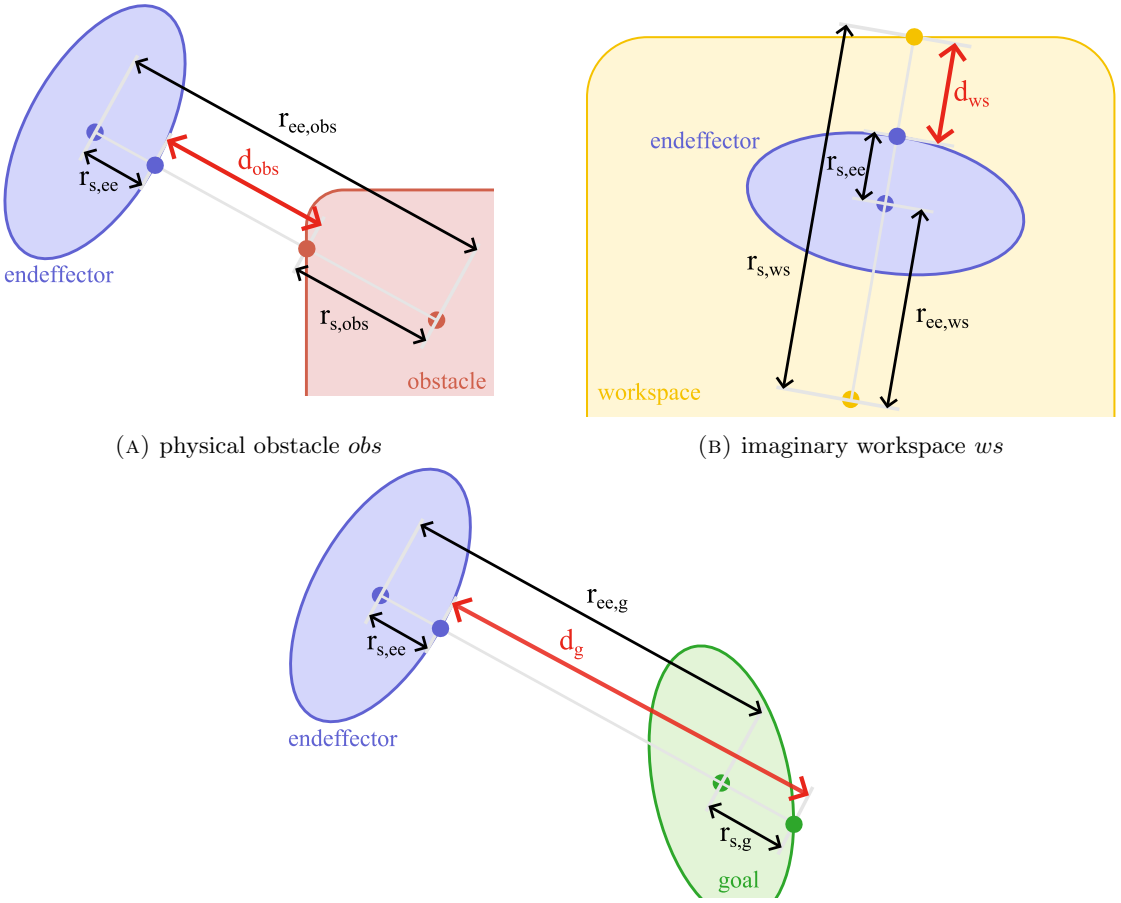

(A) physical obstacle *obs*

(B) imaginary workspace *ws*

(C) imaginary goal *g*

FIGURE 5.4: Illustration of the applied methods to approximate the seperation distances between the end-effector and surrounding environmental volumes

the method illustrated in Figure 5.4c and reads

$$\begin{aligned} d_g &= \|\mathbf{c}_{ee,g}\| - \|\mathbf{r}_{s,ee}\| + \|\mathbf{r}_{s,g}\| \\ &= \|\mathbf{c}_{ee,g}\| - \beta_{ee}\|\mathbf{c}_{ee,g}\| + \beta_c\|\mathbf{c}_{g,ee}\| \\ &= \|\mathbf{c}_{ee,g}\| \cdot \left[1 - F_{ee,g}(\mathbf{x}_{ee}, \mathbf{q}_{ee}, \mathbf{x}_g)^{-\frac{\varepsilon_{1,ee}}{2}} + F_{g,ee}(\mathbf{x}_g, \mathbf{q}_g, \mathbf{x}_{ee})^{-\frac{\varepsilon_{1,g}}{2}}\right] \\ &\textit{with}\ \ \mathbf{c}_{ee,g} = [x_{ee} - x_g\ ,\ y_{ee} - y_g\ ,\ z_{ee} - z_g]^T \end{aligned} \tag{5.14}$$

Applying the proposed distance approximation to the envisioned scene, the separation distances between the end-effector and the surrounding environmental volumes are quantified by the mathematical expressions given in (5.12), (5.13), and (5.14) and illustratively visualised in Figure 5.5. Over the course of motion, the inside-outside functions concerning the obstacle ($F_{ee,obs}$,$F_{obs,ee}$) remain > 1, the functions including the workspace boundary

remain < 1 and the goals' functions eventually shift from values above one to zero.

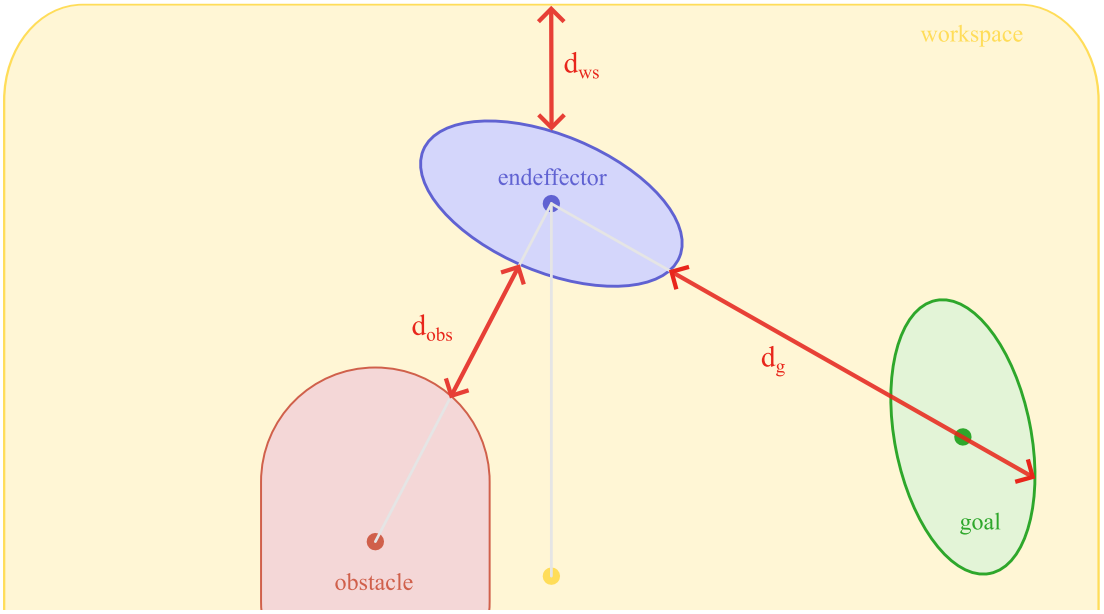

FIGURE 5.5: Illustration of the approximated distances within the given scene

5.4 Reactive Control using distance-driven Potential Fields

Following the established approximation of an encountered scene discussed in Section 5.3, four types of objects were introduced. Their relationship in the form of an analytically formulated separation distance was approximated using the rigid body radial Euclidean distance approach. In this Section, the distance is applied in a proposed modification for the creation of potential fields and their driving repulsion and attraction under consideration of the end-effector's six-dimensional freedom of motion. The method's application to CDMPs during LfD reproduction is formulated to manoeuvre a dynamic volume collision-free through the encountered scene and converging toward its final state.

Based on the existing work, the dynamic potential field after (5.8) is considered for the given path planning task. This function was originally derived from the following desired properties P1-3, as stated in [173]:

- *P1*: The magnitude of the potential decreases with the distance of the system from the obstacle
- *P2*: The magnitude of the potential increases with the velocity of the system $\|\mathbf{v}\|$ and is zero when the system is not moving.

- *P3*: The magnitude of the potential decreases with the angle between the current velocity direction $\mathbf{v}/\|\mathbf{v}\|$, and the direction towards the obstacle; and, if the system is moving away from the obstacle, the potential should vanish.

Mimicking this in the given context using the separation distance between the end-effector and the obstacle or the workspace boundary d_i with $i \in (obs, ws)$ creates the potential field function

$$U_{ee,i} \;=\; -\,\lambda \underbrace{(-\cos\theta_i)^{\iota}}_{P3} \overbrace{\frac{\|\mathbf{v}\|}{d_i^{\eta}}}^{P2}_{P1} \qquad with \;\; \cos\theta_i = \frac{\langle \nabla d_i, \mathbf{v} \rangle}{\|\nabla d_i\| \|\mathbf{v}\|} \tag{5.15}$$

for $\frac{\pi}{2} < \theta_i < \pi$ which translates to repulsive forces acting on the end-effector by applying (5.9) such that

$$\begin{aligned} \varphi \;&=\; -\,\nabla_{\mathbf{x}} \left[\, U_{ee,i} \,\right] \\ &=\; -\,\nabla_{\mathbf{x}} \left[\, \lambda (-\cos\theta_i)^{\iota} \, \frac{\|\mathbf{v}\|}{d_i^{\eta}} \,\right] \\ &=\; -\lambda \nabla_{\mathbf{x}} \left[(-\cos\theta_i)^{\iota} \right] \frac{\|\mathbf{v}\|}{d_i^{\eta}} + (-\cos\theta_i)^{\iota} \nabla_{\mathbf{x}} \|\mathbf{v}\| \left[\frac{1}{d_i^{\eta}} \right] \end{aligned} \tag{5.16}$$

To exploit the full potential of the end-effector's movement, the method discussed in Section 5.3 modelled the end-effector as a volumetric entity. As such, the expressed repulsion is to be computed for a six-dimensional wrench that covers translational and rotational variables. As this work assumes a dynamic movement of the end-effector and stationary obstacles, workspaces, and goals, the derivation refers to the absolute pose variables of the end-effector. Therefore, the original derivation operator in (5.9) is extended to rotational dimensions as expressed in (5.17). Concerning the properties P2/3 in (5.15), the rotational dimensions are also embedded in an extended velocity vector $\check{\mathbf{v}}$ as defined in (5.18). Note that the fourth rotational dimension is indirectly considered due to the intrinsic dependence of the quaternion variables [201].

$$\nabla_{\mathbf{x},\mathbf{q}} \;=\; \left[\frac{\partial}{\partial x_{ee}} \,,\, \frac{\partial}{\partial y_{ee}} \,,\, \frac{\partial}{\partial z_{ee}} \,,\, \frac{\partial}{\partial q_{x,ee}} \,,\, \frac{\partial}{\partial q_{y,ee}} \,,\, \frac{\partial}{\partial q_{z,ee}} \right]^T \tag{5.17}$$

$$\check{\mathbf{v}} = [\mathbf{v}, \dot{\mathbf{e}}_{\mathbf{q}}]^T \tag{5.18}$$

Furthermore, a modified approach is proposed to reduce the complexity resulting from $\nabla \cos\theta_i$ when determining an analytical solution of the repulsive wrench. To achieve the same characteristic expressed in P1-3 for the repulsive wrench, a modified combination of

the potential field / repulsive wrench is proposed. Instead of considering the property P3 expressed by $\cos\theta_i$ at the level of the potential function, it is transferred to the level of the repulsive wrench. As a result, the common approach expressed in (5.15) and (5.16) translates into the following modification:

$$\begin{aligned} U_{ee,i}(\mathbf{x}_{ee}, \mathbf{q}_{ee}, \check{\mathbf{v}}_{ee}, \mathbf{x}_i, \mathbf{q}_i) &= -\lambda \frac{\|\check{\mathbf{v}}\|}{d_i^{\eta}(\mathbf{x}_{ee}, \mathbf{q}_{ee}, \mathbf{x}_i, \mathbf{q}_i)} \\ \varphi_{\tilde{a}} &= -(-\cos\theta_i)^{\iota} \, \nabla_{\mathbf{x},\mathbf{q}} \, U_{ee,i}(\mathbf{x}_{ee}, \mathbf{q}_{ee}, \check{\mathbf{v}}_{ee}, \mathbf{x}_i, \mathbf{q}_i) \end{aligned} \tag{5.19}$$

where $\lambda_{ii}, \iota, \eta$ are parameters to scale each dimension, shape the direction dependency, and steepness of the potential field, respectively. Note that with this modification, the property P3 is still accomplished, but the originally influencing derivation of the velocity direction given by $\nabla_{\mathbf{x}} \cos\theta_i$ is no longer taken into account. However, it is considered to provide more value than the comparable approach in which simplification is applied by limiting the superquadrics to pre-selected roundness parameters $\varepsilon_{1,2}$ [173].

Following this method, the analytical expression is further broken down to the effected separation distances. The following provides the explanation using the example of repulsive wrenches emitted from an obstacle (for clarity of reading, the dependence of relevant pose variables of the objects has been omitted).

$$\begin{aligned} \varphi_{obs} &= -(-\cos\theta_{obs})^{\iota} \, \nabla_{\mathbf{x},\mathbf{q}} \, U_{ee,obs} \\ &= \underbrace{\lambda(-\cos\theta_{obs})^{\iota}\eta\|\check{\mathbf{v}}\| \frac{1}{d_{obs}^{\eta-1}}}_{\Lambda} \, \nabla_{\mathbf{x},\mathbf{q}} \, [d_{obs}] \\ &= \Lambda_{obs} \, \nabla_{\mathbf{x},\mathbf{q}} \left[\|\mathbf{c}_{ee,obs}\| \cdot \left[1 - F_{ee,obs}^{-\frac{\varepsilon_{1,ee}}{2}} - F_{obs,ee}^{-\frac{\varepsilon_{1,obs}}{2}} \right] \right] \\ &= \Lambda_{obs} \, \left[\nabla_{\mathbf{x},\mathbf{q}} \left[\|\mathbf{c}_{ee,obs}\| \right] \cdot \left[1 - F_{ee,obs}^{-\frac{\varepsilon_{1,ee}}{2}} - F_{obs,ee}^{-\frac{\varepsilon_{1,obs}}{2}} \right] \right] \\ &+ \Lambda_{obs} \|\mathbf{c}_{ee,obs}\| \cdot \left[\frac{\varepsilon_{1,ee}}{2} F_{ee,obs}^{-\frac{\varepsilon_{1,ee}}{2}-1} \nabla_{\mathbf{x},\mathbf{q}} \left[F_{ee,obs} \right] + \frac{\varepsilon_{1,obs}}{2} F_{obs,ee}^{-\frac{\varepsilon_{1,obs}}{2}-1} \nabla_{\mathbf{x},\mathbf{q}} \left[F_{obs,ee} \right] \right] \end{aligned} \tag{5.20}$$

In similar fashion is the repulsive wrench emitted from the workspace boundary effecting the end-effector's motion derived to

$$\begin{aligned}\varphi_{ws} &= \Lambda_{ws}\left[\nabla_{\mathbf{x},\mathbf{q}}\left[\|\mathbf{c}_{ee,ws}\|\right]\cdot\left[F_{ws,ee}^{-\frac{\varepsilon_{1,ws}}{2}} - F_{ee,ws}^{-\frac{\varepsilon_{1,ee}}{2}} - 1\right]\right] \\ &+ \Lambda_{ws}\|\mathbf{c}_{ee,ws}\|\cdot\left[-\frac{\varepsilon_{1,ws}}{2}F_{ws,ee}^{-\frac{\varepsilon_{1,ws}}{2}-1}\nabla_{\mathbf{x},\mathbf{q}}\left[F_{ws,ee}\right] + \frac{\varepsilon_{1,ee}}{2}F_{ee,ws}^{-\frac{\varepsilon_{1,ee}}{2}-1}\nabla_{\mathbf{x},\mathbf{q}}\left[F_{ee,ws}\right]\right]\end{aligned} \tag{5.21}$$

Considering a scene with multiple obstacles, and workspace boundaries, the wrenches influencing the end-effector's motion are superposed such that

$$\varphi_{repulsive} = \sum_{o=1}^{O}\varphi_{obs,o} + \sum_{w=1}^{W}\varphi_{ws,w} \tag{5.22}$$

In addition to the repulsive wrenches discussed above, approaches using potential fields also explored the creation of attractive wells that generate wrenches to guide the manoeuvring entity to its final location. In the literature, several types of static potential fields have been proposed to generate attractive wells, including linear, quadratic, parabolic, conical, and hyperbolic shapes [201, 204].

In the context of this work, an attractive wrench emitted from the modelled goal shape is derived using the quadratic potential field after [204] to support the CDMPs in converging faster to the desired goal state. As such the static potential field is expressed using the separation distance d_g and is given by

$$U_{attr} = \begin{cases}\kappa\cdot d_g\cdot d_g & \|\mathbf{c}_{ee,g}\| \leq c_0 \\ 0 & \|\mathbf{c}_{ee,g}\| > c_0\end{cases} \tag{5.23}$$

with c_0 being the desired radius of influence and κ_{ii} the scaling parameters for each dimension. The resulting attractive wrench derives with (5.9) and (5.17) to

$$\begin{aligned}\varphi_{attractive} &= -\nabla_{\mathbf{x},\mathbf{q}}\left[U_{attr}\right] \\ &= \underbrace{-2\kappa\cdot d_g}_{\Lambda_g}\nabla_{\mathbf{x},\mathbf{q}}\left[d_g\right] \\ &= \Lambda_g\left[\nabla_{\mathbf{x},\mathbf{q}}\left[\|\mathbf{c}_{ee,g}\|\right]\cdot\left[1 - F_{ee,g}^{-\frac{\varepsilon_{1,ee}}{2}} + F_{g,ee}^{-\frac{\varepsilon_{1,g}}{2}}\right]\right] \\ &+ \Lambda_g\|\mathbf{c}_{ee,g}\|\cdot\left[\frac{\varepsilon_{1,ee}}{2}F_{ee,g}^{-\frac{\varepsilon_{1,ee}}{2}-1}\nabla_{\mathbf{x},\mathbf{q}}\left[F_{ee,g}\right] - \frac{\varepsilon_{1,g}}{2}F_{g,ee}^{-\frac{\varepsilon_{1,g}}{2}-1}\nabla_{\mathbf{x},\mathbf{q}}\left[F_{g,ee}\right]\right]\end{aligned} \tag{5.24}$$

Given the nature of some expressions, the following simplifications apply to the derivation with respect to the end-effector's pose variables:

$$\nabla_{\mathbf{x},\mathbf{q}} \left[\|\mathbf{c}_{ee,i}\| \right] = \frac{1}{\|\mathbf{c}_{ee,i}\|} \cdot \left[x_{ee} - x_i \, , \, y_{ee} - y_i \, , \, z_{ee} - z_i \, , \, 0 \, , \, 0 \, , \, 0 \right]^T$$
$$\nabla_{\mathbf{q}} \left[F_{i,ee} \right] = \left[0 \, , \, 0 \, , \, 0 \right]^T \;\; as \;\; \nabla_{\mathbf{q}} \left[\mathbf{A}(\mathbf{q}_i) \right] = \left[0 \, , \, 0 \, , \, 0 \right]^T \;\; for \;\; i \in (obs, ws, g) \tag{5.25}$$

The quantified wrenches of repulsion and attraction guide the entity represented by the end-effectors superquadric through a collision avoiding path. In the context of this work, the application to LfD is discussed which build on CDMPs as learning and reproduction framework. Therefore, repulsive wrenches are introduced on the acceleration level of the transformation system, while attraction applies to the velocity level to reduce overshooting. Due to the possible simultaneous exploitation of translational and rotational deviations, the wrenches are applied to both transformation systems after (3.5) and (3.6) which now read

$$\tau \, \dot{\tilde{\mathbf{v}}}_{\mathbf{x}} = \mathbf{K}^{\mathbf{x}} \left(\mathbf{x}_T - \mathbf{x} \right) - \mathbf{D}^{\mathbf{x}} \, \tilde{\mathbf{v}}_{\mathbf{x}} - \mathbf{K}^{\mathbf{x}} \left(\mathbf{x}_T - \mathbf{x}_0 \right) s + \mathbf{K}^{\mathbf{x}} \, \mathbf{f}^{\mathbf{x}}(s) + \varphi_{repulsive,\mathbf{x}} \tag{5.26}$$
$$\tau \, \dot{\mathbf{x}} = \tilde{\mathbf{v}}_{\mathbf{x}} + \varphi_{attractive,\mathbf{x}}$$
$$\tau \, \dot{\tilde{\mathbf{w}}}_{\mathbf{q}} = -\mathbf{K}^{\mathbf{q}} \, \mathbf{e}_{\mathbf{q}} - \mathbf{D}^{\mathbf{q}} \, \tilde{\mathbf{w}}_{\mathbf{q}} - \mathbf{K}^{\mathbf{q}} \, 2 \, log(\mathbf{q}_T * \bar{\mathbf{q}}_0) \, s + \mathbf{K}^{\mathbf{q}} \, \mathbf{f}^{\mathbf{q}}(s) - \varphi_{repulsive,\mathbf{q}} \tag{5.27}$$
$$\tau \, \dot{\mathbf{e}}_{\mathbf{q}} = \tilde{\mathbf{w}}_{\mathbf{q}} - \varphi_{attractive,\mathbf{q}}$$

5.5 Experimental Evaluation

By modelling the encountered scene through the four defined types of volumetric entities and computing repulsive and attractive wrenches from established potential fields, the proposed method promises to generate a collision-avoiding path for the end-effector. Its volumetric representation allows furthermore to exploit both translational and rotational movement capabilities. The following experimental evaluation showcases the ability of the developed method to produce robust reproduction for LfD in two simulated scenarios (see Figure 5.6).

The first experiment is tailored to demonstrate the functionality of the scaling parameters that allow one to restrict dimensions of the wrenches induced on the end-effector. Given a simulated demonstration of a straight path along the x direction, an obstacle is introduced in proximity (see Figure 5.6a), such that collision-avoiding wrenches are generated. By amending the scaling parameters λ_{ii} of the repulsive wrench in (5.20), different reproducing

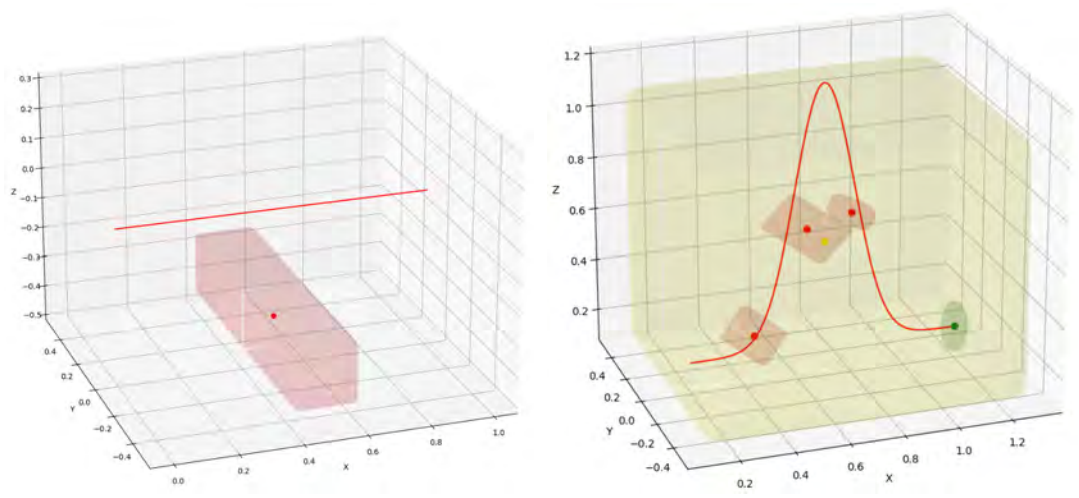

(A) Experimental setup for showcasing translation- and rotation-specific deviation

(B) Experimental setup for showcasing collision avoidance using all types of considered objects

FIGURE 5.6: Simulated setups including scene and environmental objects of validation experiments

motions are produced and introduced to the underlying CDMPs following (5.26) and (5.27). The applied parameters are reported in Appendix B.3.

Figure 5.7 illustrates the resulting motions generated for different parameter settings. A comparison is made between purely translational, which is the prevailing obstacle-avoiding approach in related work, purely rotational, enabled by the volumetric representation of the end-effector, and a combination of both movements. As can be seen, all three successfully generate deviating paths to avoid collision with the present obstacle. However, limiting to translational deviation, a considerable free space is necessary in the z direction (see Figure 5.7a). An alternative is depicted by the use of pure rotational deviation if the use case allows for this. As can be seen in Figure 5.7b, no additional free space is required, but the end-effector's shape pivots forward in proximity to the obstacle. The combination of both cases shows the most effective form of deviation, in which both movement possibilities are used and lead to smaller deviations compared to their individual use (see Figure 5.7c).

The second experiment showcases the combination of all the features promoted by the proposed method. A demonstrated trajectory that follows the shape of an e^2-function reaching 1.0 m height and taking 20 seconds is used for reproduction in the new scene, which is presented in Figure 5.6b. The scene includes three obstacles of different shapes, one workspace as a surrounding boundary, and an attractive goal in the final pose of the demonstrated path. The applied parameters are listed in Appendix B.4.

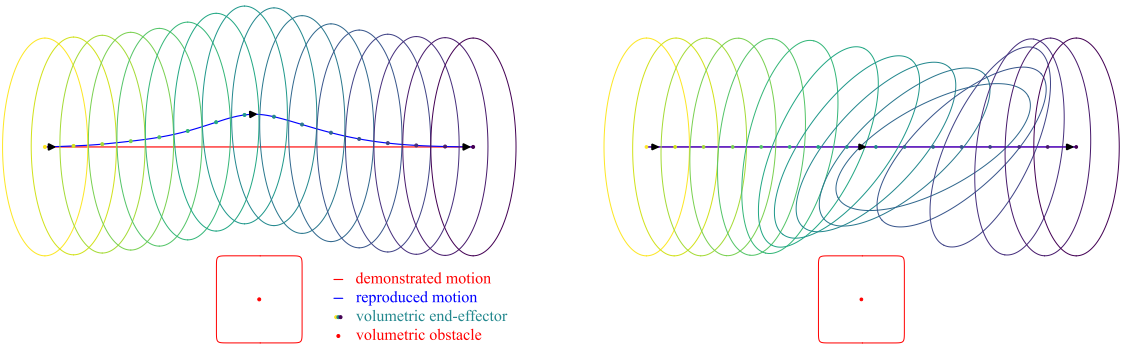

(A) $\lambda_{ii,\mathbf{x}} = 1, \lambda_{ii,\mathbf{q}} = 0$ (B) $\lambda_{ii,\mathbf{x}} = 0, \lambda_{ii,\mathbf{q}} = 1$

(C) $\lambda_{ii,\mathbf{x}} = 1, \lambda_{ii,\mathbf{q}} = 30$

FIGURE 5.7: Illustrative experiment showcasing the effect of the wrench scaling parameterisation

Figure 5.8 illustrates representative snapshots of the evolving path resulting from repulsive and attractive wrenches (see Figure 5.9) that force the dynamic volume to deviate. As can be seen, the first obstacle is occluding the path close to the starting pose of the end-effector. Due to the orientation of the obstacle, an initial downward motion is produced. It is quickly reversed upward due to the workspace boundary and the demonstrated upward movement (see Figure 5.8a). The second obstacle induces a slight pivoting behaviour on the end-effector while it reaches around the shielding its potential field (see Figures 5.8a and 5.8b). Circular motion is interrupted at an approximate height of 1.0 m due to the bounding workspace, which also prevents naive reproduction from reaching a height of 1.2 m (see Figure 5.8c). After successful avoidance of the third obstacle by exploiting a translational deviation in the +y direction, the end-effector shape reaches the final goal (see Figure 5.8d). With the elaboration of an imaginary goal volume that generates attracting wrenches acting on the end-effector's volume, the proposed method assists the CDMPs-based dynamic system to converge faster to the final state. In the given experiment, the translational accuracy of 0.001mm is achieved after 25.08 seconds when applying the attractive wrench on the velocity level compared to a duration of 36.48 seconds without the goal attraction.

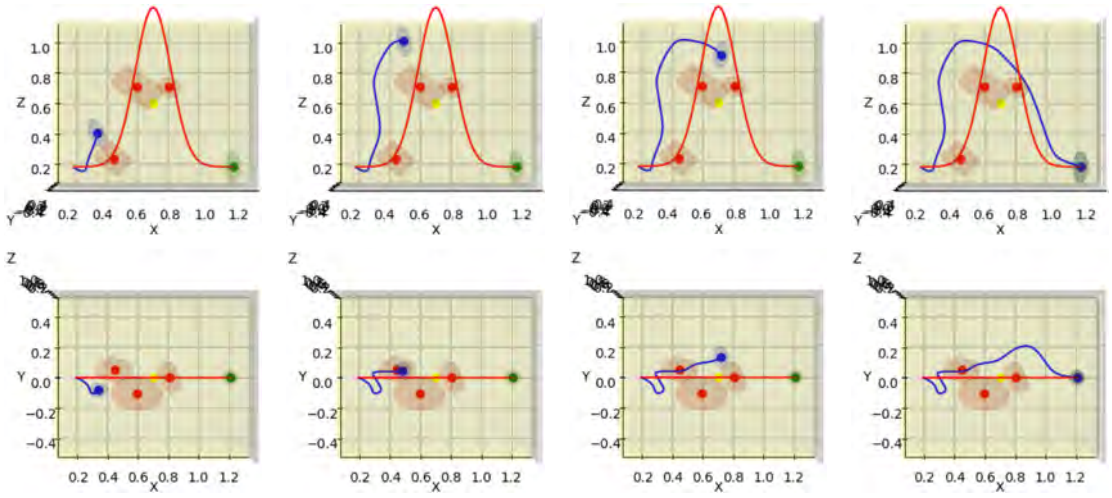

(A) $t = 6.77s$ (B) $t = 9.97s$ (C) $t = 12.46s$ (D) $t = 25.08s$

FIGURE 5.8: Snapshots of the deviating reproduction path avoiding collision with present obstacles, workspace boundary and attracting to the goal shape

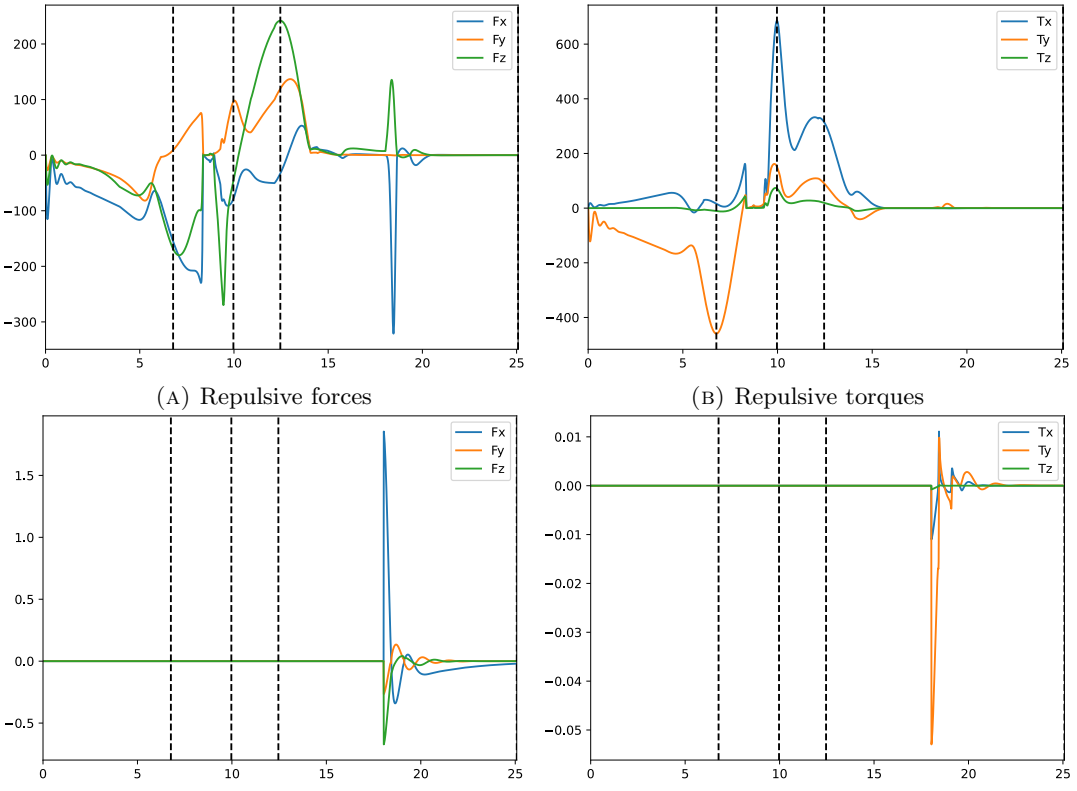

(A) Repulsive forces (B) Repulsive torques

(C) Attractive forces (D) Attractive torques

FIGURE 5.9: Repulsive and attractive wrenches emitted by environmental objects (vertical lines mark the snapshot times of Figure 5.8)

The presented experiments demonstrate how key functionalities of the proposed method using multi-superquadric potential fields allow CDMPs-based reproduction to effectively

avoid collisions and converge faster to the final state. An application to a realistic scenario is presented in Section 6.4.

5.6 Summary

During the reproduction phase, the previously taught task is carried out independently by the robot. State-of-the-art LfD solutions are expected to not only mimic an identical behaviour but rather be capable of generalising in unseen situations. Such robustness refers, in particular, to the adaptability to new scenarios caused by changed environments. DMPs feature a significant body of research on collision avoidance, where the latest trend explores the volumetric representation of physical obstacles.

This Chapter presented an extension to the prevailing method of potential field-based repulsive forces by proposing additional volumetric representations using superquadrics to better approximate the scene encountered during reproduction. A set of four different object types was proposed, which extends the existing volumetric representation of obstacles by an end-effector, workspace boundaries, and an attractive goal. Emitting repulsive and attractive wrenches from potential fields between these volumetric entities allow robust and effective manoeuvring of the end-effector around present obstacles, within the given workspace, and towards the final state. Simulative experiments were designed to demonstrate the key functionalities of the proposed method and showcased its validity.

Chapter 6

LfD-IA Framework Evaluation

The previous three Chapters examined the phases of the characteristic LfD procedure individually and discussed methods that benefit their applicability in an industry-orientated assembly scenario. As a result, the demonstration was enhanced with visual guidance that assists the human operator in finding reproducible motions considering a reproduction system with distinct kinematics (see Chapter 3). The learning framework, proposed in Chapter 4, established a method that merges the industry-known MTM-1 discretisation system with the prominent CDMPs learning technique to allow the processing of complex motion sequences. Coping with alternate scenes during reproduction is discussed in Chapter 5, which proposed an extension of CDMPs for online collision avoidance based on distance-driven potential fields between multiple volumetric entities modelled as superquadrics. Collectively, these methods comprise the Learning from Demonstration for Industrial Assembly (LfD-IA) framework aimed at in this thesis which provides the visual guidance during demonstration, the learning of the motion following the MTM-1 system and the collision avoidance capability during autonomous reproduction of desired subskills.

This Chapter presents an exemplified hardware setup to apply the proposed LfD-IA framework and provides a comprehensive summary of its discussed functionalities based on a showcased pick-and-place task. The Chapter is structured as follows: Section 6.1 begins with an explanation of a representative experimental setup and discusses the necessary preparation for use. Following the characteristic LfD procedure, the consecutive Section 6.2 describes how the demonstration phase is designed for the given task applying the features discussed in Chapter 3. The learning abilities of the framework sourced from Chapter 4 are presented in Section 6.3. Upon encountering a changed scene during reproduction, Section 6.4 demonstrates the framework's ability to produce a robust and effective

reproducing path according to the methods proposed in Section 4.3.3 and Chapter 5. A summary is provided in Section 6.5.

6.1 Experimental Setup

The three components of the LfD-IA were designed to be robot and hardware independent by mainly processing and communicating via trajectories in Cartesian space. The possibilities for hardware configuration to utilise the framework are therefore manifold.

The following showcasing of the framework's functionalities is conducted with the hardware configuration shown in Figure 6.1. As promoted in Chapter 3, the demonstration is carried out with a robot-independent demonstration device, which is tracked by a Vicon motion capture system along with the task-relevant workpiece and assembly point (introduced in Section 4.4). A television provides the human operator with the graphical interface developed in Chapter 3. Furthermore, a second monitor displays a novel LfD-IA graphical interface designed to intuitively guide the human operator through the LfD process, providing sufficient information for proper supervision of the procedure. The reproduction system consists of an Universal Robot UR5e with an OnRobot RG6 gripper. The individual components of the framework run on three different PCs, including a Windows 10 PC for Vicon Tracker 3.9 software, an Ubuntu 18.04 PC for the software associated with the visual guidance of Chapter 3, and an Ubuntu 20.04 PC for the remaining components, including the LfD-IA interface. All components are configured to communicate within one local network through Robot Operating System (ROS).

6.2 Demonstration

The demonstration phase of the proposed LfD-IA solution is carried out with a robot-independent demonstration device while being guided through the method developed in Chapter 3. The intended pick-and-place task similar to Section 5.5 is facilitated by a customised demonstration device that was designed as a passive replica of the robot's gripper (see Figure 6.2a). This simplifies the kinematic inequality between the gripper and the human hand during grasping and informs the human operator of the robot's grasping capabilities. Passive grasp functionality is achieved by a combination of rubber bands, a toothed gear, and detachable pins, as can be seen in Figure 6.2b. The guiding interface that provides information on the non-reproducible region of the kinematically constrained

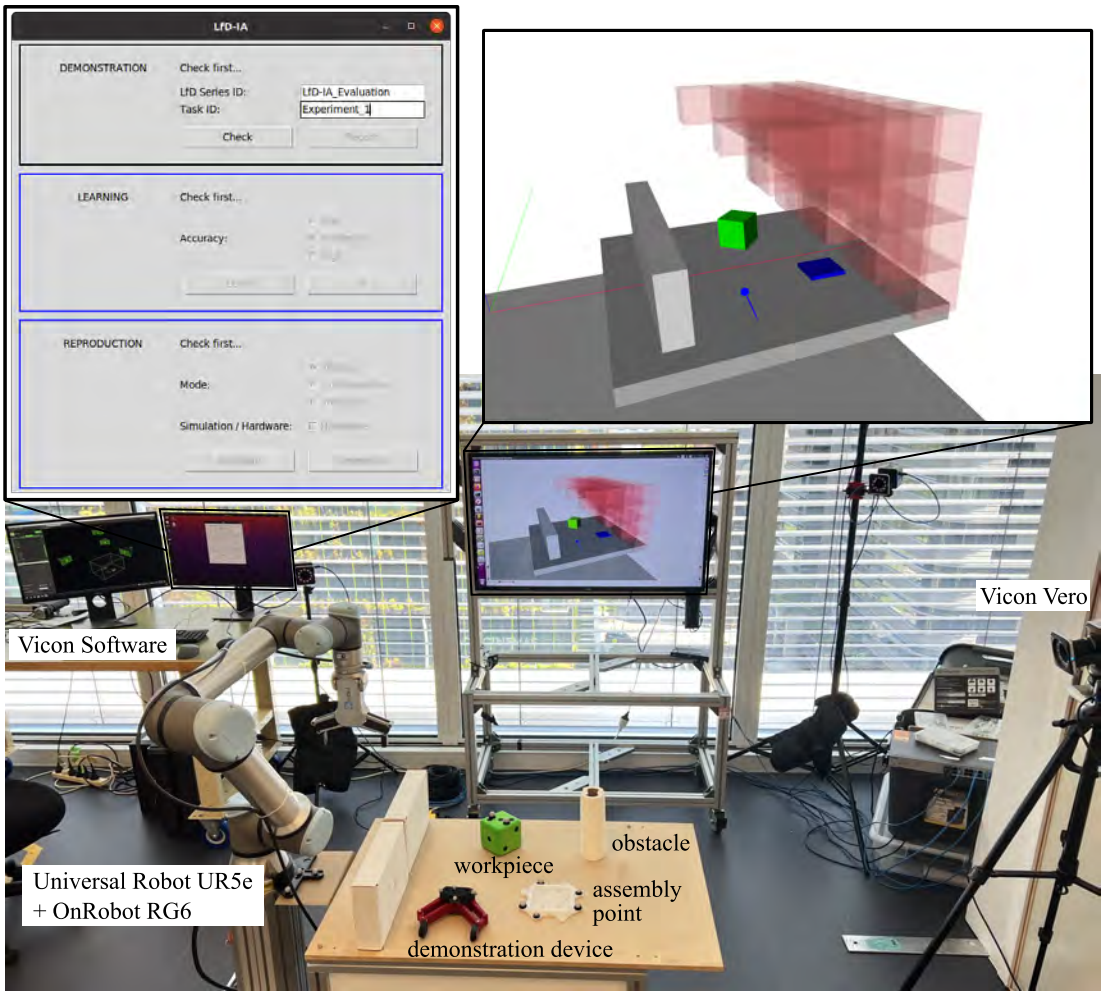

FIGURE 6.1: Hardware configuration for the experimental evaluation of the developed LfD-IA framework

UR5e is computed using the same static environment as introduced in Section 3.6 (Figure 3.3a), which mimics the real-world setup (see Figure 6.1). However, for the purpose of the intended example, the task space required by HAP was adjusted to consider only orientations roughly facing downward and being in the perspective of the grasped workpiece, which has an offset of approximately 27 cm from the tool flange.

The developed LfD-IA GUI is designed to guide the human operator through the LfD procedure. This is supported by indicative texts and the selective activation and deactivation of **buttons** and selection features based on executable *processes* and displayed information relevant to the supervision of progress. By specifying an intended LfD series ID and Task ID (see Figure 6.1), the **Check** button either activates learning and/or reproduction options for a previously recorded demonstration or activates the **Record** button if

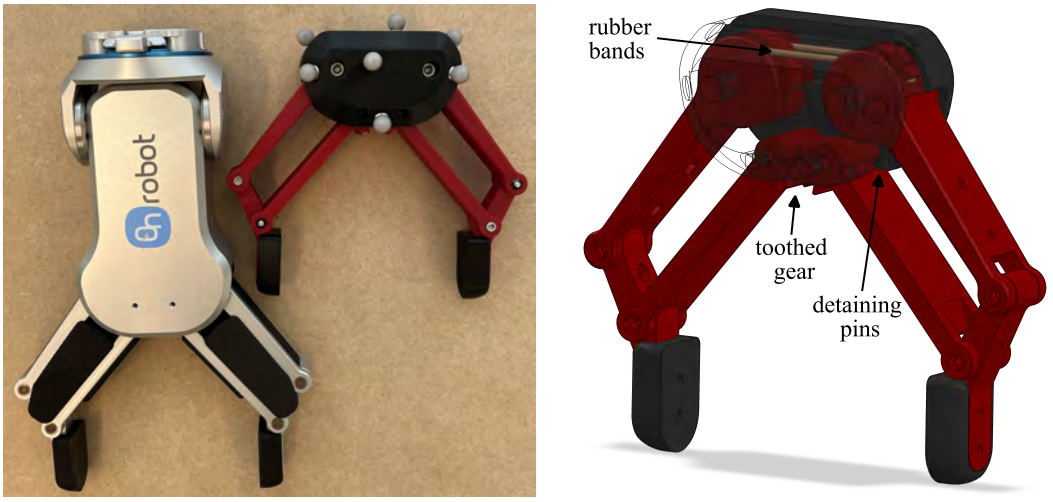

(A) RG6 gripper and its passive replica (B) CAD design

FIGURE 6.2: Designed demonstration device for pick-and-place tasks

the IDs have not been used yet. Pressing the latter displays the assisting GUI of Chapter 3 on television to guide the human operator through reproducible motions, while the robot-independent demonstration device, workpiece, and assembly point are tracked with the Vicon system (the device's finger motion is not tracked intentionally to avoid the mimicking of unnecessary finger actuation). Due to the applied CDMPs learning method, a single demonstration is sufficient for the consecutive LfD procedure. A snapshot of a performed pick-and-place demonstration is shown in Figure 6.3a. Figure 6.3b presents an illustrative example of a recorded motion of the workpiece (green) and the tool flange (blue) surrounded by the simulated static environment and the region of non-reproducible motions in the perspective of the workpiece.

After recording, an automated *data processing* algorithm is initiated, which synchronises all recorded time series and removes any stationary intervals at the beginning and end of all trajectories. The time series plots of each recorded object are presented to the human operator with the intended cropping intervals (vertical lines) as exemplified in Figure 6.4 for the above example. It allows the human operator to preliminarily verify the suitability of the demonstration performed, indicated by a smooth motion of the demonstration device and workpiece within the cropped time frame while the assembly point remains stationary.

6.3 Learning

The recorded, synchronised, and cropped demonstration trajectories of the objects in the scene serve as input to the learning phase. If the learning process is performed for the first time, pressing the **Learn** button initiates the *skill classification* as described in Section 4.3.2. The exemplary demonstration in Figure 6.4 results in the relevant distances

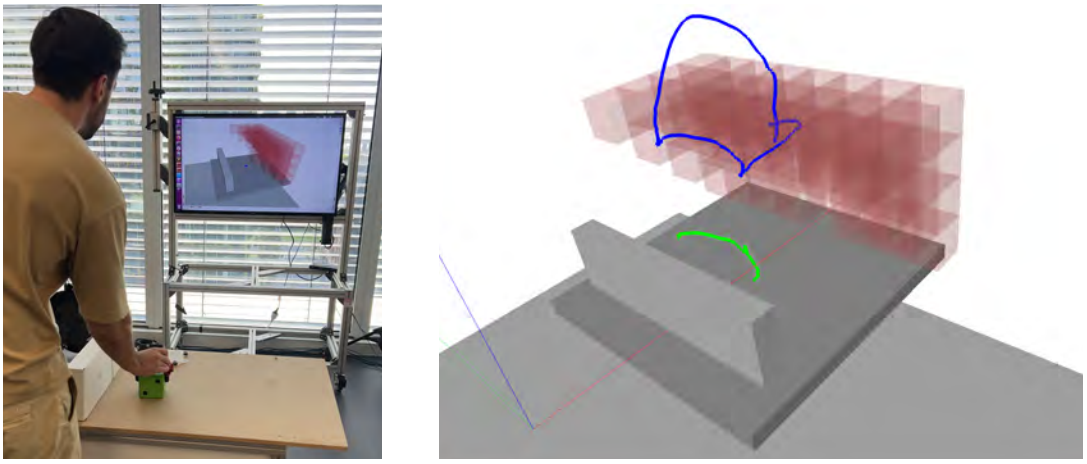

(A) human operator performing a demonstration

(B) resulting motion of the tool flange (blue) and the workpiece (green) surrounded by $\overline{\mathcal{R}^*}$ (red)

FIGURE 6.3: Guided demonstration during pick-and-place task and its resulting motion

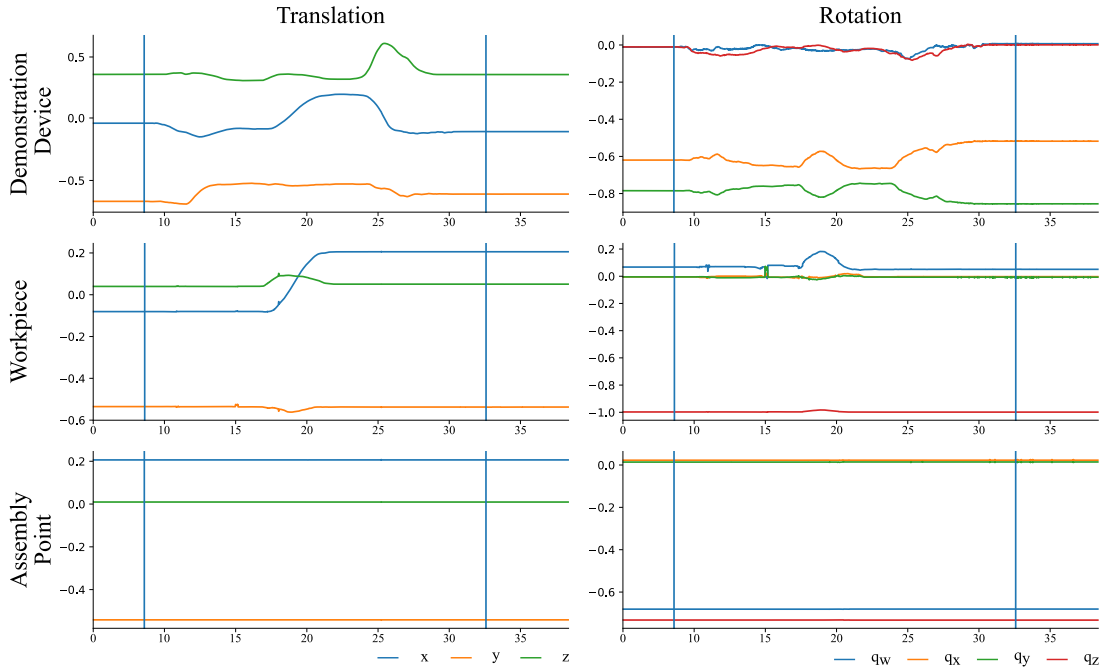

FIGURE 6.4: Recorded motion of all tracked objects during demonstration displayed to the human operator for verification

shown in Figure 6.5. The transition states are calculated from identified plateaus and are indicated by vertical red lines in the diagram of their determining distance. Furthermore, the gripper actuation is timed on the basis of the distance between the object and its latest initial and earliest final state and indicated with vertical purple lines (see Figure 6.5). The classification algorithm expects a series of skills, that is, reaching, grasping, moving, positioning, releasing, and reaching. If not identified, the demonstration is classified as a single generic skill, which is parameterised as a moving skill.

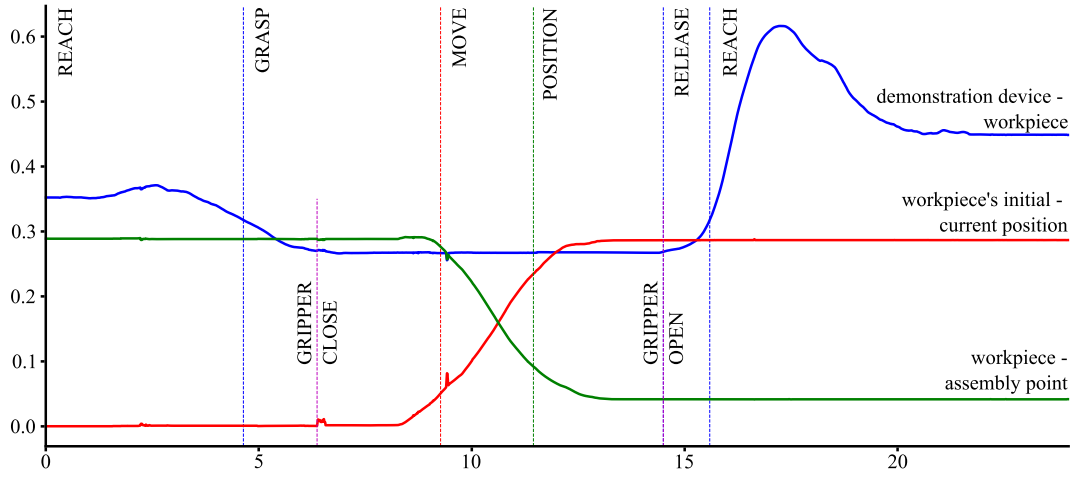

FIGURE 6.5: Distances between relevant coordinate systems to segment skills after Section 4.3.2

Once the skill classification was performed and the identified skill trajectories are stored, **Learn** automatically generates custom CDMPs for each identified skill. The LfD-IA interface provides in the learning phase a selection of the desired accuracy mode σ, which is predefined by the options low, moderate and high (see Figure 6.1). These are linked to selected values that quantify the number of RBFs applied (N) during grasping, positioning and releasing dependent on the demonstration length such that $N = \sigma \cdot T_{dem}$. The remaining parameters for the custom CDMPs are predefined according to the values summarised in Appendix B.5 and applied considering (3.4). The timing of gripper actuation is translated into the associated value of the phase variable s, which allows correct actuation despite temporal scaling (in case of more complex tools, their actuation may be translated into additional DMPs). After creating and learning skill-based CDMPs, a learnt motion of the tool flange with no spatial or temporal scaling is displayed to the human operator. Similarly to the displayed time series of the demonstrated motion, it allows the human operator to validate the robot's understanding and expected performance of the demonstrated task. Figure 6.6 shows the results for the given example with a selected low-accuracy mode. As can be seen, unnecessary jerky motion is smoothed out, especially

in the last skill, while accurate mimicking of relevant motion during grasping, positioning, and releasing is achieved.

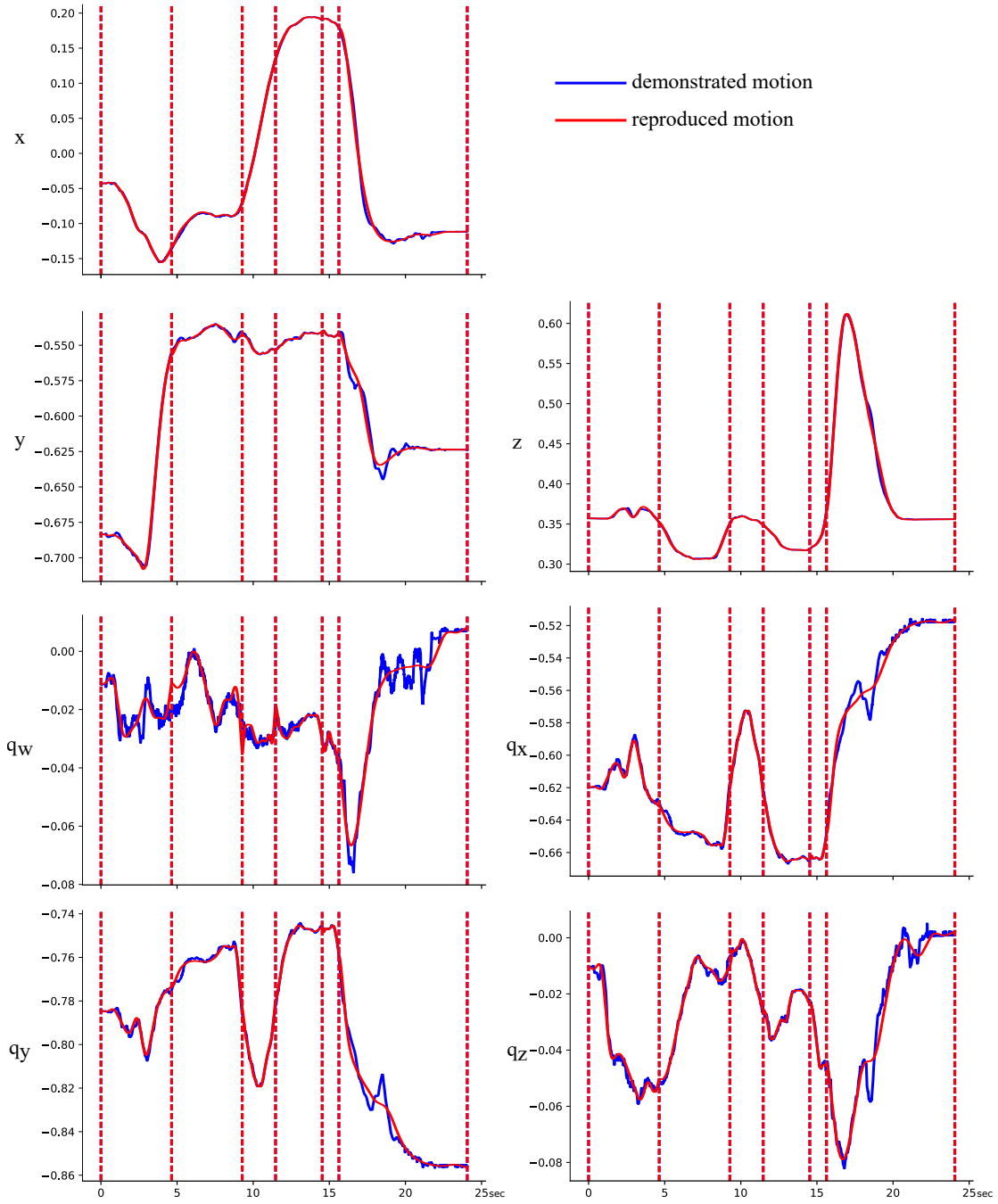

FIGURE 6.6: Learning outcome displayed to the human operator for verification

6.4 Reproduction

Once the human operator is satisfied with the mimicking behaviour of the robot, the learnt motion can be applied to autonomous reproduction within generalised situations, considering spatial and temporal scaling as well as scene-aware collision avoidance. The former scaling functionality is enabled by the MTM-inspired CDMPs learning framework presented in Chapter 4. The temporal scaling of each skill is quantified through selecting the reproduction mode on the LfD-IA interface. The three modes are linked to the temporal parameter τ_{rep} of the skills according to the following scheme: 'testing' results in a reproduction four times slower than demonstration, 'collaborative' scales the reproduction speed to a maximum speed of 250mm/s during reaching and moving, and 100mm/s for grasping, positioning, and releasing, and 'industrial' performs reproduction at the same speed as that demonstrated. Spatial scaling is enabled similarly by incorporating the relative relocation of the workpiece and the assembly point following the method proposed in Section 4.3.3. As naive relocation may result in poses that are outside the region of reproducible motion, the LfD-IA interface provides the option of accessing the GUI for guided demonstration by pressing **Relocate**. At this stage, the interface is designed to display the objects dynamically in the presence of the region of non-reproducible motion. As such, it allows the human operator to make an informed decision about where the objects can be placed, or to verify desired poses for the kinematically constrained robot in mind. An example of relocation is given in Figure 6.7 in which the workpiece was moved approximately 15cm in -x direction and the assembly point by 5cm in -y direction in combination with a rotation of 30 degrees around the z axis.

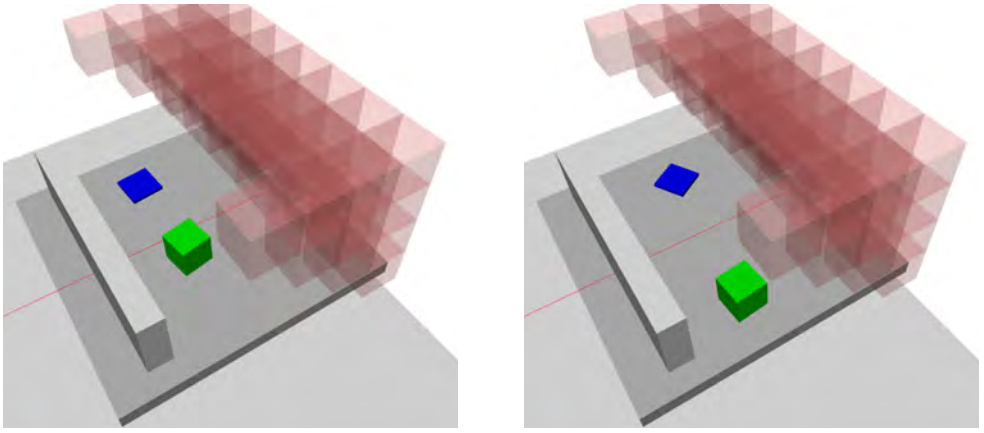

(A) Initial locations during demonstration phase

(B) Verified relocation during reproduction phase

FIGURE 6.7: Guiding interface for relocating the workpiece (green) and assembly point (blue) allowing spatial scaling during reproduction

After naturally interacting with the scaling capabilities of the LfD-IA framework, the topologically similar trajectory may collide during autonomous reproduction with pre-existing or newly introduced obstacles or result in motions that penetrate the region of non-reproducible motion. To ensure robust reproduction, the LfD-IA framework incorporates the collision avoidance method presented in Chapter 5. With a given sequence of skills, customised collision avoidance scenes are applicable to individual skills following their unique requirements. This may include distinct volumetric approximations of the end-effector, such as with or without grasped workpiece, or activation and deactivation of environmental shapes depending on their relevance. An end-effector model with a centre not being at the robot's tool flange is recognised using a transformation between the TCP and point of interest, which is applied to the repulsive/attractive wrench calculation and their effect on the tool flange's motion.

In the example of the demonstration provided in Figure 6.3, the skills of moving, positioning, and final reaching (the initial reaching skill produces reproducible motion) are designed to incorporate collision avoidance. The skill-dependent scenes used are illustrated in Figure 6.8. The applied parameters are summarised in the Appendix B.5. Due to the additional information provided by HAP about the region of non-reproducible motion for the grasped workpiece, the artificial workspace shape is extended by imaginary obstacles representing the discrete voxels. As such, these are relevant during moving and releasing, and repulsive wrenches are calculated based on the volumetric replica of the workpiece depicted in Figure 6.8c (right). As a result, the tool flange remains within the region of non-reproducible motion while simultaneously avoiding collision with physical obstacles.

The final *autonomous reproduction* of the learnt task with the desired spatial and temporal adjustments under given environmental constraints is initiated by pressing the **Reproduce** button on the LfD-IA interface. The checkbox **Simulation/Hardware** allows the human operator to select between a preliminary simulated test or direct control of the connected robotic system. In both cases, the Vicon motion capture system scans the current scene and provides the updated location of the workpiece, the assembly point, and the newly introduced obstacle to the reproducing algorithm. Figure 6.9 shows the simulation result displayed for the given example, including a trajectory comparison between the demonstration and the reproduction within the volumetric scene considered. A time series of the reproducing robot compared to the motion initially demonstrated by the human operator in a set of representative images is presented in Figure 6.10. As can be seen, the relocated workpiece is successfully grasped (Figure 6.10e) followed by a collision-avoiding behaviour that results in translational and rotational deviation due to

the newly introduced obstacle and the voxels representing the region of non-reproducible motion (Figure 6.10f). After the workpiece is successfully placed at the assembly point (Figure 6.10g), a translational deviation is induced to prevent the robot from exiting the predefined workspace (Figure 6.10h).

6.5 Summary

The presented Chapter demonstrates how the novel methods elaborated in Chapters 3 to 5 are unified to the aimed LfD-IA framework promoting LfD for assembly-orientated tasks. While the framework is robot- and hardware-independent, a physical configuration was discussed and utilised to showcase the framework's functionality. This includes methods for interactive guidance during demonstration to perform motions transferable to the robot in mind, MTM-inspired learning of complex assembly motions, and robust reproduction under desired scaling of motion and changes in the environment.

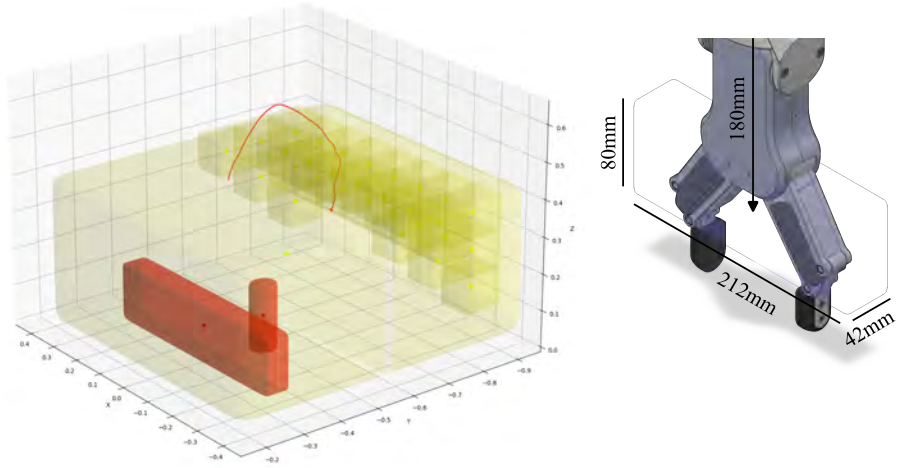

(A) Reaching

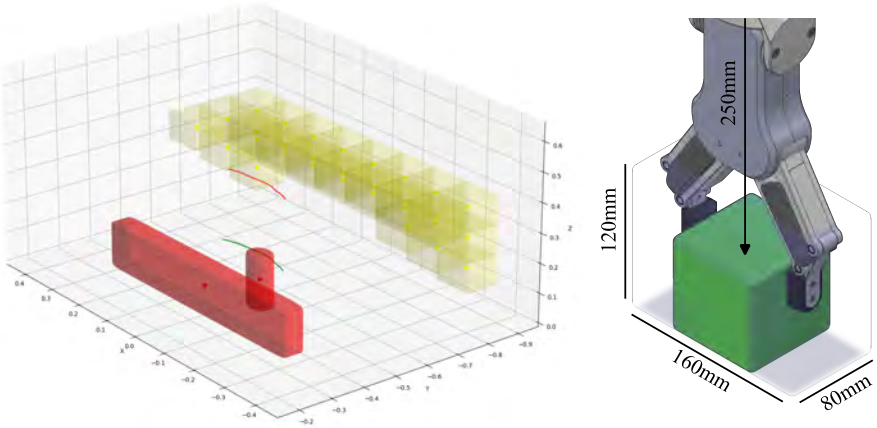

(B) Moving

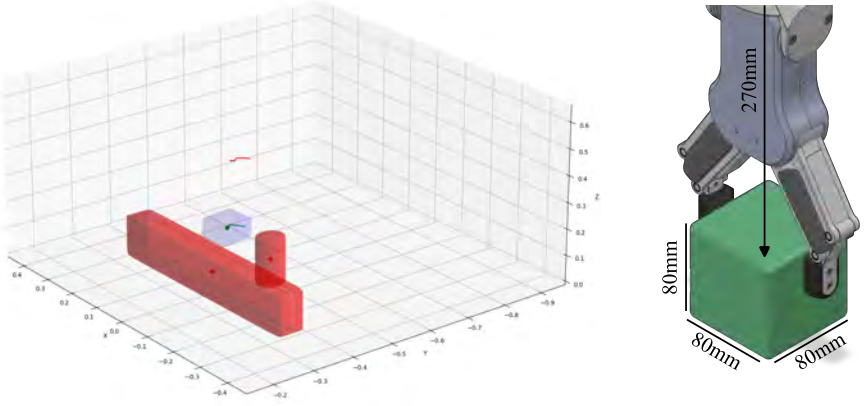

(C) Positioning

FIGURE 6.8: Skill-dependent scene approximation using physical obstacles (red), attractive goal (blue), workspace boundary (yellow), imaginary obstacles for the region for non-reproducible motion (yellow voxels) and end-effector shapes (transparent)

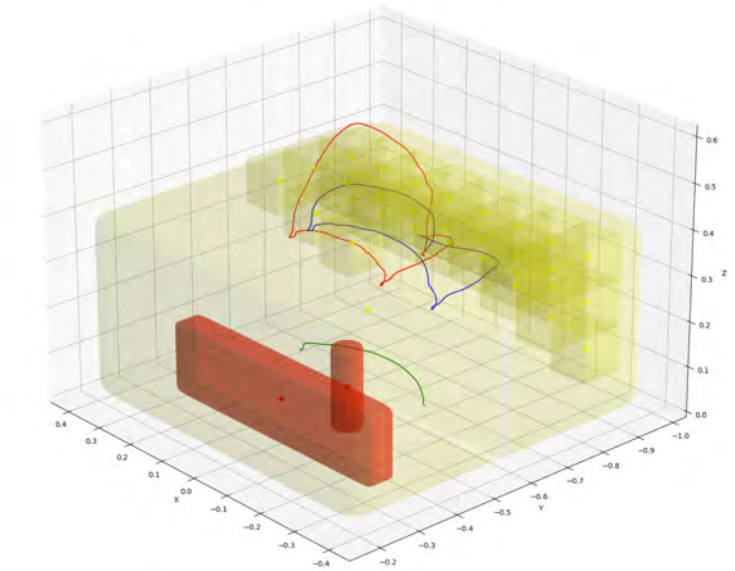

FIGURE 6.9: Displayed result of simulated test in updated scene with relocated objects after Figure 6.7b with demonstrated path (red), reproduction path (blue), and object path (green)

(A) demonstration 1

(B) demonstration 2

(C) demonstration 3

(D) demonstration 4

(E) reproduction 1

(F) reproduction 2

(G) reproduction 3

(H) reproduction 4

FIGURE 6.10: Images of the real-world human demonstration and robot reproduction

Chapter 7

Conclusion

This thesis has presented the elaboration of an LfD framework that overcomes some identified obstacles for assembly-related tasks with the aim to further promote its future deployment in the industrial sector. In light of the long-standing history in LfD research and numerous contributions in related contexts, this thesis *examined* currently prevailing methods applied in a research environment with respect to requirements and expectations in the field of application. As a consequence, key obstacles that characterise the gap between research contributions and industry requirements were identified. These informed the focus of the investigations on three novel methods by *enhancing* preexisting approaches with application-specific characteristics and functionalities. Promoting improvements in all three phases of the common LfD procedure, this thesis discussed effective demonstration, assembly-tailored learning, and robust reproduction to improve the applicability of LfD solutions in industrial settings. These individually developed components formed the basis for the *development* of the unified LfD-IA framework, which was presented in an experimental physical demonstrator. The presented investigations demonstrate that practicability, robustness, and consideration of task-specific requirements are key enabling factors to leverage the prevailing LfD approaches towards industrial assembly capabilities and outline the response to the formulated research question.

This Chapter concludes the thesis presented by outlining insights to the following: A summary of the methods that contribute to the state-of-the-art in LfD for assembly-related tasks is provided in Section 7.1. Section 7.2 discusses the identified limitations of the presented work and explores avenues for future research. A concluding remark is given in Section 7.3.

7.1 Summary of Contributions

The following provides a summary of the main contributions that emerged from the work associated with this thesis that were foreshadowed in Section 1.4 and illustrated in Figure 1.2. These are aligned with the structure of the thesis and include an application-specific systematic literature review (Chapter 2), an effective demonstration technique (Chapter 3), an assembly-tailored learning technique (Chapter 4) and a robust reproduction technique (Chapter 5).

7.1.1 Application-specific systematic literature review

Since the first ideas of programming robots naturally from human demonstrations in the 1980s, LfD has grown into a multi-discipline concept with constantly growing application potentials. It is often motivated by the desire to simplify and increase effectiveness in real-world scenarios. As such, it promotes similar increased benefits for the industrial assembly industry that is faced with emerging challenges of coping with mass customisation, labour shortage, and increased demands. Although LfD has been constantly discussed in assembly-related research, its potential has not yet gained significant foothold in the industrial sector.

Chapter 2 and the associated publication [24] contribute to the field with a comprehensive literature review that identified the state-of-the-art of LfD for assembly-related tasks. Using a systematic approach, relevant studies were thoroughly analysed with respect to the techniques used in LfD, the use cases applied, and the results achieved in real world experiments. A consecutive comparison to industrial practice for the introduction of a new assembly task outlined synergies and differences between the common characteristics of LfD solutions and traditional human operator instructions. Both aspects informed the determination of key obstacles in current LfD research that hinder the smooth integration of proposed solutions into industrial practice. As such, involved research parties, as well as industry beneficiaries, gain a clear understanding of prevailing solutions and their achievable performance while being guided towards targeted investigations resulting in effective progression.

7.1.2 Effective Demonstration through Robust Transferability

Advances in technology have established three fundamental approaches to capture human motion when demonstrating the desired task. The ability of collaborative robots to be guided passively through motion, also known as kinaesthetic teaching, is predominantly used in the research field. While this significantly simplifies further processing for the generalised reproduction movement of the robot, this medium is still to a certain extent unnatural for people unfamiliar with robots and requires rethinking of the task into the robot's perspective. The alternative, in which the demonstrating human performs a task in its own way and independently of the robot, is assumed to be more user-friendly in an industrial context. However, as the movements of humans can extend beyond the robots' capabilities, motions may be demonstrated that are not reproducible by the intended robot.

Chapter 3 and the associated publication [25] contribute to research with investigations on how robust transferability between two kinematically distinct systems is achievable. A generalised problem was formulated, resulting in the aim of finding a region of non-reproducible motions. The presented solution leverages the HAP motion planning framework, which computes the area of smooth and collision-free paths for a given environment, workspace, and robot model. The information gained about accessible regions was incorporated into a novel GUI that effectively provides the essential information to the human operator during the demonstration. As such, the user becomes capable of making informed decisions without the need of rethinking the task, passively moving a robot, or even having the robot available. While the proposed approach was motivated and evaluated in the context of LfD for assembly-related tasks, it is applicable to scenarios beyond LfD where any performed motion needs to be translated to a kinematically distinct/constrained system. Furthermore, HAP provides the ability to consider additional constraints, such as a minimum manipulability, that promote the application to contact-rich or other narrative use cases.

7.1.3 Assembly-tailored Learning through MTM-inspired skills

Research efforts in the field of LfD show great interest in assembly-orientated challenges. Motivated by individual skills, such as peg insertion, or conceptual ideas for general pick-and-place operations, promising contributions have emerged that demonstrate the theoretical strength of LfD and its justified recognition as a future-orientated technology. However, in comparison with the requirements found in practical industrial assembly, a

fundamental lack of attention is evident towards complex tasks involving a series of various skills and multi-piece handling. Given the historically evolved distinction in LfD solutions between trajectory-based and state-driven task representations for learning and reproduction, a combination of both is considered essential for achieving appropriate results.

Chapter 4 and the associated publication [26] contribute to the field of LfD research with the concept of merging the prevailing trajectory-based CDMPs learning framework with an abstraction level sourced from an industry-relevant discretisation system. A thorough selection process led to the discretisation system associated with MTM-1 that was used to define five distinct skills, including reaching, grasping, moving, positioning, and releasing. Leveraging on the multifaceted customisation ability of CDMPs resulted in unique models that adequately incorporate the individual characteristics of each skill. In addition to its proven value in the practical context, the MTM-1 method also provides reference to the standard duration of each skill when performed in manual workflows. Furthermore, reverting to methods used in the application-specific industry has the advantage that beneficiary parties familiar with the method may be more willing to use the presented robotic solution.

7.1.4 Robust Reproduction through Dynamic Potential Fields

Compared to conventional programming methods applying 'record-and-playback', LfD incorporates the decisive advantage of generalising the initially learnt behaviour to new situations. This includes mainly the ability to perform the same task despite introduced changes in motion (spatial and/or temporal adjustments), environment (appearing obstacles), or task (similar but not identical objects). The second represents a particularly essential functionality to establish robust and reliable performance in dynamic environments anticipated in industry. In the given LfD context, such a situation is possible when the scene between demonstration and reproduction changes. Considering the prominent trend of utilising potential fields from volumetric representations of physical obstacles, repulsive forces are calculated that affect the robot's motion. However, deviations are only produced translationally with no particular bounding characteristic.

Chapter 5 and the associated publication [27] contribute to the research on collision avoidance using potential fields with an extended scene approximation scheme using superquadrics as volumetric representations. In addition to physical obstacles, the suggested scheme incorporates a dynamically moving end-effector shape, which allows exploitation of all its DoF, making necessary deviations more effective. In addition, an imaginary

workspace boundary is presented that emits repulsive wrenches on the end-effector maintaining it within the designated space. To increase efficiency, a volumetric goal shape was introduced that functions as an attracting entity. By approximating the named shapes with superquadrics and applying the rigid body radial Euclidean distance calculation, an analytical solution was presented for the calculation of repulsive and attractive wrenches affecting the end-effectors path. Furthermore, its incorporation into the prominent CDMPs learning framework demonstrates its applicability to the LfD context. Although presented and promoted in the discussed context, the proposed scene approximation scheme can be considered for general collision avoidance, which is a prominent research field in robotics.

7.2 Discussion on Limitations and Future Work

The presented work shows a targeted approach to developing an LfD solution towards industrial use. While relevant narratives have been discussed and novel methods proposed, there are some limitations which need to be overcome before the framework can be fully realised in non-laboratory environments. This Section outlines identified limitations and explores promising avenues for future research.

7.2.1 Physical Demonstrator

The first point of discussion is the hardware setup used to evaluate the proposed methods and, in particular, the unified framework in Chapter 6. It exemplifies the physical realisation using several necessary components, including a Vicon motion capture system to track the human demonstration, locate the workpiece, assembly point, and obstacles in the environment. It is clear that the use of such a motion capture system is not practical for most genuine industrial applications. However, as explained in Section 6.1, the design of the framework is not dependent on this specific sensing modality, and the necessary demonstration path can be acquired differently. Other sensing systems, such as RGBD cameras, lidars, and other technologies, may be used as alternatives. Such sensors are becoming common in industrial settings, in particular for applications involving human-robot collaboration.

The evaluation was also performed on simplified tasks, which was mainly caused by available hardware. As discussed in Section 1.3, the focus of the thesis was on diversifiable contributions in the broader context of LfD which are not limited to an industry-specific

niche. Given this scope, a comprehensive evaluation of the targeted industrial assembly tasks was not attainable, but a suitable evaluation was still achievable for the aimed methodological improvements. The pursuit of such an investigation in future work is of considerable benefit to the presented work. In this context, a performance evaluation is envisioned in which the LfD-IA driven teaching of a new task is compared to teach-pendant programming with respect to efficiency, comfort, and user-friendliness.

7.2.2 Human Operator Experience

The development and design of the developed framework is orientated closely to the assumed needs of task-experienced non-robot experts, such as the achieved robot-independent demonstration phase. The analysis of relevant information that requires an interaction between humans and the LfD-IA framework resulted in the physical demonstrator presented in Chapter 6. However, future improvements are envisioned to further enhance the experience of the human operator, considering the following aspects.

The presented framework uses graphical interfaces to provide an augmented model of the environment during the demonstration and to navigate the LfD process. Although these are considered user-friendly, the use of augmented reality and sound-based communication suggests an increase in intuitiveness and a positive experience for the human operator. The latter is also applied when instructing human workers (see Section 2.3) and may present benefits for integration due to the common ground between teaching humans or robots. An investigation of their impact on the willingness to apply LfD in industrial practice is a fundamental aspect to guide future integration concepts. The user study presented in Section 3.6.2 further revealed that guiding suggestions on where to place objects would be beneficial to successfully and effectively perform the intended task, which is another important avenue to improve usability. Similarly, the selected verification method is a potential improvement aspect. As introduced to inform the human operator about the robot's learning result and intended reproduction performance, these may be substituted by more visually attractive simulations.

Providing a physical demonstrator is built suitable for industrial use, an extensive user study with real human operators in a realistic scenario is a promising measure to identify and elaborate further framework improvements. This research may involve the integration of multiple areas, such as ethical, social, and psychological considerations, as well as the selection of appropriate hardware and the development of expected software results.

7.2.3 Applied Simplifications in Framework Implementation

Throughout the development of the LfD-IA framework, some simplifications were applied that are valid in the given context but may appear as obstacles once confronted with real-world challenges. This concerns the orientations in HAP, the sequencing of individual CDMPs, and the distance approximation between superquadrics.

The current embedding of the HAP framework to inform the human operator about regions of non-reproducible motions is limited to poses approximately oriented in a nominal direction. Allowing for any greater deviations from this nominal direction results in ambiguous guidance in the GUI. For example, it may be possible to rotate the end effector about a point in the workspace in one direction, but rotating in the other direction may require a large change of joint angle to avoid self-collision or joint limits. However, this is a limitation of the GUI rather than the proposed method of finding $\mathcal{R}^*$. In order to handle this, there would need to be some notion of trajectory history encoded in the GUI. A valid workaround is to define multiple task spaces with the required nominal directions and then to carry out demonstrations independently for each of these.

Motivated by the advantages offered by MTM-1, the presented work exploited the primary classification into basic elements as the underlying discretisation system. The potential beyond this is evident in the more precise specification of the elements, the temporal comparison to manual workflows, the optimisation of skill sequences and workplace arrangement, and the use to map more complex workflows (including tool handling). However, this requires a revision of the specific assumption of manual or distance-based skill segmentation (see Section 4.3) and closer alignment to the original MTM-1 specifications. Due to the expected benefits, further exploitation of the MTM-1 method is considered a promising path to explore.

The presented method for robust reproduction applies currently the approximation method called the rigid body radial Euclidean distance to compute the distances between two superquadrics. It is considered computationally inexpensive and provides an analytical solution. Determined along the line between the volumes' centres, its approximation becomes less accurate for elongated shapes. While such situations can be overcome by conservative parameterisation, a more practical and robust solution is envisioned by computing the actual minimal distance. In addition, an extension to link collision may also benefit the robustness and is seen as a relevant aspect for future research.

7.2.4 Prerequisite Task Specification

Despite the propagated generalisability and broad applicability of most LfD-related techniques, their implementation usually requires specific adaptation and pre-engineered settings. This also applies to the presented LfD-IA framework, which includes empirically defined parameter sets and method-related design choices that do not fall at current stage into the category of natural programming and hence have to be specified by a person experienced in the system.

A set of such prerequisite task specifications is given by the input required from HAP, including the assumed static environment, a discretised task space, and a robot model. Manual quantification of the static environment can be substituted by automatic mapping using alternative sensing systems, such as RGBD cameras (see Section 7.2.1). A graphical representation of the real-time environment encountered may be presented within simulated environment that allows visual verification and the incorporation of a selection scheme for different robotic systems. The tracking of the dynamic environment can also be used to approximate the environment using superquadrics, eliminating the currently cumbersome manual specification required for robust reproduction.

Another set of pre-defined parameters is required for CDMPs. The presented work already promotes a user-centric parameterisation scheme that is suitable for all tasks encountered. Here, a user-selected accuracy mode σ is defined that calculates the actual number of RBFs required by the CDMPs using the duration of the demonstration such that $N = \sigma \cdot T_{dem}$. Further parameterisation rules for CDMPs may support more robust behaviour for a wider variety of use cases and therefore present an interesting avenue for future research.

7.2.5 Artificial Intelligence

The main purpose of the presented thesis was to analyse in detail the possibilities around LfD in the assembly industry and to promote its progress towards practical application. As discussed in Section 1.3, some constraints had to be applied to make the technical scope attainable. However, this does not imply an equivalent limitation in the applicability of the presented contributions (see Section 7.1) nor a forced exclusion of other methods to achieve the aspired goal.

A fundamental aspect to mention is the potential seen in AI and ML-based methods. Although considered outside the scope of this work, these techniques represent an increasingly prominent branch of research in the context of LfD and robotics as a whole. In

the given context, their ability to generalise is assumed to be significantly better than the trajectory-based method used by DMPs. This may be particularly relevant once the generalisation towards changes in task is of interest, e.g. the robot is expected to assemble similar but not identical objects to the ones being assembled during human demonstration. It also promotes the idea of not requiring a single fully efficient demonstration trajectory but rather learning from sparse or partial demonstrations which are optimised afterwards. While several beneficial properties are linked to AI-based solutions, the present work has identified the deterministic DMPs to be effective for the given use case. One major bottleneck seen in AI-based contributions remains their low achievable accuracy which is a key requirement for assembly tasks. However, this does not reduce the value of AI for potential incorporation in LfD solutions for industrial assembly tasks as an interesting avenue for future research.

7.3 Concluding Remark

The assembly industry is constantly interested in improving its effectiveness, cost-efficiency, and productivity to remain competitive. Current challenges including the transition into mass customisation and the labour shortage due to a demographic change promote the application of flexible, intuitively programmable robotic systems. As such, LfD promises significant advantages that may assist in keeping the assembly industry functional. This thesis investigated how LfD can be leveraged for industry practice and presented three novel methods unified in the aimed LfD-IA framework that promotes increased practicability and robustness. As a result, LfD is one step closer to becoming a reasonable candidate for the challenges of the future assembly industry. However, more work is required in terms of sophisticated solutions successfully evaluated in realistic scenarios. It is hoped that the motivation and contributions of this thesis inspire future research and industry efforts to bring both worlds together and strongly benefit from each other.

Appendices

A Material supporting the Literature Review

Table A.1: Overview of included References and their characteristics 1/2 (*rate/attempts)

Ref.	Avg. Citations	Demonstration Method	Demonstration Quantity	Learning Method
[68]	–	Kinaesthetic Teaching	10	Costs/Rewards - Trajectory Optimisation
[69]	–	Kinaesthetic Teaching	unspecified	Costs/Rewards - Trajectory Optimisation
[79]	–	Kinaesthetic Teaching	1	Policy - Trajectory
[52]	6	Kinaesthetic Teaching	"several"	Plan - Primitive Sequence
[45]	3	Kinaesthetic Teaching	"multiple"	Policy - Trajectory
[43]	3	Teleoperation	single	Policy - Trajectory
[85]	3	Kinaesthetic Teaching	4	Policy - Trajectory
[208]	3	Kinaesthetic Teaching	"few"	Policy - Trajectory
[51]	2	Passive Observation	"multiple"	Policy - Trajectory
[57]	2	Kinaesthetic Teaching	5	Policy - Trajectory
[39]	2	Passive Observation	"multiple"	Policy - Trajectory
[53]	1	Teleoperation	8	Costs/Rewards - Trajectory Optimisation
[61]	1	Kinaesthetic Teaching	"set"	Policy - Low-level Actions
[42]	1	Teleoperation	10	Policy - Trajectory
[34]	1	Teleoperation + Kinaesthetic Teaching	single	
[76]	0	Passive Observation	15	Policy - Trajectory
[84]	0	Kinaesthetic Teaching	4	Policy - Trajectory
[62]	0	Teleoperation	30	Policy - Trajectory
[38]	0	Passive Observation	single	Policy - Trajectory
[71]	0	Teleoperation	3	Costs/Rewards - Trajectory Optimisation
[70]	0	Passive Observation	30	Plan - Primitive Sequence
[78]	0	Kinaesthetic Teaching	6	Plan - Primitive Hierarchy
[58]	0	Passive Observation	single	Plan - Primitive Sequence
[89]	0	Kinaesthetic Teaching	single	Policy - Trajectory
[60]	0	Kinaesthetic Teaching	single	Policy - Trajectory

Continued on next page

Table A.1: Overview of included References and their characteristics 1/2 (*rate/attempts) (Continued)

Ref.	Avg. Citations	Demonstration Method	Demonstration Quantity	Learning Method
[67]	0	Teleoperation	single	Policy - Trajectory
[83]	0	Kinaesthetic Teaching	3	Plan - Primitive Sequence
[88]	0	Kinaesthetic Teaching	unspecified	Costs/Rewards - Trajectory Optimisation
[209]	0	Kinaesthetic Teaching	7	Policy - Trajectory
[92]	0	Passive Observation	unspecified	Costs/Rewards - Trajectory Optimisation
[77]	0	Passive Observation	3	Plan - Primitive Sequence
[72]	0	Teleoperation	15	Plan - Primitive Sequence
[75]	0	Passive Observation	10	Plan - Primitive Sequence
[91]	10	Kinaesthetic Teaching	30	Costs/Rewards - Inverse Reinforcement Learning
[47]	4.5	Teleoperation	8	Policy - Trajectory
[32]	4.5	Kinaesthetic Teaching + Passive Observation	unspecified	Plan - Primitive Sequence
[44]	4	Passive Observation	9	Policy - Trajectory
[82]	3.5	Kinesthaetic Teaching	5	Policy - Trajectory
[48]	3	Teleoperation	8	Policy - Trajectory
[74]	7.3	Passive Observation	single	Costs/Rewards - Trajectory Optimisation
[86]	6.3	Kinaesthetic Teaching	9	Policy - Trajectory
[59]	5	Kinaesthetic Teaching	8	Policy - Trajectory
[65]	4	Kinaesthetic Teaching	5	Policy - Trajectory
[63]	3.3	Teleoperation	8	Policy - Low-level Actions
[37]	14.3	Passive Observation	10	Policy - Trajectory
[49]	7	Teleoperation	4 to 7	Plan - Primitive Sequence
[33]	8.2	Passive Observation + Teleoperation	single	Plan - Primitive Hierarchy
[81]	6.4	Kinaesthetic Teaching	2	Policy - Trajectory
[35]	4.4	Kinaesthetic Teaching + Passive Observation	"multiple"	Plan - Primitive Sequence
[90]	4.4	Passive Observation	99	Policy - Trajectory
[50]	3.4	Passive Observation	single	Plan - Primitive Sequence
[73]	7.5	Teleoperation	single	Plan - Primitive Sequence
[40]	6.2	Passive Observation	single	Policy - Trajectory
[64]	5.8	Kinaesthetic Teaching	100	Policy - Trajectory
[80]	5.5	Teleoperation	4	Policy - Trajectory
[41]	4.8	Passive Observation	unspecified	Plan - Primitive Sequence
[46]	3.2	Passive Observation	single	Plan - Primitive Sequence
[66]	6.7	Passive Observation	50	Policy - Trajectory
[87]	16.3	Kinaesthetic Teaching	8	Policy - Trajectory
[36]	10.9	Teleoperation + Kinaesthetic Teaching	single	Policy - Trajectory
[56]	5.1	Kinaesthetic Teaching	single	Policy - Trajectory

Table A.2: Overview of included References and their characteristics 2/2

Ref.	Assembly Skill	Practicability	Application Scenario	Generalisability	Performance Measure
[68]	peg insertion (0.2 mm tolerance)	unrelated	–	spatial scaling + task uncertainties	success rate (100% / 10)* + efficiency + effectiveness
[69]	peg insertion (0.1 mm tolerance)	unrelated	–	spatial scaling + similar object	success rate (96% / 100 same object, 95% / 100 similar object)* + effectiveness
[79]	gluing pick-and-place	unrelated	–	unspecified	success rate (83% / 6)* + effectiveness
[52]	interlocking	related	timber structure assembly	spatial scaling + task uncertainties	success rate (93% / 100)*
[45]	peg insertion (0.5 mm tolerance)	practical	PCB assembly	spatial scaling	success rate (100% / 9)* + efficiency + effectiveness
[43]	peg insertion (0.4 mm tolerance)	related	RJ-45 connector	spatial scaling + temporal scaling + similar object	success rate (86.9% / -)* + efficiency + effectiveness
[85]	pick-and-place	unrelated	–	spatial scaling	success
[208]	peg insertion (tolerance not specified)	unrelated	–	unspecified	success
[51]	sewing	related	personalised stent grafts	spatial scaling + task uncertainties + path optimisation + similar objects	success
[57]	peg insertion (1 mm tolerance)	related	USB stick and power plug	spatial scaling + similar objects	success rate (90% / 20)* + efficiency
[39]	peg insertion (0.3 mm tolerance)	unrelated	–	spatial scaling	success rate (93.8% / 80)* + effectiveness
[53]	peg insertion (0.01 mm tolerance, interference fit)	unrelated	–	similar object	success rate (100% / 20)* + effectiveness
[61]	peg insertion (0.89 mm tolerance)	unrelated	–	spatial scaling + task uncertainties	success rate (100% / 20)* + efficiency
[42]	peg insertion (0.1 mm tolerances)	unrelated	–	spatial scaling	success + effectiveness
[34]	pick-and-place	unrelated	–	spatial scaling + similar object	success rate(82% / 50)* + efficiency
[76]	pick-and-place	unrelated	–	unspecified	success rate (90% / 10)* + accuracy error of trajectory
[84]	pick-and-place	unrelated	–	spatial scaling	success rate (85% / 20)* + efficiency + effectiveness
[62]	peg insertion (6 mm tolerance)	unrelated	–	spatial scaling + task uncertainties	success rate (90% / 30)* + effectiveness
[38]	pick-and-place	unrelated	–	path optimisation	success rate (100% / 10)*
[71]	stacking	unrelated	–	spatial scaling	success + effectiveness
[70]	stacking	unrelated	–	unspecified	success rate (100% / 5)*
[78]	pick-and-place / bin-sorting	unrelated	–	spatial scaling + sequence optimisation	success rate (100% / 20)* + effectiveness
[58]	wiring	related	NIST Assembly Board #3	spatial scaling	success + efficiency
[89]	wiring	unrelated	–	task uncertainties	success rate (100% / 10)*

Continued on next page

Table A.2: Overview of included References and their characteristics 2/2 (Continued)

Ref.	Assembly Skill	Practicability	Application Scenario	Generalisability	Performance Measure
[60]	peg insertion (1.8 mm tolerance)	unrelated	–	spatial scaling	success rate (62.5% / -)*
[67]	peg insertion (2 mm tolerance)	unrelated	–	spatial scaling + task uncertainties	success rate (96% / 50 moving hole, 98.6% / 80 error added at known location)* + effectiveness
[83]	pick-and-place	unrelated	–	spatial scaling	success rate (75% / 4)*
[88]	screwing / stacking	unrelated	–	spatial scaling + path adjustment	success
[209]	peg insertion (tolerance not specified)	unrelated	–	spatial scaling	success + effectiveness
[92]	stacking	unrelated	–	spatial scaling	success rate (96% / -)* + effectiveness
[77]	stacking	unrelated	–	sequence optimisation	success rate (77% / -)* + efficiency
[72]	stacking / pick-and-place	unrelated	–	spatial scaling	success rate (100% / 7 stacking, 100% / 7 pick-and-place)* + efficiency + effectiveness
[75]	stacking	unrelated	–	spatial scaling	success rate (>90% / 10 trained tasks, >50% / 10 unseen tasks)* + effectiveness
[91]	pick-and-place	unrelated	–	spatial scaling	success + accuracy
[47]	peg insertion (1 mm tolerance) / peg insertion (unspecified)	practical / related	condenser assembly / HDMI insertion	task uncertainties	success rate (100% / 20)* + efficiency + effectiveness
[32]	peg insertion (0.3mm tolerances) / peg insertion (0.01 mm tolerance) / bin-picking / bolting	practical	power breaker assembly + set-top box assembly	spatial scaling + path optimisation	success rate (98% / 100 grasping, 97% / 100 inserting)*
[44]	peg insertion (0.42 mm tolerance)	practical	PCB assembly	spatial scaling	success
[82]	pick-and-place	unrelated	–	spatial scaling + path adjustment	success + efficiency + effectiveness
[48]	peg insertion (1 mm tolerance) / peg insertion (unspecified)	practical / related	condenser assembly / HDMI connector	task uncertainties	success
[74]	pick-and-place / peg insertion (1mm tolerance) / bin-picking	unrelated	–	spatial scaling + path adjustment + similar objects	success rate (95% / - grasping, 72% / 10 peg insertion, 86% / - select trained objects)* + accuracy
[86]	pick-and-place	unrelated	–	path adjustment	success
[59]	peg insertion (0.2mm tolerance)	unrelated	–	spatial scaling + task uncertainties + similar objects	success + efficiency

Continued on next page

Table A.2: Overview of included References and their characteristics 2/2 (Continued)

Ref.	Assembly Skill	Practicability	Application Scenario	Generalisability	Performance Measure
[65]	peg insertion (20mm H7f7 tolerance)	unrelated	–	spatial scaling + task uncertainties	success rate (100% / 3)*
[63]	peg insertion (0.006 mm tolerance)	unrelated	–	task uncertainties	success
[37]	peg insertion (tolerance not specified)	unrelated	–	spatial scaling	success rate (86.7% / 30)*
[49]	peg insertion (0.01 mm clearance fit) / gluing / peg insertion (0.05 mm clearance fit)	practical	sleeve-cavity and coil-cylinder assembly	spatial scaling + task uncertainties	success + accuracy + effectiveness
[33]	peg insertion (tolerance not specified)	related	Cranfield benchmark assembly	spatial scaling + task uncertainties	success rate (50% / -)*
[81]	pick-and-place	unrelated	–	spatial scaling + path adjustment	success rate (100% / 5)*
[35]	hammering / bolting / screwing	unrelated	–	spatial scaling	success rate (90% / 20 hammering, 60% / 20 screwing, 75% / 20 bolting)* + effectiveness
[90]	peg insertion (tolerance not specified)	unrelated	–	spatial scaling + temporal scaling	success + accuracy
[50]	pick-and-place / screwing	practical	Switch assembly	spatial scaling	success rate (100% / 4 pick-and-place, 75% / 4 screwing)*
[73]	pick-and-place	unrelated	–	unspecified	success rate (100% / 10)*
[40]	peg insertion (0.04 mm tolerance)	unrelated	–	similar object	success
[64]	peg insertion (1 mm tolerance)	unrelated	–	spatial spacing + task uncertainties	success + efficiency + effectiveness
[80]	peg insertion (tolerance not specified)	unrelated	–	spatial scaling	success rate (100% / 4)*
[41]	pick-and-place	unrelated	–	spatial scaling	success rate (90% / 20)/*
[46]	pick-and-place	practical	PCB assembly	spatial scaling	success + effectiveness
[66]	peg insertion (25mm H7h7 tolerance + 1mm chamfer)	unrelated	–	spatial scaling + task uncertainties	success rate (98% / 25)*
[87]	screwing	unrelated	–	spatial scaling	success rate (90% / 10)*
[36]	peg insertion (tolerance not specified)	related	Cranfield benchmark assembly	spatial scaling + task uncertainties	success rate (86% / 50)* + efficiency
[56]	peg insertion (tolerance not specified)	related	Cranfield benchmark assembly	spatial scaling + task uncertainties	success rate (100% / 50 shaft and round pegs, 96% / 50 square pegs)*

B Material supporting Conducted Experiments

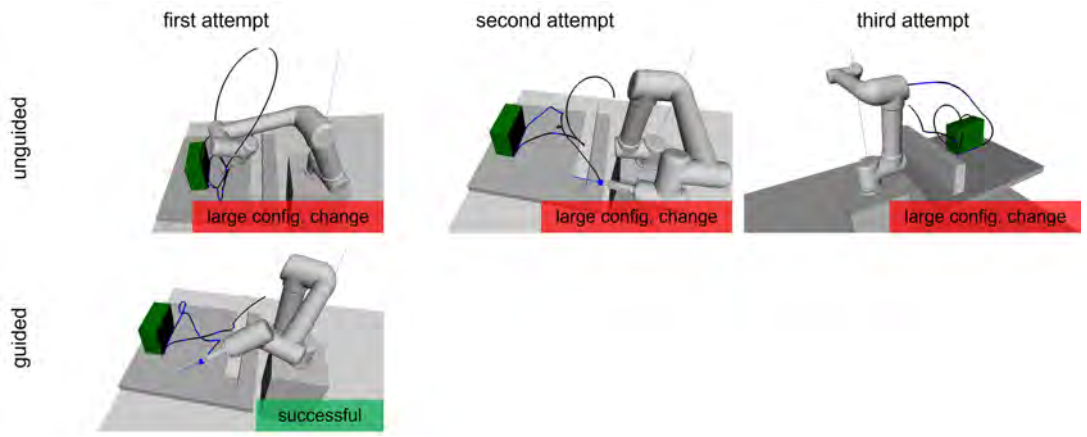

(A) Reproduction attempts of user 1

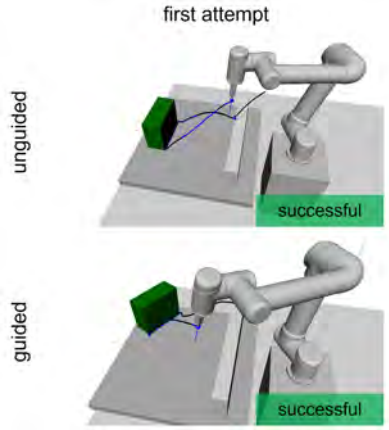

(B) Reproduction attempts of user 2

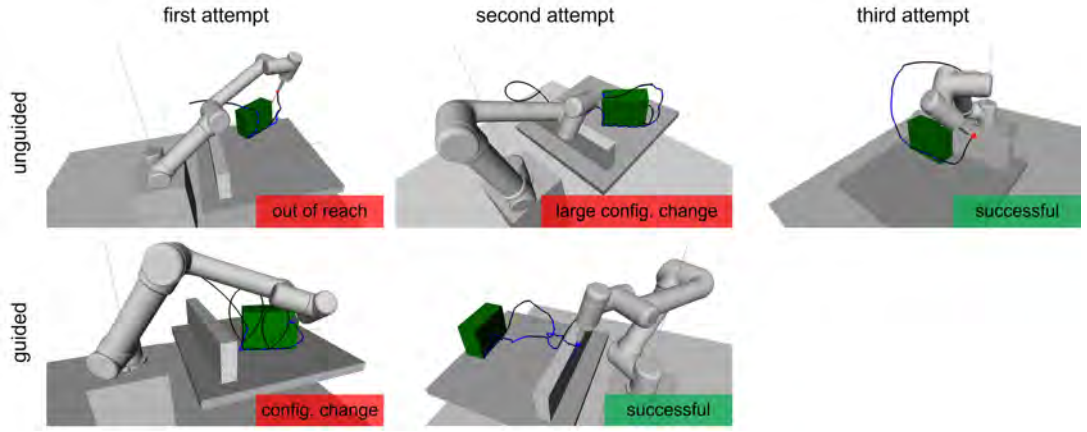

(C) Reproduction attempts of user 3

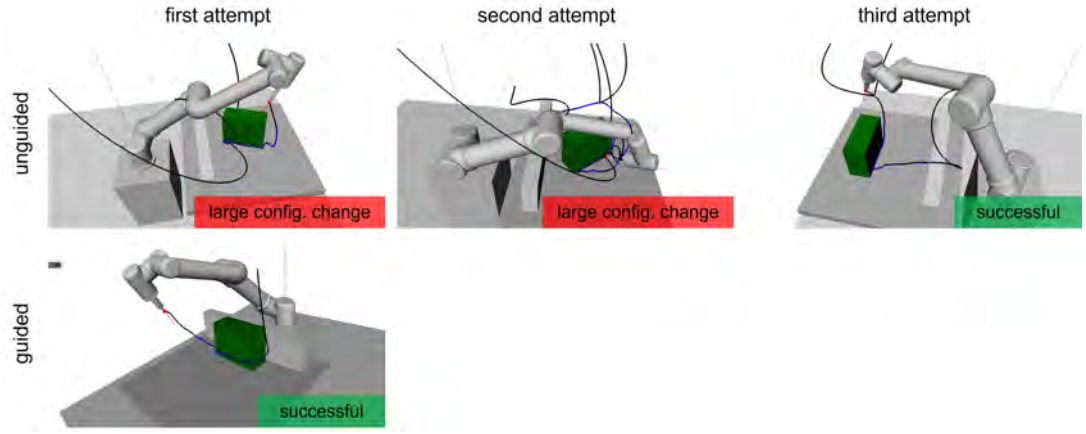

(D) Reproduction attempts of user 4

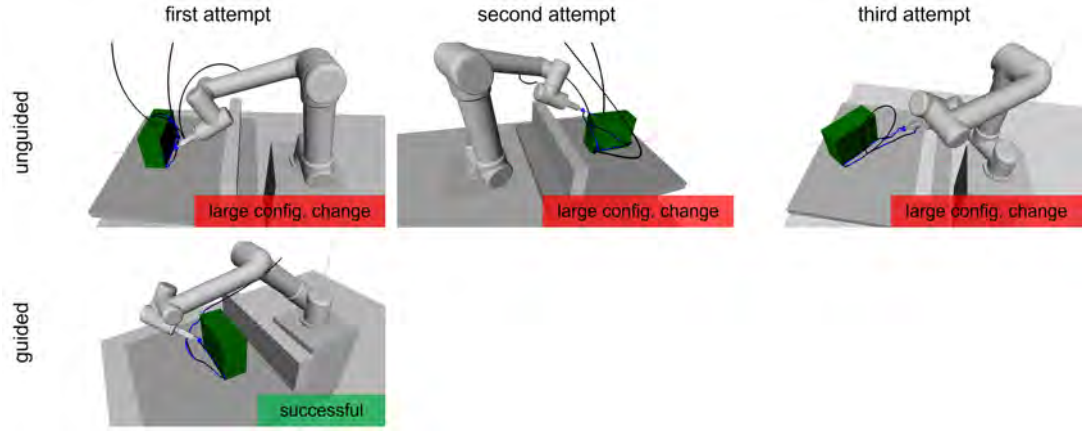

(E) Reproduction attempts of user 5

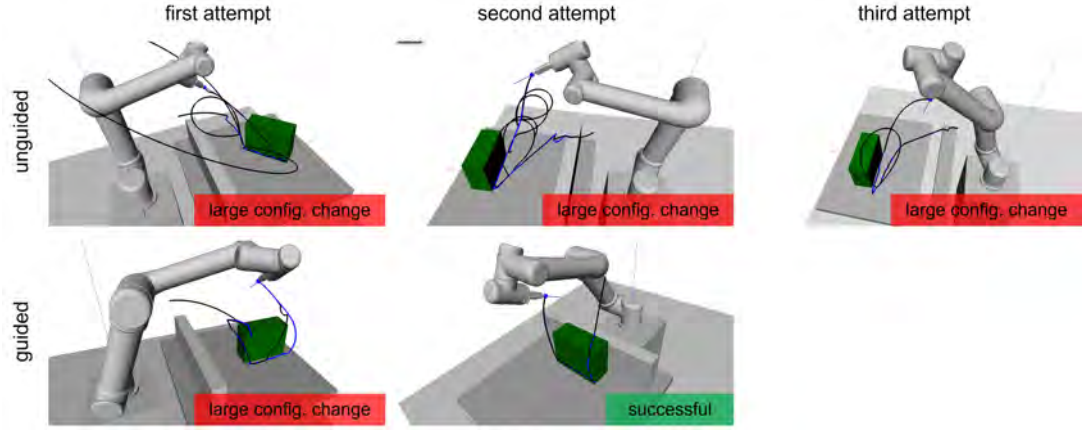

(F) Reproduction attempts of user 6

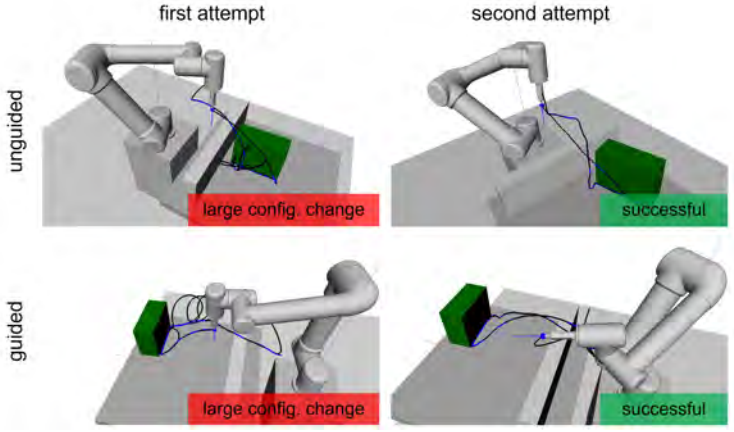

(G) Reproduction attempts of user 7

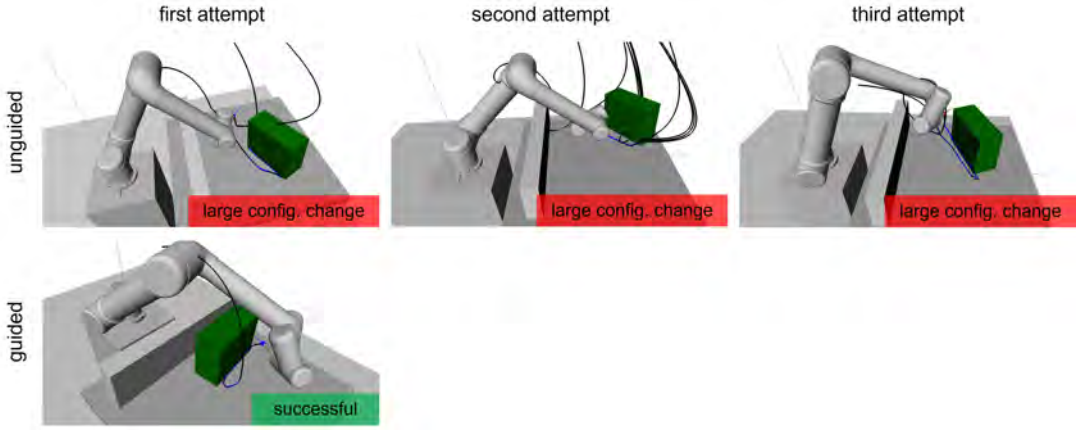

(H) Reproduction attempts of user 7

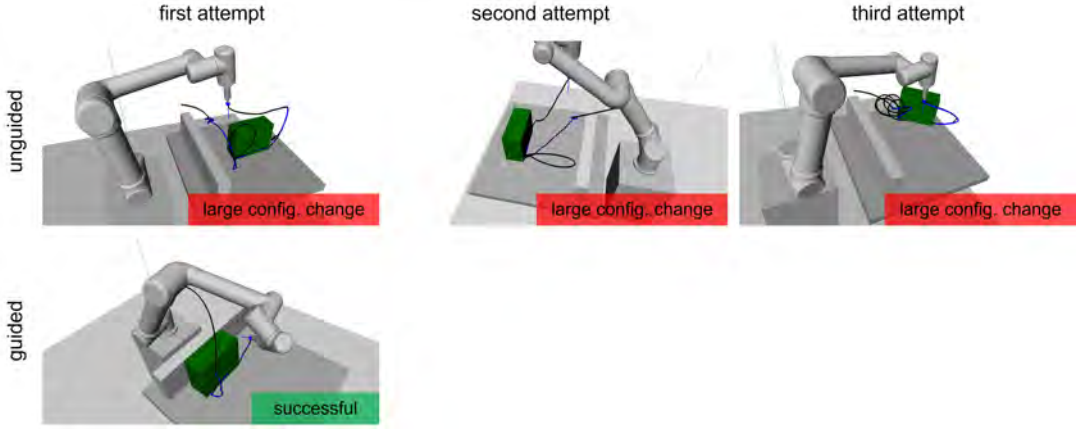

(I) Reproduction attempts of user 9

FIGURE B.1: Reproduction attempts during user study

Questionnaire

Unguided Demonstration:

Rate the following between 0-5.

- What was your confidence level when positioning the box object (5 – very confident)?
- How easy was it to demonstrate the task (5 – very easy)?
- How surprised were you by the reproduced motion (5 – very surprised)?

Guided Demonstration:

Rate the following between 0-5.

- What was your confidence level when positioning the box object (5 – very confident)?
- How easy was it to demonstrate the task while using the guidance (5 – very easy)?
- How surprised were you by the reproduced motion (5 – very surprised)?

- How effective was the GUI at improving your decision of where to place the box (post-update) (5 – very effective)?
- How intuitive was the GUI in assisting with the given task (5 – very intuitive)?
- Is the extra effort to use the GUI worth it over trial and error (i.e. without any guidance) (5 – very worth)?
- How effective was the GUI in providing spatial awareness, i.e. remain in the feasible space and avoid the infeasible space (red voxels) (5 – very effective)?

Suggested improvements to the GUI?

->

Any additional comments?

->

FIGURE B.2: Questionnaire template for user study

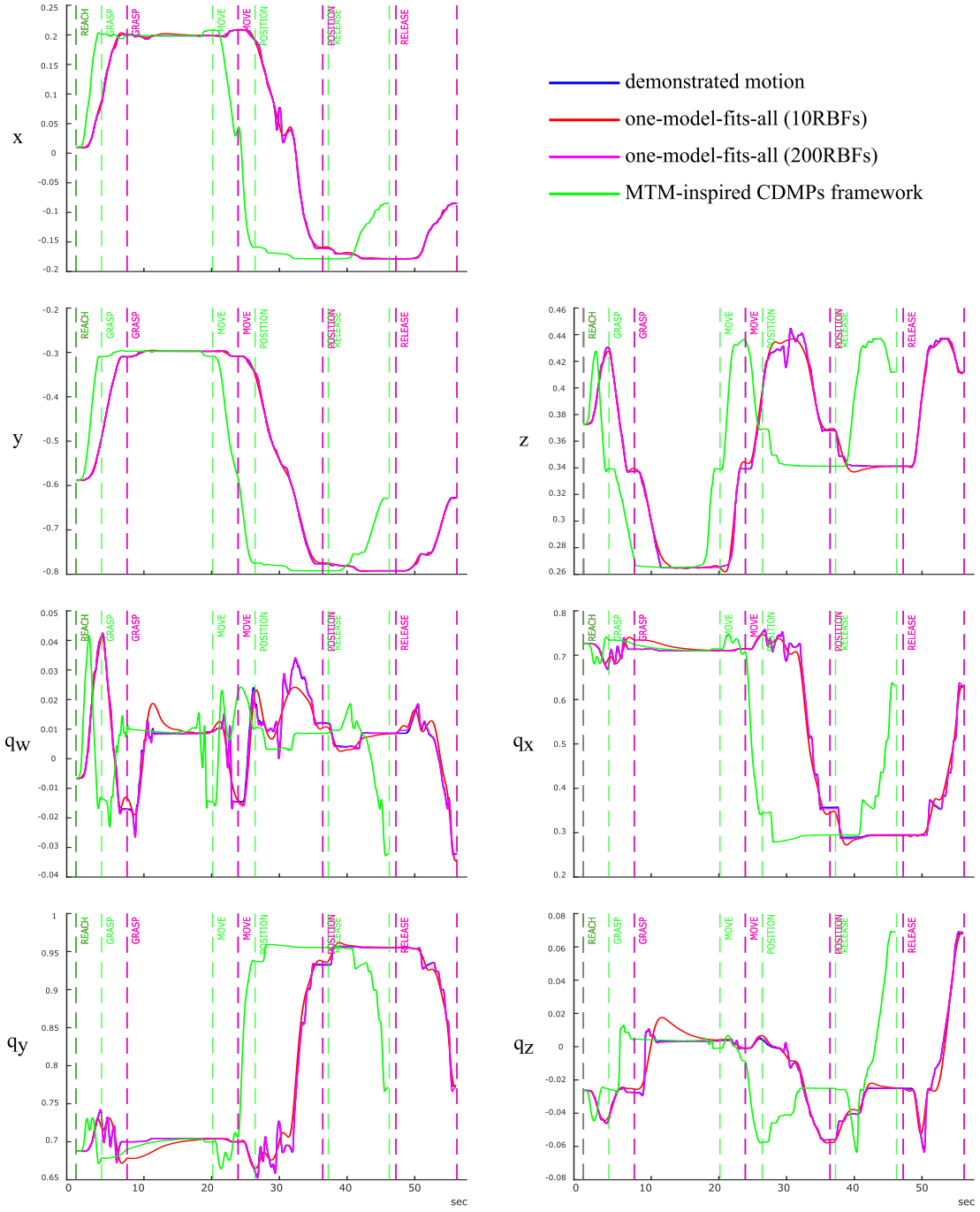

FIGURE B.3: Reproduced trajectories of developed MTM-inspired CDMPs learning framework and conventional one-model-fits-all approaches

Volumes	a, b, c	$\varepsilon_1, \varepsilon_2$	$\mathbf{x}_0$	$\mathbf{x}_T$	$\mathbf{q}_0$	$\mathbf{q}_T$
end-effector	0.10, 0.10, 0.25	1.0, 1.0	$[0.0, 0.0, 0.0]$	$[1.0, 0.0, 0.0]$	$[1, 0, 0, 0]$	$[1, 0, 0, 0]$
obstacle	0.1, 0.5, 0.1	0.1, 0.1	$[0.5, 0.0, -0.35]$		$[1.0, 0.0, 0.0, 0.0]$	
Wrenches	$\lambda_{\mathbf{x},ii}$	$\lambda_{\mathbf{q},ii}$	β	η		
obs - trans	1.0	0.0	2.0	2.0		
obs - rot	0.0	20.0				
obs - both	2.0	60.0				
LfD	α_s	K_{ii}	N	τ_{rep}		
CDMPs	7.0	600.0	40	τ_{dem}		

TABLE B.3: Applied parameter values in validation experiment 1 of potential field based robust reproduction method

Volumes	a, b, c	$\varepsilon_{1,2}$	$\mathbf{x}_0$	$\mathbf{x}_T$	$\mathbf{q}_0$	$\mathbf{q}_T$
end-effector	0.05, 0.05, 0.10	1.0, 1.0	$[0.2, 0.0, 0.2]$	$[1.2, 0.0, 0.2]$	$[1, 0, 0, 0]$	$[1, 0, 0, 0]$
obstacle 1	0.1, 0.08, 0.07	0.5, 0.1	$[0.45, 0.05, 0.25]$		$[0.71, 0.5, 0.2, -0.3]$	
obstacle 2	0.05, 0.1, 0.08	1.0, 0.1	$[0.6, -0.1, 0.7]$		$[0.6, -0.2, 0.9, 0.5]$	
obstacle 3	0.05, 0.1, 0.08	1.0, 0.5	$[0.8, 0.0, 0.7]$		$[0.8, 0.1, -0.4, 0.2]$	
workspace	0.6, 0.5, 0.5	0.1, 0.1	$[0.7, 0.0, 0.6]$		$[1.0, 0.0, 0.0, 0.0]$	
goal	0.05, 0.05, 0.1	1.0, 1.0	$[1.2, 0.0, 0.2]$		$[1.0, 0.0, 0.0, 0.0]$	
Wrenches	$\lambda_{\mathbf{x},ii}$	$\lambda_{\mathbf{q},ii}$	β	η	κ_{ii}	c_0
obstacle 1	50.0	3000.0	1.0	1.0	–	–
obstacle 2	20.0	700.0	1.0	2.0	–	–
obstacle 3	10.0	200.0	2.0	2.0	–	–
workspace	5.0	1.0	1.0	1.0	–	–
goal	–	–	–	–	10.0	0.1
LfD	α_s	K_{ii}	N	τ_{rep}		
CDMPs	7.0	500.0	80	τ_{dem}		
Demo Traj	$0.2 + e^{-0.1*(t-T/2)^2}$					

TABLE B.4: Applied parameter values in validation experiment 2 of potential field based robust reproduction method

CDMPs	α_s	K_{ii}	$\frac{N}{T_{dem}}$ (low/mod/high)	$\frac{\tau_{rep}}{\tau_{dem}}$ (test/coll/ind)
reaching	6.9	70.0	1.0 / 1.0 / 1.0	4.0 / 1.0 / 250mm/s
grasping	6.9	70.0	1.0 / 5.0 / 10.0	4.0 / 1.0 / 100mm/s
moving	6.9	500.0	1.0 / 1.0 / 1.0	4.0 / 1.0 / 250mm/s
positioning	6.9	500.0	1.0 / 5.0 / 10.0	4.0 / 1.0 / 100mm/s
releasing	6.9	70.0	1.0 / 5.0 / 10.0	4.0 / 1.0 / 100mm/s
reaching	6.9	500.0	1.0 / 1.0 / 1.0	4.0 / 1.0 / 250mm/s

Endeffector	a, b, c	$\varepsilon_{1,2}$	**x**	**q**
moving	0.08, 0.04, 0.06	0.1, 0.1	$\mathbf{x}_{TCP} + 0.25\|_z$	$\mathbf{q}_{TCP}$
positioning	0.04, 0.04, 0.04	0.1, 0.1	$\mathbf{x}_{TCP} + 0.27\|_z$	$\mathbf{q}_{TCP}$
reaching	0.106, 0.021, 0.04	0.1, 0.1	$\mathbf{x}_{TCP} + 0.18\|_z$	$\mathbf{q}_{TCP}$
for voxels	0.04, 0.04, 0.04	0.1, 0.1	$\mathbf{x}_{TCP} + 0.27\|_z$	$\mathbf{q}_{TCP}$

Environment	a, b, c	$\varepsilon_{1,2}$	**x**	**q**
wall	0.3, 0.03, 0.08	0.1, 0.1	$[0.0, -0.35, 0.087]$	$[1.0, 0.0, 0.0, 0.0]$
obstacle	0.033, 0.033, 0.09	0.1, 1.0	$[-0.05, -0.48, 0.09]$	$[1.0, 0.0, 0.0, 0.0]$
voxels	0.04, 0.04, 0.04	0.1, 0.1	$\begin{bmatrix}0.65 & -0.35 & 0.063\\ 0.85' & 0.35' & 0.363\end{bmatrix}$	$[1.0, 0.0, 0.0, 0.0]$
workspace	0.4, 0.4, 0.2	0.1, 0.1	$[0.0, -0.58, 0.213]$	$[1.0, 0.0, 0.0, 0.0]$
goal	0.04, 0.04, 0.04	0.1, 0.1	$\mathbf{x}_{TCP,T} + 0.27\|_z$	$[1.0, 0.0, 0.0, 0.0]$

Wrenches	β	η	c_0	λ / κ
wall	1.0	1.0	–	$[4.0, 4.0, 0.0, 0.0, 0.0, 500.0]$
obstacle	1.0	1.0	–	$[4.0, 4.0, 0.0, 0.0, 0.0, -1000.0]$
voxels	1.0	1.0	–	$[0.0, 0.0, 5.0, 0.0, 0.0, 0.0]$
workspace	1.0	1.0	–	$[0.0, 0.0, 5.0, 0.0, 0.0, 0.0]$
goal	–	–	0.01	$[100.0, 100.0, 0.0, 50.0, 50.0, 50.0]$

* $[0.65 - 0.85, -0.35 - 0.35, 0.063 - 0.363]$

TABLE B.5: Applied parameter values in validation experiment of LfD-IA framework

C Materials supporting Discretisation Systems

METHODS-TIME DATA

TABLE I - REACH

Case	Description	Distance moved inches	Leveled time TMU's A STD.	A Hand in Mot	A With CD or B	B Hand in Mot	C or D	E
A	Reach to object in fixed location or to object in other hand or on which other hand rests	1			2.1		3.6	
		2			4.3		5.9	
		3			5.9		7.3	
B	Reach to single object in location which may vary slightly from cycle to cycle	4	6.1	4.9	7.1	4.3	8.4	6.8
		5	6.5	5.3	7.8	5.0	9.4	7.4
		6	7.0	5.7	8.6	5.7	10.1	8.0
		7	7.4	6.1	9.3	6.5	10.8	8.7
		8	7.9	6.5	10.1	7.2	11.5	9.3
C	Reach to object in group	9	8.3	6.9	10.8	7.9	12.2	9.9
		10	8.7	7.3	11.5	8.6	12.9	10.5
		12	9.6	8.1	12.9	10.1	14.2	11.8
		14	10.5	8.9	14.4	11.5	15.6	13.0
D	Reach to very small object or where accurate grasp is required	16	11.4	9.7	15.8	12.9	17.0	14.2
		18	12.3	10.5	17.2	14.4	18.4	15.5
		20	13.1	11.3	18.6		19.8	16.7
		22	14.0	12.1	20.1		21.2	18.0
E	Reach to indefinite location to get hand in position for body balance or next motion or out of way	24	14.9	12.9	21.5		22.5	19.2
		26	15.8	13.7	22.9		23.9	20.4
		28	16.7	14.5	24.4		26.3	21.7
		30	17.5	15.3	25.8		26.7	22.9

TABLE II - MOVE

Case	Description	Distance moved inches	Leveled time TMU's A	B or E	C	D B Hand in Mot	Multiplying factor Weight	Factor
A	Move object against stop	1	1.7	1.7	1.7		Up to 5	1.00
		2	3.6	4.2	4.2		10	1.03
		3	4.9	5.7	5.7		15	1.05
B	Move object to approximate location	4	6.1	6.9	7.3	4.3	20	1.08
		5	7.3	8.0	8.7	5.0	25	1.11
		6	8.1	8.9	9.7	5.7	30	1.14
		7	8.9	9.7	10.8	6.5	35	1.16
		8	9.7	10.6	11.8	7.2	40	1.19
C	Move object to exact location	9	10.5	11.5	12.7	7.9	45	1.22
		10	11.3	12.2	13.5	8.6	50	1.25
		12	12.9	13.4	15.2	10.0		
		14	14.4	14.6	16.9	11.4		
D	Toss object aside	16	16.0	15.8	18.7	12.8		
		18	17.6	17.0	20.4	14.2		
		20	19.2	18.2	22.1	15.6		
		22	20.8	19.4	23.8	17.0		
E	Move object to indefinite location	24	22.4	20.6	25.5	18.4		
		26	24.0	21.8				
		28	25.5	23.1				
		30	27.1	24.3				

TABLE III - TURN

Deg. turned	Leveled TMU's	Deg. turned	Leveled TMU's
30°	2.8	120°	6.8
45°	3.5	135°	7.4
60°	4.1	150°	8.1
75°	4.8	165°	8.7
90°	5.4	180°	9.4
105°	6.1		

Small	No load or parts up to 2.1 lbs Use table value
Medium	Loads from 2.1 to 10 lb 1.57 x table value
Large	Loads from 10.1 to 35 lbs 3 x table value
Apply pressure 16 2 TMU's	

Turn is a special case of Reach or Move It is accomplished by a turning or torsional motion during which the hand and wrist turn When turn is combined with a normal Reach or Move, determine time for Turn and Reach or Move from the tables and use larger value

(A) Methods-time data

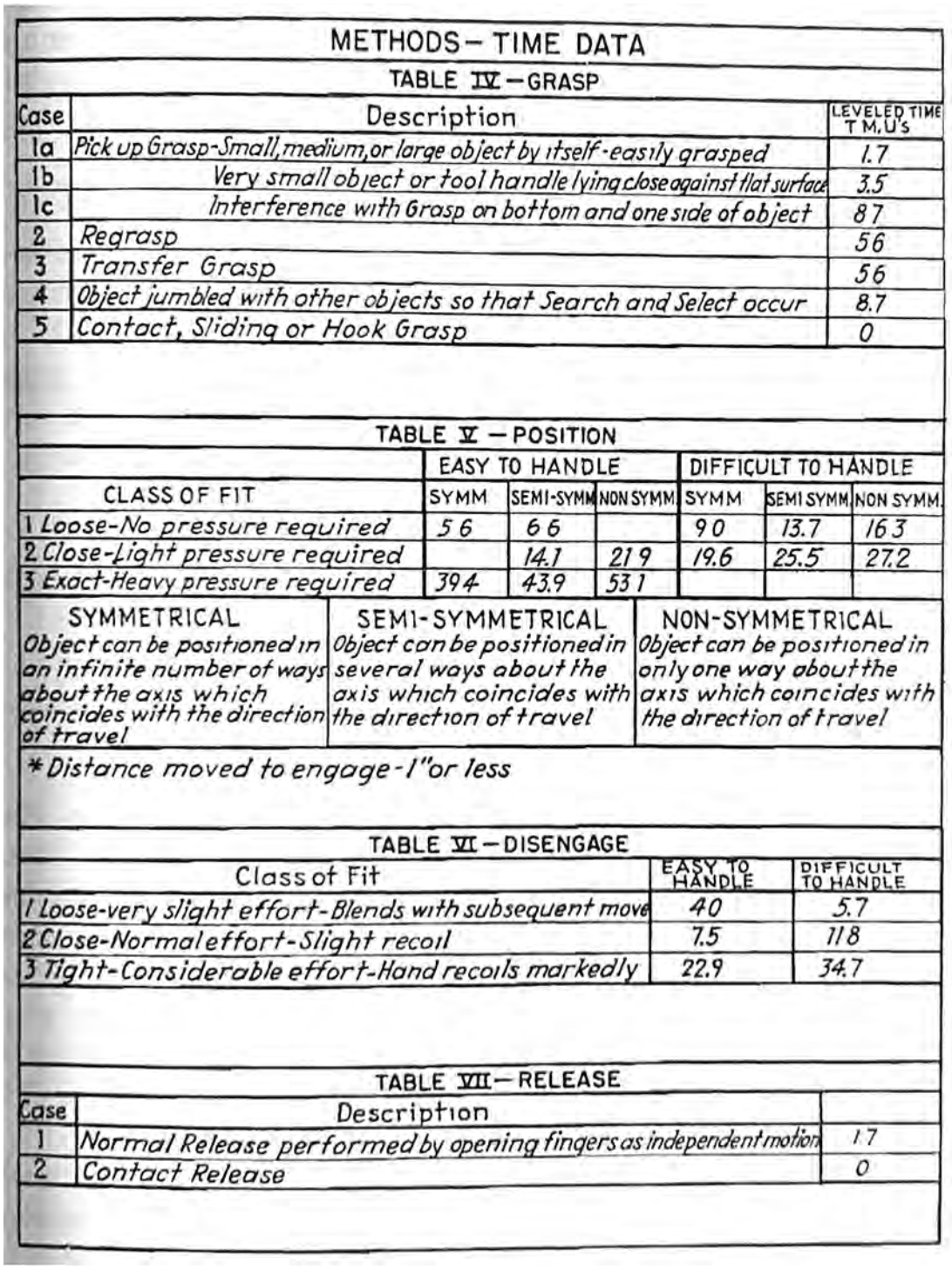

METHODS – TIME DATA

TABLE IV – GRASP

Case	Description	LEVELED TIME T.M.U's
1a	Pick up Grasp-Small, medium, or large object by itself-easily grasped	1.7
1b	Very small object or tool handle lying close against flat surface	3.5
1c	Interference with Grasp on bottom and one side of object	8.7
2	Regrasp	5.6
3	Transfer Grasp	5.6
4	Object jumbled with other objects so that Search and Select occur	8.7
5	Contact, Sliding or Hook Grasp	0

TABLE V – POSITION

	EASY TO HANDLE			DIFFICULT TO HANDLE		
CLASS OF FIT	SYMM	SEMI-SYMM	NON SYMM.	SYMM	SEMI SYMM.	NON SYMM.
1 Loose-No pressure required	5.6	6.6		9.0	13.7	16.3
2 Close-Light pressure required		14.1	21.9	19.6	25.5	27.2
3 Exact-Heavy pressure required	39.4	43.9	53.1			

SYMMETRICAL	SEMI-SYMMETRICAL	NON-SYMMETRICAL
Object can be positioned in an infinite number of ways about the axis which coincides with the direction of travel	Object can be positioned in several ways about the axis which coincides with the direction of travel	Object can be positioned in only one way about the axis which coincides with the direction of travel

*Distance moved to engage-1" or less

TABLE VI – DISENGAGE

Class of Fit	EASY TO HANDLE	DIFFICULT TO HANDLE
1 Loose-very slight effort-Blends with subsequent move	4.0	5.7
2 Close-Normal effort-Slight recoil	7.5	11.8
3 Tight-Considerable effort-Hand recoils markedly	22.9	34.7

TABLE VII – RELEASE

Case	Description	
1	Normal Release performed by opening fingers as independent motion	1.7
2	Contact Release	0

(b) Methods-time data (continued)

Figure C.1: Methods-Time Data of MTM-1 discretisation system

Bibliography

[1] Matthew J. Page, Joanne E. McKenzie, Patrick Bossuyt, Isabelle Boutron, Tammy C. Hoffmann, Cynthia D. Mulrow, Larissa Shamseer, Jennifer M. Tetzlaff, Elie Akl, Sue E. Brennan, Roger Chou, Julie Glanville, Jeremy M. Grimshaw, Asbjørn Hróbjartsson, Manoj M. Lalu, Tianjing Li, Elizabeth W. Loder, Evan Mayo-Wilson, Steve McDonald, Luka McGuinness, Lesley A. Stewart, James Thomas, Andrea C. Tricco, Vivian A. Welch, Penny Whiting, and David Moher. The prisma 2020 statement: An updated guideline for reporting systematic reviews. Medicina Fluminensis, 57(4):444–465, 2021. ISSN 18476864. doi: 10.21860/medflum2021_264903.

[2] Harold B Maynard, Gustave James Stegemerten, and John L Schwab. Methods-time measurement., 1948.

[3] A tribute to Joseph Engelberger. Unimate: The first industrial robot, 2023. URL `https://www.automate.org/a3-content/joseph-engelberger-about`.

[4] Valeria Villani, Fabio Pini, Francesco Leali, and Cristian Secchi. Survey on human–robot collaboration in industrial settings: Safety, intuitive interfaces and applications. Mechatronics, 55(March):248–266, 2018. ISSN 09574158. doi: 10.1016/j.mechatronics.2018.02.009.

[5] Aude G. Billard, Sylvain Calinon, and Rüdiger Dillmann. Springer handbook of robotics. In Springer Handbook of Robotics, chapter Learning f, pages 1995–2014. Springer, Berlin, Heidelberg, 2nd editio edition, 2016. ISBN 9783319325521. doi: 10.1007/978-3-319-32552-1_74.

[6] Aude Billard, Sylvain Calinon, Rüdiger Dillmann, and Stefan Schaal. Springer handbook of robotics. In Springer Handbook of Robotics, chapter Robot Prog, pages 1371–1394. Springer, Berlin, Heidelberg, 1st editio edition, 2008. ISBN 978-3-540-30301-5. doi: 10.1007/978-3-540-30301-5.

[7] Federico Vicentini. Collaborative robotics: A survey. Journal of Mechanical Design, 143(4):1–20, 2021. ISSN 10500472. doi: 10.1115/1.4046238.

[8] Aleksandar Vakanski and Farrokh Janabi-Sharifi. Robot Learning by Visual Observation. John Wiley & Sons, Inc., 2017. ISBN 9781119091882. doi: 10.1002/9781119091882.

[9] Harish Ravichandar, Athanasios S. Polydoros, Sonia Chernova, and Aude Billard. Recent advances in robot learning from demonstration. Annual Review of Control, Robotics, and Autonomous Systems, 3:297–330, 2020. ISSN 25735144. doi: 10.1146/annurev-control-100819-063206.

[10] Yudie Hu, Yuqi Wang, Kaixiong Hu, and Weidong Li. Adaptive obstacle avoidance in path planning of collaborative robots for dynamic manufacturing. Journal of Intelligent Manufacturing, 34(2):789–807, 2 2023. ISSN 0956-5515. doi: 10.1007/s10845-021-01825-9.

[11] Leonel Rozo, Andras G. Kupcsik, Philipp Schillinger, Meng Guo, Robert Krug, Niels van Duijkeren, Markus Spies, Patrick Kesper, Sabrina Hoppe, Hanna Ziesche, Mathias Bürger, and Kai O. Arras. The e-bike motor assembly: Towards advanced robotic manipulation for flexible manufacturing. Robotics and Computer-Integrated Manufacturing, 85:102637, 2 2024. ISSN 07365845. doi: 10.1016/j.rcim.2023.102637.

[12] Michael Sommerhalder, Yves Zimmermann, Leonardo Simovic, Marco Hutter, Peter Wolf, and Robert Riener. Trajectory optimization framework for rehabilitation robots with multi-workspace objectives and constraints. IEEE Robotics and Automation Letters, 8(10):6819–6826, 10 2023. ISSN 2377-3766. doi: 10.1109/LRA.2023.3311229.

[13] Rafael J. Escarabajal, José L. Pulloquinga, Pau Zamora-Ortiz, Ángel Valera, Vicente Mata, and Marina Vallés. Imitation learning-based system for the execution of self-paced robotic-assisted passive rehabilitation exercises. IEEE Robotics and Automation Letters, 8(7):4283–4290, 7 2023. ISSN 2377-3766. doi: 10.1109/LRA.2023.3281884.

[14] Haitao Wu, Heng Li, Xin Fang, and Xiaochun Luo. A survey on teaching workplace skills to construction robots. Expert Systems with Applications, 205:117658, 11 2022. ISSN 09574174. doi: 10.1016/j.eswa.2022.117658.

[15] Bruno Lotter and Hans-Peter Wiendahl. Montage in der industriellen Produktion: Ein Handbuch für die Praxis. Springer-Verlag, 2. edition edition, 2012.

[16] Thomas Langhoff. Den demographischen Wandel im Unternehmen erfolgreich gestalten. Springer Berlin Heidelberg, Berlin, Heidelberg, 2009. ISBN 978-3-642-01241-9. doi: 10.1007/978-3-642-01242-6.

[17] Jörn Henrik Thun, Andreas Größler, and Switbert Miczka. The impact of the demographic transition on manufacturing: Effects of an ageing workforce in german industrial firms. Journal of Manufacturing Technology Management, 18(8):985–999, 2007. ISSN 1741038X. doi: 10.1108/17410380710828299.

[18] Christoph Petzoldt, Matthias Harms, and Michael Freitag. Review of task allocation for human-robot collaboration in assembly. International Journal of Computer Integrated Manufacturing, 00(00):1–41, 2023. ISSN 13623052. doi: 10.1080/0951192X.2023.2204467.

[19] Henrik Christensen, Nancy Amato, Holly Yanco, Maja Mataric, Howie Choset, Ann Drobnis, Ken Goldberg, Jessy Grizzle, Gregory Hager, John Hollerbach, Seth Hutchinson, Venkat Krovi, Daniel Lee, William D. Smart, Jeff Trinkle, and Gaurav Sukhatme. A roadmap for us robotics – from internet to robotics 2020 edition. Foundations and Trends® in Robotics, 8(4):307–424, 2021. ISSN 1935-8253. doi: 10.1561/2300000066.

[20] Mikkel Rath Pedersen, Lazaros Nalpantidis, Rasmus Skovgaard Andersen, Casper Schou, Simon Bøgh, Volker Krüger, and Ole Madsen. Robot skills for manufacturing: From concept to industrial deployment. Robotics and Computer-Integrated Manufacturing, 37:282–291, 2016. ISSN 07365845. doi: 10.1016/j.rcim.2015.04.002.

[21] Shimon Y. Nof, editor. Springer Handbook of Automation. Springer Berlin Heidelberg, Berlin, Heidelberg, 2009. ISBN 978-3-540-78830-0. doi: 10.1007/978-3-540-78831-7.

[22] Micropsi Industries. Mirai, 2023. URL `https://www.micropsi-industries.com/product`.

[23] Shimon Y. Nof, Wilbert E. Wilhelm, and Hans-Jürgen Warnecke. Industrial Assembly. Springer Science & Business Media, 1997. doi: 10.1007/978-1-4615-6393-8.

[24] Victor Hernandez Moreno, Steffen Jansing, Mikhail Polikarpov, Marc G. Carmichael, and Jochen Deuse. Obstacles and opportunities for learning from demonstration in practical industrial assembly: A systematic literature review. Robotics and

Computer-Integrated Manufacturing, 86:102658, 4 2024. ISSN 07365845. doi: 10.1016/j.rcim.2023.102658.

[25] Fouad Sukkar, Victor Hernandez Moreno, Teresa Vidal-Calleja, and Jochen Deuse. Guided learning from demonstration for robust transferability. In IEEE International Conference on Robotics and Automation (ICRA), page accepted, 2023.

[26] Victor Hernandez Moreno, Marc G. Carmichael, and Jochen Deuse. Towards learning by demonstration for industrial assembly tasks. Manufacturing Handling Industrial Robotics (MHI) Conference, page published, 2022.

[27] Victor Hernandez Moreno, Louis F. Fernandez, and Marc G. Carmichael. Multibody collision avoidance using superquadrical repulsive wrenches. IEEE Robotics and Automation Letters, to be subm, 2024.

[28] David Denyer and David Tranfield. Producing a systematic review. In The Sage handbook of organizational research methods., pages 671–689. Sage Publications Ltd, Thousand Oaks, CA, 2009. ISBN 978-1-4129-3118-2 (Hardcover).

[29] Hannah Snyder. Literature review as a research methodology: An overview and guidelines. Journal of Business Research, 104(August):333–339, 2019. ISSN 01482963. doi: 10.1016/j.jbusres.2019.07.039.

[30] SC Score. Web of science and scopus: A comparative review of content and searching capabilities. The Charleston Advisor, 11(July):5–19, 2009.

[31] Mary M. Crossan and Marina Apaydin. A multi-dimensional framework of organizational innovation: A systematic review of the literature. Journal of Management Studies, 47(6):1154–1191, 2010. ISSN 14676486. doi: 10.1111/j.1467-6486.2009.00880.x.

[32] Sanghoon Ji, Sukhan Lee, Sujeong Yoo, Ilhong Suh, Inso Kwon, Frank C. Park, Sanghyoung Lee, and Hongseok Kim. Learning-based automation of robotic assembly for smart manufacturing. Proceedings of the IEEE, 109(4):423–440, 2021. ISSN 15582256. doi: 10.1109/JPROC.2021.3063154.

[33] Thiusius Rajeeth Savarimuthu, Anders Glent Buch, Christian Schlette, Nils Wantia, Jürgen Robmann, David Martínez, Guillem Alenyà, Carme Torras, Ales Ude, Bojan Nemec, Aljaž Kramberger, Florentin Wörgötter, Eren Erdal Aksoy, Jeremie Papon, Simon Haller, Justus Piater, and Norbert Krüger. Teaching a robot the semantics of assembly tasks. IEEE Transactions on Systems, Man, and Cybernetics: Systems, 48(5):670–692, 2018. ISSN 21682232. doi: 10.1109/TSMC.2016.2635479.

[34] Anna Meszaros, Giovanni Franzese, and Jens Kober. Learning to pick at non-zero-velocity from interactive demonstrations. IEEE Robotics and Automation Letters, 7(3):6052–6059, 2022. ISSN 23773766. doi: 10.1109/LRA.2022.3165531.

[35] Ye Gu, Weihua Sheng, Christopher Crick, and Yongsheng Ou. Automated assembly skill acquisition and implementation through human demonstration. Robotics and Autonomous Systems, 99:1–16, 2018. ISSN 09218890. doi: 10.1016/j.robot.2017.10.002.

[36] Fares J. Abu-Dakka, Bojan Nemec, Jimmy A. Jørgensen, Thiusius R. Savarimuthu, Norbert Krüger, and Aleš Ude. Adaptation of manipulation skills in physical contact with the environment to reference force profiles. Autonomous Robots, 39(2):199–217, 2015. ISSN 15737527. doi: 10.1007/s10514-015-9435-2.

[37] David A. Duque, Flavio A. Prieto, and Jose G. Hoyos. Trajectory generation for robotic assembly operations using learning by demonstration. Robotics and Computer-Integrated Manufacturing, 57(July 2017):292–302, 2019. ISSN 07365845. doi: 10.1016/j.rcim.2018.12.007.

[38] Robin Pellois and Olivier Brüls. A vision-based correction of inertial measurement of human motion for robot programming by demonstration. International Journal of Mechanical Engineering and Robotics Research, 11(6):411–416, 2022. ISSN 22780149. doi: 10.18178/ijmerr.11.6.411-416.

[39] Boyang Ti, Yongsheng Gao, Ming Shi, and Jie Zhao. Generalization of orientation trajectories and force–torque profiles for learning human assembly skill. Robotics and Computer-Integrated Manufacturing, 76(May 2021):102325, 2022. ISSN 07365845. doi: 10.1016/j.rcim.2022.102325.

[40] An Wan, Jing Xu, Heping Chen, Song Zhang, and Ken Chen. Optimal path planning and control of assembly robots for hard-measuring easy-deformation assemblies. IEEE/ASME Transactions on Mechatronics, 22(4):1600–1609, 2017. ISSN 10834435. doi: 10.1109/TMECH.2017.2671342.

[41] Yasaman S. Sefidgar, Prerna Agarwal, and Maya Cakmak. Situated tangible robot programming. ACM/IEEE International Conference on Human-Robot Interaction, Part F1271:473–482, 2017. ISSN 21672148. doi: 10.1145/2909824.3020240.

[42] Jianhua Su, Yan Meng, Lili Wang, and Xu Yang. Learning to assemble noncylindrical parts using trajectory learning and force tracking. IEEE/ASME Transactions

on Mechatronics, 27(5):3132–3143, 2022. ISSN 1941014X. doi: 10.1109/TMECH.2021.3110825.

[43] Todor Davchev, Kevin Sebastian Luck, Michael Burke, Franziska Meier, Stefan Schaal, and Subramanian Ramamoorthy. Residual learning from demonstration: Adapting dmps for contact-rich manipulation. IEEE Robotics and Automation Letters, 7(2):4488–4495, 2022. ISSN 23773766. doi: 10.1109/LRA.2022.3150024.

[44] Haopeng Hu, Zhiqi Cao, Xiansheng Yang, Hao Xiong, and Yunjiang Lou. Performance evaluation of optical motion capture sensors for assembly motion capturing. IEEE Access, 9:61444–61454, 2021. ISSN 21693536. doi: 10.1109/ACCESS.2021.3074260.

[45] Haopeng Hu, Xiansheng Yang, and Yunjiang Lou. A robot learning from demonstration framework for skillful small parts assembly. International Journal of Advanced Manufacturing Technology, 119(9-10):6775–6787, 2022. ISSN 14333015. doi: 10.1007/s00170-022-08652-z.

[46] Mathias Haage, Grigoris Piperagkas, Christos Papadopoulos, Ioannis Mariolis, Jacek Malec, Yasemin Bekiroglu, Mikael Hedelind, and Dimitrios Tzovaras. Teaching assembly by demonstration using advanced human robot interaction and a knowledge integration framework. Procedia Manufacturing, 11(June):164–173, 2017. ISSN 23519789. doi: 10.1016/j.promfg.2017.07.221.

[47] Yan Wang, Cristian C. Beltran-Hernandez, Weiwei Wan, and Kensuke Harada. Hybrid trajectory and force learning of complex assembly tasks: A combined learning framework. IEEE Access, 9:60175–60186, 2021. ISSN 21693536. doi: 10.1109/ACCESS.2021.3073711.

[48] Yan Wang, Cristian C. Beltran-Hernandez, Weiwei Wan, and Kensuke Harada. Robotic imitation of human assembly skills using hybrid trajectory and force learning. Proceedings - IEEE International Conference on Robotics and Automation, 2021-May(Icra):11278–11284, 2021. ISSN 10504729. doi: 10.1109/ICRA48506.2021.9561619.

[49] Fangbo Qin, De Xu, Dapeng Zhang, and Ying Li. Robotic skill learning for precision assembly with microscopic vision and force feedback. IEEE/ASME Transactions on Mechatronics, 24(3):1117–1128, 2019. ISSN 1941014X. doi: 10.1109/TMECH.2019.2909081.

[50] Yue Wang, Rong Xiong, Hongsheng Yu, Jiafan Zhang, and Yong Liu. Perception of demonstration for automatic programing of robotic assembly: Framework, algorithm, and validation. IEEE/ASME Transactions on Mechatronics, 23(3):1059–1070, 2018. ISSN 10834435. doi: 10.1109/TMECH.2018.2799963.

[51] Bidan Huang, Yiming Yang, Ya Yen Tsai, and Guang Zhong Yang. A reconfigurable multirobot cooperation workcell for personalized manufacturing. IEEE Transactions on Automation Science and Engineering, 19(3):2581–2590, 2022. ISSN 15583783. doi: 10.1109/TASE.2021.3092560.

[52] Aljaz Kramberger, Anja Kunic, Iñigo Iturrate, Christoffer Sloth, Roberto Naboni, and Christian Schlette. Robotic assembly of timber structures in a human-robot collaboration setup. Frontiers in Robotics and AI, 8(January):1–14, 2022. ISSN 22969144. doi: 10.3389/frobt.2021.768038.

[53] Yanqin Ma, Yonghua Xie, Wenjun Zhu, and Song Liu. An efficient robot precision assembly skill learning framework based on several demonstrations. IEEE Transactions on Automation Science and Engineering, 20(1):124–136, 2022. ISSN 15583783. doi: 10.1109/TASE.2022.3144282.

[54] NIST. Assembly performance metrics and test methods, 2018. URL `https://www.nist.gov/el/intelligent-systems-division-73500/robotic-grasping-and-manipulation-assembly/assembly`.

[55] K. Collins, A. J. Palmer, and K. Rathmill. The development of a european benchmark for the comparison of assembly robot programming systems. In Robot Technology and Applications: Proceedings of the 1st Robotics Europe Conference Brussels, June 27–28, 1984, number 2, pages 187–199. Springer, Springer Berlin Heidelberg, 1985. ISBN 0903608715.

[56] Fares J. Abu-Dakka, Bojan Nemec, Aljaž Kramberger, Anders Glent Buch, Norbert Krüger, and Aleš Ude. Solving peg-in-hole tasks by human demonstration and exception strategies. Industrial Robot, 41(6):575–584, 2014. ISSN 0143991X. doi: 10.1108/IR-07-2014-0363.

[57] Yan Wang, Cristian C. Beltran-Hernandez, Weiwei Wan, and Kensuke Harada. An adaptive imitation learning framework for robotic complex contact-rich insertion tasks. Frontiers in Robotics and AI, 8(January):1–15, 2022. ISSN 22969144. doi: 10.3389/frobt.2021.777363.

[58] Azarakhsh Keipour, Maryam Bandari, and Stefan Schaal. Efficient spatial representation and routing of deformable one-dimensional objects for manipulation. IEEE International Conference on Intelligent Robots and Systems, 2022-Octob:211–216, 2022. ISSN 21530866. doi: 10.1109/IROS47612.2022.9981939.

[59] Nam Jun Cho, Sang Hyoung Lee, Jong Bok Kim, and Il Hong Suh. Learning, improving, and generalizing motor skills for the peg-in-hole tasks based on imitation learning and self-learning. Applied Sciences (Switzerland), 10(8), 2020. ISSN 20763417. doi: 10.3390/APP10082719.

[60] Serdar Hakan Arguz, Seniz Ertugrul, and Kerem Altun. Experimental evaluation of the success of peg-in-hole tasks learned from demonstration. 2022 8th International Conference on Control, Decision and Information Technologies, CoDIT 2022, pages 861–866, 2022. doi: 10.1109/CoDIT55151.2022.9804111.

[61] Suhan Shetty, Joao Silverio, and Sylvain Calinon. Ergodic exploration using tensor train: Applications in insertion tasks. IEEE Transactions on Robotics, 38(2):906–921, 2022. ISSN 19410468. doi: 10.1109/TRO.2021.3087317.

[62] Simon Stepputtis, Maryam Bandari, Stefan Schaal, and Heni Ben Amor. A system for imitation learning of contact-rich bimanual manipulation policies. IEEE International Conference on Intelligent Robots and Systems, 2022-Octob:11810–11817, 2022. ISSN 21530866. doi: 10.1109/IROS47612.2022.9981802.

[63] Sagar Gubbi, Shishir Kolathaya, and Bharadwaj Amrutur. Imitation learning for high precision peg-in-hole tasks. 2020 6th International Conference on Control, Automation and Robotics, ICCAR 2020, pages 368–372, 2020. doi: 10.1109/ICCAR49639.2020.9108072.

[64] Aljaž Kramberger, Andrej Gams, Bojan Nemec, Dimitrios Chrysostomou, Ole Madsen, and Aleš Ude. Generalization of orientation trajectories and force-torque profiles for robotic assembly. Robotics and Autonomous Systems, 98:333–346, 2017. ISSN 09218890. doi: 10.1016/j.robot.2017.09.019.

[65] Nailong Liu, Xiaodong Zhou, Zhaoming Liu, Hongwei Wang, and Long Cui. Learning peg-in-hole assembly using cartesian dmps with feedback mechanism. Assembly Automation, 6(September):895–904, 2020. ISSN 01445154. doi: 10.1108/AA-04-2020-0053.

[66] Te Tang, Hsien Chung Lin, Yu Zhao, Yongxiang Fan, Wenjie Chen, and Masayoshi Tomizuka. Teach industrial robots peg-hole-insertion by human demonstration.

In IEEE/ASME International Conference on Advanced Intelligent Mechatronics, AIM, volume 2016-Septe, pages 488–494, 2016. ISBN 9781509020652. doi: 10.1109/AIM.2016.7576815.

[67] Devesh K. Jha, Diego Romeres, William Yerazunis, and Daniel Nikovski. Imitation and supervised learning of compliance for robotic assembly. 2022 European Control Conference, ECC 2022, pages 1882–1889, 2022. doi: 10.23919/ECC55457.2022.9838102.

[68] Shaohua Yan, De Xu, and Xian Tao. Hierarchical policy learning with demonstration learning for robotic multiple peg-in-hole assembly tasks. IEEE Transactions on Industrial Informatics, pages 1–11, 2023. ISSN 19410050. doi: 10.1109/TII.2023.3240936.

[69] Kuk-Hyun Ahn, Minwoo Na, and Jae-Bok Song. Robotic assembly strategy via reinforcement learning based on force and visual information. Robotics and Autonomous Systems, 164:104399, 2023. ISSN 09218890. doi: 10.1016/j.robot.2023.104399.

[70] Minjae Kang and Songhwai Oh. Deep latent-space sequential skill chaining from incomplete demonstrations. Intelligent Service Robotics, 15(2):203–213, 2022. ISSN 18612784. doi: 10.1007/s11370-021-00409-z.

[71] Allison Pinosky, Ian Abraham, Alexander Broad, Brenna Argall, and Todd D. Murphey. Hybrid control for combining model-based and model-free reinforcement learning. International Journal of Robotics Research, 0(0):1–19, 2022. ISSN 17413176. doi: 10.1177/02783649221083331.

[72] Dong Liu, Binpeng Lu, Ming Cong, Honghua Yu, Qiang Zou, and Yu Du. Robotic manipulation skill acquisition via demonstration policy learning. IEEE Transactions on Cognitive and Developmental Systems, 14(3):1054–1065, 2022. ISSN 23798939. doi: 10.1109/TCDS.2021.3094269.

[73] Claudia Perez-D'Arpino and Julie A. Shah. C-learn: Learning geometric constraints from demonstrations for multi-step manipulation in shared autonomy. In Proceedings - IEEE International Conference on Robotics and Automation, number d, pages 4058–4065, 2017. ISBN 9781509046331. doi: 10.1109/ICRA.2017.7989466.

[74] Lars Berscheid, Pascal Meisner, and Torsten Kroger. Self-supervised learning for precise pick-and-place without object model. IEEE Robotics and Automation Letters, 5(3):4828–4835, 2020. ISSN 23773766. doi: 10.1109/LRA.2020.3003865.

[75] Hongtao Wu, Jikai Ye, Xin Meng, Chris Paxton, and Gregory S. Chirikjian. Transporters with visual foresight for solving unseen rearrangement tasks. IEEE International Conference on Intelligent Robots and Systems, 2022-Octob:10756–10763, 2022. ISSN 21530866. doi: 10.1109/IROS47612.2022.9981832.

[76] Xinjian Deng, Jianhua Liu, Honghui Gong, Hao Gong, and Jiayu Huang. A human-robot collaboration method using a pose estimation network for robot learning of assembly manipulation trajectories from demonstration videos. IEEE Transactions on Industrial Informatics, 2022. ISSN 19410050. doi: 10.1109/TII.2022.3224966.

[77] Yi Chen, David Paulius, Yu Sun, and Yunyi Jia. Robot learning of assembly tasks from non-expert demonstrations using functional object-oriented network. IEEE International Conference on Automation Science and Engineering, 2022-Augus:2012–2019, 2022. ISSN 21618089. doi: 10.1109/CASE49997.2022.9926527.

[78] Meng Guo and Mathias Burger. Interactive human-in-the-loop coordination of manipulation skills learned from demonstration. In Proceedings - IEEE International Conference on Robotics and Automation, number ii, pages 7292–7298, 2022. ISBN 9781728196817. doi: 10.1109/ICRA46639.2022.9811813.

[79] Thomas Eiband, Johanna Liebl, Christoph Willibald, and Dongheui Lee. Online task segmentation by merging symbolic and data-driven skill recognition during kinesthetic teaching. Robotics and Autonomous Systems, 162:104367, 2023. ISSN 09218890. doi: 10.1016/j.robot.2023.104367.

[80] Affan Pervez, Arslan Ali, Jee Hwan Ryu, and Dongheui Lee. Novel learning from demonstration approach for repetitive teleoperation tasks. In 2017 IEEE World Haptics Conference, WHC 2017, number June, pages 60–65. IEEE, 2017. ISBN 9781509014255. doi: 10.1109/WHC.2017.7989877.

[81] Amir M. Ghalamzan E. and Matteo Ragaglia. Robot learning from demonstrations: Emulation learning in environments with moving obstacles. Robotics and Autonomous Systems, 101:45–56, 2018. ISSN 09218890. doi: 10.1016/j.robot.2017.12.001.

[82] Y. Q. Wang, Y. D. Hu, S. El Zaatari, W. D. Li, and Y. Zhou. Optimised learning from demonstrations for collaborative robots. Robotics and Computer-Integrated Manufacturing, 71(March), 2021. ISSN 07365845. doi: 10.1016/j.rcim.2021.102169.

[83] Matteo Iovino, Fethiye Irmak Dogan, Iolanda Leite, and Christian Smith. Interactive disambiguation for behavior tree execution. IEEE-RAS International Conference on

Humanoid Robots, 2022-Novem:82–89, 2022. ISSN 21640580. doi: 10.1109/Humanoids53995.2022.10000088.

[84] Hongmin Wu, Wu Yan, Zhihao Xu, and Xuefeng Zhou. A framework of improving human demonstration efficiency for goal-directed robot skill learning. IEEE Transactions on Cognitive and Developmental Systems, 14(4):1743–1754, 2022. ISSN 23798939. doi: 10.1109/TCDS.2021.3137262.

[85] Yu Zhang, Long Cheng, Houcheng Li, and Ran Cao. Learning accurate and stable point-to-point motions: A dynamic system approach. IEEE Robotics and Automation Letters, 7(2):1510–1517, 2022. ISSN 23773766. doi: 10.1109/LRA.2022.3140677.

[86] Emre Ugur and Hakan Girgin. Compliant parametric dynamic movement primitives. Robotica, 38(3):457–474, 2020. ISSN 14698668. doi: 10.1017/S026357471900078X.

[87] Scott Niekum, Sarah Osentoski, George Konidaris, Sachin Chitta, Bhaskara Marthi, and Andrew G. Barto. Learning grounded finite-state representations from unstructured demonstrations. International Journal of Robotics Research, 34(2):131–157, 2015. ISSN 17413176. doi: 10.1177/0278364914554471.

[88] Tian Yu and Qing Chang. User-guided motion planning with reinforcement learning for human-robot collaboration in smart manufacturing. Expert Systems with Applications, 209(August):118291, 2022. ISSN 09574174. doi: 10.1016/j.eswa.2022.118291.

[89] Roberto Meattini, Davide Chiaravalli, Kevin Galassi, Gianluca Palli, and Claudio Melchiorri. Experimental evaluation of intuitive programming of robot interaction behaviour during kinesthetic teaching using semg and cutaneous feedback. IFAC-PapersOnLine, 55(38):1–6, 2022. ISSN 24058963. doi: 10.1016/j.ifacol.2023.01.125.

[90] Timotej Gašpar, Bojan Nemec, Jun Morimoto, and Aleš Ude. Skill learning and action recognition by arc-length dynamic movement primitives. Robotics and Autonomous Systems, 100:225–235, 2018. ISSN 09218890. doi: 10.1016/j.robot.2017.11.012.

[91] Xiang Zhang, Liting Sun, Zhian Kuang, and Masayoshi Tomizuka. Learning variable impedance control via inverse reinforcement learning for force-related tasks. IEEE Robotics and Automation Letters, 6(2):2225–2232, 2021. ISSN 23773766. doi: 10.1109/LRA.2021.3061374.

[92] Xuanhui Xu, Mingyu You, Hongjun Zhou, Zhifeng Qian, and Bin He. Robot imitation learning from image-only observation without real-world interaction. IEEE/ASME Transactions on Mechatronics, pages 1–11, 2022. ISSN 1941014X. doi: 10.1109/TMECH.2022.3217048.

[93] Maria Maier, Barbara Tropschuh, Severin Teubner, and Gunther Reinhart. Methode zur gestaltung des anlernprozesses in der manuellen montage. ZWF Zeitschrift für wirtschaftlichen Fabrikbetrieb, 115(10):682–686, 2020. ISSN 09470085. doi: 10.3139/104.112423.

[94] Jürgen Berthel and Fred G. Becker. Personal-Management. Schäffer-Poeschel, 2022. ISBN 978-3-7910-5216-8.

[95] Andreas Schelten. Grundlagen der Arbeitspädagogik. Steiner Stuttgart, 2005. ISBN 3-515-8776-1.

[96] Hans Jung. Personalwirtschaft. De Gruyter, 12 2016. ISBN 9783110493092. doi: 10.1515/9783110493092.

[97] M Becker, T Hettinger, and G Wobbe. Kompendium der Arbeitswissenschaft: Optimierungsmöglichkeiten zur Arbeitsgestaltung und Arbeitsorganisation. Kiehl, 1993. ISBN 9783470454016. URL https://books.google.com.au/books?id=llRNNQAACAAJ.

[98] Verband für Arbeitsstudien und Betriebsorganisation. Methodenlehre der betriebsorganisation arbeitspädagogik. Auflage München: Hanser, 1991.

[99] Guenter Ullrich. Wirtschaftliches Anlernen in der Serienmontage. Ein Beitrag zur Lernkurventheorie. PhD thesis, Gerhard-Mercator-University, Duisburg, 1995.

[100] Tim Jeske. Entwicklung einer Methode zur Prognose der Anlernzeit sensumotorischer Tätigkeiten. Shaker, 2013.

[101] Norman G Roth and Carsten Zur Steege. Excellent Lean Production: The Way to Business Sustainability. Dt. MTM-Vereinigung, 2015.

[102] Michael Shneier, Elena Messina, Craig Schlenoff, Frederick Proctor, Thomas Kramer, and Joseph Falco. Measuring and representing the performance of manufacturing assembly robots. Nistir 8090, November, 2015.

[103] M Guertler, L Tomidei, N Sick, G Paul, S Hussain, L Frijat, A Wambsganss, and V Hernandez Moreno. Beyond technology - the cognitive and organisational impacts of cobots. In Australasian Conference on Robotics and Automation, 2022.

[104] Kevin M Lynch and Frank C Park. Modern robotics. Cambridge University Press, 2017.

[105] Yoan Mollard, Thibaut Munzer, Andrea Baisero, Marc Toussaint, and Manuel Lopes. Robot programming from demonstration, feedback and transfer. In IEEE International Conference on Intelligent Robots and Systems, volume 2015-Decem, pages 1825–1831, 2015. ISBN 9781479999941. doi: 10.1109/IROS.2015.7353615.

[106] Matthew B Luebbers, Connor Brooks, John Kim, Daniel Szafir, and Bradley Hayes. Augmented reality interface for constrained learning from demonstration. 2019.

[107] Maximilian Diehl, Alexander Plopski, Hirokazu Kato, and Karinne Ramirez-Amaro. Augmented reality interface to verify robot learning. 29th IEEE International Conference on Robot and Human Interactive Communication, RO-MAN 2020, pages 378–383, 2020. doi: 10.1109/RO-MAN47096.2020.9223502.

[108] Matthew B. Luebbers, Connor Brooks, Carl L. Mueller, Daniel Szafir, and Bradley Hayes. Arc-lfd: Using augmented reality for interactive long-term robot skill maintenance via constrained learning from demonstration. Proceedings - IEEE International Conference on Robotics and Automation, 2021-May(Icra):909–916, 2021. ISSN 10504729. doi: 10.1109/ICRA48506.2021.9561844.

[109] Fouad Sukkar, Jennifer Wakulicz, Ki Myung Brian Lee, and Robert Fitch. Motion planning in task space with gromov-hausdorff approximations. arXiv preprint arXiv:2209.04800, 9 2022.

[110] Stefan Schaal. Is imitation learning the route to humanoid robots?, 1999. ISSN 13646613.

[111] Auke Jan Ijspeert, Jun Nakanishi, Tomohiro Shibata, and Stefan Schaal. Nonlinear dynamical systems for imitation with humanoid robots. In Proceedings of the IEEE/RAS International Conference on Humanoids Robots (Humanoids2001), number CONF, pages 219–226, 2001.

[112] A.J. Ijspeert, Jun Nakanishi, and Stefan Schaal. Movement imitation with nonlinear dynamical systems in humanoid robots. In Proceedings 2002 IEEE International Conference on Robotics and Automation (Cat. No.02CH37292), volume 2, pages 1398–1403. IEEE, 2002. ISBN 0-7803-7272-7. doi: 10.1109/ROBOT.2002.1014739.

[113] Auke Jan Ijspeert, Jun Nakanishi, and Stefan Schaal. Learning attractor landscapes for learning motor primitives. In Advances in Neural Information Processing Systems, 2003. ISBN 0262025507.

[114] Stefan Schaal, Jan Peters, and Jun Nakanishi. Control, planning, learning, and imitation with dynamic movement primitives. Neuroscience, pages 1–21, 2003.

[115] Stefan Schaal, Jan Peters, Jun Nakanishi, and Auke Ijspeert. Learning movement primitives. Springer Tracts in Advanced Robotics, 15:561–572, 2005. ISSN 1610742X. doi: 10.1007/11008941_60.

[116] Stefan Schaal. Dynamic movement primitives -a framework for motor control in humans and humanoid robotics. Adaptive Motion of Animals and Machines, pages 261–280, 2006. doi: 10.1007/4-431-31381-8_23.

[117] S. F. Giszter, F. A. Mussa-Ivaldi, and E. Bizzi. Convergent force fields organized in the frog's spinal cord. Journal of Neuroscience, 13(2):467–491, 1993. ISSN 02706474. doi: 10.1523/jneurosci.13-02-00467.1993.

[118] Heiko Hoffmann, Peter Pastor, and Stefan Schaal. Dynamic movement primitives for movement generation motivated by convergent force fields in frog. In Fourth International Symposium on Adaptive Motion of Animals and Machines, Case Western Reserve University, Cleveland, OH, number 3, pages 1–2, 2008.

[119] Jens Kober, Katharina Mülling, Oliver Krömer, Christoph H. Lampert, Bernhard Schölkopf, and Jan Peters. Movement templates for learning of hitting and batting. Proceedings - IEEE International Conference on Robotics and Automation, 97:853–858, 2010. ISSN 10504729. doi: 10.1109/ROBOT.2010.5509672.

[120] Yosef Cohen and Sigal Berman. Tight dynamic movement primitives for complex trajectory generation. Proceedings - 2013 IEEE International Conference on Systems, Man, and Cybernetics, SMC 2013, (246252):2402–2407, 2013. doi: 10.1109/SMC.2013.410.

[121] Andrej Gams, Bojan Nemec, Leon Zlajpah, Mirko Wachter, Auke Ijspeert, Tamim Asfour, and Ales Ude. Modulation of motor primitives using force feedback: Interaction with the environment and bimanual tasks. IEEE International Conference on Intelligent Robots and Systems, pages 5629–5635, 2013. ISSN 21530858. doi: 10.1109/IROS.2013.6697172.

[122] Tadej Petric, Luca Colasanto, Andrej Gams, Ales Ude, and Auke J. Ijspeert. Bio-inspired learning and database expansion of compliant movement primitives. IEEE-RAS International Conference on Humanoid Robots, 2015-Decem:346–351, 2015. ISSN 21640580. doi: 10.1109/HUMANOIDS.2015.7363573.

[123] Ruohan Wang, Yan Wu, Wei Liang Chan, and Keng Peng Tee. Dynamic movement primitives plus: For enhanced reproduction quality and efficient trajectory modification using truncated kernels and local biases. IEEE International Conference on Intelligent Robots and Systems, 2016-Novem:3765–3771, 2016. ISSN 21530866. doi: 10.1109/IROS.2016.7759554.

[124] Anqing Duan, Raffaello Camoriano, Diego Ferigo, Daniele Calandriello, Lorenzo Rosasco, and Daniele Pucci. Constrained dmps for feasible skill learning on humanoid robots. IEEE-RAS International Conference on Humanoid Robots, 2018-Novem: 1032–1038, 2019. ISSN 21640580. doi: 10.1109/HUMANOIDS.2018.8624934.

[125] Weiyong Si, Ning Wang, and Chenguang Yang. Composite dynamic movement primitives based on neural networks for human–robot skill transfer. Neural Computing and Applications, 35(32):23283–23293, 2021. ISSN 14333058. doi: 10.1007/s00521-021-05747-8.

[126] Freddy Liendo, Alessandro Bozzi, Camilo Hernández, Christine Galez, Roberto Sacile, and José Jiménez. An improved dual quaternion-based dynamic movement primitives formulation for obstacle avoidance kinematics in human- robot collaboration system of systems. 2023 18th Annual System of Systems Engineering Conference, SoSe 2023, 2023. doi: 10.1109/SoSE59841.2023.10178518.

[127] Matteo Saveriano, Fares J. Abu-Dakka, Aljaž Kramberger, and Luka Peternel. Dynamic movement primitives in robotics: A tutorial survey. (February), 2021.

[128] Michele Ginesi, Nicola Sansonetto, and Paolo Fiorini. Overcoming some drawbacks of dynamic movement primitives. arXiv, 144(August):103844, 2019. ISSN 0921-8890. doi: 10.1016/j.robot.2021.103844.

[129] Fares J. Abu-Dakka and Ville Kyrki. Geometry-aware dynamic movement primitives. Proceedings - IEEE International Conference on Robotics and Automation, (0): 4421–4426, 2020. ISSN 10504729. doi: 10.1109/ICRA40945.2020.9196952.

[130] Antonis Sidiropoulos, Dimitrios Papageorgiou, and Zoe Doulgeri. A novel framework for generalizing dynamic movement primitives under kinematic constraints. Autonomous Robots, 47(1):37–50, 2023. ISSN 15737527. doi: 10.1007/s10514-022-10067-4.

[131] Peter Pastor, Heiko Hoffmann, Tamim Asfour, and Stefan Schaal. Learning and generalization of motor skills by learning from demonstration. In IEEE

International Conference on Robotics and Automation, pages 763–768, 2009. doi: 10.1109/robot.2009.5152385.

[132] Peter Pastor, Ludovic Righetti, Mrinal Kalakrishnan, and Stefan Schaal. Online movement adaptation based on previous sensor experiences. In IEEE International Conference on Intelligent Robots and Systems, pages 365–371. IEEE, 2011. ISBN 9781612844541. doi: 10.1109/IROS.2011.6048819.

[133] Aleš Ude, Bojan Nemec, Tadej Petrič, and Jun Morimoto. Orientation in cartesian space dynamic movement primitives. In Proceedings - IEEE International Conference on Robotics and Automation, number 4, pages 2997–3004, 2014. ISBN 9781479936854. doi: 10.1109/ICRA.2014.6907291.

[134] Aljaž Kramberger, Andrej Gams, Bojan Nemec, and Aleš Ude. Generalization of orientational motion in unit quaternion space. IEEE-RAS International Conference on Humanoid Robots, pages 808–813, 2016. ISSN 21640580. doi: 10.1109/HUMANOIDS.2016.7803366.

[135] Nailong Liu, Zhaoming Liu, and Long Cui. A modified cartesian space dmps model for robot motion generation. In Haibin Yu, Jinguo Liu, Lianqing Liu, Zhaojie Ju, Yuwang Liu, and Dalin Zhou, editors, Lecture Notes in Computer Science (including subseries Lecture Notes in Artificial Intelligence and Lecture Notes in Bioinformatics), volume 11745 LNAI, pages 76–85, Cham, 2019. Springer International Publishing. ISBN 9783030275280. doi: 10.1007/978-3-030-27529-7_7.

[136] Leonidas Koutras and Zoe Doulgeri. A correct formulation for the orientation dynamic movement primitives for robot control in the cartesian space. Conference on Robot Learning, (CoRL):1–10, 2019.

[137] Leonidas Koutras and Zoe Doulgeri. A novel dmp formulation for global and frame independent spatial scaling in the task space. 29th IEEE International Conference on Robot and Human Interactive Communication, RO-MAN 2020, (September): 727–732, 2020. doi: 10.1109/RO-MAN47096.2020.9223500.

[138] Richelle A.C.M. Olde Keizer, Lex van Velsen, Mathieu Moncharmont, Brigitte Riche, Nadir Ammour, Susanna Del Signore, Gianluca Zia, Hermie Hermens, and Aurèle N'Dja. Using socially assistive robots for monitoring and preventing frailty among older adults: a study on usability and user experience challenges. Health and Technology, 9(4):595–605, 2019. ISSN 21907196. doi: 10.1007/s12553-019-00320-9.

[139] I S O Iso. 9241-11: 2018 ergonomics of human-system interaction—part 11: Usability: Definitions and concepts. International Organization for Standardization. https://www. iso. org/obp/ui/# iso: std: iso, 9241(11), 2018.

[140] Auke Jan Ijspeert, Jun Nakanishi, Heiko Hoffmann, Peter Pastor, and Stefan Schaal. Dynamical movement primitives: Learning attractor models for motor behaviors, 2013. ISSN 08997667.

[141] Jing Xu, Zhimin Hou, Zhi Liu, and Hong Qiao. Compare contact model-based control and contact model-free learning: A survey of robotic peg-in-hole assembly strategies. arXiv, (March):1–15, 2019. ISSN 23318422.

[142] Kejun Ning, Tomas Kulvicius, Minija Tamosiunaite, and Florentin Wörgötter. A novel trajectory generation method for robot control. Journal of Intelligent and Robotic Systems: Theory and Applications, 68(2):165–184, 2012. ISSN 09210296. doi: 10.1007/s10846-012-9683-8.

[143] Roman Weitschat and Harald Aschemann. Safe and efficient human-robot collaboration part ii: Optimal generalized human-in-the-loop real-time motion generation. IEEE Robotics and Automation Letters, 3(4):3781–3788, 2018. ISSN 23773766. doi: 10.1109/LRA.2018.2856531.

[144] Alexandros Paraschos, Christian Daniel, Jan Peters, and Gerhard Neumann. Probabilistic movement primitives. In Advances in Neural Information Processing Systems, pages 1–9, 2013.

[145] Matteo Saveriano, Felix Franzel, and Dongheui Lee. Merging position and orientation motion primitives. Proceedings - IEEE International Conference on Robotics and Automation, 2019-May:7041–7047, 2019. ISSN 10504729. doi: 10.1109/ICRA.2019.8793786.

[146] Tomas Kulvicius, Kejun Ning, Minija Tamosiunaite, and Florentin Wörgötter. Joining movement sequences: Modified dynamic movement primitives for robotics applications exemplified on handwriting. IEEE Transactions on Robotics, 28(1):145–157, 2012. ISSN 15523098. doi: 10.1109/TRO.2011.2163863.

[147] Thomas Eiband, Matteo Saveriano, and Dongheui Lee. Learning haptic exploration schemes for adaptive task execution. Proceedings - IEEE International Conference on Robotics and Automation, 2019-May:7048–7054, 2019. ISSN 10504729. doi: 10.1109/ICRA.2019.8793934.

[148] Jerome Trommnau, Andreas Frommknecht, Jörg Siegert, Johannes Wößner, and Thomas Bauernhansl. Design for automatic assembly: A new approach to classify limp components. Procedia CIRP, 91:49–54, 2020. ISSN 22128271. doi: 10.1016/j.procir.2020.01.136.

[149] Patrick Rückert, Björn Papenberg, and Kirsten Tracht. Classification of assembly operations using machine learning algorithms based on visual sensor data. Procedia CIRP, 97:110–116, 2020. ISSN 22128271. doi: 10.1016/j.procir.2020.05.211.

[150] Jochen Deuse, Lukas Stankiewicz, Ronny Zwinkau, and Frank Weichert. Automatic generation of methods-time measurement analyses for assembly tasks from motion capture data using convolutional neuronal networks - a proof of concept. In Advances in Intelligent Systems and Computing, volume 959, pages 141–150, 2020. ISBN 9783030200398. doi: 10.1007/978-3-030-20040-4_13.

[151] Elodie Hüsing, Carlo Weidemann, Michael Lorenz, Burkhard Corves, and Mathias Hüsing. Determining robotic assistance for inclusive workplaces for people with disabilities. Robotics, 10(1), 2021. ISSN 22186581. doi: 10.3390/robotics10010044.

[152] Gualtiero Fantoni, Salam Qaddoori Al-Zubaidi, Elena Coli, and Daniele Mazzei. Automating the process of method-time-measurement. International Journal of Productivity and Performance Management, 70(4):958–982, 2021. ISSN 17410401. doi: 10.1108/IJPPM-08-2019-0404.

[153] Björn Papenberg, Patrick Rückert, and Kirsten Tracht. Classification of assembly operations using recurrent neural networks. Annals of Scientific Society for Assembly, Handling and Industrial Robotics 2021, pages 301–311, 2022. doi: 10.1007/978-3-030-74032-0_25.

[154] Joseph Haslam Quick, James H Duncan, and James A Malcolm. Work-factor time standards: measurement of manual and mental work. 1962.

[155] Kjell B. Zandin. MOST work measurement systems. CRC press, 2002.

[156] Montage und Handhabungstechnik. Vdi 2860, 1990.

[157] Deutsches Institut für Normung. Din 8593: manufacturing processes joining. Technical report, DIN, 2003.

[158] Verband Deutscher Ingenieure. VDI 2860: Assembly and handling, handling functions, handling units, terminology, definitions and symbols. VDI-Verlag, 1990.

[159] Richard P. Paul and Shimon Y. Nof. Work methods measurement—a comparison between robot and human task performance. International Journal of Production Research, 17(3):277–303, 1979. ISSN 1366588X. doi: 10.1080/00207547908919615.

[160] R L Paul and S Y Nof. Human and robot task performance. Computer Vision and Sensor-Based Robots, pages 23–50, 1979.

[161] C.K. Choi and W.H. Ip. A comparison of mtm and rtm. Work Study, 48(2):57–61, 1999. ISSN 0043-8022. doi: 10.1108/00438029910253707.

[162] Hanan Lechtman and Shimon Y. Nof. Performance time models for robot point operations. International Journal of Production Research, 21(5):659–673, 1983. ISSN 1366588X. doi: 10.1080/00207548308942402.

[163] Albert C K Choi, Andrew W H Ip, and Hong Kong. Estimation of robotic assembly time. In Sixth International Conference on Manufacturing Engineering: Manufacturing; a Global Perspective, number December, pages 325–328, 1995. ISBN 0858256339.

[164] Jaejin Jang, Pyung Hoi Koo, and Shimon Y Nof. Application of design and control tools in a multirobot cell. Computers and Industrial Engineering, 32(1):89–100, 1997. ISSN 03608352. doi: 10.1016/s0360-8352(96)00198-2.

[165] Bernhard Rembold and Shimon Y. Nof. Modelling the performance of a mobile robot with rtm. International Journal of Production Research, 29(5):967–978, 1991. ISSN 1366588X. doi: 10.1080/00207549108930113.

[166] Roman Froschauer and René Lindorfer. Workflow-based programming of human-robot interaction for collaborative assembly stations. ARW & OAGM Workshop 2019, 2019. doi: 10.3217/978-3-85125-663-5-14.

[167] Dominik Schonberger, Rene Lindorfer, and Roman Froschauer. Modeling workflows for industrial robots considering human-robot-collaboration. Proceedings - IEEE 16th International Conference on Industrial Informatics, INDIN 2018, pages 400–405, 2018. doi: 10.1109/INDIN.2018.8471999.

[168] Lukas Huber. Exact obstacle avoidance for robots in complex and dynamic environments using local modulation. Technical report, EPFL, 2024.

[169] Dae Hyung Park, Heiko Hoffmann, Peter Pastor, and Stefan Schaal. Movement reproduction and obstacle avoidance with dynamic movement primitives and potential fields. In 2008 8th IEEE-RAS International Conference on Humanoid

Robots, Humanoids 2008, pages 91–98, 2008. ISBN 9781424428229. doi: 10.1109/ICHR.2008.4755937.

[170] O. Khatib. Real-time obstacle avoidance for manipulators and mobile robots. Proceedings - IEEE International Conference on Robotics and Automation, pages 500–505, 1985. ISSN 10504729. doi: 10.1109/ROBOT.1985.1087247.

[171] Oliver Brock and Oussama Khatib. Real-time replanning in high-dimensional configuration spaces using sets of homotopic paths. Proceedings - IEEE International Conference on Robotics and Automation, 1(April):550–555, 2000. ISSN 10504729. doi: 10.1109/robot.2000.844111.

[172] Michele Ginesi, Daniele Meli, Andrea Calanca, Diego Dall'Alba, Nicola Sansonetto, and Paolo Fiorini. Dynamic movement primitives: Volumetric obstacle avoidance. In 2019 19th international conference on advanced robotics (ICAR), pages 234–239. IEEE, 2019.

[173] Michele Ginesi, Daniele Meli, Andrea Roberti, Nicola Sansonetto, and Paolo Fiorini. Dynamic movement primitives: Volumetric obstacle avoidance using dynamic potential functions. Journal of Intelligent & Robotic Systems, 101(4):79, 4 2021. ISSN 0921-0296. doi: 10.1007/s10846-021-01344-y.

[174] A. S. Phung, J. Malzahn, F. Hoffmann, and T. Bertram. Get out of the way - obstacle avoidance and learning by demonstration for manipulation. IFAC Proceedings Volumes (IFAC-PapersOnline), 44(1 PART 1):11514–11519, 2011. ISSN 14746670. doi: 10.3182/20110828-6-IT-1002.01363.

[175] Hyeonbeom Lee, Hyoin Kim, and H. Jin Kim. Planning and control for collision-free cooperative aerial transportation. IEEE Transactions on Automation Science and Engineering, 15(1):189–201, 2018. ISSN 15455955. doi: 10.1109/TASE.2016.2605707.

[176] Hyeonbeom Lee, Hoseong Seo, and Hyeong Geun Kim. Trajectory optimization and replanning framework for a micro air vehicle in cluttered environments. IEEE Access, 8:135406–135415, 2020. ISSN 21693536. doi: 10.1109/ACCESS.2020.3011401.

[177] Tomas Kulvicius, Martin Biehl, Mohamad Javad Aein, Minija Tamosiunaite, and Florentin Wörgötter. Interaction learning for dynamic movement primitives used in cooperative robotic tasks. Robotics and Autonomous Systems, 61(12):1450–1459, 2013. ISSN 09218890. doi: 10.1016/j.robot.2013.07.009.

[178] Zhangjie Tu, Tianwei Zhang, Lei Yan, and Tin Lun Lam. Whole-body control for velocity-controlled mobile collaborative robots using coupling dynamic movement primitives. IEEE-RAS International Conference on Humanoid Robots, 2022-Novem: 119–126, 2022. ISSN 21640580. doi: 10.1109/Humanoids53995.2022.10000097.

[179] Huan Tan, Erdem Erdemir, Kazuhiko Kawamura, and Qian Du. A potential field method-based extension of the dynamic movement primitive algorithm for imitation learning with obstacle avoidance. 2011 IEEE International Conference on Mechatronics and Automation, ICMA 2011, pages 525–530, 2011. doi: 10.1109/ICMA.2011.5985617.

[180] Brett R. Fajen and William H. Warren. Behavioral dynamics of steering, obstacle avoidance, and route selection. Journal of Experimental Psychology: Human Perception and Performance, 29(2):343–362, 2003. ISSN 00961523. doi: 10.1037/0096-1523.29.2.343.

[181] Andrej Gams, Bojan Nemec, Auke Jan Ijspeert, and Aleš Ude. Coupling movement primitives: Interaction with the environment and bimanual tasks. IEEE Transactions on Robotics, 30(4):816–830, 2014. ISSN 15523098. doi: 10.1109/TRO.2014.2304775.

[182] Zhuang Mei, Yang Chen, Minghao Jiang, Huaiyu Wu, and Lei Cheng. Mobile robots path planning based on dynamic movement primitives library. Chinese Control Conference, CCC, pages 6906–6911, 2017. ISSN 21612927. doi: 10.23919/ChiCC.2017.8028446.

[183] Ibrahim A. Seleem, Haitham El-Hussieny, and Samy F.M. Assal. Motion planning for continuum robots: A learning from demonstration approach. RO-MAN 2018 - 27th IEEE International Symposium on Robot and Human Interactive Communication, pages 868–873, 2018. doi: 10.1109/ROMAN.2018.8525601.

[184] Ibrahim A. Seleem, Samy F.M. Assal, Hiroyuki Ishii, and Haitham El-Hussieny. Demonstration-guided pose planning and tracking for multi-section continuum robots considering robot dynamics. IEEE Access, 7:166690–166703, 2019. ISSN 21693536. doi: 10.1109/ACCESS.2019.2953122.

[185] Iman Kardan, Alireza Akbarzadeh, and Ali Mousavi Mohammadi. Real-time velocity scaling and obstacle avoidance for industrial robots using fuzzy dynamic movement primitives and virtual impedances. Industrial Robot, 45(1):110–126, 2018. ISSN 0143991X. doi: 10.1108/IR-02-2017-0035.

[186] Clemente Lauretti, Francesca Cordella, and Loredana Zollo. A hybrid joint/cartesian dmp-based approach for obstacle avoidance of anthropomorphic assistive robots. International Journal of Social Robotics, 11(5):783–796, 2019. ISSN 18754805. doi: 10.1007/s12369-019-00597-w.

[187] Ang Li, Zhenze Liu, Wenrui Wang, Mingchao Zhu, Yanhui Li, Qi Huo, and Ming Dai. Reinforcement learning with dynamic movement primitives for obstacle avoidance. Applied Sciences (Switzerland), 11(23), 2021. ISSN 20763417. doi: 10.3390/app112311184.

[188] Zhenyu Lu and Ning Wang. Dynamic movement primitives based cloud robotic skill learning for point and non-point obstacle avoidance. Assembly Automation, 41(3): 302–311, 2021. ISSN 01445154. doi: 10.1108/AA-11-2020-0168.

[189] Zezhi Liu and Yongchun Fang. A superquadrics-based steering angle obstacle avoidance method of dmps. 2023 42nd Chinese Control Conference (CCC), pages 4273–4279, 2023. ISSN 21612927. doi: 10.23919/ccc58697.2023.10240845.

[190] Haocun Wu, Di Hua Zhai, Zhiqiang Xia, and Yuanqing Xia. A dmps-based switching motion planning method for robots with obstacles. Chinese Control Conference, CCC, 2020-July:3875–3880, 2020. ISSN 21612927. doi: 10.23919/CCC50068.2020.9188839.

[191] Takamitsu Matsubara, Sang Ho Hyon, and Jun Morimoto. Learning stylistic dynamic movement primitives from multiple demonstrations. IEEE/RSJ 2010 International Conference on Intelligent Robots and Systems, IROS 2010 - Conference Proceedings, pages 1277–1283, 2010. doi: 10.1109/IROS.2010.5651049.

[192] Freek Stulp, Ingo Kresse, Alexis Maldonado, Federico Ruiz, Andreas Fedrizzi, and Michael Beetz. Compact models of human reaching motions for robotic control in everyday manipulation tasks. 2009 IEEE 8th International Conference on Development and Learning, ICDL 2009, pages 1–7, 2009. doi: 10.1109/DEVLRN.2009.5175511.

[193] Freek Stulp, Erhan Oztop, Peter Pastor, Michael Beetz, and Stefan Schaaz. Compact models of motor primitive variations for predictable reaching and obstacle avoidance. 9th IEEE-RAS International Conference on Humanoid Robots, HUMANOIDS09, pages 589–595, 2009. doi: 10.1109/ICHR.2009.5379551.

[194] Akshara Rai, Giovanni Sutanto, Stefan Schaal, and Franziska Meier. Learning feedback terms for reactive planning and control. Proceedings - IEEE International

Conference on Robotics and Automation, pages 2184–2191, 2017. ISSN 10504729. doi: 10.1109/ICRA.2017.7989252.

[195] Zherong Pan and Dinesh Manocha. Realtime planning for high-dof deformable bodies using two-stage learning. Proceedings - IEEE International Conference on Robotics and Automation, pages 5582–5589, 2018. ISSN 10504729. doi: 10.1109/ICRA.2018.8460602.

[196] Craig Innes and Subramanian Ramamoorthy. Elaborating on learned demonstrations with temporal logic specifications. Robotics: Science and Systems, 2020. ISSN 2330765X. doi: 10.15607/RSS.2020.XVI.004.

[197] Ali H. Kordia and Francisco S. Melo. An end-to-end approach for learning and generating complex robot motions from demonstration. 16th IEEE International Conference on Control, Automation, Robotics and Vision, ICARCV 2020, pages 1008–1014, 2020. doi: 10.1109/ICARCV50220.2020.9305399.

[198] Zhenyu Lu, Ning Wang, Qinchuan Li, and Chenguang Yang. A trajectory and force dual-incremental robot skill learning and generalization framework using improved dynamical movement primitives and adaptive neural network control. Neurocomputing, 521:146–159, 2023. ISSN 18728286. doi: 10.1016/j.neucom.2022.11.076.

[199] Heiko Hoffmann, Peter Pastor, Dae-Hyung Park, and Stefan Schaal. Biologically-inspired dynamical systems for movement generation: Automatic real-time goal adaptation and obstacle avoidance. In 2009 IEEE International Conference on Robotics and Automation, pages 2587–2592. IEEE, 5 2009. ISBN 9781424427895. doi: 10.1109/robot.2009.5152423.

[200] F. Janabi Sharifi and D. Vinke. Integration of the artificial potential field approach with simulated annealing for robot path planning. pages 536–541, 1993.

[201] Ahmed Badawy. On-Orbit Manoeuvring using Superquadric Potential Fields. PhD thesis, UNIVERSITY OF STRATHCLYDE, 2007.

[202] Hiroshi Tanaka, Mamoru Minami, and Yasushi Mae. Evaluation of obstacle avoidance ability for redundant mobile manipulators. IECON Proceedings (Industrial Electronics Conference), 2005:1768–1773, 2005. doi: 10.1109/IECON.2005.1569173.

[203] Sipu Ruan, Karen L. Poblete, Hongtao Wu, Qianli Ma, and Gregory S. Chirikjian. Efficient path planning in narrow passages for robots with ellipsoidal components. IEEE Transactions on Robotics, 39(1):110–127, 2023. ISSN 19410468. doi: 10.1109/TRO.2022.3187818.

[204] Richard Alan Volpe. Real and artificial forces in the control of manipulators: Theory and experiments. Dissertation, (September):175, 1990.

[205] Alan H. Barr. Superquadrics and angle-preserving transformations. IEEE Computer Graphics and Applications, 1(1):11–23, 1981. ISSN 02721716. doi: 10.1109/MCG.1981.1673799.

[206] Aleš Jaklič, Aleš Leonardis, and Franc Solina. Segmentation and Recovery of Superquadrics, volume 20 of Computational Imaging and Vision. Springer Netherlands, Dordrecht, 2000. ISBN 978-90-481-5574-3. doi: 10.1007/978-94-015-9456-1.

[207] Richard P Paul. Robot manipulators: mathematics, programming, and control: the computer control of robot manipulators. Richard Paul, 1981.

[208] Edoardo Caldarelli, Adria Colome, and Carme Torras. Perturbation-based stiffness inference in variable impedance control. IEEE Robotics and Automation Letters, 7 (4):8823–8830, 2022. ISSN 23773766. doi: 10.1109/LRA.2022.3187866.

[209] Weitao Wang, Matteo Saveriano, and Fares J. Abu-Dakka. Learning deep robotic skills on riemannian manifolds. IEEE Access, 10(October):114143–114152, 2022. ISSN 21693536. doi: 10.1109/ACCESS.2022.3217800.